Lymphoid like stromal cells in a model of tertiary lymphoid organ formation

by

Saba Nayar

UNIVERSITY OF BIRMINGHAM

A thesis submitted to the University of Birmingham for the degree of DOCTOR OF PHILOSOPHY

School of Immunity and Infection
College of Medical and Dental Sciences
The University of Birmingham
March 2014

UNIVERSITY OF
BIRMINGHAM

University of Birmingham Research Archive

e-theses repository

This unpublished thesis/dissertation is copyright of the author and/or third parties. The intellectual property rights of the author or third parties in respect of this work are as defined by The Copyright Designs and Patents Act 1988 or as modified by any successor legislation.

Any use made of information contained in this thesis/dissertation must be in accordance with that legislation and must be properly acknowledged. Further distribution or reproduction in any format is prohibited without the permission of the copyright holder.

Abstract

Tertiary lymphoid organs (TLOs) are a hallmark of many chronic immune-mediated inflammatory diseases. However, till date the series of events leading to stromal cell activation in TLOs and their role in the inflammatory process remain unclear.

Using a model of inducible TLO formation in the salivary glands of mice we explored the role of gp38+LTβR+ lymphoid-like stromal cells (LLSc) during TLO development and show that they acquire the capability to produce lymphoid chemokines (CKs)/cytokine and drive lymphocyte compartmentalization. In this thesis, we provide evidence that stromal cell activation is a multi-step process with three distinct phases mediated by three major cytokines (IL-13, IL-22 and LTβ).

We demonstrate that during TLO formation, IL-4Rα engagement via IL-13 on quiescent tissue-resident fibroblasts induces the phenotypic acquisition of lymphoid features by LLSc. IL22 then initiates the proliferation and expansion of the LLSc population, required for the expression of lymphoid CKs/cytokines and ANA autoantibody production. Finally, we show that LTβR ligation is necessary for the establishment of a fully mature TLO structure once IL-22 driven LLSc proliferation has occurred. Based on our findings we have identified three different phases of stromal cell activation in TLOs which are all potentially targets of future therapy.

Acknowledgements

I would like to thank my supervisors, **Prof. Chris Buckley** for offering me the opportunity to undertake this project, his guidance and encouragement, and **Dr. Francesca Barone** for investing her faith in me and bringing me to do a PhD with her in Birmingham, I am really thankful for her invaluable and patient supervision on a daily basis, and her constant support throughout my PhD. Additionally, I am very grateful for the endless mice cannulations that Francesca has done for me during my PhD. I would also like to thank my PhD co-supervisor **Prof. Peter Lane** for his invaluable discussion of my project.

Many others have provided technical assistance during my PhD; **Dr. Debbie Hardie** for her assistance in establishing the MoFlo sorting of stromal cells, and guidance in developing the image analysis method, she can only be described as 'the Expert', **Roger Bird** for his help in cell sorting the 'fastidious stromal cells' always with a smile and patience, and **Mehmood Khan** for teaching me tissue sectioning and not fear the cold machine called the Cryostat. I have to especially thank both **Gemma** and **Dennis**, our lab technicians who prepared large batches of virus for me to use for my experiments. A big thank you to the medical intercalators; **Tom Cloake** for all his help in pushing the IL-22 project in the right direction, **Ming-May Chung** and **Philip Ranklin** for helping me with the tedious image analysis.

I will also like to thank **Dr. David Withers** and **Dr. Andrea White** for their constant help and technical advice throughout my PhD, they truly have been my saviours especially during my first year of PhD.

The team at the BMSU have also been superb, in particular Ian and Jenny, who have been patient and always helpful.

A huge thanks to Buckley group and entire RRG, past and present, for all the help and advice over the years, and especially for making the lab a fun place to work. **Joana, Niharika, Julia and Dominika** thank you for being such great friends and support throughout.

This acknowledgement would not be complete without thanking Francesca, Inus, Jon, Lucrezia, Jessica and Chocolate for being my family here.

Thank you to all my friends from school and undergraduate years, you all have been instrumental in some way or the other in helping me get through these long four years.

Finally, I thank my long suffering family, who have shared every inch of my pain over these past four years. Mom, Dad, Nana, Nani, Tanvir, and all my aunts and cousins. This thesis wouldn't be possible without your love, support and patience.

List of Abbreviations

-/-	Knock-out
+	positive
-	negative
ADSCs	Adipocyte derived stromal cells
AdV	Adenovirus
Ag	Antigen
AID	Activation induced cytidine deaminase
Akt	Ak thymoma/ Protein kinase b
aly	alymphoplasia
ANA	Anti-nuclear antibodies
APC	Antigen presenting cells
ARTN	Artemin
ATLOs	Artery tertiary lymphoid organs
BAFF	B-cell activating factor
B cell	Bursa/bone-marrow derived lymphocyte
Bcl-6	B cell lymphoma-6
BCR	B-cell receptor
BEC	Blood endothelial cells
Blimp-1	B lymphocyte-induced maturation protein-1
BM	Bone-marrow
BP-3	Bone marrow stromal cell antigen-1
BrdU	Bromodeoxyuridine
BSA	Bovine serum albumin
C/EBPα	CCAAT/enhancer-binding protein alpha
CAFS	Cancer associated fibroblasts
CCL11	C-C motif chemokine ligand 11
CCL19	C-C motif chemokine ligand 19
CCL20	C-C motif chemokine ligand 20
CCL21	C-C motif chemokine ligand 21
CCL5	C-C motif chemokine ligand 5
CCL7	C-C motif chemokine ligand 7
CCR6	Chemokine (C-C motif) receptor 6
CCR7	Chemokine (C-C motif) receptor 7
CD	Cluster differentiation
cDNA	Complementary deoxyribonucleic acid
cKit	proto-oncogene c-Kit/CD117
Clec-2	C-type lectin-like receptor 2
CMV	Cytomegalovirus
CNS	Central nervous system
CSR	Class switch recombination
CXCL1	C-X-C motif chemokine ligand 1
CXCL10	C-X-C motif chemokine ligand 10
CXCL11	C-X-C motif chemokine ligand 11
CXCL12	C-X-C motif chemokine ligand 12
CXCL13	C-X-C motif chemokine ligand 13
CXCL9	C-X-C motif chemokine ligand 9
CXCR5	Chemokine (C-X-C motif) receptor 5
DCs	Dendritic cells
DMEM	Dulbecco's Modified Eagle's Medium
DN	Double negative
DNA	Deoxyribonucleic acid

DNase	Deoxyribonuclease
DT	Diphtheria toxin
E11	Embryonic day 11
E13	Embryonic day 13
E15	Embryonic day 15
EAE	Experimental autoimmune encephalomyelitis
EC	Endothelial cells
EDTA	Ethylenediaminetetraacetic acid
ELISA	Enzyme-linked immunosorbent assay
EMT	Epithelial-mesenchymal transition
EPCAM	Epithelial cell adhesion molecule
ERTR7	Clone of antibody that detects reticular fibroblasts and reticular fibres in lymphoid organs
FACS	Fluorescence activated cell sorting
FAE	Follicle associated epithelium
FAM	Fluorescein amidite
Fc	Fragment constant
FCS	Fetal calf serum
FDC	Follicular dendritic cells
FDC-M1	Clone of antibody that recognizes follicular dendritic cells and their dendritic processes
FRC	Fibroblastic reticular cells
GC	Germinal centers
GFP	Green fluorescent protein
GL-7	Clone of monoclonal antibody that reacts with a cell-surface protein found on activated T and B lymphocytes
GlyCAM-1	Glycosylation-dependent cell adhesion molecule-1
gp38	Glycoprotein 38/podoplanin
GPS	Glutamine Penicillin Streptomycin
HCV	Hepatitis-C virus
HEV	High endothelial venules
hi	High
HLA	Human leukocyte antigen
HOX	Homeobox
iBALT	Inducible bronchus associated lymphoid tissue
I or ICAM-1	Intercellular adhesion molecule 1
ICOS	Inducible T-cell costimulator
ICOSL	Inducible T-cell costimulator ligand
Id-2	Inhibitor of DNA binding-2
IFN	Interferon
Ig	Immunoglobulin
Ikaros	Member of a family of Krüppel-like zinc finger transcription factors
IκB	inhibitor of kappa B
IL-13Ra	Interleukin-13 receptor α
IL-17	Interleukin-17
IL-21	Interleukin-21
IL-22Ra	Interleukin-22 receptor α
IL-4	Interleukin-4
IL-4Ra	Interleukin-4 receptor α
IL-6	Interleukin-6
IL-7	Interleukin-7
IL-7R	Interleukin-7 receptor
ILC	Innate lymphoid cells
ILF	Inducible lymphoid tissue
int	intermediate

IPAH	Idiopathic Pulmonary Arterial Hypertension
IRF	Interferon regulatory factor
Ki67	Ki-67 protein (also known as MKI67) is a cellular marker for proliferation
KO	Knock-out
LEC	Lymphatic endothelial cells
LIGHT	Homologous to LT, inducible expression, competes with herpes simplex virus (HSV) glycoprotein D for HSV entry mediator (HVEM), a receptor expressed on T lymphocytes
LLSc	Lymphoid like stromal cells
LN	Lymph node
lpr	lymphoproliferation
LPS	Lipopolysaccharide
LTα	Lymphotoxin alpha
LTα1β2	Lymphotoxin alpha 1 beta 2
LTα3	Lymphotoxin alpha 3
LTβ	Lymphotoxin beta
LTβR	Lymphotoxin beta receptor
LTi	Lymphoid tissue inducer
LTin	Lymphoid tissue initiator
LTo	Lymphoid tissue organizer
LYVE-1	Lymphatic vessel endothelial receptor 1
MACS	Magnetic cell sorting
MADCAM-1	Mucosal vascular addressin cell adhesion molecule 1
MALT	Mucosa associated lymphoid tissue
MFI	Mean fluorescent intensity
MHC	Major histocompatibility complex
mLN	Mesenteric lymph node
MRC	Marginal reticular cells
mRNA	Messenger r nucleic acid
NALT	Nasal associated lymphoid tissue
NEAA	Non-essential amino acids
NFκb	Nuclear factor kappa b
NK cells	Natural killer cells
NKT cells	Natural killer T cells
NOD	Non-obese diabetes
O.D.	Optical density
p.c.	Post-cannulation
PALS	Periarteriolar lymphoid sheath
PBMC	Peripheral blood mononuclear cells
PBS	Phosphate buffer saline
PDGF	Platelet derived growth factor
PdgfRα	Platelet derived growth factor receptor alpha
PdgfRβ	Platelet derived growth factor receptor beta
pLN	Peripheral lymph nodes
plt	paucity of lymph node T cells
PNA	Peanut agglutinin
PNad	Perpheral Node addressin
PP	Peyer's patch
PROX-1	Prospero homeobox protein 1
r.p.	Recombinant protein
RA	Rheumatoid arthritis
RAG	Recombination activating gene
RALDH2	Retinaldehyde dehydrogenase 2
RANK	Receptor activator of nuclear factor kappa-B
RANKL	Receptor activator of nuclear factor kappa-B ligand

RASF	Rheumatoid arthritis synovial fibroblasts
RET	Rearranged during transfection
RFs	Reticular fibres
RIP	Rat insulin promoter
RLT	Lysis buffer for lysing cells and tissues prior to RNA isolation when using Qiagen RNA extraction kit
RNA	Ribonucleic acid
RNase	Ribonuclease
RORc	RAR-related orphan receptor C
RORg	RAR-related orphan receptor gamma
RPE	Buffer for washing membrane-bound RNA when using Qiagen RNA extraction kit
rpm	Revolutions per minute
RPMI	Roswell Park Memorial Institute
RQ	Relative quantitation
RT-PCR	Reverse transcriptase polymerase chain reaction
RW1	Buffer for washing membrane-bound RNA when using Qiagen RNA extraction kit
Sca-1	Stem cell antigen-1
SCID	Severe combined immunodeficiency
SCS	Subcapsular sinus
SHM	somatic hypermutation
SLE	systemic lupus erythematosus
SLOs	Secondary lymphoid organs
SMC	Smooth muscle cells
SNP	Single nucleotide polymorphism
SS	Sjogren's Syndrome
STAT	Signal Transducer and Activator of Transcription
T cell	Thymus-derived lymphocyte
TCR	T cell receptor
Tfh	T follicular helper
Tg	Transgenic
Th2	T helper 2
TLO	Tertiary lymphoid organs
TNF	Tumor necrosis factor
TNFR1	Tumor necrosis factor receptor 1
TRAF	TNF receptor associated factor
TRANCE	TNF-related activation-induced cytokine
TRANCE-R	TNF-related activation-induced cytokine receptor
V or VCAM-1	Vascular cell adhesion protein 1
VEGFR	Vascular endothelial growth factor receptor
WT	Wild-type
γc	Gamma chain

List of Figures

List of Tables

Table of Contents

Chapter 1

Introduction

1.1 General

The functioning of the immune system requires highly complex and dynamic interactions between various cell populations which protect the body against insults by pathogens and noxious antigens. This includes a wide range of physiological phenomena such as generation of diverse and functionally mature (albeit naïve) T and B lymphocytes, regulation of immune tolerance through T- and B-cell receptor repertoire screening and selection to control escape of auto-reactive lymphocytes, antigen drainage from peripheral tissues and blood, initiation of the adaptive immune response, generation of immunological memory and control of commensal microbiota homeostasis. Over the years, many studies have documented the location and organization of these complex activities within specialized lymphoid organs [1-4].

Broadly the immune system is made up of primary and secondary lymphoid organs. Primary lymphoid organs like bone marrow and thymus are specialized environments where lymphocytes are produced, differentiated and selected according to their 'non-self-reactive' specificity but all of this happens in an antigen-independent manner [5]. Secondary lymphoid organs (SLOs) are anatomically distinct tissues that are situated throughout the body at strategic sites where foreign antigens are most likely to be encountered, thus each SLO is uniquely equipped to 'sample' antigens, efficiently trap and concentrate these foreign antigens to be delivered to lymphocytes that recirculate in these SLOs, [1-4] in order to mount an appropriate adaptive immune response. The spleen, for example, is important for detection of and protection against blood-borne pathogens, whereas draining lymph nodes are found along the lymphatic bed that drains antigen and antigen-presenting cells (APC) from the peripheral tissue [1-4].

The mucosal lymphoid organs, Peyer's patches (PP), nasal-associated lymphoid tissue (NALT), cryptopatches and inducible lymphoid follicles (ILF) provide protection at mucosal surfaces, 'collecting' antigens directly from the local environment via the mucosal epithelium. These lymphoid organs lack afferent lymphatic vessels. Taken together these SLOs form a highly diverse and complex system that provide a specialized architecture and microenvironment to support the controlled interactions between APCs and rare, antigen-specific lymphocytes, provide the necessary factors for the survival and differentiation of lymphocytes to pre-empt a rapid and appropriate immunological response to foreign agents and also promote stimulation of long-lived, protective immunity. Furthermore they have been recently recognized as sites for regulation of peripheral tolerance to control escape of auto-reactive lymphocytes that escape central tolerance barriers operating in primary lymphoid organs [1-4].

Over the past years, numerous studies have described immune cell location and organization in both primary and secondary lymphoid organs. For all these years, stromal cells which form the lymphoid tissue parenchyma have been assigned to play only a structural role of forming the scaffold of the lymphoid organs within which the immune cells perform their functions. However, it's only recently that studies have started to highlight how the leukocytes in these lymphoid organs are actively engaged in functional interactions by the non-haematopoietic stromal cells (which include mesenchymal and endothelial stromal cell subsets and in case of thymus also includes epithelial cells) [1, 6, 7].

In the thymus, stromal cells have been demonstrated to be necessary for survival and proliferation of thymocytes. Furthermore, the active interaction between stromal cells and immature thymocytes has been shown to be critical to drive the self-tolerant T cell maturation process in the thymus [8]. Correspondingly in SLOs, the stromal cell compartment provides lymphocyte survival signals, chemokine cues which allows migration of T and B cells within SLOs that allows appropriate conservation of SLO architecture and function, Stromal cells also provide channels for delivery of antigen and inflammatory stimuli within SLOs [1].

Stromal cell networks are a dynamic component of SLOs which consist of a variety of cell subsets with specific but overlapping functions [1, 6, 7]. Moreover, stromal cells are not only important for proper functioning of the lymphoid organs in adulthood; studies have also underlined their necessity in development of these lymphoid organs. For example, a study in 1960 showed that removal of the surrounding mesenchymal layer from 12-day-old embryonic thymus lobes prevented normal thymus development [8, 9]. The importance of thymic mesenchymal stromal cells was further emphasized in a study where extirpation of the neural crest cells- resulting in lack of thymic mesenchymal stromal cells- led to abortive thymic formation and function [8, 10]. Similarly, in SLOs (such as LNs) lack of lymphoid stromal cell maturation signals during development results in disrupted LN formation [6, 11].

For the purpose of this thesis only aspects of SLO (in particular LN) development, structure (including different lymphoid stromal subsets) and function will be further discussed. This introductory chapter will also discuss tertiary lymphoid organs (TLOs) in detail. TLOs are ectopic accumulations of lymphocytes commonly found at non-lymphoid site of inflammation and infection. They architecturally resemble SLOs, with segregated T and B cell areas, presence of specialized populations of DCs, differentiated lymphoid stromal cells and high endothelial venules (HEVs). Even though TLOs are often associated with local pathology observed in chronic inflammatory or infectious diseases but there are also examples in which TLOs are reported to contribute to protective immune responses like their SLO counterparts [12-14] . Therefore, it remains unclear whether TLOs are beneficial or not and whether their presence in tissues should be encouraged or prevented.

1.2 Development of secondary lymphoid organs (SLOs)

Irrespective of differences in anatomical location and organization, the development of most SLOs follows a similar script with some variations. A relatively common programme of organogenesis seems to underlie the development of LNs, PP, NALT and ILF whereas the organogenesis of the more complex organ the spleen, which consists of white and red pulp, involves different genes [4, 11, 15, 16]. For the purpose of this thesis we will not discuss the development of spleen.

The process of secondary lymphoid organ development (also termed secondary lymphoid organogenesis) occurs mostly independent of antigen or pathogen recognition with the exception of ILF development which only takes place when the intestine is colonized by bacteria. The foundation for lymphoid tissue ontogeny is established at predetermined sites throughout the body as a result of complex and critical interactions between hematopoietic, mesenchymal and endothelial cells [4, 11, 15, 16]. The knowledge on the cellular and molecular interactions involved in the formation and maintenance of SLO architecture has mostly derived from the analysis of various gene-deficient mice that show different degrees of defective lymphoid organogenesis [4, 11, 15, 16]. The results of deletion of individual cytokines, chemokines, receptors and transcription factors have been catalogued in Table 1.2A.

Table 1.2A

Mutation	Signalling pathway	Cells affected	mLN	pLNs	PPs	NALT	References
Lta$^{-/-}$	LTβR	stroma	± *	−	−	± **	[17-20]
Ltb$^{-/-}$	LTβR	stroma	±	−	−	±	[17, 20, 21]
Ltbr$^{-/-}$	LTβR	stroma	−	−	−	±	[17, 20, 22]
Light$^{-/-}$	LTβR	stroma	+	+	+	ND	[23]
Light/Ltb$^{-/-}$	LTβR	stroma	−	−	−	ND	[23]
Aly/aly	LTβR	stroma	−	−	−	±	[17, 20, 24]
Il7ra$^{-/-}$	IL-7R	LTi	+	+	−	±	[17, 20, 25, 26]
Il2rg/rag$^{-/-}$	IL-7R	LTi	+	+	−	−	[27]
Jak3$^{-/-}$	IL-7R	LTi	+	+	−	ND	[25, 26]
Trance$^{-/-}$	TRANCE-R	LTi	−	−	+	+	[20, 28, 29]
Rank$^{-/-}$	TRANCE-R	LTi	−	−	+	ND	[30]
Traf6$^{-/-}$	TRANCE-R	LTi	−	−	+	ND	[31]
Rorc$^{-/-}$		LTi	−	−	−	+	[20, 32, 33]
Id2$^{-/-}$		LTi	−	−	−	−	[17, 34]
Ikaros$^{-/-}$		LTi	−	−	−	ND	[35]
Cxcl13$^{-/-}$	CXCR5	LTi/B	−	−	−	±	[36, 37]
Cxcr5$^{-/-}$	CXCR5	LTi/B	−	−	−	ND	[38]
Plt/plt	CCR7	LTi/B/T	+	+	+	+	[24, 37]
Ccr7$^{-/-}$	CCR7	LTi/B/T	+	+	+	ND	[39]
Cxcl13/Ccl19/21$^{-/-}$	CXCR5/CCR7	LTi/B/T	−	−	−	±	[37]
Ret$^{-/-}$	RET	LTin	ND	ND	−	ND	[40]
Gfra$^{1/1}$	RET	LTin	ND	ND	±	ND	[40]

(Adapted from Randall et al., 2008; Mebius 2003 [11, 16])

***small mLNs developed in few mice
***small disorganized NALT developed
ND, not determined

Table 1.2A Mutations that impair lymphoid organogenesis.

LN and PP Organogenesis

The development of LNs and PP is initiated approximately at E11 and E15 respectively and continues for several weeks after birth. The process starts with LN and PP anlagen formation that entails development of the necessary stromal microenvironment which contains reticular cells, fibroblasts and endothelial cells, and the recruitment of lymphoid tissue inducer (LTi) cells of hematopoietic origin. The iterative interaction between stromal cells (referred as lymphoid tissue organizer cells or LTo) and LTi, which is reinforced by several cytokine/chemokine feedback loops, lays the foundation for the subsequent development of mature lymphoid organ [11, 16, 41].

In this section the development of LN and PP will be discussed, with a focus on LTi and LTo cells, the cellular and molecular axis involved in the organogenesis of these lymphoid tissues and finally the organization of LN and PP in their characteristic mature architecture with segregated T and B cell areas.

Generation of lymphoid tissue inducer (LTi) cells during secondary lymphoid organogenesis: The Hematopoietic Instructor Paradigm

Cells of hematopoietic origin which include CD3-CD4+cKit+IL7Rα+α4β7+ LTi cells and a distinct population of CD3-CD4-cKit+IL7Rα-α4β7+CD11c+ lymphoid initiator (LTin) cells, start to colonize pre-defined future sites of lymphoid organs between embryonic day 9.5 (E9.5) and 16.5 (E16.5), depending on the type and location of the SLO [11, 16, 42-48].

LTi were first discovered by Kelly and Scollay in 1992, in a study designed to better understand the initial colonization of neonatal LNs by T cells. The study showed that during the first few days of life a high proportion of neonatal CD45+ cells in the LN were CD4+CD8- cells but the majority of them were CD3- cells. These cells lacked surface expression of B220 and Mac-1 and were found to be Thy-1loCD44+. The CD3-CD4+ population did not increase greatly in number after birth and rapidly diminished in proportion as the number of CD3+ cells increased [49].

Several years' later CD45+CD4+CD3- cells were found to be the earliest hematopoietic cells colonizing the fetal LN and PP anlagen. CD45+CD4+CD3- cells were found in mice lacking spleen (HOX11-/- mice) or thymus (nude mice), demonstrating that these organs were not mandatory for generation of fetal LTi cells [47, 50, 51]. Fetal LTi cells are the progeny of Lin-cKit+IL7Rα+ common lymphoid progenitors (CLPs) residing in the fetal liver, which can also give rise to NK, DC, T and B cells [50, 52, 53]. IL7Rα+ precursor cells depend on Ikaros for their development, since Ikaros deficiency results in the absence of LTi, NK, DC, T and B cells [42, 54]. LTi differentiate from common IL7Rα+ precursor by suppression of E2A-encoded protein, by expression of the helix-loop-helix protein inhibitor of DNA binding 2 (ID2), which prevents differentiation to B cells [55, 56]. Down modulation of Notch signalling prevents their differentiation to T cells and results in up-regulation of α4β7 expression [57]. Finally expression of transcription factor retinoic acid-related orphan receptor γt (RORγt) is required for final differentiation of LTi cells [33, 48, 56, 58].

Detailed phenotype analysis of LTi cells over the years, has revealed that apart from CD4, they are negative for lymphoid and erythroid lineage markers, can be identified by expression of RORγt in conjugation with IL7Rα chain (nearly 75% of these cells also express IL-2Rγ and IL-2Rα), in addition they express c-Kit, integrins α4β7 and α4β1, TRANCE-TRANCE-R (RANKL-RANK), chemokine receptors CXCR5, CCR7 and most importantly lymphotoxin (LT) α1β2. Signalling either through IL7Rα or tumor necrosis factor-related activation induced cytokine receptor (TRANCE-R) leads to expression of LTα1β2 by LTi cells, which allows them to be functional instructor cells for lymphoid tissue formation [11, 26, 28, 46, 56, 59]. In view of the necessity of lymphotoxin in lymphoid organ development, LTi are main protagonists of SLO development. Absence of LTi, as documented in mice deficient in Ikaros, Inhibitor of DNA-binding 2 (Id-2) or RORγt result in LNs and PP development failure [54, 55, 58]. Moreover, reaggregate LN grafting assays showed that addition of wild-type LTi cells to E15 LTα-/- iLNs resulted in formation of mature lymphoid structures [60]. Besides, adoptive transfer of LTi cells in mice with impaired SLO development was shown to rescue

the organogenesis of PP [61] and NALT [17]. Moreover increased LTi numbers caused by transgenic overexpression of IL7 resulted in formation of higher number of LN and PP [62]. Interestingly, even though treatment with LTβR agonist can rescue development of LN and PP in LTα-/- mice, the same treatment fails to rescue development in RORγt-/- mice [58] and TRANCE deficient mice (which have severely reduced number of LTi cells) [28, 46]. This indicates that LTi cells apart from providing LTα1β2 also provide additional signals to the developing anlage. Overall, these lines of evidence support a role of LTi as instructor cells in lymphoid organ formation.

LTin cells were first described in the gut anlage in 2007 [40, 63-65] where it was demonstrated that partial depletion of LTin cells, through administration of diphtheria toxin (DT) to CD11c-DT receptor embryos, or deficiency of tyrosine kinase receptor RET (a neuroregulator) expression on LTin cells resulted in abrogated PP formation. This suggests that LTi cells are necessary but not sufficient for PP development. Further supporting this concept, RET ligand (ARTN) induced formation of ectopic lymphoid primordial structures and LTin are the first hematopoietic cells to cluster with VCAM-1+ stromal cell at the site of PP formation, although LTi cells are scarcely detected at this stage, but a subsequent extensive accumulation of LTi cells follows LTin cell aggregation [40, 43].

Generation of lymphoid tissue organizer (LTo) cells during secondary lymphoid organogenesis: The Stromacentric Illustration

Upon arrival in the SLO anlagen, LTi (and LTin in case of PP genesis) cells are believed to establish an interplay with their mesenchymal counterparts, lymphoid organizer (LTo) cells, in order to trigger lymphoid organogenesis [11, 16].

Stromal organiser cells are believed to develop from mesenchymal cells. It has been suggested that this mesenchymal specification to lymph node organiser cell occurs independently from LTβR signalling [60, 66]. The mesenchymal progenitor cells are characterized as CD45-, PDGFRα+, LTβR+, VCAM-1-, ICAM-1- [67]. The origin and identity of signals that induce specification of mesenchymal progenitor cells prior to LTi arrival at the

site of lymph node formation to assure SLO organogenesis to take place at defined positions along the body axis remain largely unknown [67].

A century ago, Sabin identified that the earliest event underpining the developing LN anlage is the formation of lymph sacs (that are earliest developments of the lymphatic vasculature) by endothelial-cell budding from the larger veins around embryonic day 10.5 (E10.5) [68-71]. Subsequently, the lymph sac endothelial cells sprout, to give rise to the lymphatic vasculature network and to the LN subcapsular sinus. This process requires expression of the early lymphatic markers such as homebox gene Prox-1 and Lyve-1 and, later, podoplanin (human) or gp38 (mouse) [11, 45, 72]. At E13, the primitive LN anlage consists of a spherical shaped bud of tightly packed gp38/podoplanin+ endothelial cells forming lymph sac surrounded by layers of fibroblastic-like cells, which express several molecules characteristic of mesenchymal cells, such a PDGFRα, the extracellular matrix protein ERTR7, fibronectin, and hyaluronic acid receptor CD44. In contrast, the central bud of gp38+ cells expresses endothelial markers ICAM-1, CCL21 and extracellular matrix proteins laminin α5 and collagen type 1 which is separated from the outer layers of ER-TR7+ fibroblastic cells by an intact and thin layer of Perlecan+ basement membrane [66]. By E14.5 ERTR7+ cells start to invade the endothelial core and migrate to form proper internal stromal compartment of LN anlage, it is at this stage when first entry of CD4+ and CD4- LTi cells is detected [60, 66]. Detailed FACS analysis of CD45- cell populations in E14.5 LN anlagen identified the presence of newly specified mesenchymal cells that are positive for PDGFRα but negative for ICAM-1 and VCAM-1(I^-V^-) and which correlate with the fibroblast-like cells of the mesenchyme that surround the gp38/podplanin+ lymph sac and $I^+V^-gp38^+$MadCAM-1^+VEGFR3$^-$ endothelial cells. The I^+V^- endothelial population becomes positive for both VEGFR3 and lymphatic marker Lyve-1 between E15-E17 [66], indicating the ongoing differentiation process towards lymphatic endothelial cells. This topologically and chronologically controlled process led to the hypothesis that LNs arise from lymph sacs [45, 66, 67].

However, Vodenhoff *et al*. have shown that Prox-1 null and Prox1 conditional mutant embryos that lack lymphatic vasculature, the LN anlage still forms and hence initiation of LN development does not require lymph sacs. However, the LN anlage is hypoplastic and fails to efficiently cluster LTi cells, which are reduced in number. These findings indicate that lymphatic endothelium might not be required for positioning of LTi, but signals from lymphatic endothelial cells do play an important role in generation and/or maintenance of the LN hematopoietic cell niche by specifying the surrounding mesenchyme in order to complete lymphoid organ formation [72, 73]. Furthermore, Onder *et al*. recently reported that endothelial cells (EC)-specific ablation of LTβR in mouse embryo resulted in failure to develop 20% to 40% of all peripheral LNs in these mice. This study identifies endothelial cells as a potential LTo population, but further studies are required to understand which of the two EC populations; lymphatic endothelial cells or blood endothelial cells, function as an endothelial LTo cells [74]. This observation by Onder *et al*. where they suggest endothelial cells as potential source of LTo cells is supported by a previous study in 2007, where analysis of LN anlage not only identified presence of I+V- endothelial cells which expressed Prox-1 and Lyve-1 but this population expressed similar mRNA levels of LTβR, Relb, NFκb2, and target genes of this pathway [60].

By E15.5, these I^-V^- mesenchymal cells precursors differentiate into $PDGFR\alpha^+I^{int}V^{int}gp38^+RANKL^{int}$ "primed" mesenchymal LTo cells independently of LTi cells and LTβR signalling as accumulation of this intermediate population is present in RORc-/-, LTβR-/- and LTα-/- embryonic LNs. The signal/s that prime I^-V^- to $I^{int}V^{int}$ mesenchymal cells are still not very well understood. However, by E17 primed $I^{int}V^{int}$ cells further differentiate into $I^{hi}V^{hi}MADCAM^+RANKL^{hi}$ mature LTo cells, this maturation step is instead dependent on the presence of both LTi cells and LTβR signalling as $I^{hi}V^{hi}$ LTo cells are absent in LN anlagen of RORc-/-, LTα-/- and LTβR-/- and thus LN development is regressed in these mice. Interestingly, differentiation of $I^{int}V^{int}$ cells to $I^{hi}V^{hi}MADCAM^+RANKL^{hi}$ mature LTo cells coincides with accumulation of LTi cells in the LN anlagen [66].

Gene expression profiles of the three CD45- stromal cell populations present in the LN anlagen ($I^{-}V^{-}$, $I^{int}V^{int}$ and $I^{hi}V^{hi}$), surprisingly showed expression of TNFR1, CCL21 along with LTβR on all three subsets but the LTβR signalling downstream effector, the transcription factors Relb and NFκb2 (members of the NFκb family member) were only detected in the $I^{int}V^{int}$ and $I^{hi}V^{hi}$ cells correlating with their higher levels of expression of CCL21, CCL19, CXCL13, RANKL and IL7 with respect to the $I^{-}V^{-}$ precursor cells. However, the highest expression of these genes is detected in the $I^{hi}V^{hi}$ cells, confirming their greater potential to attract LTi [60, 66, 75]. mLN from E15-16.5 LTβR-/- embryos, whose stromal cells are blocked at the $I^{int}V^{int}$ cell stage showed similar level of CXCL13 and IL7 transcripts as found in E15 mLN anlagen of WT mice, indicating that these genes are less dependent on LTβR engagement at this stage [66]. These results are in agreement with findings of Moyron-Quiroz *et al*. showing LT independent expression of CXCL13 and CCL21 during iBALT formation [76].

In contrast $I^{int}V^{int}$ cells showed a failure to induce RANKL and MadCAM in LTβR-/- stromal cells, highlighting the importance of LTβR in expression of these molecules [66]. Absence of RANKL compromise the survival and maturation of LTi cells, which are dependent in the RANK signalling, indicated by the reduced number of LTi found in the mLN of newborn mice deficient in RANKL/RANK or TRAF6, the intracellular adaptor protein via which RANK signals as well as mice that are treated with RANK-Ig fusion protein [28, 31, 46]. Recent reports from Hess *et al*. [77] and Sugiyama *et al*. [78], have indicated a function of RANK signalling in LN stromal cell proliferation and development of LN microarchitecture. Therefore, in absence of full maturation of stromal cells as in case LTβR-/- mice, only rudimentary mLN are found in these mice at birth.

Various studies in SLO organogenesis have identified two LTo populations based on their differential expression of ICAM-1 and VCAM-1, the $I^{int}V^{int}$ and $I^{hi}V^{hi}$ both in LNs and PP [79, 80]. LTo cells are not identical in all SLOs, for example LTo from LNs express RANKL while their PP counterparts lack expression of this molecule. In addition, microarray analysis of LN

and PP LTo showed that mLN LTo cells express high levels of chemokines and cytokines CCL11, CXCL1, CCL7, IL7 and IL6, LTo cells from PP have higher levels of CXCL13, CCL19 and CCL21. Moreover, LN and PP LTo cells also displayed differences in expression of various transcription factors such as Meox2, Prrx1 and Lhx8, functional relevance of these factors is unclear [80]. LTo show differences between LNs. The $I^{int}V^{int}$ LTo cells are relatively more abundant in mLN when compared to other peripheral LNs where LTo cells mainly comprise of $I^{hi}V^{hi}$ subset [79]. This study proposes that the difference in representation of the LTo subsets provides a reasonable explanation for differential developmental requirements between mLN and pLN. For example, targeted deletion of either LTβ, CXCL13/CXCR5 pair or components of the IL7R signalling complex [21, 38, 41, 79, 81, 82] has little effect on mLN development but disrupts the development of pLN. The authors argue that because $I^{int}V^{int}$ LTo cells express higher level of LTβR, the decrease of this population in pLNs could be the limiting factor in case of sub-optimal LTβR stimulation during development, as in the case of LTβ-/- mice. Furthermore, in absence of IL-7R signalling, RANK/RANKL is still able to induce surface expression of LTα1β2 on LTi cells [26, 79]. However, if a reduction in LTα1β2-inducing signals leads to reduced numbers of cells with LT signals, again LTβR levels could be limiting. The same holds true for CXCL13/CXCR5 disruption which controls the accumulation of LT expressing inducer cells at sites of LN development [41, 50, 79, 81, 82]. Overall, these differences in SLO LTo cells strongly support the notion that heterogeneity might result in different LTo cells which preferentially interact and provide different cues to different hematopoietic cells, and thus consequently determines the key molecular signalling axes that are used in different organs.

In 2009, van de Pavert *et al*. showed nerve fibres that are near the site of developing LNs express RALDH2, main enzyme crucial for generation of retinoic acid (RA) which induces expression of CXCL13 in mesenchymal cells, suggesting this to be a possible mechanism for mesenchymal cell specification [83]. This expression of CXCL13 is required for the initial recruitment of LTi cells to form clusters at the site of LN formation, as in absence of RALDH2

LTi clusters failed to form and hence most peripheral LNs were absent in in RALDH2 mutant mice. Further evidence that supports the notion that CXCL13 expression by early LN mesenchyme is part of the initiating event and precedes LTβR signalling comes from the observation that CXCL13 can be detected in the developing LN of LTα-/- embryos [56, 66, 83]. In addition majority of LNs (except mesenteric and cervical LNs) fail to develop in the absence of CXCL13 or its receptor CXCR5, and analysis of embryos of these mice showed that initial clustering of LTi cells did not occur in the absence of CXCL13 or CXCR5. Overall, van de Pavert *et al*. proposed that neuron-derived RA induces mesenchymal specification by inducing CXCL13 expression in these cells and this process determines the location of lymph nodes by attracting the first LTi. The mechanism by which RA is transferred from nerve fibers to adjacent mesenchymal cells is unknown, but effects of RA in the immune system has been described previously [56, 84, 85]. Furthermore, even though the RALDH2 is expressed throughout the nerve fibre, but LNs are not formed the entire length of the neurons, based on observations that LNs always form at location where blood vessels branch, its suggested that these locations somehow instruct nerve fibers to release RA, but exact mechanism is still to be elucidated. Given the pleiotropic role of RA during vertebrate development in processes such as regulation of cell-fate and differentiation [56, 85], it is likely that in addition to CXCL13, RA activates a set of downstream target genes, for example HOX genes, required for organ patterning and cell fate specification during embryogenesis, thus representing them to be candidate factors involved in specifying the mesenchymal cells and patterning of the early LN anlage. It has already been shown by Okuda *et al.* [44] that LTo cells from mesenteric LNs and PP express different HOX genes [67]. Moreover, presence of mesenteric and/or cervical LNs in CXCL13-/-, CXCR5-/- and RALDH2-/-, argues that different specification signals exist depending on location of the organs [83]. CCL21 derived from lymphatic endothelium is shown to be involved in guiding LTi cells to the developing cervical LNs in CXCL13-/-, CXCR5-/- and RALDH2-/- mutant embryos, and hence allow interaction between the LTi and mesenchymal organizer cells [83]. In line with this conclusion cervical LNs fail to form in CXCR5-/- CCR7-/- mice, which lack ability to respond to both

CXCL13 and CCL21. However, plt/plt CXCL13-/- mice which retain CCL21 expression on lymphatic endothelium, still develop cervical LNs [81-83].

Recent work from Benezech *et al*. have demonstrated that adipocyte precursor cells (pre-adipocytes) that develop into adipose cells, also have the potential to give rise to lymphoid tissue organizer cells on LTβR engagement, which represents the key molecular switch in the choice between the two cell lineages, whereby LTβR ligation by LTα1β2-expressing hematopoietic cells activates the alternative NFκB signalling pathway in pre-adipocytes which blocks adipogenic differentiation and induces their maturation towards lymphoid tissue stromal cells (LTo). The pre-adipocytes on LTβR engagement begin to express group of genes characteristic of LTo namely those encoding cell-adhesion molecules, such as ICAM-1 and VCAM-1, chemokines such as CXCL13, CCL19 and CCL21 and additionally the survival factor IL-7. Embryonic adipocyte precursor cells expressed stem cell marker CD24, Sca-1, CD34, Pref-1 (a transmembrane protein expressed in mesenchyme and adipocyte progenitors but down-regulated in adipocytes), in addition showed high gp38 and LTβR expression but were negative for mature adipocyte markers C/EBPα and Perilipin along with being c-Kit- and CD31-. Consistent with their mesenchymal origin adipocyte precursors were PDGFRα+ and VCAM-1+. Phenotypically pre-adipocytes strongly resembled the PDGFRα+VCAM-1+ gp38+ LTβR+ LTo mesenchymal progenitor cells previously described in E14-15 LN anlage [86]. Embryonic adipocyte precursors were localized around vasculature in the developing fat pads and also found surrounding and residing within the developing LN anlage. The perivascular location of these cells and their LTβR expression makes them appropriately positioned and equipped to interact with incoming LTα1β2+ LTi cells during LN formation. Interestingly, the pre-adipocytes found in adult mice fat pad, were phenotypically and functionally similar to their embryonic counterparts [86, 87].

Intriguingly, nerve endings are positioned in the very specific regions of the fat pad that eventually encapsulate the developing LN. Hence this could suggest that paracrine provision of retinoic acid from nerve cells to pre-adipocytes might initiate their spatially restricted

cellular differentiation into CXCL13 expressing prospective LN organizer cells, that lead to LTi recruitment and clustering, which in turn allows efficient LTβR engagement on locally present pre-adipocytes, resulting in their maturation into LTo. This will also ensure only some but not all pre-adipocytes in the fat pad are engaged by LTβR signalling [87].

Cellular and Molecular signalling axis in LN and PP development

On the basis of various gene-targeted mice (overviewed in table 1) that lack some or all LNs and PP a generally accepted model of lymphoid organogenesis has been developed. The first signalling pathway shown to be critical for LN and PP formation was LTβR triggering via LTα1β2, which results in downstream activation of the NFκB pathway leading to expression of adhesion molecules and chemokines that are central to lymphoid tissue formation and maturation. Histological analysis of LN and PP anlagen formation at different stages and experiments with mutant chimeric mice showed the source of LTα1β2 was circulating cells (LTi) whereas LTβR+ cells that express NFκB must be resident stromal cells (LTo) [11, 16, 67, 88, 89]. More recently new insights in the initiating events during LN and PP have further helped complete this picture.

The lymph node anlagen was described to be formed at locations where the lymph sac (which gives rise to the lymphatic vasculature) forms around larger blood vessel that consist of VEGFR1+VEGFR2+MECA32+ endothelial cells. For decades lymph sacs were thought to be pre-requisite for LN formation [59, 72]. However, this concept was challenged in 2009 by Vodenhoff *et al*. This study revealed that initiation of LN development, marked by recruitment of LTi cells, was unaffected in Prox-1 null and conditional embryos which lack lymph sac formation. Nevertheless, LTi cell clustering was less efficient in the prospective LN site in these mutant mice [73], strongly suggesting that lymphatic endothelial cells are important in generating an environment conducive for LN development [60, 74]. The current paradigm of LN development (illustrated in Figure1.2A) suggests that the first instructive signal for LN anlage formation might derive from outgrowing nerves in which neurons express enzyme RALDH2 that converts retinal to retinoic acid. Retonic acid then induces CXCL13 expression

in local mesenchymal cells. This allows initial attraction of CXCR5+ LTi cells and initiation of LN development. Owing to the importance of CXCL13 in LN formation, CXCL13-/- and CXCR5-/- embryos lacked clusters of LTi cells and LN anlagen (except some cervical or facial LNs). In addition to its role in recruitment of LTi cells [83], CXCL13-mediated triggering of CXCR5 has been shown to activate α4β1 intergrin on LTi cells [61]. This enhances their binding to VCAM-1+ stromal cells and form tight clusters of LTi-LTo cells which is essential for LTβR signalling. Early expression of CXCL13 was detected between E12.5-13.5 in LN anlage and was shown to be independent of LTβR signalling, as comparable levels of CXCL13 mRNA was detected in WT and LTα-/- mice at this stage. However, at later stages, CXCL13 production is dependent on LT mediated signalling [83]. To further support this concept, studies have shown that LTi recruitment is independent of LT, since LTi cells are observed in LTα-/- mice at the site of anlage formation [59]. Interestingly, the first CXCR5+ LTi cells, recruited to the site of LN formation, express both RANK (TRANCE-R) and it ligand RANKL (TRANCE) rather than LTα1β2 [59].

At later stages in LN development, RANKL has been shown to be majorly expressed by LTo cells [59, 78]. The RANK-RANKL mediated paracrine interaction between LTi cells is important for initial clustering of LTis and up-regulation of LTα1β2 on these cells [46, 75]. LTα1β2 then signals via LTβR to drive surrounding stromal cells or pre-adipocyte cells to differentiate into LTo [11, 67, 75, 86]. LTα1β2/LTβR axis results in initiation of two sequential NFκB signalling pathways (Fig1.2B). The first signal belongs to the classical pathway which involves RelA, p50 and IκBα, and initiates the expression of adhesion molecules such as VCAM-1 [11, 88, 89]. Increased expression of VCAM-1 aids in retention and prolonged interaction of the LTi (which α4β1, ligand for VCAM-1) with LTo cells. The prolonged triggering of LTβR, results in activation of alternative NFκB pathway via the NFκB-inducing kinase (NIK), IκB kinase α and RelB [11, 88, 89]. This second pathway leads to production of chemokines (CXCL13, CCL21 and CCL19), expression of adhesion molecules (VCAM-1, ICAM-1 and MADCAM-1) and up-regulation of IL-7 and RANKL in LTo [11, 66, 75, 88, 89].

Moreover, LTβR triggering is mandatory for stromal cell proliferation and survival. This stromal cell activation allows establishing a positive feedback loop which allows the further recruitment, retention and survival of haematopoietic cells from circulation in the expanding lymphoid anlagen [11, 60, 88, 90]. Accordingly, combined ablation of CXCR5 and CCR7 or CXCL13, CCL21 and CCL19 resulted in failure of LN and PP development [81, 82, 90].

Various studies have shown that for successful formation of LNs, its absolute necessary not only to recruit but also to maintain a critical number of LTi which express LTα1β2. Mice deficient in TRANCE, TRANCE-R or a critical component of TRANCE signalling pathway, TRAF6, all did not develop any LNs (although some cervical LNs have been observed in TRANCE-/- mice, but even these LNs are small and poorly populated), however, PP formation is intact in these mice. The defect observed in LN development in TRANCE-TRANCE-R-/- mice is not due to the absence of LTi cells, but due to severely reduced numbers of LTi cells which fail to properly induce the differentiation of LTo cells. Hence, in the absence of TRANCE signalling, the VCAM-1+ ICAM-1+ LTo cells fail to appear and thus LNs fail to complete their program of development. This is supported by the fact that upon transgenic expression of TRANCE in TRANCE-/-, numbers of LTi increase, rescuing formation of several LNs. However, transgenic expression of TRANCE in LTα-/- mice, which have significant number of LTi cells to start with, fails to restore LN formation. The LTi cells recruited in LTα-/- at sites of LN formation fail to cluster due to their inability to activate stromal cells which results in abrogated LN formation [28, 31, 46]. Overall, these observations suggest that both TRANCE and LTα1β2 regulate the colonization and cluster formation by LTi cells which is important for surrounding stromal cell activation, thereby establishing a positive feedback loop, allowing a successful cross talk between inducer and organizer cells that involves ligands-receptors of the tumour necrosis family (TNF), various chemokines and cytokines which allows completing the process of LN organogenesis.

The steps in the organogenesis of PP are similar to LN development. However, there are some differences. Firstly, unlike LNs development that always occurs at pre-defined

positions in the body, the PPs form in variable numbers and not in fixed positions along the gut [16, 45, 47, 51]. Secondly, in addition to LTi cells, another subset of hematopoietic cells, the LTin has been demonstrated to be crucial for PP formation [40, 45, 63, 64]. Another major difference in PP and LN development is in their requirement of IL-7 and TRANCE. In contrast to LNs, PP development is completely intact in TRANCE-/- mice whereas it is absent in IL-7Rα-/- mice [15, 16, 45]. Another signalling pathway, which is differently used in LN and PP genesis, is the TNFR1. Even though LN development is intact in TNFR1-/- mice, the PP development has been shown to be defective in these mice [15, 16, 45].

Figure 1.2A

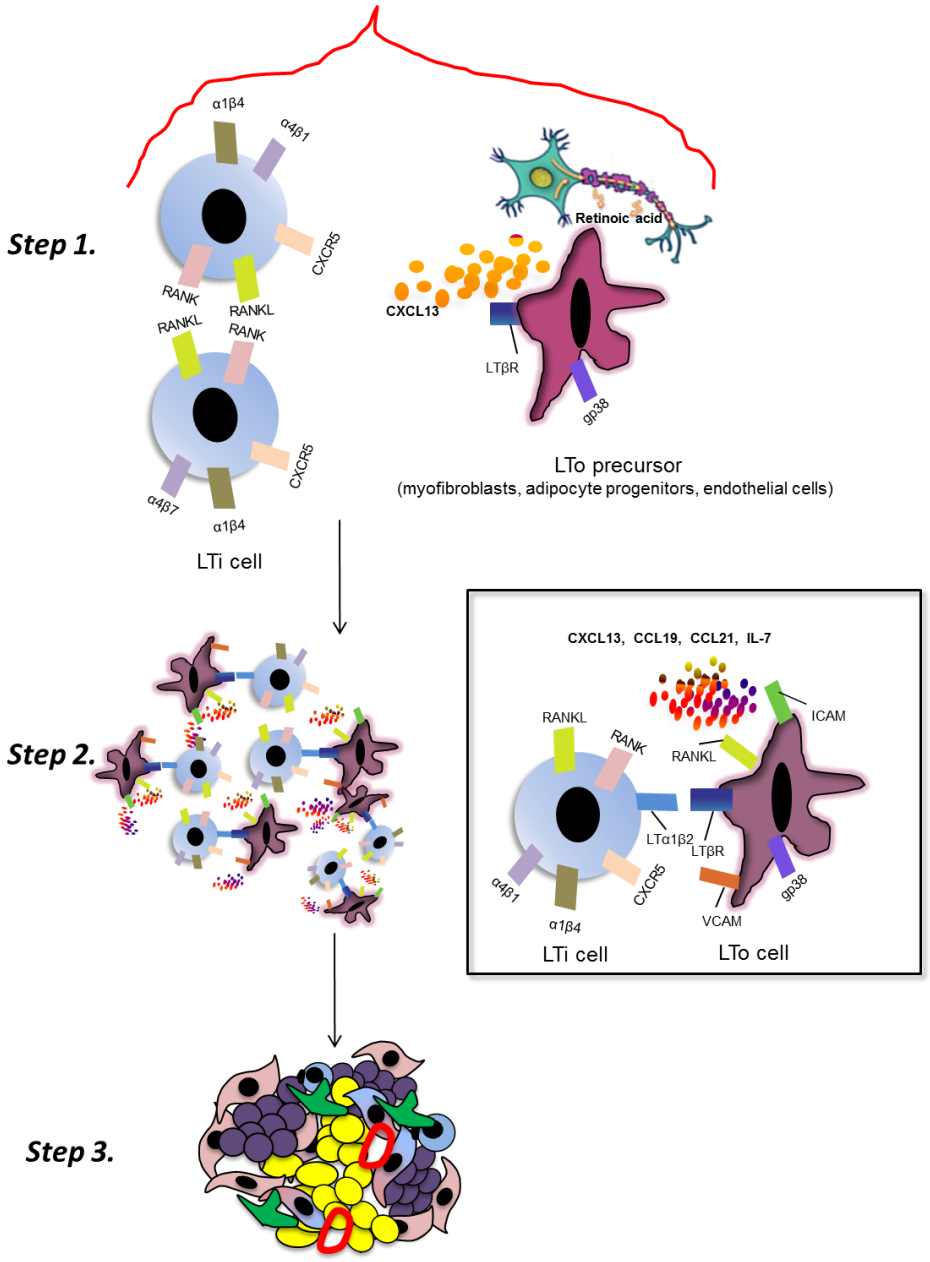

Figure 1.2A Model of Lymph node (lymph node) organogenesis. *Step 1*: Retinoic acid produced by neurons, stimulate LTo precursor cells to express chemokine CXCL13. CXCL13 expression by LTo precursor cells attracts CXCR5+ LTi cells to the site where LNs will develop. LTi cells will cluster and signal in trans to each other through RANKL-RANK. RANK signalling on LTi cells will induce high expression levels of LTα1β2. ***Step 2 and 3*:** Binding of the LTα1β2 to LTβR on LTo precursor will induce differentiation into mature LTo cells that express cell adhesion molecules VCAM-1, ICAM-1, and MAdCAM-1 as well as CXCL13, CCL21, and CCL19. This will subsequently attract large numbers of LTi cells which are now in close contact with increasing numbers of stromal cells. This results in increased LTβR triggering and thereby a positive-feedback loop is initiated which leads to accumulation of more haematopoietic cells (such as B and T lymphocytes), differentation of LTo cells to various stromal cell subsets and formation of HEVs. Thus the formation of the structure of the organs (Adapted from [6, 22, 26, 29, 30, 32, 33, 46, 59, 66, 67, 74, 75, 78, 83, 91-97])

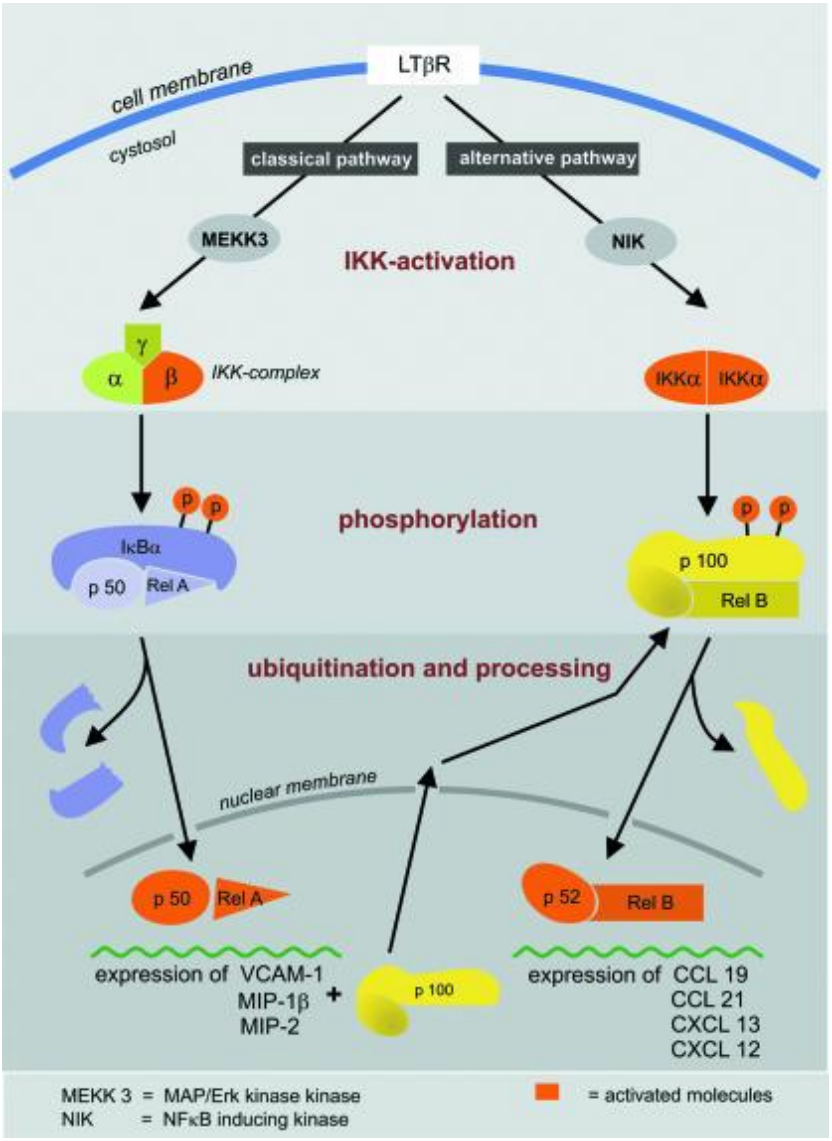

Figure 1.2B Activation of NF-κB via the classical and the alternative pathway. Signalling via the LTβR can initiate both NF-κB activation pathways. The classical pathway leads to the expression of the inflammatory molecules VCAM1, MIP-1β and MIP-2, and an increase of p100. The first step in this cascade is the activation of the β unit of the IKK complex. This activated IKKβ complex leads to phosphorylation and ubiquitination of the IκBα, which allows the p50-RelA heterodimer to translocate to the nucleus and bind to the DNA. The alternative pathway follows a similar mechanism: after activation of the IKKα complex, p100 is phosphorylated and processed to p52. The remaining p52-RelB heterodimer induces the expression of the homeostatic cytokines CCL19, CCL21, CXCL13 and CXCL12, after translocation into the nucleus (Taken from Blum and Pabst 2006 [88]).

Lymphocyte Recruitment and Formation of Follicular Structures in Lymph Nodes and Peyer's Patches during their organogenesis

Clusters of IL7Rα+CD4+CD3-LTi cells and VCAM-1+ICAM-1+ mesenchymal LTo cells begin to segregate into follicular micro-domains around E18 in PP and day 1 postnatally in LNs, with LTi cells at the centre and LTo cells at the periphery [11, 16, 94, 98, 99]. Around the same time, CD11c+ cells are also seen at the periphery of these follicle-like sub-regions in the PP, though it's still unclear if these cells are CD11c+ LTin cells or whether they are CD11c+ DCs that have differentiated in situ from LTi cells [16, 50, 52]. The initial follicular structure micro-domain formation is dependent on LTαβ expression, but not B and T cells, demonstrated by the fact that the initial architectural organization is intact in SCID mice [16, 94, 98]. The recruitment of lymphocytes, segregation of T and B cell in separate zones and formation of mature B cell follicles occurs in the final stages of mature LN and PP development. In mouse LNs this process occurs at day2-3 after birth [100] following the expression of PNAd on HEVs [16, 100, 101]. Before day 2-3, HEVs only express MAdCAM-1 [100], therefore the only cells that can enter the developing LNs at this time are α4β7 integrin expressing IL7Rα+CD4+CD3- LTi cells and γδ T cells [16, 50, 52, 101]. However, around day 3 onwards, LN HEVs down-regulate the expression of MAdCAM-1 and start expressing PNAd, which allows entry of mature naïve T and B cells [16, 100] that express CD62L, ligand for PNAd. When B and T cells enter in the LNs, they ultimately "replace" the LTi cells in their role, providing the LTαβ necessary to maintain differentiation and survival of the LTβR expressing stromal cells. At this stage, CXCL13 expression is still dependent on LTαβ+ LTi cells [11, 16, 94] as the first B cells that enter in the LN lack expression of LTαβ [11, 16, 94]. B and T cell then start to segregate leading to formation of more organized LN [16]. This initial segregation is independent from CXCL13, as at this stage only LTi cells can respond to this chemokine. From day 4, B cells start expressing LTαβ and respond to CXCL13. At this stage their segregation into distinct follicular structures begins [11, 16, 94]. Mice lacking T, B and NK cells develop initial LN anlagen but fail to persist after birth [16, 27].

SLO Organogenesis is confined to a strict developmental window

LNs have been demonstrated to develop in a characteristic order based upon *in vivo* blocking experiments with LTβR-Ig fusion proteins. They begin to be formed at E10.5 with the mesenteric lymph nodes, followed by cervical lymph nodes at E11.5 and then the brachial and axillary lymph nodes after E12.5 [11, 16, 102, 103]. The development of inguinal LNs and PP begins at E16 but the PP continues development until after birth. Finally, the NALT develops after birth. The development of PP and NALT appears to be last, as LT signalling disruption, just before birth, blocked PP formation [16, 102], whereas the adoptive transfer of LTi cells restored development of PP in CXCR5-/- [16, 61] and development of NALT in Id2-/- mice [16, 17]. Each LN has been shown to have its own set of developmental cues and signalling, because when different elements are blocked in the signalling pathway, varying LNs are differentially affected [11, 102-104]. It is possible that these differences are sustained by the differences in the stromal cell compartment of the diverse LNs [11, 16, 79]. In fact, the organogenesis of LN and PP must occur within a strict developmental window, because once this window has passed, their development cannot take place even if LT signalling pathway is restored [11, 16]. In contrast, ILF formation does not follow a strict developmental window. Even though, LT signalling has been shown to be necessary for mature ILF development [16, 105, 106], ILF structures were restored in adult LTα-/- mice, when these mice were reconstituted with normal (LTα+) hematopoietic cells [16, 106]. However, it is not very clear why ILFs lack a fixed developmental window. ILFs are derived from cryptopatches and RORγt expressing adult LTi cells, and are majorly found at these sites in adults [16, 32]. Thus availability of LTi cells at the location of each lymphoid organ might confine it to a particular developmental window [16]. Interestingly, gp38+ stromal cells in the T cell area of the spleen, are also restricted to a developmental window, and require LTαβ expressing B cells during this neonatal period [16, 107]. As a result, splenic gp38+ stromal cells cannot be restored in adult LTα-/- or B-cell knockout mice even after reconstitution with normal bone-marrow derived hematopoietic cells [16, 107]. However, most of the other splenic architecture defects, including the expression of homeostatic

chemokines, FDC differentiation and formation of germinal centres post-immunization, can be reversed in LTα-/- mice when they are reconstituted with LTα+/+ bone-marrow cells from adult WT mice [16, 108-111].

The development of the NALT and ILF follows a slightly different dynamic to that described for LN. This will not be discussed in this dissertation.

Role of Lymphotoxin and TNF in the maintenance of lymphoid architecture

Both LT and TNF expression has been demonstrated to be essential for proper homing and segregation of T and B lymphocytes within SLOs as well as for the maintenance of SLO architecture. For instance, the spleens of LTαKO mice exhibit disorganized T and B cell zones, germinal centres and marginal zones. Furthermore, failure in FDC development is noticed in the absence of LT or TNF signalling [16, 18, 19, 108-110, 112, 113]. LT expression has also been demonstrated to be important for development of CCL21 expressing gp38 stromal cells and subsequent T cell organization in the spleen [16, 107, 114]. As in LN organogenesis the expression of LT and constitutive lymphoid chemokines (CXCL13,CCL19,CCL21) are inter-dependent on a positive-feedback loop; similarly in adult SLOs, LT promotes expression of lymphoid chemokines by stromal cells [16, 115-117]. This controls steady state homing and correct positioning of T and B cells and lymphoid chemokines particularly CXCL13 also play a role in maintenance of LTαβ expression on lymphocytes, thereby sustaining the positive feedback loop to maintain the structure and function of SLOs [16, 36, 115-117]. Evidence suggests that the maintenance of lymphoid chemokine expression and FDCs in B cell follicles is dependent on LTαβ and TNFα expression on mature B cells [16, 108, 118]. However, normal levels of chemokines, and B cell follicles with FDCs were detected in the LNs of mice that lack LTβ, specifically on B cells. Hence, in this case, it was been shown that LTαβ-expressing T lymphocytes are sufficient to maintain LN structure and function [16, 119, 120]. Altogether, this data indicates that expression of LTαβ by both T and B lymphocytes is necessary for proper conservation of lymphoid architecture in adult SLOs. In addition, LT has been suggested to play a role in

maintenance of DC numbers [121], as well as their activation and maturation during an immune response [122]. Furthermore, continual expression of PNAd and structural integrity of HEVs is dependent upon LTβR signalling, because in its absence the HEVs collapse [96, 123, 124]. Interestingly, soluble LTα3, membrane bound LTαβ and TNFα have overlapping yet distinctive functions in regulating many aspects of SLO micro-architecture, for example, spleens of LTαKO [19] and LTβRKO [22] showed more severe disorganization of the T and B cell zones than spleens of LTβKO [21], indicating that LTα3 signalling through TNFR1 as well as LTβR mediated signalling are important for appropriate organization of lymphocytes within SLOs [16]. Similarly, FDC differentiation and maintenance requires TNFα, LTα and LTαβ [108, 110, 111, 125]. On the contrary, the presence of DC in spleens, expression of MADCAM-1 in splenic marginal zones, and development and function of HEVs in LNs are dependent on LTαβ/LTβR axis and not on TNFα, LTα, or TNFR1 [16, 103, 121].

1.3 Adult SLO Organization and Function

SLOs are highly organized encapsulated aggregations of lymphocytes in a framework of non-leukocyte stromal cells, which not only provide basic structural organization to the tissue but also provide survival signals to help sustain lymphocyte survival. In addition to lymphocytes, SLOs also contain resident macrophages and dendritic cells [3].

Of all SLOs, the microarchitecture of LNs (Fig1.3A) has been most fully characterized and hence, is commonly studied as the prototypical SLO. LNs are situated at the points of convergence of vessels of the lymphatic system throughout the body. A LN consists of sub-capsular sinus (SCS), an outermost cortex, paracortex and an inner medulla [3, 88, 126]. Immediately beneath the LN capsule is the SCS, in which the afferent lymphatics empty their content, delivering antigens, molecules and APCs from the draining tissues and organs. Lymphatic endothelial vessels express Lyve 1, as well as other adhesion molecules and CCL21, which are all involved in cell entry into the lymphatics. LN resident-macrophages line the SCS and capture antigens and particles that enter via the lymph [3, 88, 126].

Lymphocytes enter LNs from the blood by extravasation across specialized high endothelial venules (HEVs). HEVs are arranged in regions between the B and T cell zones known as cortical ridges. HEVs have a distinct morphology (a cobblestone like appearance) and express molecules that are crucial for lymphocyte entry into the lymph node, such as peripheral noode addressin (PNAd) and CCL21 [3, 88, 126]. Below the SCS, is the cortex that contains lymphoid nodules called primary follicles. These are composed of B cells and follicular dendritic cells (FDCs). It is here that B cells undergo proliferation after encountering their specific antigen and their cognate T cells, thus forming secondary follicles termed germinal centres. Inside the cortex is the paracortex which is composed of T cells and DCs [3, 88, 126].

The medulla consists of strings of macrophages and antibody secreting plasma cells known as the medullary cords. Filtered lymph and cells leave the LN via efferent lymphatics for later

delivery to the venous blood. The structure and organization of the LN allows maximal interaction between antigen presenting cells and the few lymphocytes, specific for any given antigen. Such features make LNs optimal sites for inducing adaptive immune response. The antigen-bearing DCs and macrophages actively migrate into the lymph node under the chemotactic influence of the lymphoid chemokines such as CCL21 and CCL19 [3, 88, 126]. The same chemokines also attract lymphocytes from the blood, and these enter via the HEVs. Since both lymphocytes and antigen presenting cells are attracted to the same chemokines, they become localized in the same area of the LN. Free antigen diffusing through the LN becomes trapped on resident DCs. The juxtaposition of the antigen, antigen-bearing cells and naïve T cells creates an ideal environment where naïve T cells can bind their antigen and become activated. Since both B and T cell lymphocytes enter the LN via the paracortical area where HEVs are situated, this ensures that before entering the follicles, naïve B cells pass through the T cell zone, where they can encounter both their antigen and their cognate helper CD4 T cells and become activated. These activated B cells undergo intense proliferation and form germinal centres where they differentiate into antibody-producing plasma cells and memory B cells. Of note, B cells also express receptor for lymphoid chemokine CXCL13 which allows their homing to the follicular compartment after their entry via HEVs [3, 88, 126, 127].

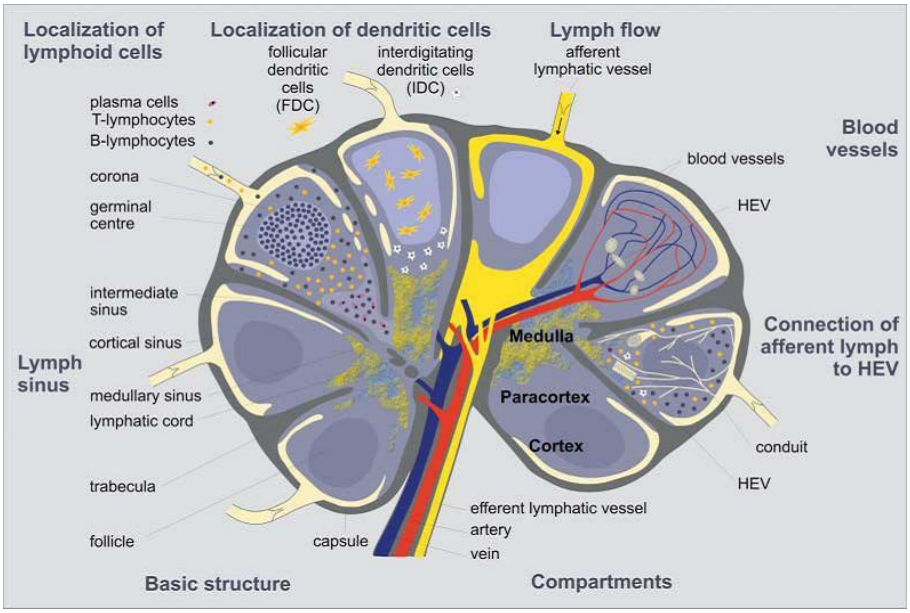

Figure 1.3A Lymph node structure

The lymph node consists of three main regions; the cortex, paracortex and medulla. The cortex consists mainly of B cells organised as primary or secondary follicles. The migration of these cells towards the follicles is mediated by follicular dendritic cells (FDC). T cells migrate to the paracortical region, neighbouring the cortex, and interact with the interdigitating dendritic cells (IDC). The central region, the medulla, mostly contains plasma cells and B cells. The lymphocytes enter the lymph node via the afferent lymphatic vessel or through transmigration of the high endothelial venules (HEV). Both systems, the lymph vasculature and the blood vasculature, are connected via a conduit system (Adapted from Blum et al, 2006 [88]).

Mucosa associated lymphoid tissues (MALT) including PP, NALT have a general structure similar to LNs, with T and B cells segregated in distinct areas. The T cell areas contain substantial number of DCs and primary B cell follicles, where antigen activated B cells undergo germinal centre reaction, during which B cells expand and mature to become antibody producing cells and memory B cells [127-129]. However, MALT differs to LNs in the pathway by which antigen gains entry. Unlike LNs where antigen traffics through afferent lymphatic vessels, antigen enters MALT directly across mucosal epithelium (known as FAE i.e follicle associated epithelium), immediately overlying the follicles of MALT. The FAE has specialized antigen sampling cells termed Microfold (M) cells, which can directly uptake antigen from the lumen of the mucosa and deliver antigens by trans-epithelial vesicular transport to the sub-epithelial lymphoid tissue (such as lamina propria of intestinal and respiratory tracts and nasopharynx glandular tissue). M cells are capable of transporting particles as large as intact micro-organisms. Lymphocytes enter the blood circulation via efferent lymphatic vessels located at abluminal surface of the MALT. These lymphatic vessels ultimately join the thoracic duct like efferent lymphatic vessels from LNs [127-129].

The spleen, the single largest lymphoid organ in mammals, contains up to 25% of the body's mature lymphocytes, and is separated into two major compartments; the red pulp and the white pulp [127, 130]. The red pulp consists of reticular network containing stromal cells and large proportion of macrophages. It primarily serves as a site where aged or damaged erythrocytes are filtered out of circulation. The white pulp represents the organized lymphoid compartment of the spleen where activation and maturation of antigen specific T and B cells occur. Immune cells and antigens enter the spleen with blood via single vascular supply, the splenic artery which branches into trabecular arteries and ultimately into central arterioles that penetrate the periarteriolar lymphoid sheath (PALS) in the white pulp. PALS are T cell-rich compartments surrounding the central arterioles. This area also contains abundant inter-digitating DCs that serve as important APCs early in immune response in the spleen [127,

130]. After penetrating the PALS, the central arteriole forms a marginal sinus that is lined by MADCAM-1 expressing endothelium.

A specialized layer of metallophilic macrophages are associated with marginal sinus endothelium, and are thought to regulate entry of antigen into the white pulp area. Within the white pulp, B cells are organized into two compartments. The first is the marginal zone B cells, which includes of naïve B cells and at least some memory B cells, located adjacent to MADCAM-1 expressing marginal sinus. The other compartment of B cells is the FDC containing primary B follicles surrounding PALS. The arrangement of these follicles resembles primary follicles in LN. This highly ordered structure of the splenic white pulp is critical for proper regulation of immune responses within the spleen [127, 130].

Stromal cell subsets in SLOs

Stromal cells are important for the organization, maintenance and function of secondary lymphoid organs both in resting and inflammatory conditions. Lack of stromal cells in SLOs results in aberrant T/ B cell segregation and failure to generate appropriate immune responses [126]. Stromal Cell subsets in SLOs are overviewed in Table 1.3A.

Mesenchymal organizer stromal cells are thought to represent the precursors of three mature stromal cell subsets observed in the T and B cell areas in adult LNs (described below) [6]. However, the contributions of the organizer cells to stromal subsets in adult organs, and signals that induce their differentiation are still poorly understood.

Fibroblastic reticular cells (FRCs)

In the T cell zones of LN, FRCs surround HEVs forming a dense network filled with CD4+ T cells, CD8+ T cells and subsets of DCs. FRCs produce CCL21 and CCL19 to attract CCR7+ T cell and DCs to the T zone in the LN [126, 131-133]. The CCL21 protein can attach to the negatively charged glycosaminoglycans on the surface of FRCs; this promotes lymphocyte motility on the FRC network that can contribute to increased lymphocyte-DC encounters [126, 131, 134]. Besides regulating T cell trafficking, FRCs produce extracellular matrix,

forming a system of microchannels (conduits) connecting the SCS with the paracortex and the HEVs. This allows rapid transport of small soluble molecules, such as antigens, to DCs in the T cell zone, and thereby has a functional role in antigen presentation, and transport of chemokines to HEVs, which are then presented on the luminal side of HEVs which will ultimately affect lymphocyte entry [126]. FRCs are also a source of IL-7 which in combination with CCL19, sustains naïve T cell survival within the LN T zone and thereby maintains T cell homeostasis in the periphery [135].

Owing to the above mentioned features, FRC are actively involved as positive regulators of T cell responses during immune responses. However, during an acute immune response the FRCs also attenuate excessive proliferation of neighbouring T cells by transiently expressing nitric oxide, thus preventing excessive expansion and inflammatory activity of antigen specific T cells. This helps conserve LN integrity and function during rapid LN growth [136-139]. FRC express and present a range of peripheral tissue antigens, thus participating in peripheral tolerance induction of self-reactive T cells [136, 140].

FRCs is usually defined on the basis of expression of gp38, ER-TR7 and high levels of VCAM-1 and ICAM-1. They are also known to express intracellular molecules which are found in some fibroblasts, including desmin, α-smooth muscle actin, and transglutaminase, and are involved in the formation, expansion, and contraction of their collagen rich reticular fibres [126]. The full function of FRCs, at least in vitro, depends on expression of LTαβ by lymphocytes, presumably due to LTβR:LTαβ cross-talk between FRCs and lymphocytes [141]. However, it has recently been shown that myofibroblastic FRC precursor cells are able to generate the basic T cell zone infrastructure even in absence of LTβR triggering. However their full maturation and function was dependent on LTβR [142].

Follicular dendritic cells (FDCs)

FDCs are the main B cell zone stromal cell population where they are the main source of CXCL13, which is critical for homing of CXCR5+ B cells to the follicular compartment. FDCs cluster in the centre of B cell follicles and form a dense network in which B cells search for

antigens and receive differentiation signals after they are activated [6, 126, 143-145]. FDCs express Fc receptors such as CD16, CD23, and CD32 and complement receptors such as CD21 and CD35 that enables FDCs to capture and present unprocessed antigen, particularly in the form of immune complexes [145]. Furthermore, FDCs secrete cytokines and growth factors that support germinal centre B cell survival and activation such as BAFF [145, 146].

FDCs are characterized by expression of markers such as FDC-M1 (milk fat globule epidermal growth factor 8), FDC-M2 (complement C4) and CD157 (BP-3). They also express high levels of VCAM-1 and MAdCAM-1, as well as molecules that are common to other lymphoid stromal cell populations such as vimentin and desmin [6, 126, 145].

Recently, it has been shown that FDCs originate from perivascular progenitor cells expressing PDGFRβ and Mfge8 genes, and ablation of PDGFRβ+ cells induces collapse of FDC networks [147]. Of note, TNFR and LTβR signalling is critically required for the maintenance of FDCs, as evidenced by their rapid disappearance upon TNFR or LTβR-Ig treatment in mice [145, 148].

Marginal reticular cells (MRCs)

More recently, another lymphoid stromal cell population, localized underneath the SCS in LNs, has been characterized as marginal reticular cells (MRCs) because they exhibit a phenotype that is distinct from B and T cell zone stroma zones [149, 150]. Although MRCs express many markers (VCAM-1, ICAM-1, MadCAM-1, BP-3 and gp38), which are in common with other subsets of lymphoid stromal cells [6, 126, 149], they seem to uniquely express RANKL and thus, are thought to be the adult equivalent of embryonic LTo cells with a role in organising the structure of adult SLOs [149, 150]. MRCs are localized at the edges of the B cell follicles and express CXCL13, similar to the centrally located FDCs. They also form conduit network that can deliver Ag from the LN SCS to the B cell follicles [6, 126, 149, 151, 152]. Altogether, this suggests an important role for MRCs in the homeostasis of B cells and capture and delivery of Ag [6, 126, 149, 150]. MRCs maintenance, like FDCs, fully depends on continuous LTβR signalling [6, 126, 149, 151].

Table 1.3A

	Tissue & location	Phenotype	Functions
Fibroblastic Reticular cells (FRC)	Lymph nodes, spleen, peyer's patches, MALT, tertiary lymphoid tissues. T cell zones.	ER-TR7, podoplanin (gp38), laminin, desmin, α-SMA, fascin, 1BL-10, 1BL-11, LTβR, TNFR1/2, VCAM-1, ICAM-1, PDGFRα/β, CD171, CD157, hyaluronan, CD44, transglutaminase, collagen I, II, IV, cytokeratin 8 & 18, fibronectin, vitronectin, vimentin, fibrillin, tenascin, hepatocyte growth factor, integrin α1, α4, β1, MHC-I, VEGF, CXCL16, CCL21, CCL19, IL-7.	Structural support; production & secretion of reticular fibers & formation of conduit network; chemokine production & expression; substrate for lymphocyte migration; substrate for DC adhesion; IL-7 production & T cell homeostasis; antigen presentation.
Follicular Dendritic cells (FDC)	Lymph nodes, spleen, peyer's patches, MALT, tertiary lymphoid tissues. B cell zones.	CD35 (CR-1), CD21 (CR-2), FcγR-IIb (CD32), FceR-II (CD23), FcγR-III (CD16), FDC-M1, FDC-M2 (complement C4), CD157, VCAM-1, ICAM-1, MAdCAM-1, CD40, CD73, laminin, desmin, fibronectin, tenascin, α-SMA, CXCL13, CXCL12, BAFF.	Antigen capture & presentation of immune complexes; chemokine production & presentation; B cell homeostasis.
Marginal Reticular cells (MRC)	Lymph nodes, spleen, peyer's patches, MALT. SCS (LN) & MZ	ER-TR7, VCAM-1, ICAM-1, MAdCAM-1, TRANCE (RANKL), laminin, desmin, PDGFRa/b, 1BL-11, CD157, CXCL13.	Structural support; chemokine production (CXCL13); conduit function.
Red-pulp fibroblasts	Spleen.	ER-TR7, desmin, laminin, perlecan, integrin α3, α4, α5, β1, PDGFRα/β, ICAM-1, IL-6, CXCL12, IL-2.	Construct splenic cords & direct blood flow; assist in removal of dying red blood cells; expansion & contractile capabilities to control splenic blood flow & function, macrophage and plasma cell attraction and retention.
LN medullary fibroblasts	Lymph node	ER-TR7, desmin, laminin, collagen III, CXCL12(?).	Macrophage and plasma cell attraction and retention?, Mast cell retention and function?
Lymphatic endothelial cells (LEC)	Lymph nodes, spleen (?), peyer's patches, MALT, tertiary lymphoid tissues.	CD31, LYVE-1, VCAM-1, ICAM-1, ICAM-2, ER-TR7, podoplanin (gp38), laminin, VE-cadherin, VEGFR3, catenin, claudin-5, JAM-A, Prox1, Toll-like receptors, CCL21, S1P.	Transport of lymph from the tissues; transport of antigens & cells; allow entry of lymphocytes & APC into lymphatics, chemokine production & presentation.
Vascular endothelial cells (VEC)	Lymph nodes, spleen, peyer's patches, MALT, tertiary lymphoid tissues.	PNAd (LN), CD31, CD34, VE-Cadherin, TNFR1, LTβR, VEGFR2, laminin, collagen IV, JAM-A/B/C, ZO-1/2, ESAM-1, claudin-5, catenin, desmoplakin, endoglin, meca-32, CCL21 (mice).	Transport of blood; entry of cells including lymphocytes from the blood into tissues.

(Adapted from Mueller and Germain 2009 [126]; Fritz and Gommerman 2011 [7])

Table 1.3A Stromal cell subsets in SLOs.

Germinal centre reaction

Germinal centres (Figure1.3B) develop in B-cell follicles of SLOs in response to antigen challenge. Mature B cells continuously recirculate through SLOs in search of signs of infection. Migrant B cells pick up antigens from sub capsular sinus macrophages and bring them to the centre of the follicles. The selective localization of B cells within follicles of SLOs is mediated by CXCL13 (i.e. produced by follicular stromal cells mainly FDCs) which is recognized by the receptor CXCR5 and are highly expressed on B cells [153-156].

On antigen encounter, B cells up-regulate the chemokine receptor CCR7 (specific for chemokine found in T cell area) and congregate at the boundary between B-cell and T-cell areas in search of T-cell help. Cognate encounters with activated T cells, specific for the same antigen, at the T-B boundary drive initial B-cell proliferation. This is particularly mediated by a synapse of CD40 and ICOSL, which is constitutively expressed by B cells, and its ligand, CD40L (CD154) and ICOS, which is expressed by activated T helper cells [153-156]. At this stage B cells can generate an extra follicular immune response where they undergo rapid transformation into plasmablasts (that give rise to short-lived plasma cells) or migrate back into the follicle where they undergo intense proliferation accompanied by the process of somatic hypermutation (SHM). SHM is regulated by the enzyme activation-induced cytidine deaminase (AID), which introduces single base-pair substitutions into the variable regions of antibody gene segments. Thus, SHM drives B cell receptor (BCR) diversification and creates a series of related clones of B cells that differ subtly in their specificity and affinity for the same antigen.

Following SHM, B cells stop proliferating and undergo the process of affinity maturation. During this process, the BCR presented on the surface of generated B cell clones interact with the antigens trapped on FDCs networks. The B cells bearing receptors with the highest affinity for the antigen are favoured for survival and can undergo further rounds of proliferation and SHM. B cell clones that do not bind antigen, or bind with very low affinity, do not receive survival signals from the FDCs and die in situ by apoptosis and are engulfed by

tingible body macrophages in the GC. FDCs have been shown to be important source of IL-6 and BAFF during the GC reaction. These signals are important for terminal differentiation process such as SHM and B cell survival respectively [153-156].

After BCR selection, B cells undergo class switch recombination (CSR), i.e. the process of isotype switching and this is also regulated by AID. The specificity of the B cell response is determined by processes of SHM and affinity maturation (mentioned above), but its effector actions is determined by CSR that helps produce the immunoglobulins isotype more appropriate for the type and the site of the immune response (eg. IgA for mucosal sites) [153-156].

GC B cells, bearing high affinity BCR, strongly express Bcl-6. This promotes their survival and it is down regulated once these cells terminate their cycles of proliferation, followed by strong expression of Blimp-1. Blimp-1 drives B cell commitment towards the plasma cell fate. GC B cells bearing intermediate-affinity BCR are committed to become memory B cells. They do not express Blimp-1 and maintain a low level of Bcl-6 expression (that is sufficient to inhibit plasma cell differentiation) [153-156].

Of note, a GC reaction is heavily dependent on CD4 T helper cells. In addition to expressing CD40L, activated T helper cells also secrete cytokines such as IL-21 and IL-4 that deliver signals to drive B-cell proliferation, survival and differentiation [153-156].

In summary, the primary function of GCs is to generate the high-affinity antibody-secreting plasma cells and memory B cells that will not only ensure sustained immune protection but also a rapid recall response against the previously encountered foreign antigens. However, the processes such as SHM during an active germinal centre reaction, carry potential risks; generation of potentially pathogenic autoantibody specificities and unintended oncogenic mutations [154, 156].

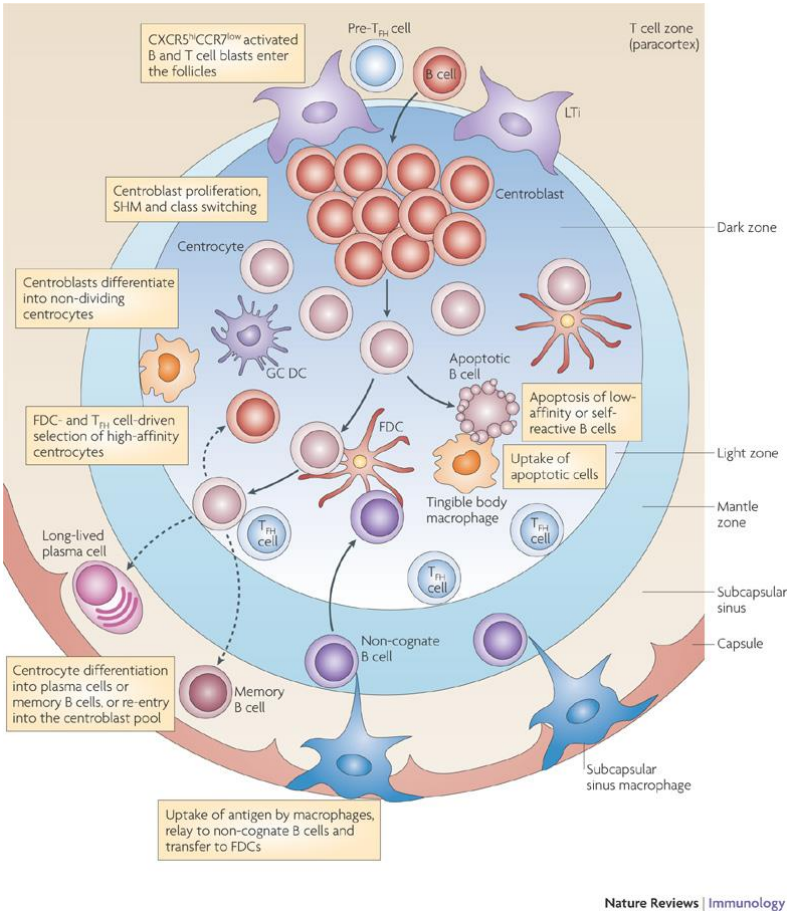

Figure 1.3B Germinal centre reaction.

A small number of activated B cells seed the follicles to grow and initiate germinal centre (GC) reactions. T follicular helper (T_{FH}) cells that have established stable interactions with B cells at the outer T cell zone also enter follicles. Proliferation of GC B cells displaces naive circulating B cells that now form the follicular mantle zone. Two zones can be identified: the dark zone and the light zone. The dark zone is full of dividing GC B cells, known as centroblasts, although some proliferating B cells can also be found in the light zone. The light zone is rich in follicular dendritic cells (FDCs) that have antigen bound on their surface. Antigen can be picked up by subcapsular sinus macrophages from the lymph and delivered to non-cognate B cells that transfer the antigen to FDCs. FDCs bind the antigen in the form of immune complexes. Dividing centroblasts acquire somatic hypermutation (SHM) in their immunoglobulin variable-region genes; their non-dividing progeny, centrocytes, are selected after a successful interaction with FDCs, uptake of antigen through the B cell receptor and presentation of this antigen to T_{FH} cells. Selection can lead to terminal differentiation into long-lived plasma cells or memory B cells or can induce centrocytes to re-enter the cell cycle and undergo further rounds of SHM. It is possible that selection signals are also received by B cells in the dark zone. Failure to receive these survival signals leads to apoptosis in situ. Apoptotic cells are cleared by tangible body macrophages (Vinuesa C.G et al., 2009 [154]).

1.4 Ectopic Lymphoid Neogenesis: The process of tertiary lymphoid organ formation

Tertiary lymphoid Organs (TLOs) are accumulations of lymphoid cells within non-lymphoid organs that share the cellular compartments, spatial organization, vasculature, chemokines and function with SLOs, especially LNs. TLOs organize into a separate T cell compartment and B cell compartment which contain germinal centres with follicular dendritic cells (FDCs). In most cases TLOs contain PNAd (Peripheral Node addressin) expressing high endothelial venules (HEVs). TLOs are also commonly referred to as ectopic lymphoid structures owing to their propensity to develop in typically non-lymphoid locations. TLOs have been described in various mouse models of inflammation (overview in Table 1.4A) and shown to be associated with a wide range of autoimmune diseases. Lymphoid neogenesis has also been documented in a few chronic infections that include Helicobactor pylori-induced gastritis where high degree of TLO organization and a large number of locally generated IgA-producing plasma cells, specific for H.pylori antigens, have been detected. TLO formation has also been reported in chronic hepatitis C virus (HCV) infection, in lyme disease and influenza A virus infection. Other than these, TLOs have been described in chronic allograft rejection, atherosclerosis, allergic lung disease and cancer (for example ectopic and functional germinal centres have been detected in breast cancer) (overview in Table 1.4B) [4, 12, 14].

Table 1.4A

Disease	Target tissue	Microarchitecture of lymphoid infiltrates	Immunological correlates
Autoimmune disease			
Autoimmune gastritis	Stomach	B-cell follicles with FDCs but rare PNA+ GCs; no CCL21+PNAD+ HEVs	Increased titre of serum gastric-mucosa-specific autoantibodies; TH1-cellbiased microenvironment
Autoimmune thyroiditis (Autoimmune-prone biobreeding (BB) rats were used in these experiments)	Thyroid gland	B-cell follicles and HEVs	Serum colloid-specific antibodies
Prediabetic NOD mice	Pancreatic islets; salivary and lacrimal glands	Lymphoid aggregates with CCL21+ stromal cells and CCL21+HEC-GlcNAc6ST+MADCAM1+ HEVs	Not determined
Collagen-induced arthritis	Joints	B-cell follicles with GL7+ GCs	Not determined
Experimental autoimmune encephalomyelitis (chronicrelapsing form)	Central nervous system	Intrameningeal B-cell follicles with FDCs and GCs	Not determined
Allergic disease			
Airway antigenic challenge	Lungs	B-cell follicles with FDCs and PNA+ GCs	IgE production
Infectious disease			
Helicobacter pylori-induced gastritis	Stomach	B-cell follicles with GCs; T-cell areas with CD62Lhi naive T cells and MADCAM1+PNAD+HEVs	Weak correlation with H. pylori-specific antibody responses
Propionibacterium acnes-induced granulomatous liver disease	Liver	B-cell follicles with FDCs without GCs; T-cell areas with PNAD+ HEVs	Not determined
Influenza A virus	Lungs	B-cell follicles with FDCs and GCs; T-cell areas with CCL21+PNAD+ HEVs	Influenza-virus-specific CD8+ T cells and antibodies
Transplantation			
Allograft rejection	Heart	B-cell follicles; T-cell areas with PNAD+ HEVs	Not determined
Ectopic expression of:			
Lymphotoxin-α	Pancreatic islets, kidneys	B-cell follicles with or without FDCs; T-cell areas with CCL21+MADCAM1+PNAD+ HEVs	Production of antibodies to foreign antigen
	Tumours		T-cell responses against tumour antigens
Lymphotoxin-αβ	Pancreatic islets	B-cell follicles with FDCs; T-cell areas with CD62Lhi naive T cells, CD11c+ DCs and CCL21+HEC-GlcNAc6ST+MADCAM1+PNAD+ HEVs	Not determined
LIGHT	Tumours	Infiltrating CD62Lhi naive T cells and CCL21+MADCAM1+ stromal cells	Intratumoral expansion and activation of tumourantigen-specific T cells
CCL19	Pancreatic islets	Non-organized B- and T-cell infiltrates; MADCAM1+PNAD+ HEVs	Not determined
CCL21	Pancreatic islets, thyroid gland	B-cell follicles without FDCs; T-cell areas with CD11c+ DCs, MADCAM1+PNAD+ HEVs and stromal cells	Not determined
CXCL12	Pancreatic islets	B-cell, plasma-cell and DC infiltrates	Not determined
CXCL13	Pancreatic islets	B-cell aggregates without FDCs; T-cell areas with stromal cells and MADCAM1+PNAD+ HEVs	Not determined

(Adapted from Aloisi 2006; Drayton 2006 [4, 14])

Table1.4A Mouse models of inflammation and transgenic mouse models accompanied by ectopic lymphoneogenesis.

Table 1.4B

Disease	Target tissue	Percentage of patients with ectopic follicles that contain CD21+ CD35+ FDCs or GCs	T-cell aggregates with CCL19+CCL21+stromal cells, DCs and HEV-like vessels	Antigen recognized by antibodies generated in ectopic GCs
Autoimmune diseases				
Rheumatoid arthritis	Diarthrodial joints	10–35%	Present; PNAD–CCL21+ blood vessels and PNAD+CCL21+HEVs	Rheumatoid factor
Hashimoto's thyroiditis (hypothyroidism)	Thyroid gland	100%	Present; HECA-452+CCL21+HEVs	Thyroglobulin, thyroperoxidase
Graves' disease (hyperthyroidism)	Thyroid gland	54–63%	Present; HECA-452+CCL21+HEVs	Thyroglobulin, thyroperoxidase
Myasthenia gravis	Thymus	Mainly patients with early-onset myasthenia gravis	Present	Nicotinic acetylcholine receptor
Sjogren's syndrome	Salivary glands	17%	Present; PNAD+CCL21+ HEVs	SSA/Ro; SSB/La
Multiple sclerosis	Central nervous system	30–40% of patients with secondary progressive multiple sclerosis	Absent	Not determined
Cryptogenic fibrosing alveolitis	Lungs	83–90%	Not determined	Not determined
Primary sclerosing cholangitis and primary biliary cirrhosis	Liver	None	Present; CCL21+MADCAM1+HEVs	Not determined
Other chronic inflammatory diseases				
Ulcerative colitis*	Gut	27%	Present; CCL21+PNAD- blood vessels	Not determined
Crohn's disease*	Gut	Not determined	Present; CCL21+PNAD- blood vessels	Not determined
Atherosclerosis	Arteries	32%	Present; HECA-452+ HEVs	Not determined
Infectious diseases				
Chronic hepatitis C	Liver	33–85%	Not determined	Not determined
Helicobacter pylori-(orCampylobacter pylori)-induced gastritis	Stomach	27–100%	Present; PNAD+ HEVs	Bacterial antigens
Chronic Lyme disease	Joints	17%	Present	Not determined
Tumours				
Ductal breast carcinoma	Breasts	33–100%	Not determined	Tumour-associated and normal breast tissue antigens

(Adapted from Aloisi 2006; Lambrecht 2012 [12, 14])

Table1.4B Human inflammatory diseases, infections and cancer with lymphoid neogenesis.

Lessons Learnt From Transgenic Models of TLO Formation

Transgenic (Tg) mouse models of chronic inflammation that over-express inflammatory cytokines, for example TNF and LTα develop TLOs [157-160]. For example, LTα over-expression in mice pancreas, under the control of rat insulin promoter (RIP), led to formation of inflammatory lesions that were organized like LNs with separate T and B cell areas, specialized stromal cells (FDC and ER-TR7+ stromal networks) and HEVs, in the pancreas and kidney of these RIP-LTα Tg mice. LTα expression in the pancreas can promote expression of lymphoid chemokines CCL21 and CXCL13 that enable T and B cell organization, germinal centres formation and isotype switching in B cells. This process is dependent on TNFR1 suggesting that signals through TNFR1, rather than LTβR, are sufficient for TLO development [157-160].

Similarly, engineered LTα expression in tumor cells has been demonstrated to lead the formation of intratumoral lymphoid tissue, able to sustain an efficient immune response, suggesting that signalling through LT and its receptors play a role in the induction of functionally competent TLOs [161]. However, the mice that expressed both LTα and LTβ in the pancreas had much larger infiltrates with better segregated T and B cell areas and higher expression of lymphoid chemokines CXCL13, CCL19 and CCL21 in the pancreatic islets than those observed in the LTα single Tg mice [4]. This suggests that the simultaneous expression of LTα and LTβ is more efficient in promoting TLO formation, and highlights distinct roles for LTα and LTαβ in lymphoid neogenesis [4].

LIGHT which is also known to signal via the LTβR, has also been implicated in formation of TLOs [23, 162, 163]. LIGHT expression has been reported in the islets of NOD mice that develop TLO and diabetes [163, 164], and LIGHT overexpression in the pancreas of NOD mice has been shown to accelerate diabetes [163, 164]. Hence, blockade of LTβR in NOD mice has been shown to disrupt organization of TLOs and prevent diabetes [164]. These studies are the first line of evidence to support the notion that lymphoid neogenesis during inflammation could involve the same signalling pathways which are involved in the

physiological development of lymphoid organs, and clearly endorse the view that expression of LTα, LTαβ and LIGHT can all contribute to formation of TLOs via signalling through TNFR1 and LTβR. [159, 165]. However, the inflammatory environment in RIP-TNFα Tg, RIP-LTα Tg and RIP-LTα/LTβ Tg mice did not lead to tissue destruction and type 1 diabetes, unless an additional co-stimulatory signal was provided in the form of B7.1 or IFNg or IL-2 co-expression in the islets, which could activate infiltrating T cells resulting in beta cell destruction [166-168].

Further studies by Cyster's group and others, addressed the role of individual chemokines in TLO formation [169-174] . Mice expressing CXCL13 in the pancreas developed TLOs that contained B and T cell zones. CD11c+ DCs were also present in the T cell area, and in most cases the T cells and DC co-localized. A dense BP-3+ stromal cell network was observed extending through most of the ectopic lymphoid structures, PNAd+ and MadCAM-1+ HEVs were also evident in these structures and remarkably, CCL21 was detectable on a subset of HEVs as well as in a dense network in the T cell-rich area. The authors further demonstrated that this phenomenon of TLO development was dependent on B cells and LTα1β2 [169]. Likewise, other studies showed that overexpression of CCL21 in non-lymphoid tissue, such as the pancreas (under the control of rat insulin promoter) [173, 174] and thyroid (under the control of thyroglobulin promoter) [170-172], is sufficient to activate a pathway of events that promote development of TLOs. Pancreatic islets of RIP-CCL21Tg mice contained infiltrates that consolidated into organized lymphoid tissues, containing T cell/DC clusters with B cells at the perimeter. gp38+, BP-3+ and ERTR7+ stromal cell networks, as well as MadCAM-1 and PNAd expression on vascular endothelium (that showed morphological resemblance to HEVs) were detected in these ectopic lymphoid structures. However, neither of the CCL21Tg mouse models showed evidence of development of CD35+ FDC or CXCL13-expressing stromal cells. Though, Chen *et al*. [174] reported occasional weak staining for FDC-M1, a marker of FDC, within B cell follicles in CCL21-induced TLOs.

Similarly, TLOs formed in the thyroid had separate T and B cell areas, as well as HEV and lymphatic vessels, surrounding the ectopic follicles. Further investigation revealed that even though HEVs expressing PNAd were frequently observed in the thyroid tissue, lymphocyte recruitment was independent of L-selectin and LTα but does require CCR7. However, the ability to form segregated lymphoid aggregates in the thyroid tissue that develop PNAd+ HEV and lymphatic vessels was dependent on LTα expression and LTβR signalling as well as on the activities of lymphocytes. Interestingly, initiation of lymphangiogenesis in this model was dependent on LT-expressing CD4 T cells rather than B cells [170-172].

Of note, CXCL13, CCL21, CCL19 and CXCL12 are not equal in their ability to promote TLO neogenesis. Overexpression of CCL19 or CXCL12 is not able to induce fully mature aggregates. Possibly this is related to their differential ability to promote LTαβ expression on lymphocytes. CXCL13 has been shown to trigger LTαβ expression on B cells, while CCL21, and to lesser extent CCL19 but not CXCL12, promotes LTαβ expression on CD4 T cells [175]. Interestingly, in particular for human pathology, cytokines such as IL-7 and IL-4 have been shown to be able to induce LTαβ expression on naïve T [175]. In this context Tg co-expression of IL-6 and IL-6R under the Class I and β-actin promoters, as well as IL-5 overexpression has been shown to induce the formation of iBALT in the lung [176]. Not in all cases the transgene induced TLO formation is accompanied by pathology [13].

Lymphoid Neogenesis in Experimental Disease Models and Human Disease

More direct evidence for the cellular and molecular mechanisms in TLO ontogeny is derived from immunohistochemical and gene expression analysis of patient tissue specimens (such as salivary glands from Sjogren's patient and synovium of rheumatoid arthritis patients), as well as experimental disease models (for example NOD mice). Increased expression of lymphoid chemokines (CXCL13, CCL21, CCL19 and CXCL12), LTα, LTβand PNAd+ and/or MadCAM-1+ HEVs have been reported in most of the chronically inflamed tissues that harbour TLOs. Remarkably, a correlation between the expression of LTα/LTβ and/or lymphoid chemokines and lymphoid organization has been observed in experimental disease

mouse models and human autoimmune lesions, which supports a causative involvement of these mediators in TLO formation [12-14, 177-183].

Features of ectopic lymphoid neogenesis have also been detected in animal models of autoimmunity, such as insulitis that spontaneously develops in non-obese diabetic (NOD) mice, with most organized structures generally being associated with the chronic disease phases. Astorri *et al*. have recently demonstrated in the pancreas of NOD mice that TLOs are critical in promoting chronic inflammation during autoimmune insulitis and diabetes. They showed that T and B cell infiltration follows a highly regulated process with the formation of lymphoid aggregates characterized by T/B cell segregation, follicular dendritic cell networks, and differentiation of germinal center B cells during progression from peri- to intrainsulitis in early diabetic mice. This process is preceded by local upregulation of lymphotoxins alpha/beta and lymphoid chemokines CXCL13 and CCL19. Upon development, TLOs were fully functional in supporting autoreactive B cell differentiation *in situ*, indicated by the expression of activation-induced cytidine deaminase, the enzyme required for B-cell affinity maturation and class switching, and the presence of plasma cells displaying anti-insulin reactivity [181].

Increased size and organization of TLOs in various autoimmune tissues have been shown to correlate with increased local expression of homoeostatic cytokines and chemokines including LTα, LTβ, CXCL13, CCL21 [13, 14, 160, 179, 180, 183-186] and CXCL12 [13, 14, 160, 186, 187]. Although different patterns of lymphoid arrangements usually coexist in the same patient tissues, tissues with highly organized ectopic lymphoid follicles tend to express much higher levels of LTα, CXCL13 and CCL21 than those with diffuse lymphoid infiltrates [13, 14, 160, 179, 180, 182, 184, 186, 188]**.** In fact, the expression levels of CXCL13 and LTβ has been suggested to be highly predictive of the presence of ectopic GC in synovial biopsies of patients with RA. The expression of CXCL13 also correlates with the presence of highly organized B cell follicles in patients with Sjogren's syndrome [13, 14, 177, 180, 188]. Expression of CXCL13 and BAFF were shown to be increased with meninges associated

ectopic GC formation in a mouse model of CNS inflammation [189]. In a spontaneous mouse model of autoimmune gastritis, CXCL13 and LTβ were highly expressed in the ectopic lymphoid follicles that develop in the stomach of these mice. The number and size of these follicles correlated with the serum autoantibody titre [190]. Formation of TLOs has also been documented in Helicobacter pylori-induced gastritis, which is dependent on the CXCL13/CXCR5 signalling axis since these structures fail to form in CXCR5-/- mice [191]. In fact Wegner *et al*. demonstrated in a mice model of chronic antigen-induced arthritis that the development and organization of TLOs was impaired in absence of CXCR5 and CCR7 [192].

Apart from autoimmune and infectious diseases, TLO formation has also been reported in other diseases such as atherosclerosis and allergic lung disease. LTβR signalling was demonstrated to promote the adventitial aortic tertiary lymphoid organs (ATLOs) and interruption of this signalling axis achieved by administering LTβR-Ig fusion protein to a mouse model of ATLO, strongly reduced CXCL13 and CCL21 expression and HEV structures and disrupted the structure and maintenance of ATLOs in these mice [193]. LTβR-Ig administration in other mouse model such as NOD mice also resulted in disruption of TLOs [163].

The ability of local TLOs to locally produce antibodies is still debated. Highly organised TLOs are characterised by FDC expression, that associate with the expression of AID (activation induced cytidine deaminase), enzyme important for B-cell somatic mutation and isotype class switching, and have been detected in the TLOs [194]. Accordingly, analysis of the DNA sequence analysis of synovial isolated germinal centre B cells demonstrated a restricted number of heavy and light chain rearrangements, consistent with oligoclonal B cell expansion in the inflamed synovial tissue [195, 196]. Furthermore, demonstration that these cells undergo somatic hypermutation in the Ig variable regions *in situ* has been provided [196]. A similar phenomenon of oligoclonal B cell expansion and somatic hypermutation of Ig variable genes have also been demonstrated within the TLOs that form in the salivary glands of

patients with SS, in the thymus of patients with myasthenia gravis and in the CSF of multiple sclerosis patients [4, 14, 197-201].

Finally, plasma cell-derived autoantibodies have been detected in TLO associated GC in rheumatoid arthritis, Hashimoto thyroiditis and Sjogren's syndrome, as well as plasma cells secreting anti-SRBC antibodies in RIP-LTα Tg mice kidneys after SRBC immunization [159, 202]. Likewise, large numbers of locally generated IgA-producing plasma cells specific for H.pylori antigens have been detected in Helicobacter pylori-induced TLOs. In some studies, a correlation has been found between autoantibody serum levels and ectopic GCs which has raised the possibility that TLOs contribute to the disease process [14, 178, 190, 203-206]. However, it remains unclear whether plasma cells actually develop in TLOs or migrate from canonical SLOs. Nonetheless, all these studies in several human diseases and animal models collectively suggest that TLOs can support germinal centre reaction characterized by somatic hypermutation of Ig variable genes, affinity maturation, isotype switching and terminal differentiation of B cells differentiation into plasma cells.

T cell priming and epitope spreading have been shown to occur in TLOs formed in the brain of experimental models. Reactivity to CNS antigens has been observed [207] as well as proliferation of adoptively transferred T cells only in the CNS but not in the draining LN [207]. In addition, there is another study which has reported presence of restricted T cell repertoire in tumor-associated TLOs suggesting that naïve T cell priming can occur within TLOs [161].

There has been a long-standing conundrum surrounding the functionality of ectopic GCs to mount and sustain local immune responses. This question has been elegantly addressed by Moyron-Quiroz *et al*. [76] in spleen-, lymph node-, Peyer's patch-deficient (SLP) mice, in which iBALT (inducible bronchus-associated lymphoid tissue) formed in the lung of SLP mice upon influenza virus infection were able to generate a robust primary T and B cell responses to influenza, and clear influenza infection. The investigators found the generation of influenza-specific CD8α T cells in these iBALT structures. Additionally GL7+PNA+ GC B cells

were detected in iBALT and they were shown to support production of influenza specific antibodies. Interestingly, these mice were able to survive higher doses of virus compared to wild-type mice [76]. Likewise, another study using SLO deficient mice provided evidence that TLOs formed at the site of allografts post-transplantation were able to generate effector and memory T cells from transferred naïve T cells, which lead to allograft rejection in these mice [208].

TLOs and their potential role in tumors

Various studies have reported lymphoid neogenesis at tumor sites. Schrama *et al.* and Yu *et al.* have shown that induction of TLOs at the site of tumors results in regression of the tumor. Moreover, analysis of T cell within these TLOs revealed presence of tumor-specific T cells and these T cells exhibited enhanced proliferation activity. Both these studies suggested that TLOs may be beneficial for local presentation of tumor antigens and induction of anti-tumor immunity [161] [209]. On the contrary, TLOs have also been demonstrated to promote tumor formation and metastasis. For example in some chronic inflammatory diseases, such as Hashimoto thyroiditis and SS, TLOs have been indicated to provide local molecular environment to support continual B cell proliferation which results in development of lymphomas in these diseases [160, 194]. Similarly, in hepatitis C virus infection and Helicobacter pylori infection, chronic inflammation has been reported to lead to progression of TLO into cancer [210, 211].

Role of LTi cells in TLO formation

The role of LTi cells in the formation of TLO is still controversial. Adoptive transfer of LTi cells to ectopic sites, such as skin in neonatal mice, triggers TLO development [212]. Similarly, Tg overexpression of IL-7 which results in abnormally high number of LTi cells in these mice form TLOs in the pancreas and salivary glands. Interestingly, when IL-7 transgenic mice are crossed with RORγ-/- mice, which lack LTi, these mice do not develop any SLOs (LNs and PPs) or TLOs. Thus, in this model, IL-7 by itself is not sufficient to drive development of these ectopic lymphoid tissues, but in fact requires LTi cells [62]. Furthermore, in transgenic

mice, that overexpress CXCL13 in the pancreas, CD4+CD3- cells are the first hematopoietic cell type recruited to the pancreatic islets very early after birth, suggesting that LTi cells may be involved in formation of the TLO that eventually develop in this location [169, 213]. However, in these models, lymphoid neogenesis is triggered before birth or at the neonatal stage and not in the adult, which means that the requirement of LTi cells could be overestimated. It therefore remains unclear from these studies whether this is due to a coincidence in timing or due to a causal relationship of LTi and TLO development. This notion is further supported in an adoptive transfer study, where adoptive transfer of LTi into the skin of adult mice results in disorganized accumulations of lymphocytes with no FDC and HEVs [212]. However, there are some human TLOs, such as those seen in idiopathic pulmonary arterial hypertension (IPAH), where RORc+CD4-cKit+ LTi have been detected [12].

Id2-/- or RORγt-/- mice, which lack LTi cells, when infected with influenza virus or exposed to LPS, develop normal iBALT structures in the lung [76, 214, 215]. Similarly, another study demonstrated development of TLOs in colon of RORγt-/-mice [216]. Studies using mice that express CCL21 in the thyroid suggested that LTi cells are not required for TLO neogenesis, instead, in this model, CD3+CD4+ T cells were the first cell to appear in the thyroid and interact with local DCs. This subsequently leads to production of homoeostatic and inflammatory chemokines, recruitment of lymphocytes and DCs which organize into lymphoid structures with appearance of PNAd+ HEV like vessels. Importantly, when CCL21 transgenic mice were crossed with Id2-/- mice, they still formed TLOs in the thyroid despite absence of LTi cells [217]. This suggests that the formation of TLOs does not require Id2-dependent LTi cells but depends on program initiated by mature CD4+T cells. During chronic inflammation, within TLOs, the presence of inflammatory lymphocytes that are able to express LTαβ is likely to compensate for the lack of LTi. [36, 217] [218-220]. Finally, the role of DCs has been highlighted in TLO development. DC might contribute to this by providing antigen presentation to the T cells or directly providing LTβ and lymphoid chemokines CXCL13 and

CCL21/CCL19. Hence, depletion of DCs result in disappearance of existing TLO structures [218-220].

Stromal cells in Ectopic Lymphoneogenesis

It is believed that stromal cells, in particular fibroblasts, contribute to the microenvironment in chronic inflammation, by providing pro-survival and retention signals via production of factors, such as B cell survival factors (BAFF) and the inflammatory chemokines (e.g., IL-8, CCL5, CXCL1). Pathogenic tissue fibroblasts play, not only a key role in immune cell recruitment to the site of inflammation, but have also been implicated in the formation of organized aggregation of infiltrating immune cells (TLOs) at these sites by virtue of their capability to produce lymphoid chemokines CXCL12, CCL21 and CXCL13 [221-223].

The central role of stromal cells in the development of TLOs was shown by intradermal injections of cell suspensions obtained from the neonatal LNs. These injections resulted in ectopic LN like structure formation and the cells that were of donor origin within these structures turned out to be stromal cells, which not only demonstrated the capacity to attract and retain host- derived T and B lymphocytes, but organize themselves into distinctive micro-domains [212]. The central role of stromal cells for TLO formation is further supported by studies in which artificial LNs were created by implantation of stromal cell scaffolds under the kidney capsule. These structures were shown to attract cells that are present in a normal LN and organize them in distinctive B and T cell areas, which support bona fide immune responses [126, 224]. Thus, these studies indicate an overriding capacity of stromal cells to contribute to TLO development and predict stromal cells pivotal role in the formation of ectopic lymphoid structures that develop during chronic inflammation. Indeed, in a model of atherosclerosis which develops adventitial aortic tertiary lymphoid organs (ATLOs), the investigators showed that the mouse aorta smooth muscle cells (SMC) were activated and acquired features of LTo cells, such as expression of VCAM-1 and lymphorganogenic chemokines CXCL13 and CCL21, that supported formation of ATLOs [193]. Signalling through both LTβR and TNFR1 was shown to activate SMCs [225]. Once established, the

ATLOs could be disrupted by LTβR blockade in vivo [193]. Likewise, Peduto *et al.*, [226] elegantly demonstrated that local resident fibroblasts give rise to LTo-like cells in experimental models of cancer and local inflammation by mechanical and inflammatory stimuli. Intriguingly, the induction of LTo like cells was shown to be independent of TLR or TNF signalling, but most probably linked to the presence of polymorphonucleated cells in the first phases of the inflammatory process. gp38, marker of lymph node stromal cell, was used to identify and isolate these LTo-like stromal cells that acquire during inflammation the capability to express genes essential in lymphoid tissue genesis and in the recruitment and survival of leukocytes. The gp38+LTo like cells expressed elevated levels of IL-7, CXCL13, CCL19, CCL21, CXCL12, TRANCE, VCAM-1, BP-3, etc [226].

Reticular networks of ER-TR7+, podoplanin+ and BP-3+ stromal cells have also been observed in pancreatic infiltrates of RIP-CXCL13, RIP-LTα/LTβ Tg and NOD mice [213] [159, 169, 227] and other refs). These cells, like lymphoid stromal cells, expressed LTβR, VCAM-1, CCL19, CCL21 and IL-7 and have been suggested to differentiate from tissue-resident myofibroblasts [213]. Additionally, podoplanin+ stromal networks, co-localizing with lymphoid chemokines such as CCL21, CCL19, have been detected in ectopic infiltrates associated with human diseases such as rheumatoid arthritis [179, 228] and Sjogren's syndrome [213]. Moreover, numerous reports in mice models and human diseases have documented the presence of CD35+/FDC-M1+ FDCs networks within B-cell areas of TLOs. Like their SLO counterparts these FDCs are also associated with CXCL13 expression [229] Recently, Krautler *et al*., showed that PDGFRβ^{+} stromal-vascular cells from non-lymphoid organs have the capacity to differentiate into FDCs upon LTβR and TNF triggering, suggesting that this cell population may be the source of FDC in TLOs. Moreover, this study further reiterates the capability of non-lymphoid tissue-resident stromal to undergo lymphoid conversion [147].

Altogether, these observations suggest that the stromal cells in inflammation recapitulate the ontogeny of lymphoid stromal cells, which lays the foundation for the development of TLOs, by providing factors and signals critical for lymphoid neogenesis.

TLO development does not necessarily copy secondary lymphoid organogensis

The similarities between SLO and TLOs, in terms of structure and to an extent function as well as insights from mouse and human studies, suggest that SLO and TLO development might employ similar pathways. However, studies from some groups have challenged this paradigm. Randall's group in 2011 proposed the idea that inflammatory cytokines such as IL-17 could initiate TLO formation using a mouse model of iBALT formation. The study demonstrated that the formation of iBALT did not require LTi and lymphotoxin mediated signals; instead it was dependent on IL-17 produced by CD4+ T cells, indicated by failure to form iBALT structures in the lungs of IL-17Rα-/- and IL-17-/- mice. More surprising was the finding that IL-17, in addition to its ability to induce expression of inflammatory chemokines, such as CXCL10, CXCL11 and CXCL9 (which in turn recruit inflammatory cells at the effector site), could also directly stimulate the expression of CXCL13 and CCL21 in stromal cells [214]. This observation explained their previous finding in 2004, which had shown that expression of homeostatic chemokines expressed within iBALT in lungs of influenza infected mice was independent of LTα and TNFα mediated signals [76]. Even though induction of iBALT was independent of lymphotoxin signalling, it was crucial for maintenance and organization of these structures in the infected lung tissues, as these lymphoid structures were highly disrupted in LTα-/- mice [214]. Supporting a role for IL-17 in TLO formation, Kuchroo's group showed that Th17 cells specifically induced ectopic lymphoid follicles in the CNS, in the experimental autoimmune encephalomyelitis (EAE) mouse model. Intriguingly, the Th17 cell signature cytokine IL-17 and cell surface molecule podoplanin (expressed on CNS infiltrating Th17 cells) directly contributed to TLO formation in this model, as the lymphoid follicle were significantly reduced in IL-17Rα-deficient mice, and inhibition of podoplanin with blocking antibody also partially inhibited the formation of these ectopic lymphoid follicles [230].

Overall, these recent studies propose an interesting possibility that ectopic organogenesis can be driven by inflammatory cytokines rather than constitutive lymphoid cytokines. This

opens a new perspective to understand the role of stromal cells and cytokine signalling pathways involved in TLO formation.

Figure 1.4A

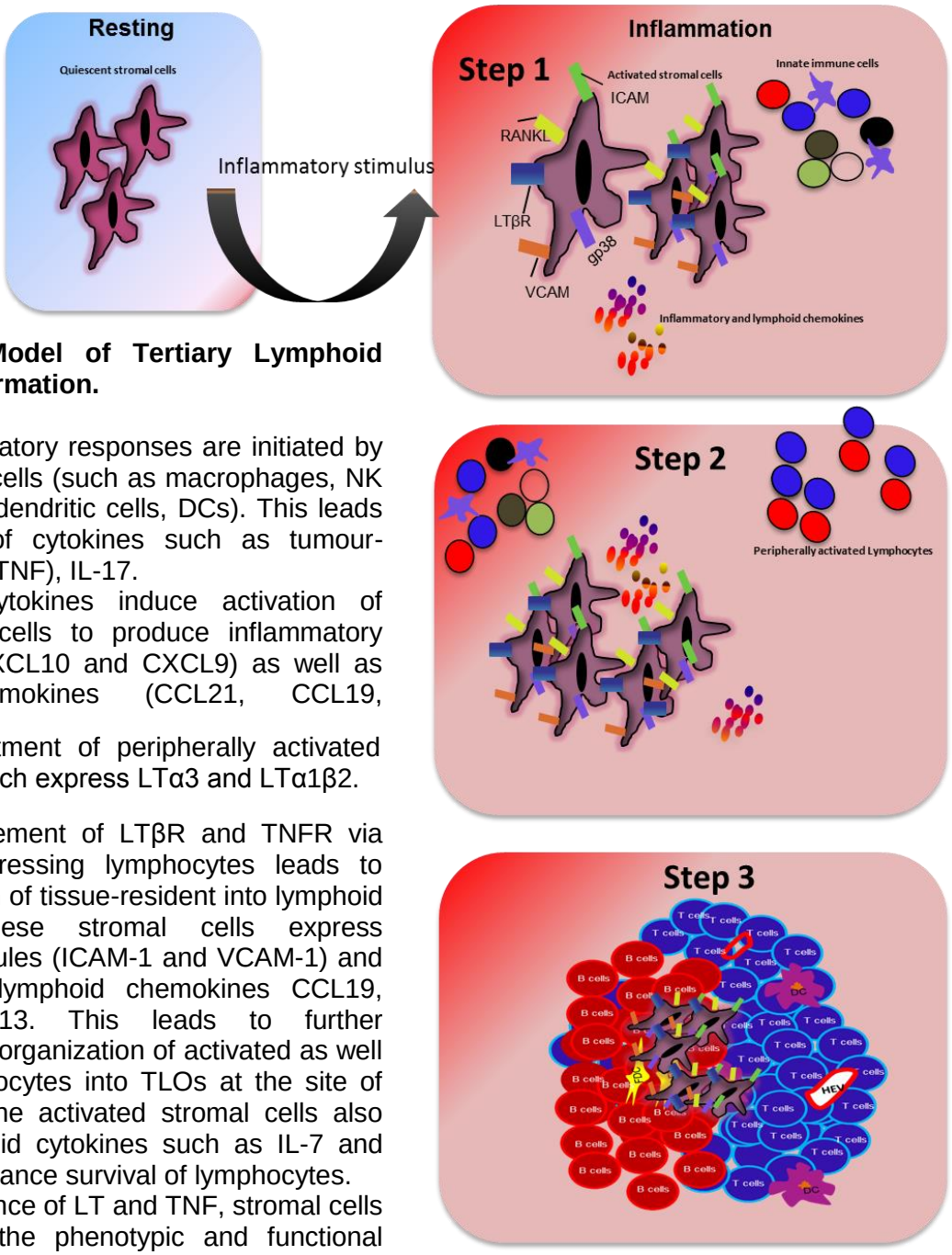

Figure 1.4A Model of Tertiary Lymphoid Organ (TLO) formation.

Step 1. Inflammatory responses are initiated by innate immune cells (such as macrophages, NK cells, ILCs and dendritic cells, DCs). This leads to production of cytokines such as tumour-necrosis factor (TNF), IL-17.
Inflammatory cytokines induce activation of tissue stromal cells to produce inflammatory chemokines (CXCL10 and CXCL9) as well as lymphoid chemokines (CCL21, CCL19,

Step 2. Recruitment of peripherally activated lymphocytes which express LTα3 and LTα1β2.

Step 3. Engagement of LTβR and TNFR via lymphotoxin-expressing lymphocytes leads to further activation of tissue-resident into lymphoid phenotype. These stromal cells express adhesion molecules (ICAM-1 and VCAM-1) and expression of lymphoid chemokines CCL19, CCL21, CXCL13. This leads to further recruitment and organization of activated as well as naïve lymphocytes into TLOs at the site of inflammation. The activated stromal cells also produce lymphoid cytokines such as IL-7 and BAFF which enhance survival of lymphocytes.
Under the influence of LT and TNF, stromal cells would acquire the phenotypic and functional properties of FDCs, including CXCL13 production, which promote germinal-centre organization. Cytokines that mediate lymphocyte survival, differentiation and/or proliferation, such as BAFF, IL-2-family members (IL-2, IL-4, IL-7, IL-15 and IL-21) and IL-6, might contribute, together with antigen, to establish optimal niches for germinal centre reaction.

(Adapted from [4, 12, 14, 76, 154, 157, 160, 165, 169, 171, 173-175, 180, 181, 183, 185, 188, 193, 194, 214, 216, 217, 220, 226, 227, 230-235].

1.5 Sjogren's syndrome: An illustration of ectopic lymphoneogenesis in inflammation, infection and cancer

Sjogren's Syndrome (SS) is a chronic inflammatory disease that primarily affects the exocrine glands (particularly salivary and lacrimal glands) and leads to their functional impairment. SS occurs either independently as a primary disease or as a secondary manifestation to other rheumatic diseases, most commonly rheumatoid arthritis [23-25]. Primary SS is a common autoimmune disease, affecting 0.1-0.4% of general population, and is more prevalent in females with a female to male ratio of 9:1. Being commonly affected and easily accessible, salivary glands are the most studied exocrine glands in SS. SS is an intriguing example of an immune mediated inflammatory disease in which there is evidence of an antigen driven immune response to infection, autoimmunity and development of cancer [18, 23-25].

Pathology

SS is characterized by peri-epithelial mononuclear cell infiltration of exocrine glands. Histopathologically, these are focal aggregates of at least 50 lymphocytes, plasma cells and macrophages that surround the ducts and subsequently replace the acini which are the secretory units leading to sicca symptoms of dry eyes and dry mouth (typical clinical manifestations studied in patients with SS). There is progressive acquisition of lymphoid features by salivary gland inflammatory aggregates observed in patients of Sjogren's syndrome. Within the inflammatory foci the presence of T/B cell segregation, formation of follicular dendritic cell networks within the germinal centres (GC) [178, 180] and local expression of AID (activation induced cytidine deaminase), the enzyme, instrumental for B cell affinity maturation, has been demonstrated [194].

Salivary gland lymphoid organization is accompanied by the ectopic production of the chemokines (CKs) CXCL13, CCL21 and CXCL12. The cellular localization of these molecules is mostly consistent with that observed in B- and T-cell areas of SLOs. Such pathological lesions are indicative of chronic lymphocytic sialadenitis [177, 180, 183, 231].

Moreover, deregulated B-cell hyperactivity, expressed by the presence of anti-SSA and anti-SSB autoantibodies, hypergammaglobulinemia and cryoglobulinemia, is a common finding in SS patients. Other autoantibodies found in 50% of SS patients include autoantibodies against muscarinic M3 receptors that can induce decreased secretory function. This category is associated with increased morbidity and risk for lymphoma development [24, 25]. The expression of lymphoid chemokines significantly increases, together with the production of B cell survival factors, in patients with SS as they develop Mucosal Associated Lymphoid Tissue (MALT) lymphoma [18, 236].

Sjogren's Syndrome: Genetic factors

The high incidence of autoimmune diseases in families of patients with SS is supportive of a genetic predilection to the disease. Alleles of HLA-DR and HLA-DQ, which are a region within the major histocompatibility complex (MHC) class II gene, are implicated in the pathogenesis of SS. Patients of diverse ethnic origin that carry different HLA susceptibility alleles. Patients from North America and from Northern and Western Europe show a high prevalence of B8, DRw52 and DR3 genes whereas Greek and Scandinavian patients with SS display strong linkages to the DR5 and DR2 genes. However, it has been shown that these HLA class II alleles are associated with the presence of specific subtypes of autoantibodies rather than the disease itself. For instance, presence of the MHC class II alleles DRB1*0301, DRB1*0201 and DRB1*0501 is linked with production of anti-Ro52 autoantibodies [23, 24, 26].

Genome-wide association studies (GWAS) in patients with SS have highlighted several other gene polymorphisms of genes outside the HLA locus. These include IRF5 and STAT4, pivotal genes that encode transcription factors involved in IFN pathways. One study has confirmed the genetic association of IRF5 rs2004640 T allele with predisposition to develop SS and in another study it revealed a correlation between development of SS and in SNP rs10488631 within IRF5 gene and SNP rs7582694 within STAT4 gene. Moreover, studies at

both glandular and systemic levels have demonstrated the presence of type1 IFN and IFN-producing cells in salivary glands of patients with SS, activation of IFN pathways in PBMCs of these patients. Furthermore, the IFN signature is enhanced in patients with autoantibodies and suggests a relationship between IFN pathways and B-cell activation. Overall, these findings suggest that a genetic susceptibility favouring a higher interferon (IFN) response to different stimuli (classically stimulated by infectious agents such a viruses) could be a key event in the onset of the disease [23, 24, 26].

Sjogren's Syndrome: Hormonal factors

SS is predominantly observed in postmenopausal women, and moreover, results from several experimental mouse models have indicated a role for estrogen deficiency in SS. Mice, that lack aromatase and therefore have deficiency in estrogen, develop a lymphoproliferative disease that resembles SS. In another mouse model, overexpression of retinoblastoma-associated protein 48 (also known as histone binding protein RBBP4) in the exocrine glands, induced estrogen-deficiency-dependent apoptosis which resulted in an age-dependent SS-like autoimmune exocrinopathy. Further analysis revealed that the salivary gland epithelial cells in these transgenic mice functioned as antigen-presenting cells that directly up-regulated MHC class II molecules expression, secreted IL-18 and IFNγ and hence led to CD4+ T cell activation and glandular inflammation. These findings strongly indicate that estrogen deficiency could stimulate epithelial cells via up-regulation of RBBF4, to present an autoantigen to T cells in order to perpetuate disease pathogenesis and induce lesions observed in SS [23-25].

Infection and Sjogren's Syndrome

A number of infectious agents have been implicated in the initiation and pathogenesis of SS. Diseases and pathogens that may drive SS include tuberculosis, leprosy, hepatitis C, dengue fever, malaria, subacute bacterial endocarditis, HIV, infections by parvovirus B19 and spirochetes. Certain viruses display tropism for lacrimal and salivary glandular tissue,

especially the Herpesviridae family, which is a large family of DNA viruses that include Epstein-Barr virus (EBV), cytomegalovirus (CMV) and human herpes virus (HHV). Furthermore, several serological, epidemiological and experimental pieces of evidence incriminate retroviral infections- especially human T-lymphotropic virus type 1 (HTLV-1), HIV and human retrovirus-5 (HRV-5) - as triggering factors for the development of SS. Although a number of viruses have been implicated in SS, the evidence is circumstantial and not conclusive in regard to their exact role in the disease. It has been suggested that cryptic antigens displayed on the cellular surface of the glandular epithelium upon virus-mediated infection in the association with the aberrant class II MHC expression, by same epithelial cells, play a key role favouring the activation of self-reacting lymphocytes and perpetuating the inflammatory process. The presence of molecular memory between viral antigens and self-epitopes has been widely supported [23, 24, 26, 28].

1.6 Cannulation model of salivary gland inflammation

To address the aims and objectives of this thesis we will validate and utilize a new transient mice model of salivary gland inflammation established in Prof. Pitzalis's lab by Dr. Francesca Barone and Dr Michele Bombardieri. In this mice model we can induce salivary gland inflammation in wild-type animals, in response to selective submandibular gland administration of a replication-defective adenovirus 5 (AdV5) [237]. The replication deficient AdV5, encoding for the firefly luciferase gene (LucAdV) is administered into the submandibular salivary glands using customised glass cannulae via the excretory duct. Using this technique of cannulation preliminary experiments showed that increasing luciferase activity was observed using increasing doses of LucAdV within the first week post-cannulation (p.c.), which then decreased over the next two weeks (Fig 1.6.1). Histological analysis of the cannulated glands demonstrated that AdV doses of 10^8 pfu per gland, but not vehicle control (or doses <10^7 pfu, data not shown), induced the formation of periductal inflammatory infiltrates organized as TLOs (Fig 1.6.2), similar to human SS, with evidence of ectopic expression of lymphoid chemokines and functional B cell activation, that spontaneously resolves with virus clearance. Importantly, not only AdV5 infection reproduces the phenotypic features of SS, but also functionally leads to the development of humoral autoimmunity to nuclear antigens and decrease in salivary flow [237]. Thus, this novel model offers the unique possibility to dissect the cellular and molecular mechanisms regulating TLO formation during inflammation.

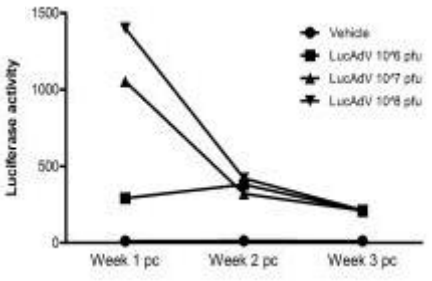

Figure 1.6.1 Representative dose-response time-course experiments of luciferase activity following delivery of LucAdV at 10^6, 10^7 and 10^8pfu/gland and vehicle control showing dose-dependent enzymatic activity within the first week. Dose dependency is lost at week 2 and 3 despite persistent transgene expression.

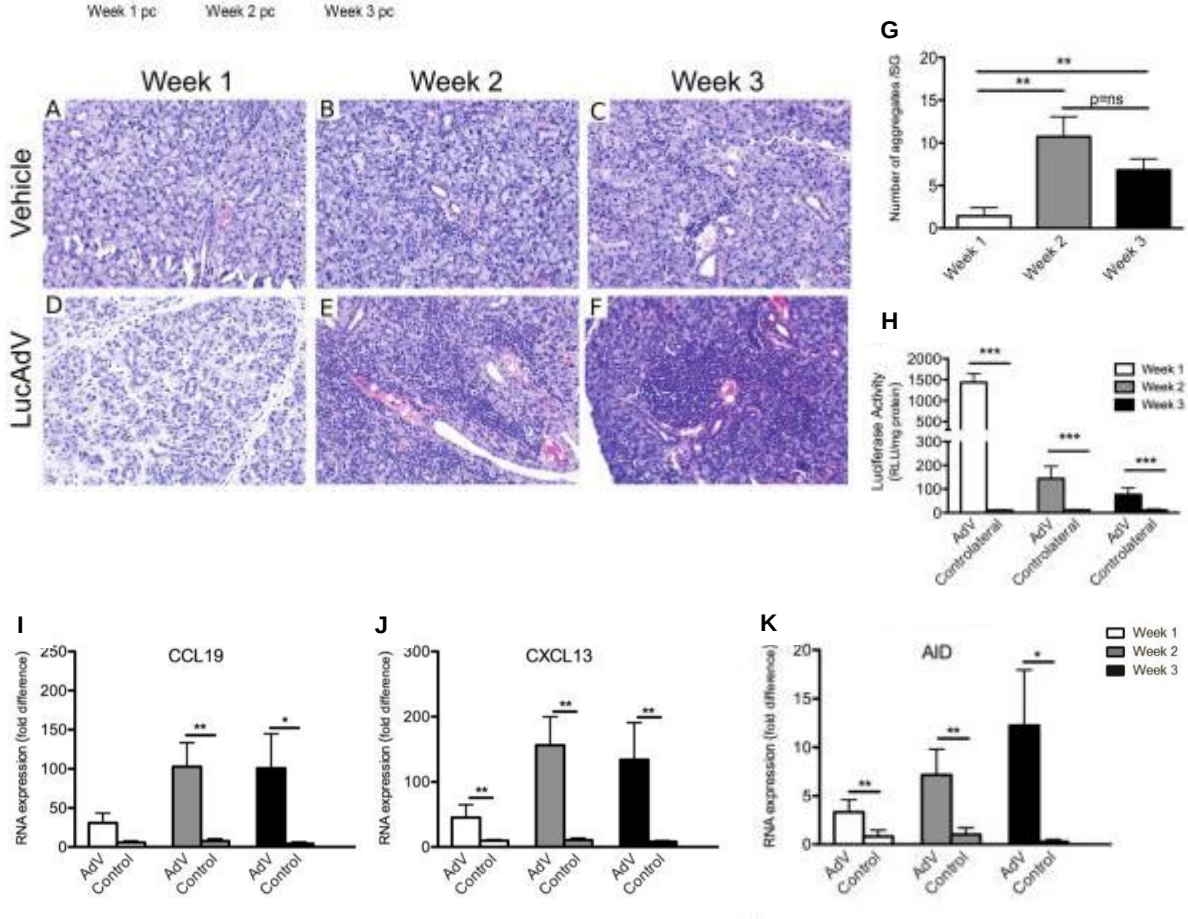

Figure 1.6.2 Representative microphotographs showing inflammatory responses induced by local administration of either vehicle **(A-C)**, LucAdV **(D-F)**. After AdV delivery, diffuse lymphomonocytic infiltration in the first week **(D)** is followed by progressive organization of periductal inflammatory aggregates during week 2 **(E)** and week 3 pc **(F)**. Vehicle delivery induces negligible inflammation **(A-C)**.

The mean ± SEM of the number of periductal foci/gland following LucAdV delivery at different time points is reported in **G**. (**p<0.01 between AdV and vehicle-treated mice at each time point, minimum of 10 mice per time point).

High sensitivity luciferase activity assay in LucAdV-infected glands shows persistent signal well above background levels up to three weeks pc (**K,** mean ± SEM of luciferase activity. Original magnification in A-F x100. (***p<0.001 between AdV-treated and vehicle-treated mice at each time point, minimum of 10 mice per time point).

Quantitative TaqMan real-time PCR time-course analysis of CCL19 **(I)** CXCL13 **(J)**, and AID **(K)** mRNA transcripts showing abundant up-regulation following AdV-delivery in the submandibular glands. Data are expressed as mean ± SEM of the fold-increase compared to an internal calibrator. (*p<0.05, **p<0.01 and ***p<0.001 between AdV-treated and vehicle-treated mice at each time point, minimum of 10 mice per time point).

1.7 Aims and Objectives of Thesis

Lymphoid stromal cell activation and maturation is crucial for the development of SLOs. Stromal cells not only provide the structural framework for immune cells to mount an effective immune response but they also actively direct the course of the inflammatory process that takes place within SLOs.

The formation of tertiary lymphoid organs (TLOs), defined as aggregates of lymphoid cells, developing ectopically in non-lymphoid locations, characterized by B/T cell segregation, differentiation of high endothelial venules (HEV), and development of follicular dendritic cells (FDC) networks, supporting a germinal centre response, is a common histological feature associated with autoimmunity, chronic inflammation and cancer [14]. This ectopic lymphoid organization of immune cells is accompanied by the production of lymphoid chemokines and cytokines, responsible for leukocyte organization and survival. Interestingly, many of these factors detected within lymphoid structures are derived from non-hematopoietic stromal cells [222]. This suggests that stromal cell activation is critically important for the maintenance and organization of tertiary lymphoid organs in inflammatory conditions.

However, relatively little is known about the structure and function of stromal cells in TLOs. gp38 or podoplanin expressed on stromal cells in secondary lymphoid organs has recently been utilized to identify and isolate activated stromal cells at sites of transient inflammation, autoimmunity and cancer. These gp38+ stromal cells secrete and bind soluble factors similar to their lymhoid organ counterparts suggesting that inflammation " recapitulates the ontegeny of lymphoid stromal cells" [226]. Of late, effector cytokines such as IL-17 have been shown to directly stimulate the expression of lymphoid chemokines in stromal cells at sites of TLO formation [214]. Nonetheless, the signals that drive the aquisition of a lymphoid phenotype by tissue-resident stromal cells, and differences in the degree of stromal cell activation during TLO compared to SLO formation, remain contentious.

Hypothesis

Stromal cells, at the site of TLO development during an inflammatory process, undergo dramatic changes in order to acquire phenotypic and functional features that resemble lymphoid stromal cells. **We propose that distinct signals are involved in the induction, proliferation and maintenance of these lymphoid like stromal cells in a dynamic model of TLO formation.**

Aims of the thesis

1. To examine the dynamic changes occurring in the stromal component during TLO formation in a resolving model of salivary gland inflammation.
2. Identify signal/s that regulate(s) lymphoid stromal cell activation at different phases of the inflammatory process using knockout and cytokine blocking strategy.

Plan of Investigation

We planned to perform the following set of experiments:

- Validation of the model of TLO formation during salivary gland inflammation by adenoviral cannulation and identification of the different stages of the inflammatory process in a detailed time course analysis.
- Phenotypical and functional characterization of lymphoid stromal cells in inflamed salivary glands at different phases of the inflammatory process, by using immunofluorescence (IF), flow cytometry and quantitative RT-PCR in tissue isolated from WT, KO and mice challenged with blocking agents.
- Phenotypical and functional analysis of the effect of lymphocyte interactions on stromal cell induction, maturation and maintenance by using KO mice for lymphocyte, lymphocyte-derived factors or blocking antibody experiments.

Chapter 2
Materials and Methods

2.1 Mice

il4rαko [238], *il4ko* [239], *il13ko* [240], *il22ko* (generated at Lexicon Genetics in collaboration with Pfizer, Boston), *il22rαko (*sourced from EMMA (European Mouse Mutant Archive) Sanger Center, UK*), rorγko* [33], *ltβrko* [22], *ragko* [241] , *cd3ε*^{tg26} [242] and *b-cell knockout (ko)* mice (generated from breeding out the QM IgH transgene from QM mice, which have the other IgH locus inactivated) [243, 244], were bred in the Biomedical Service Unit (BMSU) at the University of Birmingham. *c57bl/6* mice were from external supplier Harlan and *balb/c* mice were from an internal colony of BMSU. All mice were maintained under specific pathogen-free conditions in the Biomedical Service Unit at the University of Birmingham according to Home Office and local ethics committee regulations. All mice used were 8-12 weeks old.

il13gfp bone-marrow chimera experiments were performed at University of York in collaboration with Dr. Mark Coles. *c57bl/6* mice were irradiated with two doses of 475 rad and were reconstituted with bone-marrow cells from *il13gfp* mice [245]. The *il13gfp* mice had the il13 gene locus replaced (knocked-in) with the *gfp* gene [245], and therefore, these mice not only help track il13 producing cells but also serve as *il13ko* mice. All il13gfp bone-marrow chimera mice were maintained under specific pathogen-free conditions in the Biomedical Service Unit at the University of York according to Home Office and local ethics committee regulations.

2.2 Virus preparation and salivary gland cannulation

Concentrated stocks of E1-E3 replication-deficient human AdV5 (adenovirus serotype 5) encoding for firefly luciferase (LucAdV) (obtained from our collaborator Dr. Michele Bombardieri at Queen Mary University of London [237], were used to produce bulk amount of viral particles. Hek293 cells were infected with the concentrated stock of AdV5. The AdV5

infected Hek293 cells were then subjected to freeze-thaw cycles three times to ensure lysis of infected cells and release of virus particles in the supernatant. This supernatant was centrifuged to get a supernatant with only virus particles and clear off any cell debris. The virus particles in the supernatant were purified using a discontinuous CsCl gradient. Finally, AdV particles were transferred into a Slide-a-lyzer dialysis cassette (Slide-A-Lyzer 3.5K MWCO, Thermo Scientific) and dialyzed overnight against a solution consisting of 1 mM MgCl2, 10 mM Tris (pH 7.4), and 150 mM NaCl with 10% glycerol (vol/vol)[237]. AdV particles collected from dialysis cassette were titrated using the BD Clontech^{TM} Adeno-X Rapid Titre Kit (Clontech Laboratories.inc) as per manufacturer's instructions. In brief serial dilutions of the AdV solution was prepared and seeded with Hek293 cells in a 12 well culture plate, incubated for 48 hours at 37^0C. On day 3, cells are fixed and stained with a HRP-conjugated AdV specific antibody followed by staining with DAB, a chromogenic substrate for HRP. The infected cells turned brown in contrast to infected cells. The numbers of infected cells were counted in a given area and the titre was determined using a formula as per to manufacturer's instructions.

Retrograde mouse submandibular salivary gland cannulation was performed, as described in [237]. Briefly, mice were anaesthetized with ketamine (76mg/kg) and domitor (1mg/kg) (i.p.). Mice were also injected subcutaneously with analgesia Buprenorephine (0.03mg/kg). Then the submandibular salivary glands of the mice were cannulated **(Figure 2.2.1)** via the excretory duct using heat-drawn glass gas chromatography tubing (0.1 mm internal diameter; Sigma Aldrich). Approximately 30 µl of adenovirus solution, corresponding to 1×10^8-1×10^9 pfu of luciferase reporter-encoding AdV5, was injected into the salivary gland using an attached Hamilton syringe (Sigma Aldrich) [237]. After cannulation procedure, mice were then recovered with atipamezole at a dose of 0.15mg/mouse (s.c.).

Blood was obtained by performing cardiac puncture on mice under anesthesia (Isoflurane) and then these mice were sacrificed with terminal anesthesia (Euthal) after 3 hours, or at day 2, 5, 8, 15 and 23, post-cannulation (p.c.). Salivary glands were dissected from these mice.

In-vivo stimulation of salivary glands with recombinant cytokines and IL-22 blocking

2ug/ml of recombinant cytokine/s in PBS or PBS (Table 2.1A) was directly cannulated into the submandibular glands of anaesthetized female *c57bl/6* mice (8-12 weeks old). Glands were harvested 48 hours p.c.

Rat anti mouse IL22 Ab-03 and Rat IgG2a isotype antibody was obtained from Pfizer, Boston and used as previously described [17]. Briefly, starting at either day 2 or day 8 post-cannulation mice were administered a dose of 200ug of anti-IL22 antibody via i.p injection followed by subsequent injections at the same dose at a frequency of three times per week. Anti-IL22 treated and untreated matched control mice were taken for analysis at indicated time-points.

Sample processing

Submandibular glands from cannulated mice were harvested at designated/various time-points. Every gland was split for histology, stromal digestion, evaluation of the mRNA levels of molecules of interest and a very tiny piece to test luciferase activity.

Figure 2.2.1

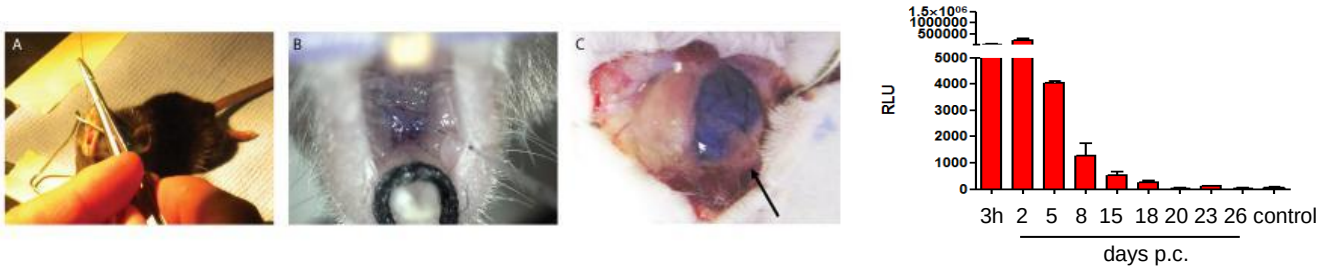

Figure 2.2.1 AdV delivery via retrograde mouse submandibular gland excretory duct cannulation. (A-B) A glass cannula is inserted in the excretory orifice of the submandibular gland of a 12 weeks-old *c57bl/6* mouse. **(C)** Representative picture of a cannulated NOD mouse demonstrating that delivery of 50µl of bromophenol blue dye is sufficient to permeate the cannulated submandibular gland with no spillage to the contralateral gland or the adjacent sublingual gland (arrow). **(D)** Expression of luciferase activity (normalised to protein levels) in pieces of tissue taken from cannulated glands infused with AdV containing the luciferase transgene [237].

Table 2.1 Reagents used for the *in vivo* cytokine cannulation experiments

Recombinant cytokine/PBS	Clone/Catalogue number	Supplier
IL-4	214-14	Peprotech
IL-13	210-13	Peprotech
IL-22	210-22	Peprotech
LTβR agonist antibody	clone 4H8	Novus Biologicals
TNFα	315-01A	Peprotech
Dulbecco's Phosphate Buffered Saline	D5652	Sigma-Aldrich

2.3 Luciferase Assay

At the time of dissection, a small portion of AdV cannulated salivary gland was stored in 50µL of RNAlaterR (Life Technologies Corporation) at -20^{0}C. This tissue was processed to quantify the degree of viral infection in the salivary gland. Samples were thawed and salivary gland pieces removed from RNAlaterR. These salivary gland pieces were transferred into bijous containing 350µL of GloLysis Buffer (Promega Corporation) and homogenised. Homogenised cell suspensions were centrifuged at 1300rpm for 10 minutes to sediment the cell debris and leave a supernatant. 25µL of the supernatant was the transferred in triplicates to a flat-bottomed, 96-well plate. 25µL of Luciferase substrate (Promega Corporation) was added to each well and incubated for 5 minutes. The Luciferase activity was determined using Berthold Technologies CentroLB 960 with MikroWin 2000 software.

2.4 Histology

Tissue processing and sectioning

Salivary glands from cannulated and control mice were dissected, snap-frozen in OCT over liquid nitrogen. All tissues were then stored in −80 °C until use. Six-seven microns sections were obtained by cutting the specimens in a cryostat (Bright) and mounted on X-tra Adhesive glass slides (Leica). Salivary gland sections were taken from the cutting level at which cellular infiltration was detected by Toluidine blue staining. Slides were left overnight at room temperature to dry. The next day, slides were stored in slide boxes at −80 °C until required.

Immunofluorescence (IF) Staining

Prior to staining, each slide was allowed to come to room temperature and then fixed for 20 minutes in ice-cold acetone; slides were then left to dry for at least 30 minutes and hydrated in PBS. For immunofluorescence staining, all dilutions of reagents and antibodies were made in PBS with 1% BSA (Sigma Aldrich) and slides were always incubated in a humid chamber in the dark. Firstly, to block endogenous biotin, sections were treated with 0.05% Avidin (Sigma Aldrich) and then 0.005% Biotin (Sigma Aldrich) for 15 minutes each. The slides were

washed for 5 minutes with PBS in between the two incubations. Following avidin-biotin blocking step, the sections were treated with 10% horse serum solution for 10 minutes to prevent non-specific staining by blocking Fc receptors. Excess horse serum was removed from the slides and sections were then incubated with primary antibodies for one hour, and then washed for 10 minutes with PBS. Wherever relevant, sections were then stained with sequential secondary, tertiary and quaternary antibodies for 30 minutes each. After each incubation, slides were washed for 10 minutes in PBS. All secondary, tertiary and secondary antibodies were pre-adsorbed in 100ul of 10% mouse serum for 30 minutes prior to their use. Finally, after the final incubation, slides were mounted with Prolong Gold (Invitrogen) and stored in -80^{0}C until acquisition of images.

Image acquisition

Images were acquired on a Zeiss LSM 510 laser scanning confocal head with a Zeiss Axio Imager Z1 microscope. Digital images were recorded in four separately scanned channels with no overlap in detection of emissions from the respective fluorochromes. Confocal micrographs were stored as digital arrays of 1024×1024 or 2048×2048 pixels with 8-bit sensitivity; detectors were routinely set so that intensities in each channel spanned the 0-255 scale optimally. The LSM510 Image Examiner Software was used to process these images. Leica DM6000 Fluorescent Microscope was used to obtain tile scans for the whole salivary gland section in order to perform fraction area analysis (as described in image analysis section).

Image analysis

Fraction area analysis

In order to assess the dimension of lymphocytic aggregates and the degree of lymphoid organization in cannulated salivary glands over a time-course, fraction area analysis system was used. For this analysis system we used CD3 and CD19 for identifying T cells and B cells respectively. CD3/CD19 double stained slides were analysed on Leica DM6000 Fluorescent

Microscope and tile scans for the whole salivary gland section were taken **(Figure 2.4.1)**. A region around the aggregates was manually drawn on the electronic pictures in the ImageJ software, and then both, the area of the aggregates and the area for the whole tissue section, were determined using the software. This numerical data was used to calculate the size of the aggregates i.e. the ratio of the aggregate area to the total tissue area, expressed in percentage. Thus, size of the aggregates was calculated as percentage of total tissue area (fraction area analysis).

On the basis of CD3/CD19 double staining, we also counted foci that were segregated (i.e. aggregates in which T and B cells are organised in separate areas) as an indicator of lymphoid organization. Single images **(Figure 2.4.1)** were acquired for all lymphoid follicles observed in the tile scans to calculate the size of lymphoid follicle size, the numerical data was expressed as μm^2. All measurements were performed in a masked fashion by observers in a blinded manner.

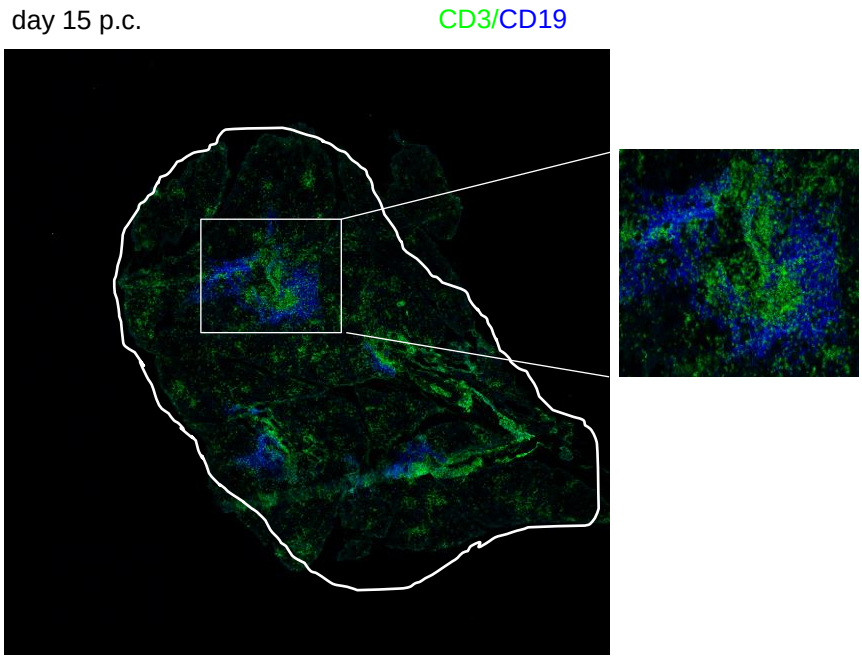

Figure 2.4.1 Example of a tile scan taken to study T cell (green) and B cell (blue) infiltration virus infected salivary gland at day 15 p.c.

Quantitation of T and B cell densities

CD3/CD19 double stained slides were visualized on LSM510 confocal microscope (Zeiss, Germany) and images taken using Zeiss LSM image software (Zeiss). Image of T/B cell infiltrates, indicated by CD3 and CD19 positive staining respectively, were acquired and this was repeated in several fields of view, covering the whole tissue section. Images were processed in the ImageJ software. A binary histogram was created by thresholding the red colour of CD3 (T cell) staining and blue colour of CD19 (B cell) staining respectively, and a threshold was chosen, based on the staining intensity. Using the histogram, the software estimated the area positive for the staining and it calculated the volume fraction area between the staining positive and negative areas. This value was used to determine the T and B cell densities for each image. The data was plotted as a ratio of B/T cell. All measurements were performed in a masked fashion by two observers.

Quantitation of gp38 and CD4 immunostaining

CD4/gp38 double stained slides were visualized on LSM510 confocal microscope and images taken using Zeiss LSM image software. Image of the aggregate indicated with CD4 and its underlying gp38+ stromal cells were acquired and this was repeated in several fields of view, covering the whole tissue section. The LSM510 Image Examiner Software was used to analyze the images. A region around aggregate was drawn, its area was determined and pixels count for gp38 and CD4 channel is calculated by the software. Correlation analysis between gp38 (no. of pixels/unit area) and CD4 (no. of pixels/ unit area) was then performed. All measurements were performed in a masked fashion.

Antinuclear antibodies (ANA) Detection

Hep-2 slides (IMMCO Diagnostics) were taken and were washed in PBS. Animal sera, obtained from spinning whole blood at 13000 r.p.m., and isolating the non-corpuscular component, was diluted in PBS (1:80) and deposited on each well. WT and KO mice sera were incubated for 1 h at room temperature, washed twice in PBS, and incubated with FITC

anti-mouse IgG (Sigma, Poole, U.K.) for 30 min in the dark. Slides were washed twice in PBS, mounted, and observed at fluorescence microscope for ANA staining.

Table 2.4.1 Primary Antibodies used for Confocal Microscopy

Antibody	Clone	Format	Supplier	Dilution Used
Hamster anti-mouse gp38	8.1.1	unconjugated	In house	1:10
Goat anti-mouse CXCL13	AF470	unconjugated	R&D Systems	1:100
Goat anti-mouse CCL21	AF457	unconjugated	R&D Systems	1:100
Hamster anti-mouse CD3e	eBio500A2 (500A2)	biotin	ebiosciences	1:50
Rat anti-mouse/human B220	RA3-6B2	eFluor450	ebiosciences	1:50
Rat anti-mouse CD19	eBio1D3 (1D3)	eFluor660	ebiosciences	1:50
Rat anti-mouse CD19	eBio1D3 (1D3)	Alexa-Fluor647	ebiosciences	1:50
Rat anti-mouse CD31	390	FITC	ebiosciences	1:100
Rat anti-mouse CD21/CD35	eBio4E3 (4E3)	FITC	BD biosciences	1:50
Hamster anti-mouse CD11c biotin	N418	biotin	ebiosciences	1:50
Rat anti-mouse IL-22Rα	MAB4294	unconjugated	R&D Systems	1:50
Rat anti-mouse/human RORγt	AFKJS-9	unconjugated	ebiosciences	1:20
Rat anti-mouse IL-7Rα	A7R34	Alexa-Fluor647	ebiosciences	1:20
Rat anti-mouse CD4	RM4-5	Alexa-Fluor647	ebiosciences	1:200
Rat anti-mouse FDCM1	FDCM1	unconjugated	BD biosciences	1:50
Rat anti-mouse EpCAM	G8.8	APC	ebiosciences	1:50
Rat anti-mouse CD8α	53-6.7	PE/ biotin	ebiosciences	1:50
Rat anti-mouse CD11b	MCA74G	unconjugated	AbD Serotech	1:100
Rat anti-mouse Gr1	RB6-8C5	biotin	AbD Serotech	1:100
Rat anti-mouse F4/80	MCA497G	unconjugated	AbD Serotech	1:100
Rat anti-mouse PNAd	MECA-79	unconjugated	BD biosciences	1:50

Table 2.4.2 Secondary Antibodies used for Confocal Microscopy

Antibody	Format	Supplier	Dilution Used
Goat anti-hamster	biotin	Biolegend	1:100
Goat anti-rabbit FITC	Alexa-Fluor488	Invitrogen	1:100
Rabbit anti-FITC	unconjugated	Invitrogen	1:200
Goat anti-mouse IgG	FITC	Southern Biotech	1:100
Donkey anti-goat	FITC	Jackson Immunoresearch Laboratoies Inc.	1:100
Donkey anti-rabbit	Alexa-Fluor647	Invitrogen	1:100
Goat anti-rat IgG	Alexa-Fluor546	Invitrogen	1:100
Donkey anti-rat IgG	FITC	Southern Biotech	1:100
Goat anti-rat IgM	Alexa-Fluor594	Invitrogen	1:100
Goat anti-gfp	FITC	Abcam	1:50
Streptavidin 555	555	Invitrogen	1:500
Streptavidin 647	647	Invitrogen	1:300

2.5 Flow cytometry

Isolation of stromal cells

Harvested salivary glands from mice were cut into small pieces and digested for 40 min at 37^0C with gentle stirring in 1.5 ml RPMI 1640 (Sigma Aldrich) medium containing collagenase D (3.7 mg/ml; from Roche), DNAse I (30ug/ml; from Sigma Aldrich) and 2% (vol/vol) FCS. The suspension was gently pipetted at 15min intervals to break up aggregates. The remaining fragments were further digested for 20 min at 37 °C with medium containing collagenase dispase (3.7 mg/ml; from Roche) and DNAse I (30ug/ml). The suspension was then gently pipetted to break up remaining aggregates until no visible fragments remained. During the final pipetting, EDTA (Sigma Aldrich) was added to a final concentration of 5 mM to further reduce cell aggregates. Cells were then passed through a 70-um mesh, were washed twice and were re-suspended in RPMI 1640 medium containing 10% (vol/vol) FCS.

Isolation of leukocytes

Cannulated salivary glands were harvested and chopped into small pieces and digested for 20 min at 37^0C with gentle stirring in 2 ml RPMI 1640 medium, containing collagenase dispase (250ug/ml; from Roche), DNAse I (25ug/ml; from Sigma) and 2% (vol/vol) FCS. The suspension was gently pipetted to break up aggregates. During the final pipetting, EDTA was added to a final concentration of 10mM to further reduce cell aggregates. Cells were then passed through a 70-um mesh with a syringe, were washed twice and re-suspended in MACS buffer and kept on ice until staining.

In-vitro stimulation for cytokine production

Isolated leukocyte or stromal cells were re-suspended in DMEM (with 10% FCS, 1%GPS, 1% NEAA, 1%HEPES and 50μM β-mercaptoethanol) for in vitro stimulation culture and were incubated with 50ng/ml PMA (Phorbol 12 Myristate 13 Acetate), 750ng/ml Inonomycin, 10ug/ml BrefeldinA (all from SIGMA), 10ul of 10^8-10^9 pfu of adenovirus for 4 h at 37°C.

10ug/ml recombinant IL-23 (Biolegend) was also added to the stimulation media for intracellular IL-22 cytokine assay.

Flow cytometric staining and analysis

Single cells suspensions were stained for 30 minutes in PBS (with 0.5% BSA and 2Mm EDTA) with desired 'cocktails' of antibodies indicated in Table 3.2.

Intracellular staining for cytokine production was performed (BD Cytofix/Cytoperm) according to the manufacturer's protocol. In brief, following surface staining with cocktails of desired antibodies, cells were washed in PBS (with 0.5% BSA and 2Mm EDTA), re-suspended in 150 µl Cytofix/Cytoperm (BD Pharmingen) and incubated overnight at 4°C. Cells were washed twice with the BD Perm/Wash Buffer, and subsequently, intra-cellular cytokine antibody was added and incubated at 4°C for 30–40 minutes. Afterwards, cells were washed twice, re-suspended in MAC buffer.

Data was acquired using a Cyan-ADP (Dako) with forward/side scatter gates set to exclude non-viable cells. Data were analyzed with FlowJo software (Tree Star).

For cell sorting, stained cells were sorted using MoFlo-XDP (Beckman Coulter Inc). The purity of sorted stromal populations routinely exceeded 96%. Gating strategy for stromal cell sorting is shown in **(Figure 2.5.1)**.

In vitro stimulation of sorted stromal cells with recombinant cytokines

Isolated stromal cells subsets were re-suspended at the same cell density in 500µl of DMEM (with 10% FCS, 1%GPS, 1% NEAA, 1%HEPES and 50µM β-mercaptoethanol) for *in vitro* cytokine stimulation assay in 48 well plates. All recombinant cytokines were reconstituted in DPBS (Sigma Aldrich). Cells were then incubated with 2ug/ml of recombinant IL-22 (Peprotech) alone, 2ug/ml LTβR agonist antibody (Novus Biologicals) plus 500ng/ml recombinant TNFα (Peprotech), 2ug/ml IL-22ug/ml plus LTβR agonist antibody plus

500ng/ml TNFα or only DPBS (Sigma Aldrich) for 24 hours at 37°C. Cells were harvested after 24 hours and taken for quantitative PCR analysis.

Figure 2.5.1

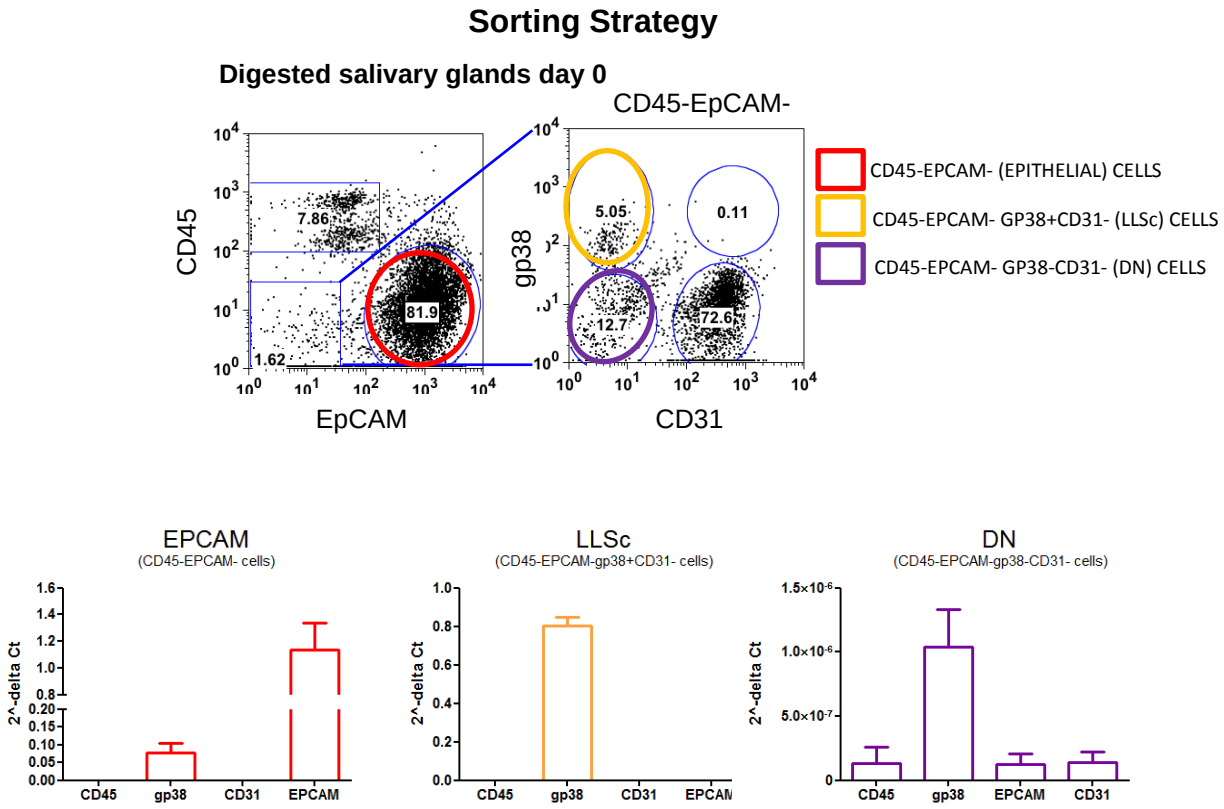

Figure 2.5.1 Gating strategy for different stromal cell subset analysis and sorting. The cells from the forward scatter and side scatter gate were plotted with CD45 against EPCAM, this allowed exclusion of CD45 hematopoietic cells and enrichement of CD45-EPCAM+ (epithelial) cells as well as the CD45-EPCAM- l cell component (consisting of endothelial cells and non-hematopoiteic, non-epithelial, non-endothelial stromal cells). Further gating of the CD45-EPCAM- cells with gp38 (stromal and lymphatic cell marker) and CD31 (endothelial cell marker) allowed us to identify gp38+CD31- lymphoid like stromal cells (LLSc) and gp38-CD31- double negative (DN) cells. The graphs show gene expression analysis for CD45, EPCAM, CD31 and gp38 in the three stromal subsets post-sorting, to confirm purity of the sort.

Table 2.5.1 List of Antibodies used for Flow Cytometry

Antibody specificity	Isotype	Clone	Format	Supplier	Dilution used
CD45 (all isoforms) LCA, Ly-5	Rat IgG2b	30-F11	PERCPCy5.5/ PECy7/ APC-Cy7	ebiosciences	1:200/1:500/ 1:800
Podoplanin (gp38)	Hamster IgG	ebio8.1.1	PE	ebiosciences	1:50
CD31 (PECAM-1)	Rat IgG2a	390	FITC/PECy7	ebiosciences	1:50
CD326 (EpCAM)	Rat IgG2b	G8.8	PECy7	ebiosciences	1:200
ICAM-1	Rat IgG2b	YN1/1.7.4	APC	Biolegend	1:200
VCAM-1	Rat IgG2a	429 (MVCAM.A)	PERCPCy5.5	Biolegend	1:50
RANKL	Rat IgG2a	IK22/5	Biotin	Biolegend	1:50
MadCAM-1	Rat IgG2a	MECA-367	Biotin	Biolegend	1:50
IL-22Rα	Rat IgG2a	FAB42941A	APC	R&D Systems	1:50
Ki67	Mouse IgG1	B56	Alexa-Fluor647	BD biosciences	1:50
BrdU	Mouse IgG1	3D4	Alexa-Fluor647	BD biosciences	1:50
CD3e	Hamster IgG	145-2C11	PECy7	BD biosciences	1:100
B220 (CD45R)	Rat IgG2a	RA3-6B2	APCCy7	BD biosciences	1:100
CD4	Rat IgG2a	RM4-5	efluor 450	ebiosciences	1:50
CD8α	Rat IgG2a	53-6.7	PE-TexasRed	BD biosciences	1:200
CD62L	Rat IgG2a	MEL-14	PE	ebiosciences	1:100
CD44	Rat IgG2b	IM7	FITC	ebiosciences	1:100
CD19	Rat IgG2a	eBio1D3 (1D3)	APC	ebiosciences	1:100
NK1.1	Rat IgG2a	PK136	FITC	ebiosciences	1:50
CD11b	Rat IgG2b	M1/70	PERCPCy5.5	ebiosciences	1:200
Gr1	Rat IgG2b	RB6-8C5	FITC	ebiosciences	1:50
CD11c	Hamster IgG	N418	PE/PECy7	ebiosciences	1:100
IL-7Rα	Rat IgG2a	A7R34	Alexa-Fluor647	ebiosciences	1:50

2.6 Enzyme-linked immunosorbent assay (ELISA)

Relative virus-specific serum antibody titres were evaluated by ELISA (protocol adapted from Ruth Elizabeth Coughlan, Prof. Adam Cunningham's Lab at University of Birmingham). Peripheral blood obtained by cardiac puncture from *wt* and *gene knockout* mice at specified time-points, post cannulation, was allowed to clot at room temperature and serum was separated from corpuscular component by spinning at 13000 r.p.m for 10 minutes. Sera were aliquoted and frozen at -20^{0}C until further use. To measure for viral-specific antibody titre, the AdV solution (that is used to cannulate mice) was used to coat ELISA plates (MaxiSorp plates, Nunc) at 5µg/ml in coating buffer (1 capsule of Sigma carbonate-bicarbonate buffer /100mldH_2O). After an overnight incubation at 4^{0}C, plates were washed three times with PBS and blocked with 100µl of PBS/1% BSA for 1 hour at 37^{0}C, to prevent non-specific binding in subsequent steps. Post incubation, plates were washed again three times with PBS. Sera were diluted at 1:20 ratio in PBS/1% BSA/0.05%Tween 20 and added to the first row of the 96 well ELISA plate. For each of the samples further four-fold serial dilutions in PBS/1% BSA/0.05%Tween 20 were prepared in each column and then the plate was incubated for 1 hour at 37°C followed by three times washing with PBS. AP-conjugated goat anti-mouse IgM and IgG secondary antibodies (all from Southern Biotechnology) diluted at 1:1000 in PBS/1% BSA/0.05%Tween 20, were added to the appropriate wells, and incubated for 1 hour at 37^{0}C. Plates were then washed three times with PBS. Antibodies were detected using Sigma fast p-Nitrophenyl phosphate solution (prepared using manufacturer's instructions). 100µl of substrate was added to each well and incubated at 37^{0}C until the desired positivity was obtained. Optical densities (O.D.) values at 405nm were obtained using the softmax Pro programme. Relative antibody titres for each sample were obtained by plotting the dilution against the O.D. values and then taking the dilution at which the O.D. value was set in the mid-exponential phase of the curve.

2.7 Quantitative Real-Time Polymerase Chain Reaction

Extraction of total RNA from mouse tissues

Samples of cannulated salivary glands for RNA extraction were obtained by tissue sectioning at the cutting level, which showed infiltration detected by Toluidine blue staining. Briefly, after cryosectioning tissues for histology, a further five 25 microns thick tissue sections were taken and transferred in a RNAase-free tube for each sample, which were stored at -80ºC until further use. RNA was extracted using the Qiagen RNeasy mini kit, according to manufacturer's instructions. Tissues stored at -80°C were defrosted on ice, and 200ul of RLT buffer (containing 10ul of β-Mercaptethanol/ ml of buffer) were added to each tube. The tissue lysis was carried out by vortexing each sample tube for at least 30-50 seconds until the sample was uniformly homogeneous. Tissue lysates were centrifuged very briefly at maximum speed (13000rpm) to collect the sample at the bottom of the tube. An equal volume of 70% ethanol was added to the lysate and immediately mixed by pipetting in order to precipitate RNA, which remains in the aqueous phase. The sample (400ul) were added to the RNeasy mini column placed in a 2 ml collection tube and centrifuged for 1 minute at 13,000 rpm to allow the RNA to bind to the silica column. The flow-through was discarded, and 350 µl of RW1 Buffer were added to the column, centrifuged for 1 minute at 13,000 rpm and the flow-through discarded. To avoid any possible DNA contamination, a DNase step was included according to manufacturer' instructions.10 µl of DNAse I stock solution (previously prepared by dissolving solid DNase I (1500 Kunitz units) in 550 µl of RNase-free water) were added to 70µl of Buffer RDD, gently mixed and added to the RNeasy mini column silica-gel membrane. Following 15 min incubation at room temperature (RT), 350 µl of Buffer RW1 were added to the column, centrifuged for 1 minute at 13,000 rpm and the flow-through discarded. The RNeasy column was transferred into a new 2 ml RNase free collection tube. In order to wash away contaminants (residual DNA and proteins) in the organic phase, 500 µl of Buffer RPE were placed onto the RNeasy column and centrifuged for 1 minute at 13,000 rpm to wash the column. The flow-through was then discarded and

another 500 µl Buffer RPE added to the RNeasy column. The tube was centrifuged for 2 min at 13,000 rpm to dry the RNeasy silica-gel membrane and the flow-through discarded. To eliminate any chance of possible Buffer RPE carryover, the tube was centrifuged again for 1 min at 13,000 rpm. For elution, the RNeasy column was transferred to a new RNAse free 1.5 ml collection tube, and 25 µl of RNase-free water were pipetted directly onto the RNeasy silica-gel membrane and the tube centrifuged for 1 min at 13,000 rpm. The eluted RNA for each sample was immediately frozen at -80°C until required.

Extraction of total RNA from mouse cells

Isolated stromal cell subsets were obtained by cell sorting (described in section 2.5). Following sorting, cells were centrifuged and cell pellets were stored at -80ºC until further use. Prior to RNA extraction cell pellets were thawed and lysed in 350µl buffer RLT (Qiagen). Then RNA was extracted from cell lysates using the QiagenRNAeasy Micro Kit following manufacturer's instructions. Cell lysates were centrifuged very briefly at maximum speed (13000 r.p.m) to collect the sample at the bottom of the tube. An equal volume of 70% ethanol was added to the lysate and immediately mixed by pipetting in order to precipitate RNA, which remains in the aqueous phase. The sample (700µl) were added to the RNeasy mini column placed in a 2 ml collection tube and centrifuged for 1 minute at 13,000 rpm to allow the RNA to bind to the silica column. The flow-through was discarded, and 350 µl of RW1 Buffer were added to the column, centrifuged for 1 minute at 13,000 rpm and the flow-through discarded. To avoid any possible DNA contamination, a DNase step was included according to manufacturer' instructions.10 µl of DNAse I stock solution (previously prepared by dissolving solid DNase I (1500 Kunitz units) in 550 µl of RNase-free water) were added to 70µl of Buffer RDD, gently mixed and added to the RNeasy mini column silica-gel membrane. Following 15 min incubation at room temperature (RT), 350 µl of Buffer RW1 were added to the column, centrifuged for 1 minute at 13,000 rpm and the flow-through discarded. The RNeasy column was transferred into a new 2 ml RNase free collection tube. In order to wash away contaminants (residual DNA and proteins) in the organic phase, 500 µl

of Buffer RPE were placed onto the RNeasy column and centrifuged for 1 minute at 13,000 rpm to wash the column. The flow-through was discarded and then 500 µl Buffer of 80% ethanol was added to the RNeasy column. The tube was centrifuged for 2 min at 13,000 rpm to dry the RNeasy silica-gel membrane and the flow-through discarded. To eliminate any chance of possible ethanol carryover, the tube was centrifuged again for 1 min at 13,000 rpm. For elution, the RNeasy column was transferred to a new RNAse free 1.5 ml collection tube, and 12.5 µl of RNase-free water were pipetted directly onto the RNeasy silica-gel membrane and the tube centrifuged for 1 min at 13,000 rpm. The eluted RNA for each sample was immediately frozen at -80°C until required.

Reverse Transcription PCR and generation of a cDNA template

In Reverse-Transcription PCR (RT-PCR), complementary DNA (cDNA) is synthesized from mRNA using a reverse transcriptase. Reverse transcription was carried out using the High capacity reverse transcription cDNA synthesis kit (Applied biosystems) according to the manufacturer's guidelines in a 96 well plate. Briefly, 25ul of total RNA for each sample was mixed with 5 ul 10x Buffer, 5ul 10x Random Primers, 2ul 100nM dNTPs, 2.5ul Reverse transcriptase enzyme and brought to 50ul volume reaction with DNase/RNase-free water After mixing and a brief spin down of the 96 well plate, the reverse transcription to cDNA was carried out on Techne 312 Thermal Cycler PCR machine using the following conditions: 25ºC for 10 min and 37ºC for 120 min. Finally, the completed cDNA was diluted with 50ul DNase/RNase-free water in a 1:1 ratio. The cDNA was then stored at -20ºC until further use.

Quantitative Taqman real-time PCR (qPCR)

Relative expression of the gene of interest was quantified by TaqMan RT-PCR. Reactions were carried out in a 384-well optical reaction PCR plate (Applied Biosystems) in a final volume of 5.1µl. The reaction mix contained a forward primer, a reverse primer and a probe, specific to the gene of interest or the housekeeping gene (β-actin). Already published TaqMan probes and primers from Applied Biosystems were used. Primer and probe sequences can be viewed in table 2. These were diluted to their optimal pre-determined working concentrations. Probes for both the house-keeping and target gene were labelled with FAM. 2.8µl of Taqman gene expression master mix (Applied Biosystems) was also added to each reaction, along with 2.3µl of cDNA template. Before running the reaction, the plate was sealed using a MicroAmp™ Clear Adhesive Film (Applied Biosystems) and centrifuged for 1 min at 350 x g. The quantitative real-time PCR were run in duplicates per gene for each sample and detected by the ABI PRISM 7900HT Instrument. The standard thermal cycling conditions were used that comprised of a 2 min UNG activation step at 50 ºC, a 95 ºC Taq polymerase enzyme activation step for 10 min, and cycles of 95 ºC denaturation for 15 sec and 60 ºC anneal/extension for 60 sec. Results were then analysed after 40 cycles of amplification using the ABI PRISM 7900HT Sequence Detection System Version 2.1 (SDS 2.1). Cycle thresholds (Ct) were determined within the logarithmic phase of the PCR for the house-keeping gene and the target gene. β-actin and PDGFRβ were used as an endogenous control. We used the mean of two technical replicates (Ct values) to calculate the ΔCt value for which the *C*t of the β-actin was subtracted from the Ct of the target gene C_t value and the relative amount was calculated as $2^{-\Delta Ct}$. Stromal cell dependent genes were normalized to PDGFRβ instead for β-actin in order to account for differences in percentage of infiltrating cells between *wt* and *ko* mice. RQ values were calculated as $2^{-\Delta\Delta Ct}$ where *ΔΔC*t is the difference between the ΔCt values of cannulated salivary glands and the ΔCt of non-cannulated salivary glands. Ct values above 34 were not accepted, and neither were technical replicates with more than two cycle differences between them.

Table 2.7.1 Primers and probes used for Quantitative PCR

Gene	mRNA Accession number	Assay ID	Source
Mouse β-actin	NM_007393.3	Mm01205647_g1	Applied Biosystems
Mouse Pdgfrβ	NM_001146268.1 NM_008809.2	Mm00435546_m1	Applied Biosystems
Mouse AICDA	NM_009645	Mm00507774_m1	Applied Biosystems
Mouse BAFF	NM_028075	Mm00840578_g1	Applied Biosystems
Mouse CXCL13	NM_018866	Mm00444533_m1	Applied Biosystems
Mouse CXCR5	NM_007551	Mm00432086_m1	Applied Biosystems
Mouse CCL19	NM_011888	Mm00839967_g1	Applied Biosystems
Mouse CCR7	NM_007719	Mm01301785_m1	Applied Biosystems
Mouse LTβ	NM_007986	Mm00484254_m1	Applied Biosystems
Mouse LTα	NM_007986	Mm00484254_m1	Applied Biosystems
Mouse IL-7	NM_007986	Mm00484254_m1	Applied Biosystems
Mouse IL-4	NM_007986	Mm00484254_m1	Applied Biosystems
Mouse IL-13	NM_007986	Mm00484254_m1	Applied Biosystems
Mouse IL-23	NM_007986	Mm00484254_m1	Applied Biosystems
Mouse IL-22	NM_008337	Mm01168134_m1	Applied Biosystems
Mouse IL-17α	NM_007986	Mm00484254_m1	Applied Biosystems
Mouse IL-22	NM_007986	Mm00484254_m1	Applied Biosystems
Mouse IL-6	NM_008366	Mm00434256_m1	Applied Biosystems
Mouse IL-2	NM_008371	Mm00434291_m1	Applied Biosystems
Mouse IFNγ	NM_008518	Mm00434774_g1	Applied Biosystems
Mouse TNFα	NM_013693	Mm00443258_m1	Applied Biosystems
Mouse ICAM-1	NM_009506	Mm00437310_m1	Applied Biosystems
Mouse VCAM-1	NM_001025250	Mm01281449_m1	Applied Biosystems
Mouse LTβR	NM_007986	Mm00484254_m1	Applied Biosystems

2.8 Statistical Analysis

Data Set

Each experiment was performed atleast two times with minimum of two mice used per experiment unless mentioned. Both salivary glands from mice were used to generate data sets. Each figure legend contains the information about the number of times a particular experiment was performed as well as the number of mice (biological replicates) used in each repeat experiment.

Statistics

Statistics were calculated using the student's *t* test. All p values were calculated using the statistics programme included in GraphPad Prism and p values of ≤ 0.05 were accepted as significant.

Chapter 3

Expansion of lymphoid like stromal cells in a model of TLO formation in the salivary glands of wild-type mice

Introduction

Stromal cells in SLOs, commonly termed lymphoid stromal cells, express cytokines and chemokines that regulate lymphocyte survival, differentiation and migration [6, 246]. In SLOs, mainly three different types of lymphoid stromal cells have so far been identified: fibroblastic reticular cells (FRCs), marginal reticular cells (MRCs) and follicular dendritic cells (FDCs) [6]. Podoplanin/gp38+ER-TR7+ FRCs reside in the T cell zone and produce the T cell and DC attracting chemokines CCL19 and CCL21 [6, 133, 141]. FRCs also secrete lymphoid cytokine IL-7 that is necessary for survival and homeostasis of T cells [6, 135]. MRCs express MAdCAM-1, RANKL as well as B cell recruiting chemokine CXCL13, and are found underneath the marginal sinus at the edges of the B cell follicles [6, 149, 247]. CD35+gp38/Podoplanin+ FDCs, located in the light zone of germinal centres, secrete CXCL13 and BAFF (B cell survival factor) and regulate B cells affinity maturation [6, 144].

Numerous reports in mice and human inflammatory conditions have reported the expression of lymphoid stromal markers such as ICAM-1, VCAM-1, FDC markers (CD21/35) and the production of survival factors and chemokines in resting stroma [76, 159, 160, 177-179, 185, 226, 248, 249].

The differentiation and maintenance of lymphoid stromal cells in secondary lymphoid organs has been demonstrated to be dependent on LT and TNFα signalling [6, 7, 107, 115, 117, 141, 144, 250]. Expression LT and TNFα has been detected in various inflammatory diseases. Furthermore, Tg mice over-expressing these molecules in the pancreas, develop functional TLOs [157, 158, 251]. Altogether, these data suggest that TLOs and secondary lymphoid tissues engage similar pathways in their formation [165, 252, 253].

However, the signals that drive the differentiation of lymphoid like stromal cells during inflammation and the possible functional relevance of these stromal cells during the process of tertiary lymphoid organogenesis are not very clear. We aimed to address these questions by using an inducible model of TLO formation in the salivary glands of wild-type mice [237].

This chapter first describes in detail a new mouse model of salivary gland inflammation and validates its use as model of TLO formation. In particular we will discuss the acquisition of lymphoid features by the inflammatory infiltrates in relation to the expression of factors involved in TLO development. The second part of the chapter delineates the phenotypical and functional changes occurring to resident stromal cells in the cannulated salivary glands, which enable the stromal cells to modulate the formation, organization and maintenance of the lymphoid aggregates.

Results

3.1 Histomorphological characterization of cellular infiltrates in submandibular glands of cannulated mice

To assess the dynamic progression and evaluate the acquisition of lymphoid features by the infiltrating cells, histological analysis was performed using CD3/CD19 and FDC-M1 (to identify follicular dendritic cells). Total aggregate area as percentage of total tissue area and size of the lymphoid aggregates was calculated. Finally, the prevalence of organized aggregates with T/B cell segregation in discrete areas was determined using image analysis system as described in the material and method section.

Peri-ductal lymphocytic infiltrates typically develop in cannulated mice. Early stage, day 5 post cannulation (p.c.), of the inflammatory process was characterized by T cell infiltration with very few B cells **(Figure 3.1Ai)**. From day 8 p.c. onwards a trend towards progressive increase in T and B cells was observed **(Figure 3.1Ai-ii)**. FDC-M1+ cells closely co-localized with the B cell rich areas, acquiring the typical morphology of GC **(Figure 3.1Bi)**. Of note, FDCs were not always present in characteristic reticular networks but showed scattered cellular staining within the B area **(Figure 3.1Bii)**.

Fraction area analysis demonstrated that day 8 p.c. was characterized by larger total lymphoid area i.e. ~10% of fraction area ($p>0.005$) with presence of T cell/B cell segregation in ~30% of inflammatory foci **(Figure 3.1C-D)**. By day 15 p.c. we observed a reduction in the total lymphoid area **(Figure 3.1C)**, while the aggregates displayed higher degree of organization both in terms of segregation (more than 45% of the foci were segregated at day 15 p.c.) **(Figure 3.1Aiii and D)** and presence of FDC networks **(Figure 3.1Aiii and Bi-ii)**. Nearly 30% at day 8 p.c. and 60% of mice at day 15 p.c. were positive for FDC-M1 staining **(Figure 3.1E).** The average size of lymphoid follicles observed at day 8 p.c. was around 7-8x10^4 µm^2 whereas at day 15 it was 10-12x10^4 µm^2 **(Figure 4.1F)**. At day 23 p.c. aggregates showed not only resolution of the structural organization but a significant decrease in the

fraction area; from a 8-10% total aggregate area at day 8-15 p.c. to <2% at day 23 p.c. ($p<0.005$) **(Figure 3.1Aiv and C)**.

Figure 3.1

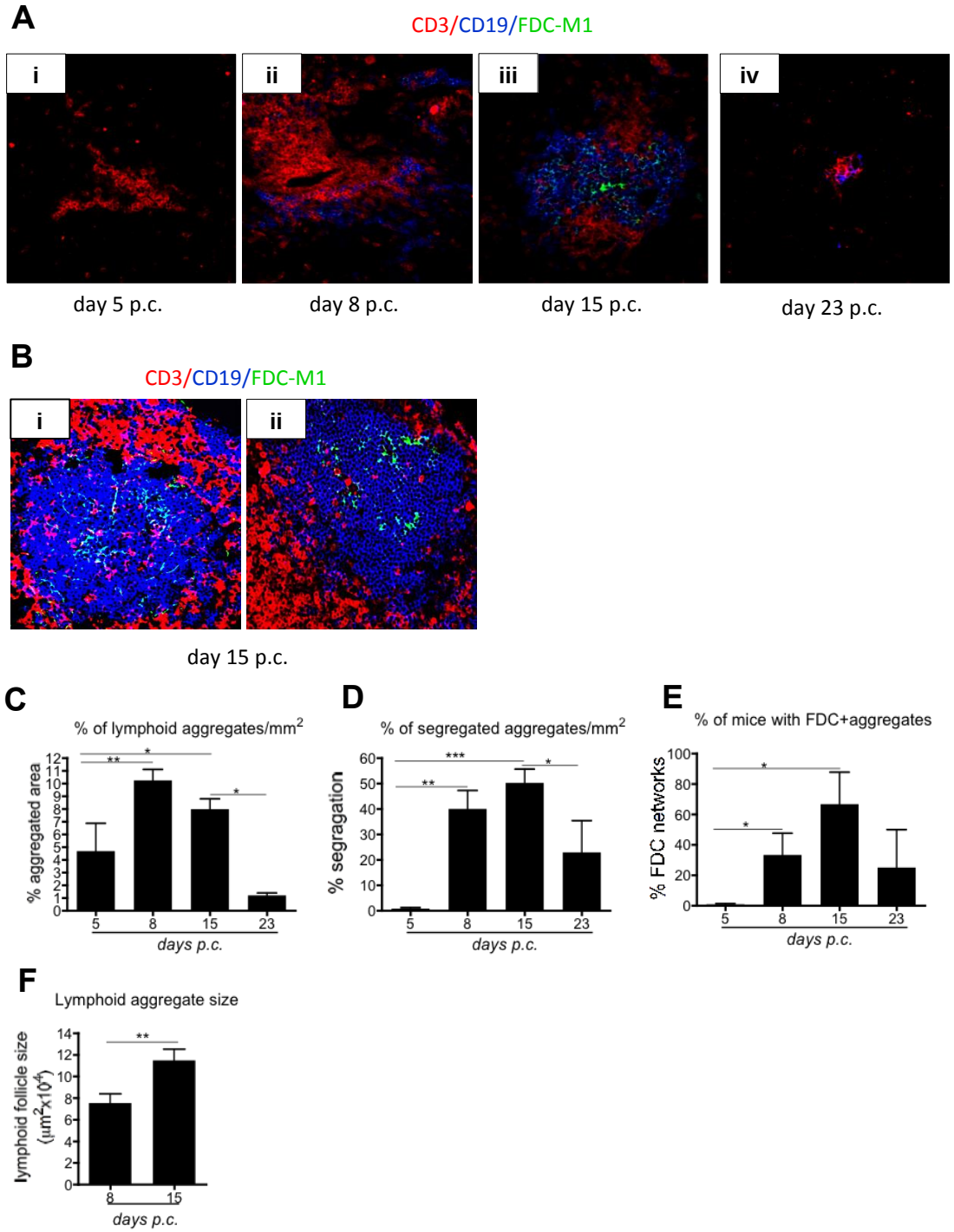

Fig 3.1 Characterization of cellular infiltrate and fraction area analysis of salivary glands from mice cannulated with with 10^8 pfu of replication deficient adenovirus. Salivary glands sections of virus infected mice at day 5, day 8, day 15 and day 23 p.c. were stained with CD3 (red), CD19 (blue) and FDC-M1 (green). Around day 5 p.c. only diffuse CD3+ infiltrates were observed, B cells are absent **(Ai)**. Day 8 p.c cannulation is characterized by influx of B-cells, significant increase in the aggregates **(Aii)**. Day 15 aggregates are characterized by increase in organization i.e. separate T cell area and B cell area and presence of FDC **(Aiii)**. FDC-M1 staining was not always detected in characteristic reticular networks **(Bi)** but also as scattered cellular staining **(Bii)** within B cell area. The software *ImageJ* was used to calculate; the area of the tissue and the relative area covered by lymphoid aggregates **(C)**, how many of these aggregates were segregated **(D)**, positive for FDC-M1 **(E)** and also size of lymphoid follicles **(F)** (*p>0.05; **p>0.01; ***p>0.001).

3.2 FACS analysis infiltrating T and B lymphocytes, and their proliferation status in cannulated salivary glands

FACS analysis for CD3+ and CD19+ cells infiltrating the salivary glands supported the histological findings. The dynamic of T and B cell infiltration within the glands was expressed as percentage of the CD45+ cells. CD3+ cells were observed infiltrating salivary glands **(Figure 3.2C)** by day 2 p.c. followed by a progressive increase, and peak T cell infiltration observed between 8-15 p.c. However, a decline in the percentage of T cells was observed at day 23 p.c. Ki67 staining on CD3+ cells demonstrated their ability to proliferate in situ **(Figure 3.2Bi and D)**. The dynamic of CD19+ B cell infiltration **(Figure 3.2C)** was different to T cells. Only 0.5% of B cells were observed at day 2, with a progressive increase observed at day 5 and day 8. Peak infiltration was observed at day 15 with ~20% of the CD45 compartment constituted by CD19+ cells **(Figure 3.2A)**. B cells also exhibited the capability to proliferate within cannulated salivary glands, verified by the Ki67+ staining on the CD19+ cells **(Figure 3.2Bii and D)**.

Figure 3.2

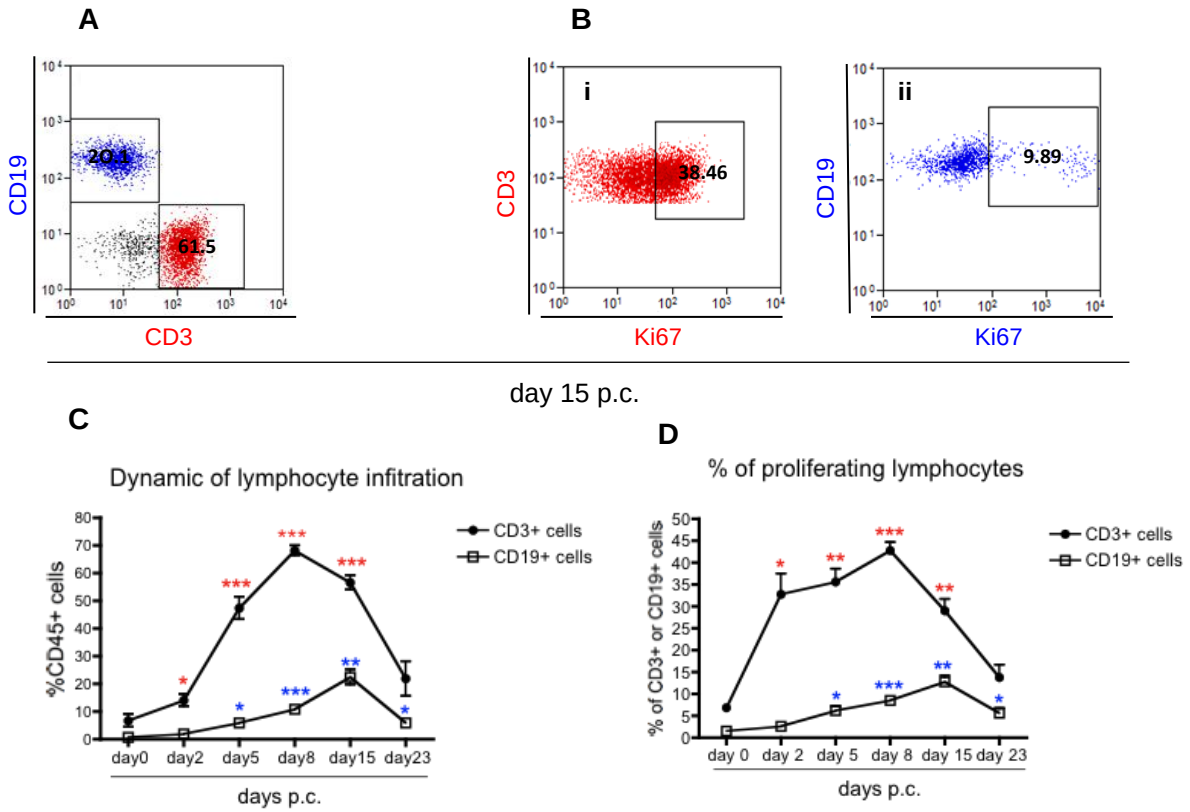

Figure 3.2 FACS analysis of infiltrating T and B lymphocytes, and their proliferation status in cannulated salivary glands. Representative dot plots showing flow cytometry analysis of CD3e+ and CD19+ cells i.e. T and B cells respectively within CD45+ cells **(A)**, Ki67+CD3e+ cells **(Bi)** and Ki67+CD19+ cells **(Bii)** from salivary glands isolated at day 15 p.c. Graph summarizing the percentage T and B lymphocytes in the CD45+ leukocyte population **(C)** and proliferating T and B lymphocytes **(D)** at day 0, day 2, day 5, day 8, day 15 and day 23 p.c. Data are representative of three different experiments with three mice per experiment and expressed as differences between given time-points and percentage of the cell population at day 0 (*p<0.05; **p<0.01; ***p<0.001).

3.3 Phenotyping of T cell subsets within salivary glands during TLO formation

Further evaluation of the T cell subsets based on differential expression of CD62L and CD44 revealed that 50-70% and 20-25% of the CD3+cells infiltrating virus infected salivary glands displayed respectively an activated (CD62L-CD44+) and memory (CD62L+CD44+) phenotype. Interestingly, even though only 5-10% naïve (CD62L+CD44-) T cells were observed at day 2 and 5, there was nearly 15-17% increase witnessed in this population at later time-points **(Figure 3.3A)**.

CD4 and CD8 staining was performed on cannulated salivary gland to further characterize the CD3+ T cell population. FACS analysis showed that the majority of the infiltrating T cells observed in the salivary glands were CD4+ T cells ($p<0.05$-0.001), 30% CD3+ cells were CD8α T cells at day 2 and 5 p.c. whereas at later-time points only 18-20% CD8α+ T cells were observed **(Figure 3.3B)**.

Of interest, CD3+ cells at day 0 were predominantly γδ T cells, however a switch in the phenotype of T cells was detected upon inflammation ($p<0.05$-0.01), 70-80% of CD3+ cells in inflamed salivary glands were αβ+T cells **(Figure 3.3C)**.

Figure 3.3

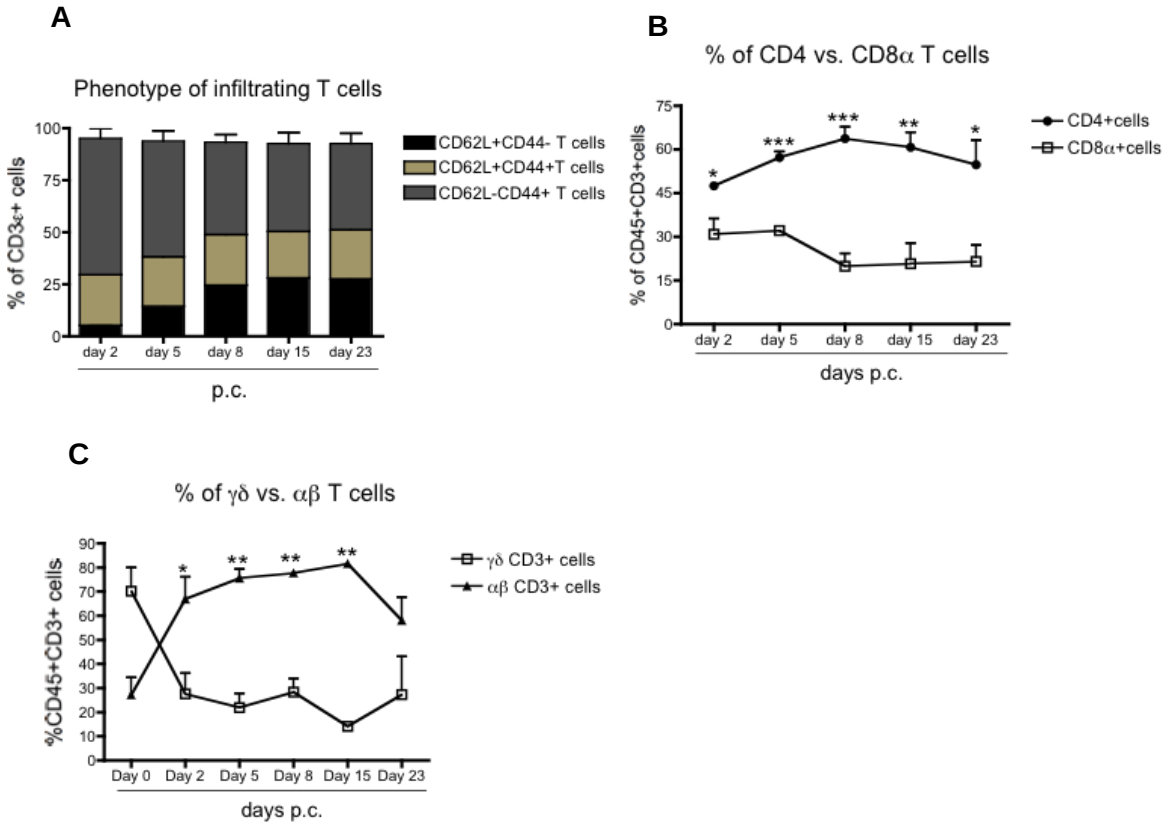

Figure 3.3 Phenotyping of T cell subsets within salivary glands during TLO formation. Flow cytometry analysis was performed on salivary glands that were stained for CD3, CD4, CD8α, CD62L, CD44, αβTCR and γδTCR antibodies to differentiate between CD8 T cells (CD3+CD8α+), CD4 T cells (CD3+CD4+), αβ T cells (CD3+αβ+), γδ T cells (CD3+γδ+) and within T cell subsets; naïve T cells (CD62L+CD44), memory T cell (CD62L+CD44+) and activated effector T cells (CD62L-CD44+). Graph summarizing the relative distribution of naïve, memory and activated effector T cells **(A)** within cannulated salivary glands at day 2, day 5, day 8, day 15 and day 23 p.c. Plots showing relative percentage of CD4 versus CD8α T cells **(B)** and αβ versus γδ T cells **(C)** infiltrating cannulated salivary glands at different time-points p.c. Data are representative of three different experiments with three mice per experiment (*p<0.05; **p<0.01; ***p<0.001).

3.4 Investigation of other leukocyte populations found in cannulated salivary glands

The other leukocyte cell populations apart from lymphocytes, observed in salivary glands were the CD11c+ cells, NK1.1 cells and CD11b+Gr1+ cells and ILCs.

Normal SGs were characterized by the presence of a large network of CD11c+ cells by IF **(Figure 3.4Ai)**. Post-cannulation there was progressive T cell infiltration observed with aggregation of CD11c+ cells at the edges of the infiltrated areas **(Figure 3.4Aii)**. FACS analysis also showed the presence of nearly 70% CD11c+ cells, ~3% ILC (Lineage-IL-7Ra+ cells) and ~10% NK1.1+ cells in resting salivary glands. Interestingly, a decline (50-60%) was observed in CD11c+ cells until day 15 **(Figure 3.4D)**.

The majority of the infiltrating cells at day 2 were CD11bGr1+ cells (40-45%), and NK cells (25-30%) **(Figure 3.4D)**. The CD11b+ and Gr1+ cells observed at day 2 p.c. were polymorphonuclear cells **(Figure 3.4Bi-iv)**. While NK cells were still largely detected in salivary glands at day 5 **(Figure 3.4Ci)** and day 8 p.c., the CD11bGr1+ cells showed a significant decrease after day 2 **(Figure 3.4D)**.

ILCs were identified as IL-7Ra+Lineage- cells, with the lineage markers including CD3, B220, CD11b, CD11c, CD5. The highest percentage of ILC (i.e. 2-3%) was observed in salivary glands at resting conditions. This population did not increase post infection **(Figure 3.4D)**.

Figure 3.4

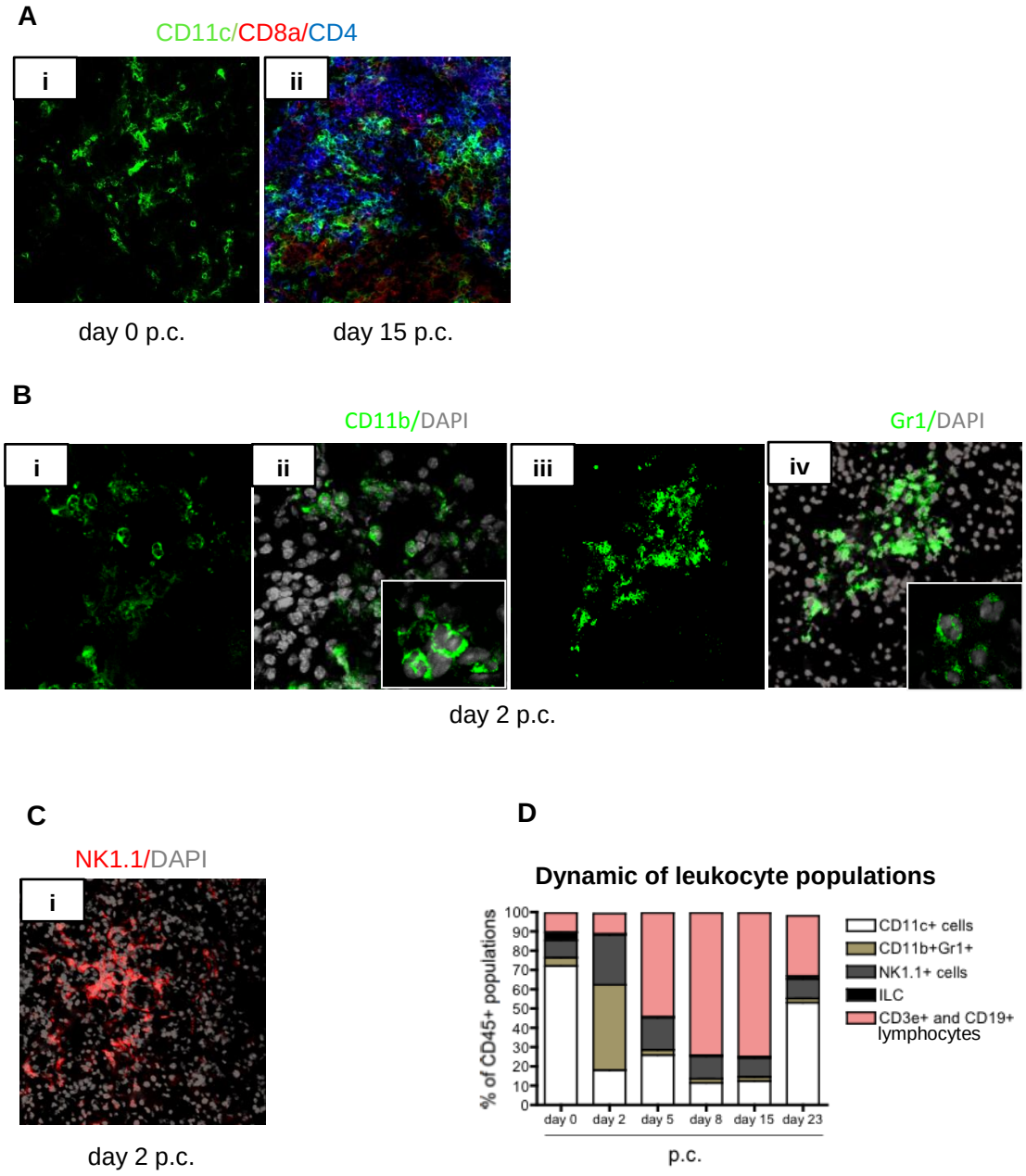

Figure 3.4 Investigation of other leukocyte populations found in cannulated salivary glands. Immunofluorescence of WT cannulated salivary glands at day 0 **(Ai)** and 15 **(Aii)** p.c. CD4 (blue), CD11c (green), CD8a (red). Original magnification 25X. Immunofluorescence of WT cannulated salivary glands at day 2 p.c. DAPI (grey), CD11b **(Bi-ii)** and Gr-1 **(Biii-iv)** (green) and NK1.1 (Ci) (red). Original magnification 25X **(Bi-iv and Ci)** and 60X **(Bii and iv)**. Graph summarizing the relative distribution of different leukocyte cells **(D)** within cannulated salivary glands at day 0, day 2, day 5, day 8, day 15 and day 23 p.c. Data are representative of three different experiments with three mice per experiment

3.5 CXCL13 and CCL21 expression increases with increasing level of lymphoid organization of the inflammatory foci in cannulated salivary glands

To evaluate the expression of constitutive lymphoid chemokines as factors in the progressive acquisition of the lymphoid organization of submandibular inflammatory foci, the expression of CXCL13 and CCL21 in relationship to lymphoid aggregates was examined. Diffuse weak expresion of CXCL13 was observed at early time points **(Figure 3.5.1Ai).** From day 8 p.c. when progressive increase in B cell infiltration was observed, we noticed a significant increase in CXCL13 expression. The CXCL13 expression appeared to be more prevalent in segregated versus non-segregated aggregates **(Figure 3.5.1Bi-ii)**. Expression of CXCL13 was mainly confined to B cell areas and B cell/FDC–rich areas suggesting relationship between ectopic expression of CXCL13 and B cell infiltration **(Figure 3.5.1Ci-ii)**. CXCL13 could also be detected in salivary gland epithelial ducts, surrounded by periductal infiltrates and non-infiltrated ducts **(Figure 3.5.1Aii)**.

CCL21 expression was first detected as early as day 5 in CD3+ foci **(Figure 3.5.2Ai)**. Its expression was always confined to T-cell rich areas **(Figure 3.5.2Ai-iii)** and showed a strict association with CD31+/LYVE-1+ lymphatic vessels **(Figure 3.5.2Bi)**. Interestingly, CD3+ T cells were often seen in close association or within these CCL21+ lymphatic vessels **(Figure 3.5.2Bi-ii)**.

Figure 3.5.1

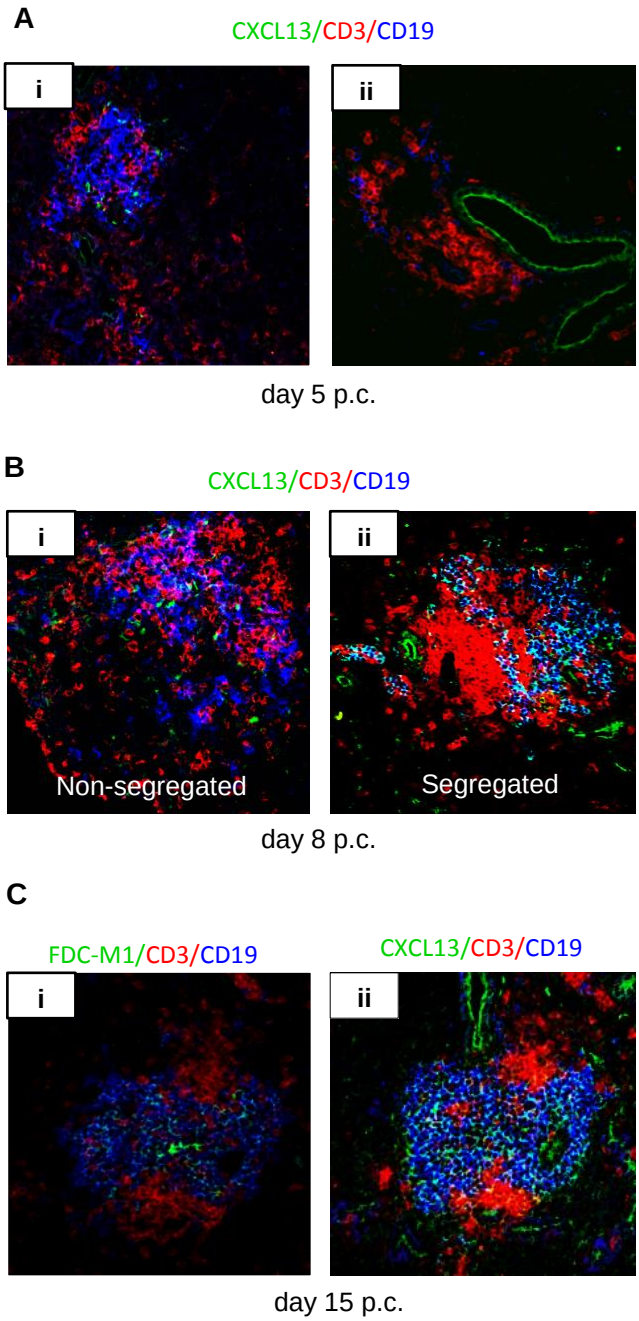

Figure 3.5.1 CXCL13 expression increases with the increasing level of lymphoid organization of the inflammatory foci in salivary glands of cannulated mice. Microphotographs showing CXCL13 protein expression (green) with T cell (CD3; red) and B cell (CD19; blue) aggregates in cannulated salivary glands of *wt* mice at day 5 **(Ai-ii)**, day 8 **(Bi-ii)** and day 15 **(Cii)**. Original magnifications 25X. CXCL13 staining is also detected in salivary gland ductal epithelial cells **(Aii)**. CXCL13 expression in in non-segregated **(Bi)** versus segregated **(Bii)** lymphocytic aggregate at day 8 p.c. **(Ci)** Day 15 p.c. salivary gland section stained with CD3 (red) , CD19 (blue) and FDC marker FDC-M1 (green). **(Cii)** Sequential section of day 15 p.c. salivary gland showing CXCL13 (green) expression in FDC rich area in T cell (red) and B cell (blue) aggregate.

Figure 3.5.2

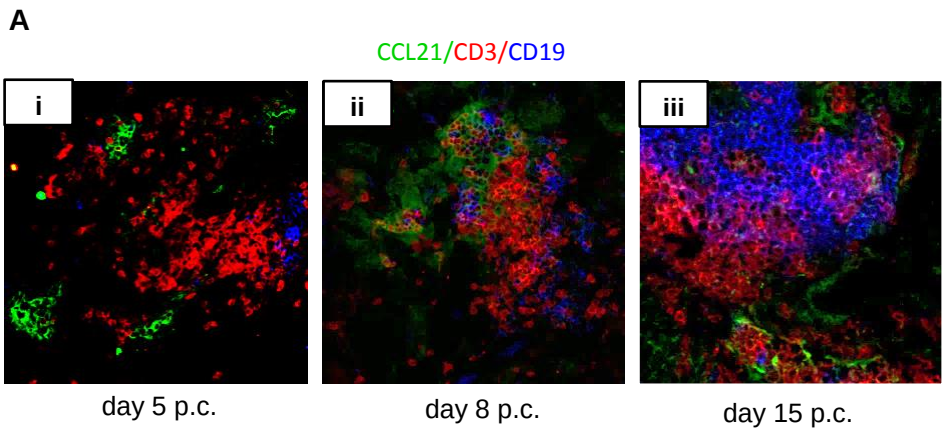

Figure 3.5.2 Patterns of CCL21 expression with increasing level of lymphoid organization increasing level of lymphoid organization of the inflammatory foci in salivary glands of cannulated mice. Microphotographs of CCL21 staining (green) by immunofluroscence show a trend in the colocalization of CCL21 with the CD3+ (red) T cell-rich area of aggregates at day 5, day 8 and day 15 p.c. B cell are also shown with CD19 (blue) staining **(Ai-iii).** At day 5 is CCL21 expression was scarce **(Ai)** but showed progessive increase with higher degree of infiltration **(Aii-iii)**. CCL21+ cells were mostly present on the edge of the aggregates at day 8 and day 15 p.c. **(Aii-iii)**. CCL21 (green) was detected in association with LYVE-1+ (red) CD31+ (blue) lymphatic vessels **(Bi)** in the CD3+ (red) T cell area **(Bii)**.

3.6 Vascular organization of lymphoid aggregates in cannulated salivary glands

The lymphocyte aggregates were characterized by formation of CD31+ vessels, some of which showed a cobblestone-like appearance resembling HEVs. MECA-79 staining was performed on salivary glands of cannulated mice in order to assess the presence of HEV-like vessels identified by expression of PNAd, known to regulate naïve cells homing in secondary lymphoid organs. PNAd+ expression was detected on all the HEVs like structures in close association with the T-cell rich area of the inflammatory foci. The PNAd+ HEVs were primarily observed at the edges of the lymphoid aggregates at day 8 and day 15 p.c. **(Figure 3.6Ai-iii)**. Additionally, the presence of lymphatic vessels was ascertained by examining the expression of LYVE-1 and gp38. Lymphatic vessels, positive for LYVE- and gp38, were found mainly in the periphery and occasionally in the midst of lymphocytic infiltrates **(Figure 3.6Bi-ii and Ci)**. These vessels were more abundant in the areas containing aggregates than in the non-infiltrated areas.

Figure 3.6

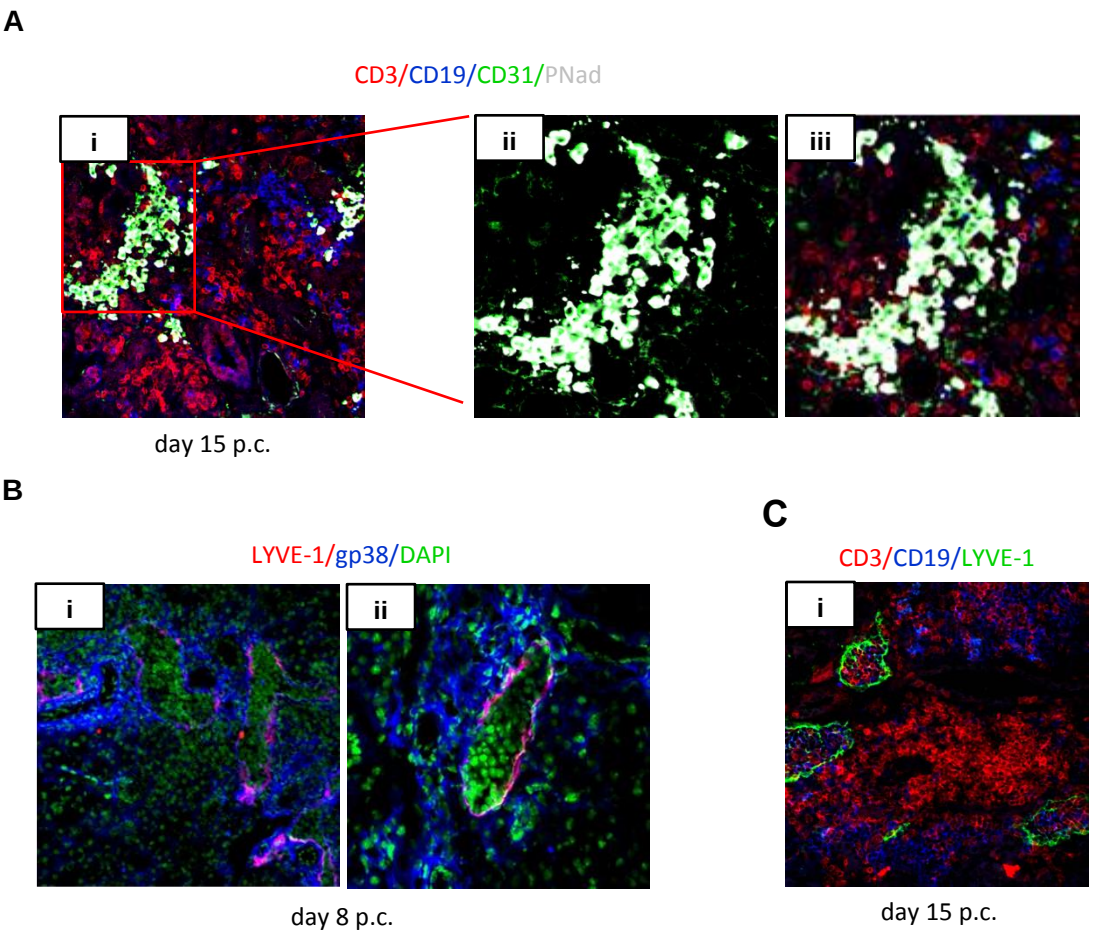

Figure 3.6 Histological characterization of vascular compartment in the virus infected salivary glands of WT mice. Immunofluorescence analysis of CD31 (green), PNad (white), CD3 (red) and CD19 (blue) showed that some CD31+ vessels acquired HEV-like phenotype i.e. cobblestone appearance with PNad expression and were mainly confined to the periphery of aggregates (**Ai-iii**). Original magnification at 25X (**Ai**) and 60X (**Aii-iii**). Immunofluorescence staining for DAPI (green in **Bi-ii**), Lyve (red in **Bi-ii** and green in **Ci**) and gp38 (blue) showed lymphatics, characterized by gp38 and Lyve co-expression **(Bi-ii)**, engulfed with cells. Lymphatic vessels were found both at the periphery and midst of lymphoid aggregates **(Bi-ii and Ci)**. Original magnification at 10X **(Bi)** and 25X **(Aii and Ci)**.

3.7 Local expression of genes regulating TLO formation and functionality characterise disease evolution in salivary glands of cannulated mice

Development of TLOs is believed to be reliant on ectopic expression of a critical set of genes, such as lymphotoxin and lymphoid chemokines [14, 160]. Additionally, presence of various lymphoid cytokines/growth factors is required for lymphocyte survival, proliferation, and function within TLOs. Thus, we examined whether evolution of TLOs in salivary glands of virus-cannulated mice was accompanied with a concomitant up-regulation of these genes.

CXCL13/CXCR5 and CCL19/CCR7 mRNA transcripts **(Figure 3.7A-D)** were significantly up-regulated in the salivary glands of virus-canulated mice as compared to non-cannulated mice, and their expression was consistent with the progressive detection of TLO in the salivary glands, reaching their peak of expression between day 8-15 p.c. Interestingly, CXCL13/CXCR5 and CCL19/CCR7 mRNA showed significant up-regulation already at day 5 p.c. and thus preceded the development of TLO. Importantly, both LTα and LTβ, recognised to be essential for the induction of lymphoid chemokines [115, 117], were highly expressed in virus cannulated salivary glands, but not non-cannulated mice. Moreover, LTα and LTβ expression displayed a similar trend to lymphoid chemokine expression **(Figure 3.7E-F)**. LTβR expression was also abundantly up-regulated in virus infected salivary glands as compared to resting salivary glands **(Figure 3.7G)**.

IL-7 has been suggested to play an key role in ectopic lymphoid neogenesis, analogous to its role in the development and homeostasis of SLOs [254]. In contrast to chemokines and (LTβ), signal for IL-7mRNA **(Figure 3.7H)** was detected as early as day 2 p.c. with a significant deflection at day 8 and its level were maintained until the resolution phase of the inflammatory process.

Formation of B cell rich aggregates coincided with the in situ up-regulation of BAFF, a crucial B cells survival and proliferating factor [153, 155]. Of interest, the acquisition of functional features of TLOs was also associated with the significant expression of BAFF at day 15 p.c. **(Figure 3.7I)**. Of notice, IL-2 mRNA **(Figure 3.7J)** expression in cannulated salivary glands

appeared to mirror expression pattern of the lymphoid chemokines and LTβ. Gene expression profiles of TNFα and IFNγ show a significant increase early in the inflammatory process between day 5 and day 8 p.c. with a significant drop observed in their levels from day 8 onwards **(Figure 3.7K-L)**.

Of notice, the expression of germinal center cytokines IL-21 and IL-4 [155, 156], was also observed in cannulated salivary glands from day 8 onwards coinciding with appearance of TLOs **(Figure 3.7M-N)**.

Figure 3.7

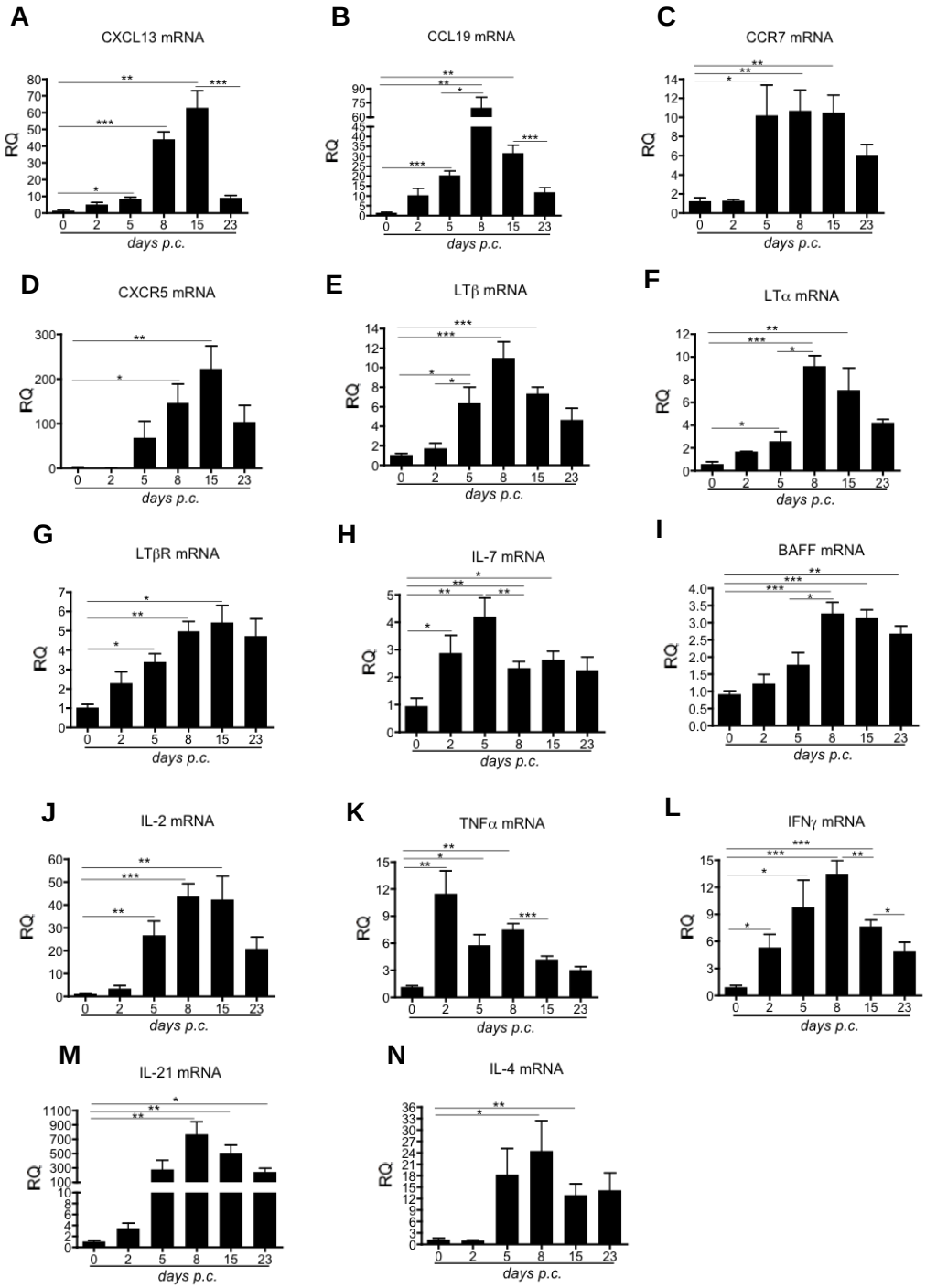

Figure 3.7 Development of aggregates in cannulated salivary glands is accompanied by upregulation of genes regulating tertiary lymphoneogenesis. A-N, Graphs showing mRNA transcript levels of CXCL13 **(A)**, CCL19 **(B)**, CCR7 **(C)**, CXCR5 **(D)**, LTβ **(E)**, LTα **(F)**, LTβR **(G)**, IL-7 **(H)**, BAFF **(I)**, IL-2 **(J)**, TNFα **(K)**, IFNγ **(L)**, IL-21 **(M)**, IL-4 **(N)** in *wt* mice salivary glands at day 0, day 2, day 5, day 8, day 15 and day 23 p.c. Transcripts were normalized to β-actin or pdgfrβ (for CXCL13, CCL19, LTβR, IL-7 and BAFF) and results are presented as relative quantitation (RQ) values calculated with calibrator day 0 untreated salivary glands. Data are representative of three-four different experiments with atleast three mice per experiment (*p<0.033, **p<0.005, ***p<0.0005).

3.8 Humoral response in the cannulation model of salivary gland inflammation

FACS analysis showed the presence of CD138+ cells in cannulated salivary glands and both CD138+B220+ plasmablasts and CD138+B220- plasma cells were detected **(Fig 3.8A-B)**. Furthermore, GL7+ B cells **(Figure 3.8C-D)** were also present in cannulated salivary glands of mice at day 8 (4-5%; $p<0.01$) and day 15 (9-10%; $p<0.001$). Of interest, AID mRNA **(Figure 3.8E)** was strongly up-regulated in the cannulated salivary glands; its expression parallels the histological detection of ectopic GC formation, as the peak of AID expression signal was observed at day 15 p.c. These findings suggested to us that the machinery, able to sustain the process of class switch recombination and somatic hyper-mutation [153-156], is present within our target organ.

To probe for virus-specific B-cell responses, serum samples were collected from cannulated WT mice at day 5, 8, 15, 23 p.c. and analysed for viral-specific Ig isotypes; IgM and IgG by ELISA **(Figure 3.8F-G)**. Significant levels of adenoviral-specific IgM and IgG were detected in the serum of cannulated mice as compared to controls (non-cannulated animals). IgM antibodies peaked early in the time course by day 5 p.c. but showed a significant increase by day 15 p.c. ($p<0.055$), while viral-specific IgG antibodies continued to increase significantly up to day 26 p.c ($p<0.03$-0.005).

We next investigated whether there was any evidence of anti-nuclear (ANA) IgG autoantibody in this model. ANA were observed by week 3 p.c. in ~66% of cannulated mice **(Figure 3.8H-I)**. Remarkably, ANA detection closely paralleled the development of AID expression in the salivary glands, suggesting that salivary gland TLOs contribute towards breach of tolerance towards auto-antigens and development of class-switched antibodies.

Figure 3.8

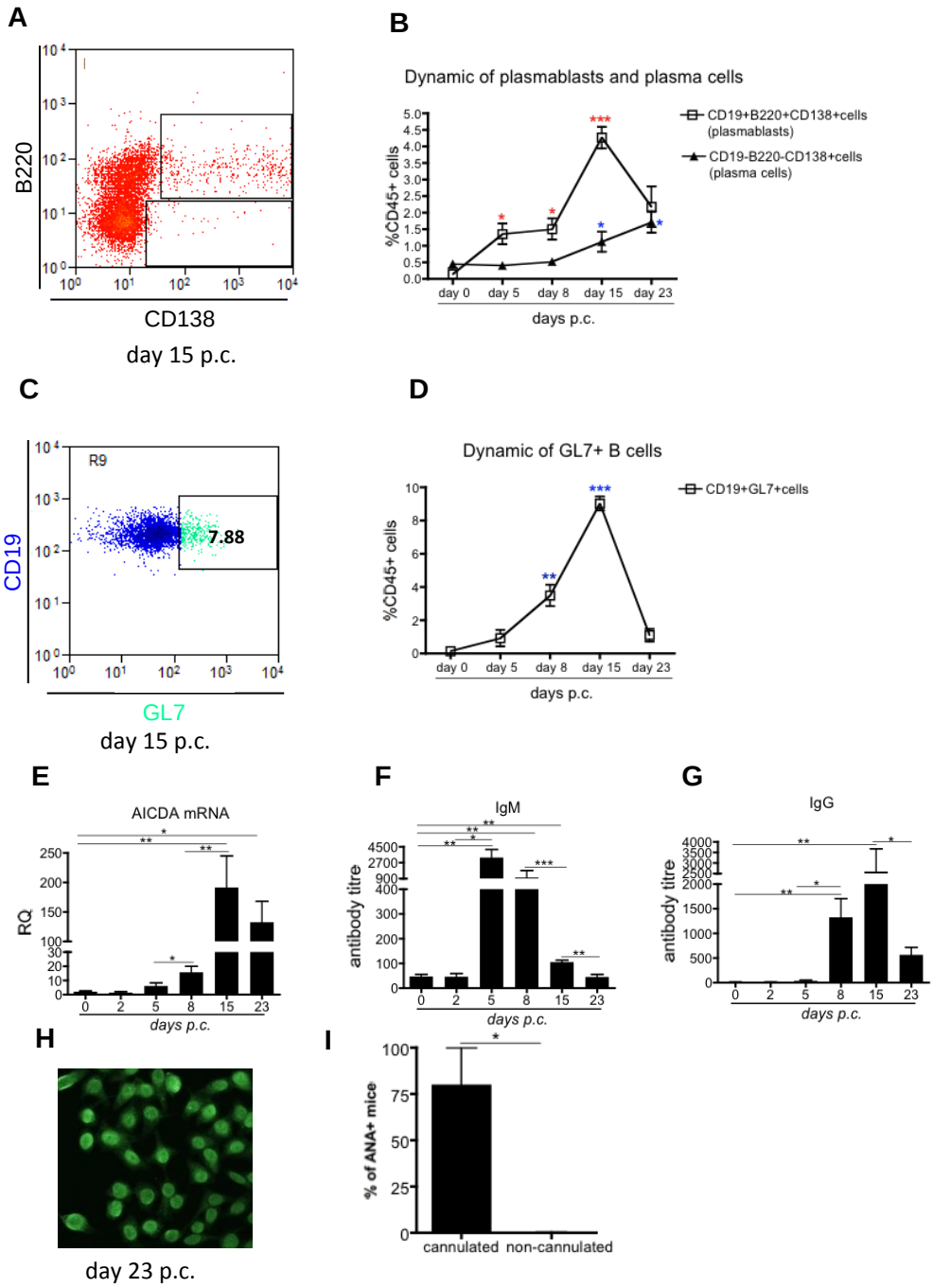

Figure 3.8 Humoral response in the cannulation model of salivary gland inflammation. (A), Flow cytometry analysis for B220 and CD138 was performed in cannulated salivary glands. Representative dot plot shows presence of both plasmablasts (B220+CD138+) and plasma cells (B220+CD138+) in salivary glands at day 15 p.c. **(B)**, Graph summarising the dynamic of plasmablasts and plasma cells at day 0, day 5, day 8, day 15 and day 23. **(C)**, Representative dot plot presenting percentage of GL7+ B cells at day 15 p.c. **(D)**, Graph displaying percentage of GL7+ B cells at day 0, day 5, day 8, day 15 and day 23 p.c. **(E)**, AID mRNA transcripts levels that were normalized to β-actin and results are presented as relative quantitation (RQ) values calculated with calibrator day 0 untreated salivary glands. **(F-G)**, Quantitative evaluation of serum viral antibodies in cannulated mice demonstrate an anti-viral IgM response **(F)** early in the inflammatory process whereas anti-viral IgG antibodies **(G)** increase is concomitant with the formation of TLOs from day 15 p.c. onwards. **(H)**, Representative microphotographs of immunofluorescent detection of anti-nuclear autoantibodies (ANA) using Hep2 cells as substrate. **(J)**, Sera (a dilution 1:80) from 75% mice three weeks p.c. was positive for ANA. Data are representative of three experiments with atleast three mice per experiment (*p>0.033, **p>0.005, ***p>0.0005).

3.9 Histological characterization of Lymphoid like stromal cell (LLSc) in inflamed salivary glands

Expression of the lymphoid stromal cell marker gp38 on non-lymphoid tissue stromal cells has been described during inflammation [226]. Therefore, the stromal cells underlying the lymphoid aggregates were examined for the presence of gp38+ lymphoid like stromal cells in cannulated salivary glands.

Expression of gp38 by EPCAM+ myoepithelial cells on acini and ducts in resting salivary glands has been reported by Hata et al. [255]. In accordance with these reports, we detected constitutive gp38 expression on EPCAM+ epithelial cells while little expression of this glycoprotein was detected on CD45-EPCAM- stromal cells in salivary glands at day 0, (shown in **Figure 3.9Ai)**. However, in inflamed salivary glands, gp38 expression showed an increased diffuse web-like staining pattern in close association with the inflammatory foci denoted by CD4+ cells by day 5 p.c. **(Figure 3.9Avi-x)**. Lack of co-localization between gp38 and EpCAM was observed in the aggregate area, suggesting that gp38+ cells within the foci are non-epithelial cells **(Figure 3.9Avi)**. The gp38+ cells also expressed other lymphoid stromal cells markers, such as ICAM-1, VCAM-1 and ER-TR7, in inflamed salivary glands **(Figure 3.9Avii-ix)**; however expression of these markers was negligible in day 0 salivary glands **(Figure 3.9Aii-iv)**. gp38 expression on stromal cells underlying lymphoid aggregates was observed in TLOs at day 8 and day 15p.c. **(Figure 3.9Bi-iv),** and at these sites, gp38 expression was found to correlate with the increase in size of the aggregates as measured by image analysis **(Figure 3.9C)**. Since gp38 expression can also be found on lymphatic vessels, day 8 cannulated salivary gland sections were stained with CD3, CD19, gp38 and CD31 to understand the distribution of the gp38+ endothelial component in relation to the aggregates, as shown in **Figure 3.9Di-ii.** gp38+ detected within the aggregate did not show co-localization, thus confirming the non-endothelial nature of the gp38+ cells observed within aggregates.

Overall, the histological data showed an accumulation of non-epithelial, non-endothelial lymphoid stromal cells within inflamed salivary glands when compared to non-cannulated resting salivary glands.

Figure 3.9

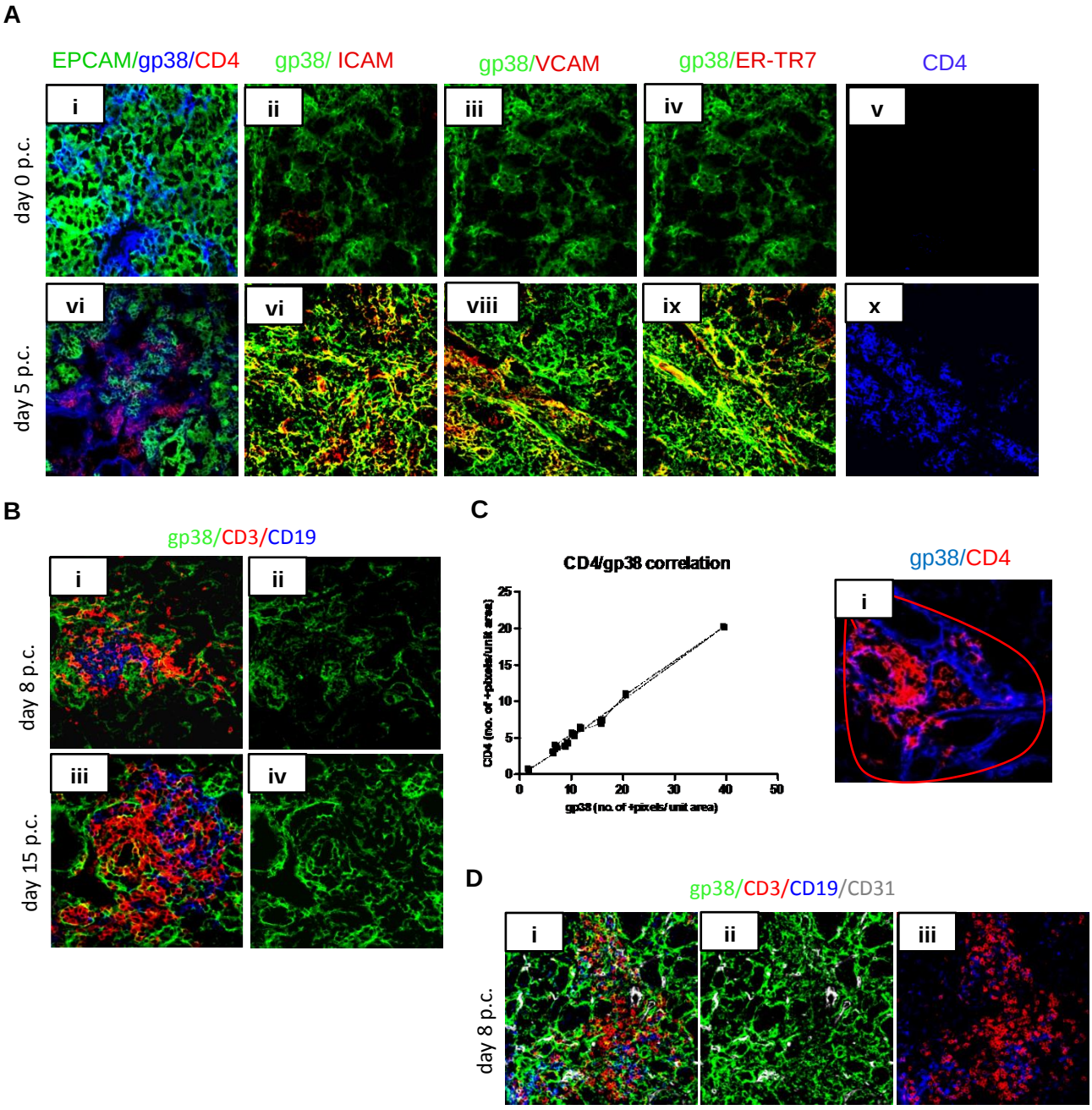

Figure 3.9 Histological characterization of Lymphoid like stromal cell (LLSc) in inflamed salivary glands. (Ai-x) Immunofluorescence of WT cannulated salivary glands at day 0 and 5 p.c. CD4 (blue), gp38 (green), EpCAM, ICAM-1 and VCAM-1 (red). Original magnification 25X. Histological analysis illustrates increased non-epithelial gp38 expression **(Avi)** in the areas covered by the aggregates shown here by CD4+ cells **(Avi and x)** in salivary glands at day 5 p.c. as compared to day 0 p.c. gp38 expression at day 0 is mostly confined to epithelial (EPCAM+) cells **(Ai)**. Expression of other lymphoid stromal markers: VCAM-1/ICAM-1/ER-TR7 by gp38+ stromal cells sitting under the aggregate confirmed their lymphoid phenotype **(Avii-ix)**. **(Bi-iv)** gp38 (green) expression showed a web-like staining pattern in close association with the CD3+ (red) and CD19+ (blue) lymphocytic foci and appear to progressively increase from day 8 **(Bi-ii)** upto day 15**(Biii-iv)** p.c. in association with aggregate size **(C)** Image analysis of gp38 and CD4 positive areas in salivary gland tissue sections at different time-points p.c. Area expressed as number (no.) of pixels per unit area. Dots represent mean of aggregate area in each gland. Eleven glands from different mice were analysed in total. **(Ci)** Representative immunfluorescence picture of CD4 (red) and gp38 staining (blue) in salivary glands, as described in Materials and Methods. **(Di-ii)** Immunofluorescence of WT cannulated salivary glands at 8 p.c. CD3 (red), gp38 (green), CD3 (red) and CD31 (white). Original magnification 25X.

3.10 Phenotypical and functional analysis of Lymphoid like stromal cell (LLSc) in inflamed salivary glands

We next performed a detailed FACS analysis of the changes occurring in the stroma post-cannulation. Following viral cannulation of the salivary glands, we observed progressive enrichment of EPCAM-CD45-gp38+CD31- cells **(Figure 3.10.1Ai** day 0 and **Figure 3.10.1Ai** day 5 p.c.). RANKL **(Figure 3.10.1B)** and MadCAM-1 **(Figure 3.10.1C)** expression was detected on the EPCAM-CD45-gp38+CD31- cells in salivary glands at day 5p.c. when compared to day 0 salivary glands. Expansion of these gp38+CD31- cells was accompanied by enrichment in CD45-EPCAM-CD31-VCAM-1^{int}ICAM-1^{int} and VCAM-1^{high}ICAM-1^{high}cells **(Figure 3.10.1D-F)**, similar to that observed in the early phases of lymph node anlagen embryogenesis and has been associated with stromal cell maturation in the embryonic lymph node anlagen [60, 79, 256]. Between 50-70% VCAM-1^{int}ICAM-1^{int} cells and upto 10% and VCAM-1^{high}ICAM-1^{high} cells were observed in cannulated salivary glands ($p<0.01$-0.05). gp38 expression was primarily confined to these two VCAM-1^{int}ICAM-1^{int} and VCAM-1^{high}ICAM-1^{high}cells **(Figure 3.10.1G-H)**.

FACS sorting of the gp38+CD31- cells at day 5, 8 and 15 p.c. identified mRNA expression the lymphoid chemokines CXCL13 **(Figure 3.10.2A)**, CCL19 **(Figure 3.10.2B)** and CCL21 **(Figure 3.10.2C)** as well as the lymphoid cytokines BAFF **(Figure 3.10.2D)** and IL-7 **(Figure 3.10.2E)** that progressively and significantly increased in the gp38+CD31- component but not in the double negative gp38-CD31- cells (in the CD45-EPCAM- compartment), epithelial cells (CD45-EPCAM+ compartment) or in the small gp38+cd31- cells present in resting salivary glands. Furthermore, LTβR **(Figure 3.10.2F)** and TNFR1 **(Figure 3.10.2G)** mRNA was significantly up-regulated on the LLSc when compared to the DN and epithelial cells, thus demonstrating the enhanced ability of LLSc to be able to respond to lymphotoxin stimulation and up-regulate lymphoid chemokines similar to the lymphoid stromal cells.

We named the CD45-EPCAM-CD31-gp38+ stromal cells, lymphoid like stromal cells or LLSc because their phenotypical appearance and ability to secrete lymphoid chemokines and survival factors was not confined to just one cell type but resembled different lymphoid stromal cell subsets (i.e. both T cell and B cell stroma).

Figure 3.10.1

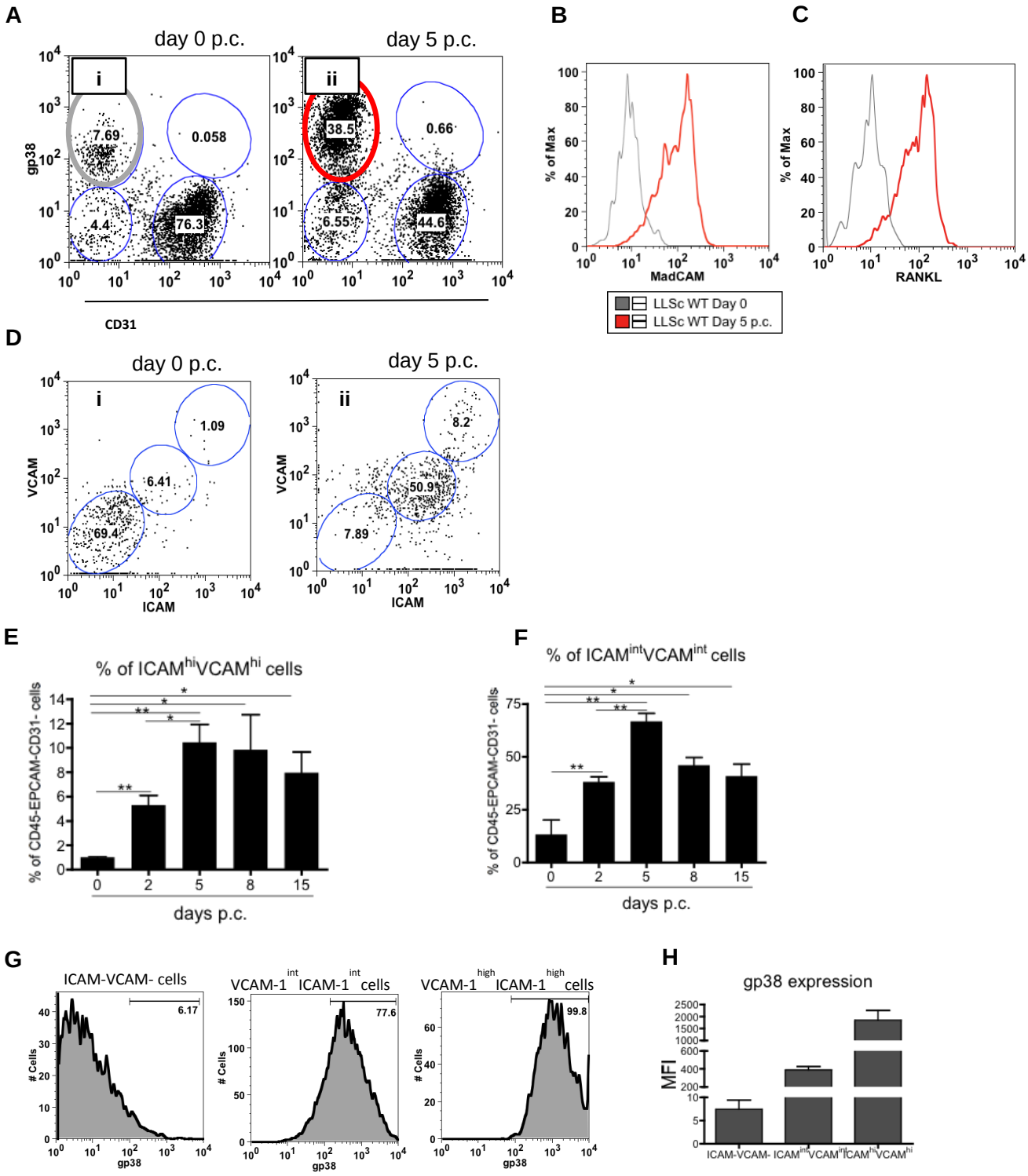

Figure 3.10.1 Phenotypical and functional analysis of Lymphoid like stromal cell (LLSc) in inflamed salivary glands. FACS histogram representing LLSc expansion in WT mice salivary glands at day 5 p.c. as compared to day 0 p.c. **(A)**. Induction of lymphoid stromal markers MadCAM **(B)** and RANKL **(C)** on gp38+CD31- cells is shown in histograms from cannulated salivary glands at day 5 p.c. (red line) compared to day 0 salivary glands (grey line)**.** FACS plots representing expansion of ICAM-1^{hi}VCAM-1^{hi} and ICAM-1^{int}VCAM-1^{int} cells within CD45-EPCAM-CD31- component in WT mice salivary glands at day 5 p.c. **(Dii)** as compared to day 0 salivary glands **(Di)**. Time course of CD45-EpCAM-CD31- ICAM-1^{hi}VCAM-1^{hi} **(E)** and ICAM-1^{int}VCAM-1^{int} **(F)** cells following cannulation as determined by flow cytometry in cannulated WT mice at day 0, day 2, day 5, day 8 and day 15 p.c. Histogram **(G)** and graph **(H)** showing the MFI of gp38 on ICAM-1^{hi}VCAM-1^{hi}, ICAM-1^{int}VCAM-1^{int} and ICAM-1-VCAM-1- cells.

Figure 3.10.2

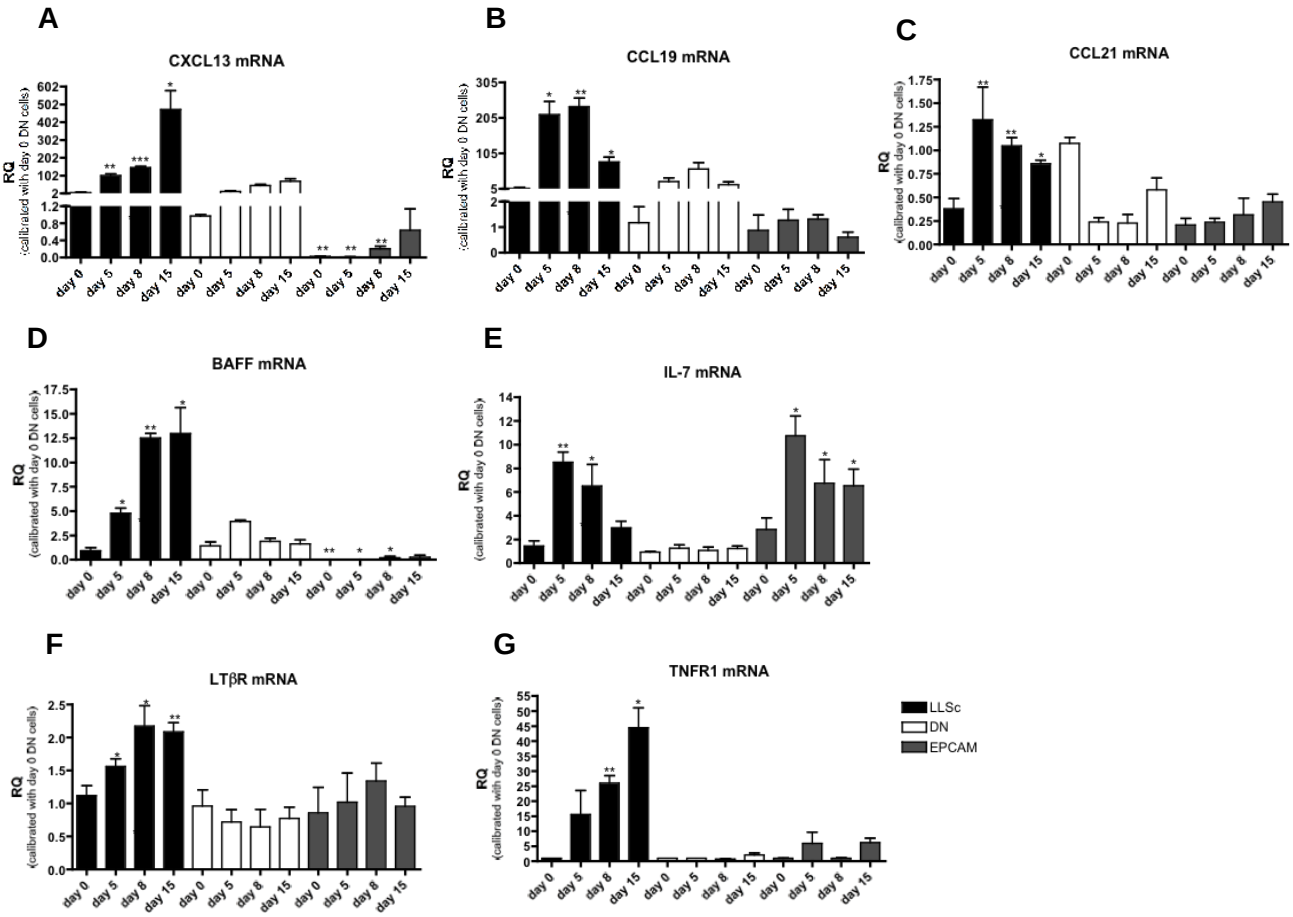

Figure 3.10.2 Phenotypical and functional analysis of Lymphoid like stromal cell (LLSc) in inflamed salivary glands. Expression of CXCL13 **(A)**, CCL19 **(B)**, CCL21 **(C)**, BAFF **(D)**, IL-7 **(E)**, LTβR **(F)** and TNFR1 **(G)** on sorted CD45-EpCAM-CD31-gp38+ cells (black bars) in comparison to CD45-EpCAM-CD31-gp38- cells (white bars) and CD45-EPCAM+ epithelial cells (grey bars). Transcripts encoding the indicated genes were quantified by quantitative RT-PCR and normalized to housekeeping gene β-actin. Relative quantitation (RQ) calculated with calibrator day 0 CD45-EpCAM-CD31-gp38- cells. Data are representative of two independent experiments with three mice per group. * $p < 0.05$; ** $p < 0.01$; unpaired t test.

3.11 LLSc expansion during the inflammatory process

In order to evaluate the changes occurring to the LLSc in the salivary glands post-infection, we performed FACS analysis of the single cell suspensions isolated from salivary glands at different time-points post cannulation **(Figure 3.11A-B)**. We observed a significant increase in the percentage of LLSc between 3 hours ($p<0.05$) to day 2 p.c. ($p<0.01$). The highest percentage of LLSc were observed at day 5 p.c. (over 40% LLSc are observed in the CD45-EPCAM- stromal component as compared to only 7% gp38+CD31- cells detected within the CD45-EPCAM- stromal compartment in a resting non-cannulated glands; $p<0.001$). Day 8 p.c. shows a deflection in percentage of this population compared to day 5, nevertheless, the gp38+LLSc are maintained between a percentage of 20-25% from day 8 to day 20 p.c. ($p<0.0002$). A gradual decline in percentage of LLSc is observed from day 23 p.c. which coincides with resolution of lymphoid aggregates. By day 26 p.c. the proportion of gp38+ fibroblasts detected in salivary glands is similar to day 0 salivary glands. Absolute number of LLSc was also determined at different time-points p.c., and it showed similar trend in LLSc expansion as mentioned above **(Figure 3.11C)**.

Figure 3.11

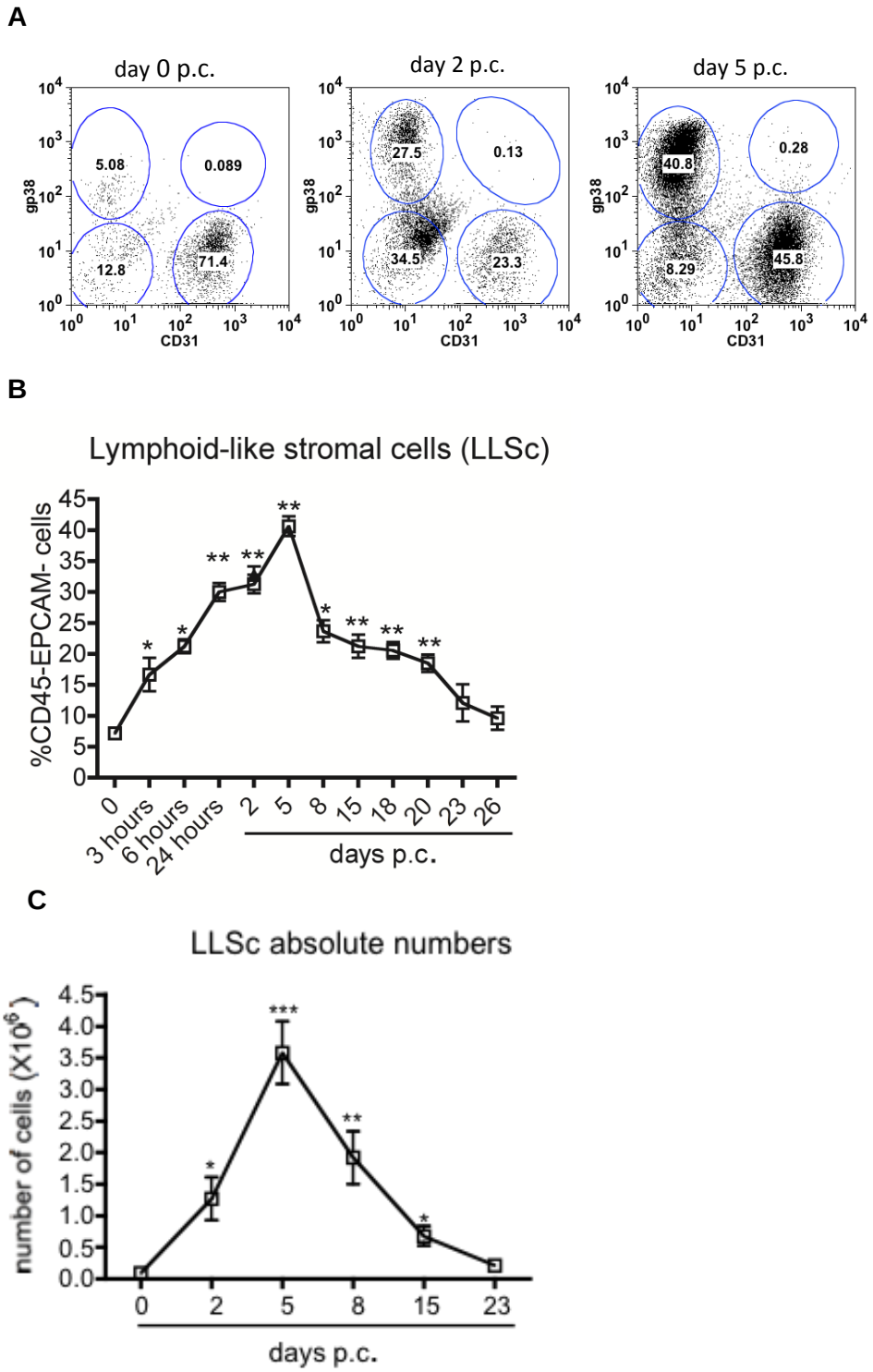

Figure 3.11 Dynamic of LLSc expansion during the inflammatory process. FACS histogram representing LLSc expansion in WT mice salivary glands at day 0, day 2 and day 5 p.c. **(A)**. Time course of the percentage **(B)** and absolute number **(C)** of CD45-EpCAM-CD31-gp38+ cells (LLSc) following cannulation as determined by flow cytometry in cannulated WT mice. Data presented as the mean ± s.e.m. of two-three independent experiments with at least two mice analysed per time-point. * $p < 0.05$; ** $p < 0.01$; *** $p < 0.001$, unpaired t test, comparing LLSc population at each time point with day 0 p.c.

3.12 Proliferative status of LLSc at different time-points post-cannulation

In order to study the proliferative status and understand the proliferating ability of the LLSc population, both Ki67 and BrdU staining was performed on the digested stromal cells from salivary glands at different time-points **(Figure 3.12A-C)**. This approach exploited the differences in the properties of the data obtained by Ki67 and BrdU staining, i.e that Ki67 only stains active proliferating cells whereas BrdU is incorporated in all proliferating cells, thus labelling both actively proliferating cells and also cells that have proliferated since BrdU was first administered to the mice. For the purpose of this experiment, mice were given BrdU water from day 0. Ki67 data **(Figure 3.12B)** exhibited that LLSc were undergoing active proliferation from as early as 3 hours p.c to day 15 p.c. ($p>0.01$-0.05) between 5-10% of LLSc were Ki67+. However, negligible percentage of cell showed Ki67 staining at day 23 p.c. which coincides with the resolution of inflammation in salivary glands. The BrDU staining **(Figure 3.12C)** demonstrated that LLSc were undergoing multiple rounds of proliferation and more than 50 percent of LLSc observed between day 2-day 15 p.c. ($p<0.001$-0.05) was derived from proliferation. The maximum proliferative activity is observed between day 2 and day 5 p.c. leading to expansion of LLSc compartment observed at day 5 p.c.

Figure 3.12

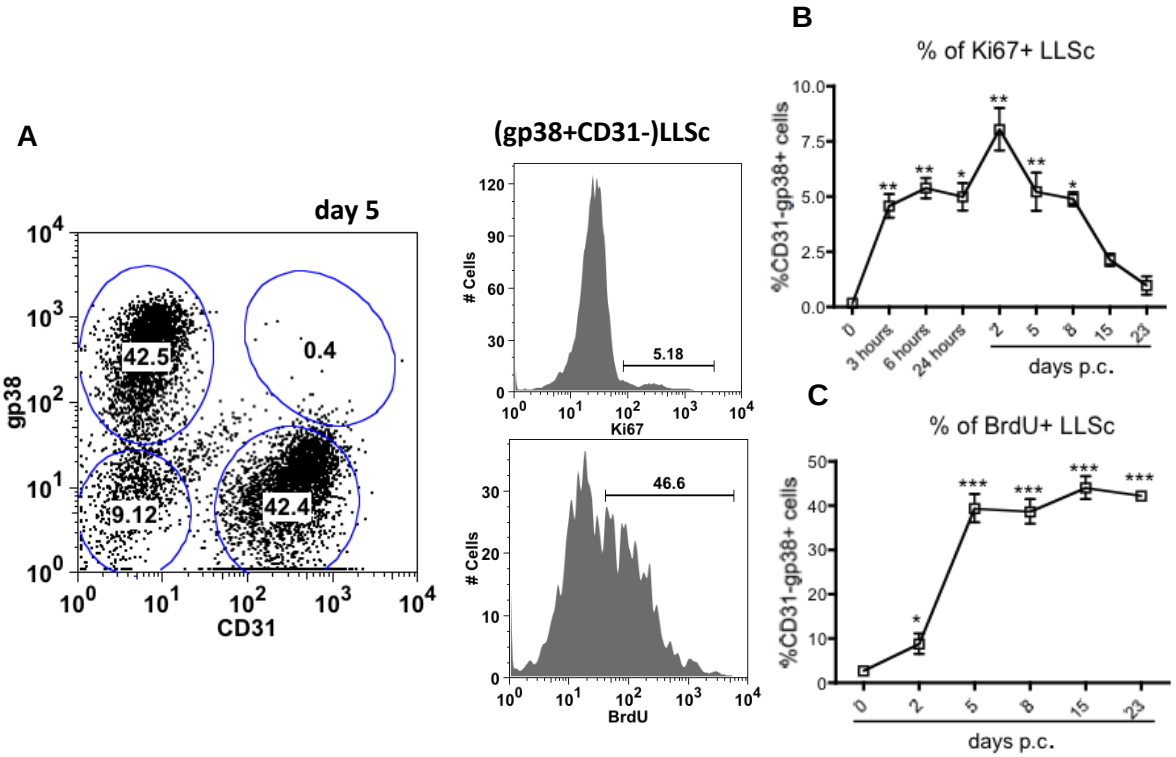

Figure 3.12 Proliferative status of LLSc at different time-points post-cannulation. FACS histogram representing Ki67+ **(Aii) and** BrDU+ **(Aiii)** LLSc in WT mice salivary glands at day 5 p.c. **(Ai)**. Graphs showing proliferation, both Ki67 **(B)** and BrdU **(C)**, of CD31-gp38+ (LLSc) in the CD45-EPCAM- cell population. ** $p < 0.01$, *** $p < 0.001$ versus day 0 wt mice. Data are from three to four independent experiments with two to four mice analysed per group.

Discussion

Current understanding of the fundamental cellular and molecular events that trigger and regulate the formation of TLOs in the salivary glands, is insufficient and restricted to cross-sectional analysis of salivary glands patients with Sjogren's Syndrome (SS) and spontaneous autoimmune prone murine models of exhibiting Sjogren's-like syndrome [237, 257, 258]. The most commonly used model to study SS is the NOD mice, which develop salivary gland inflammation that resembles many features of the human SS. However, this model has major limitations which prevent its use to address functional aspects of ectopic lymphoid neogenesis. Firstly, the onset of disease in NOD mice is quite variable, i.e. not all mice develop the disease at the same age. Secondly, the penetrance of disease is not one hundred percent i.e. not all mice develop the disease. Thirdly, it's a spontaneous model of autoimmunity, where the exact triggers of disease are unknown. Finally, NOD mice have a complex genetic background, hence, crossing these mice with other mice strains, such as knockout mice for inflammatory genes, is not easy and this limits the feasibility to study role of specific genes in these mice. When SS is studied in NOD mice, it is important to take in consideration the presence of type 1 diabetes. All mice develop diabetes by 15 weeks of age, and thus the highly activated inflammatory environment provides additional confounding factors to study and manipulate the disease process in NOD mice [259-262].

Other models of SS are dependent on transgenic expression of inflammatory cytokines, such as IL-14 and BAFF [259-262]. Additional models of inducible salivary gland inflammation, that share some features of SS, have been reported. Nonetheless, these models rely either on the use of replication-deficient adenovirus vectors harbouring pro-inflammatory genes [237, 263] or infection of autoimmune prone mice (such as *lpr/lpr* mice) with fully infectious and replicating sialotropic viruses [237, 264, 265]. The dependence of these models on pro-inflammatory mediators or autoimmune prone mice prevents the study of the inflammatory process in physiological settings. Additionally, to our knowledge, models using viral induced inflammation do not provide a clear demonstration as to whether they can progress towards

the formation of functional TLOs and exhibit the main characteristic of SS, which is the formation of autoantibodies [237]. Furthermore, in humans it is unethical to perform a dynamic evaluation of the cellular and molecular mechanisms involved in the formation of ectopic lymphoid structures, and thus AN understanding of the role played by stromal cells in this process is prevented by the impossibility of performing repeated biopsies from a patient or other functional studies in vivo. Therefore, in order to overcome this limitation, we developed a mouse model of inducible salivary gland inflammation [237].

The work presented in this chapter established that upon delivery of replication-deficient AdV vector, directly into the salivary glands of wild-type mice, a true phenomenon of ectopic lymphoneogenesis occurs within virus infected salivary glands which resemble SS. In this model, immune cell infiltration rapidly progresses from a diffuse inflammatory process towards the formation of periductal lymphocytic aggregates which further evolve into highly organised TLOs. This process is highly reproducible and synchronous with the lymphocytic foci development in one hundred percent of the mice by day 5 p.c. It evolves between 8-15 days p.c. into fully formed TLOs characterized in over 70% of mice by T/B cell segregation, and formation of FDC-M1 and GL-7 positive GC-like structures displaying high similarity to the human counterpart SS patient salivary glands [178, 180, 237]. The development of FDC was exclusively present within the B cell area and associated with the presence of segregation of T and B cells in distinct areas.

In this chapter, we also showed that post-virus infection, there is early up-regulation of lymphoid chemokines CXCL13, CCL19, and CCL21 mRNA which precedes the development of TLOs, and their expression peaks in parallel with full acquisition of lymphoid organization of lymphocytic foci. Lymphoid chemokines retained their distinct expression pattern observed in secondary lymphoid tissues, with CXCL13 confined to the B cell-rich areas of the lymphoid aggregates and CCL21 in the surrounding T cell area and lymphatic vessels [3, 237]. During embryonic secondary lymphoid organogenesis, the expression of lymphoid chemokines CXCL13, CCL19 and CCL21 by VCAM-1+ICAM-1+LTβR+ mesenchymal “organizer” (LTo) is

chiefly dependent on LTβR/LTα1β2 signalling axis. This signal establishes a positive feedback loop between lymphoid chemokines and LTβ which is absolutely crucial in promoting further immune cell recruitment and development of mature LNs [11, 36]. Consistent with this evidence, we showed that LTβ and LTα are significantly up-regulated in parallel with CXCL13/CCL19 induction, suggesting that LT/chemokine positive feedback loop is active within salivary glands during TLO formation [160].

In our model, despite the detection of FDC-M1+ reticular staining in the B cell zone, the FDC structures did not display the typical FDC network pattern observed in SLOs. In SLOs it has been demonstrated that B cells and sustained B cell-derived LT/TNF is important for formation and maintenance of FDC networks [144, 266] However, in our model major B cell infiltration is only detected between day 8-day 15 p.c. and resolution of lymphocytic structures is observed from day 23 onwards Therefore, we hypothesize that the late and transient B cell-derived LT/TNF signal, present in the salivary gland, is not sufficient to allow full formation of FDCs.

TLO have been shown to support functional B cell activation with expression of AID, the enzyme which initiates somatic hypermutation (SHM) and class switch recombination (CSR) of the Ig genes [194, 267], leading to affinity maturation and differentiation of memory B and plasma cells [155, 156, 268]. We demonstrated that in our model, increased expression of AID in the salivary glands coincided with the formation of TLOs acquiring markers of germinal centres such as FDC networks and GL7. Of relevance, ectopic induction of AID associated with the expression of several cytokines such as BAFF, IL-21 and IL-4, known to support a germinal centre reaction by enhancing B cell survival and promoting AID expression in B cells. [154-156, 269]. Moreover, both plasmablasts and plasma cells were detected in cannulated salivary glands. Overall, the data demonstrates that following AdV infection, TLOs acquire the molecular machinery required for the development of functional niches for B cell activation.

Because the cellular and molecular features of TLO in this model were remarkably similar to those observed in SS [18, 178, 180, 183], we looked for the presence of circulating autoantibodies [178, 237, 270, 271]. Of interest, at week 3 pc, sera from 75% of the AdV-cannulated mice showed positivity for IgG anti-nuclear autoantibodies (ANA) [237]. The presence of these circulating antibodies in the blood of the cannulated animals indicates the possibility of breakage of tolerance, likely by exposure of nuclear material in the context of the formation of TLOs with active GCs in the salivary glands. The possibility of *in situ* production of anti-viral antibodies and ANA is currently under investigation. We suspect this to be the case since the ectopic GCs seem to possess the machinery for their active function [194, 237].

Altogether, the data demonstrates that this inducible model of TLO formation, during salivary gland inflammation, is a suitable tool to dissect the dynamic and hierarchical significance of the critical factors regulating stromal cell activation, thus, allowing us to better understand functional relevance of this phenomenon during TLO formation in vivo.

It is increasingly becoming clear, that non-lymphoid tissue stromal cells are not merely sessile bystanders during an inflammatory response*s,* but many factors, such as chemokines, cytokines, that we detect in TLO-associated inflammatory disease are derived from these non-hematopoietic stromal cells [1, 222, 248]. In physiologic lymphoid organs, gp38+ lymphoid stromal cells secrete factors and chemokines that are responsible for leukocyte organization, survival and function [6]. Large body of evidence indicates towards presence of lymphoid-like stromal cells at the site of inflammation [76, 159, 160, 177-179, 185, 226, 248, 249]. However, formal realization came from the work of Peduto et al., who demonstrated that during inflammation, the tissue-resident fibroblasts acquire the phenotypical and functional ability of lymphoid stromal cells that allows recruitment and organized aggregation of lymphocytes inside tissue target of inflammatory processes [226]. These cells were identified and isolated by their expression of gp38. However, currently none of the studies provide the dynamic of stromal cell activation during inflammatory process and

moreover the identity of signal/s regulating this pathological conversion of tissue resident fibroblasts is still obscure.

This chapter also examined the presence of lymphoid-like stromal cells and ascertains a dynamic of stromal cell activation during TLO formation. gp38 or podoplanin is a stromal cell marker, expressed on specialized stromal cells present in secondary lymphoid organs [1, 226, 272, 273]. On resting conditions fibroblasts in non-lymphoid organs express only negligible amount of gp38, while EpCAM+ salivary glands and kidney epithelial cells, alveolar cells in the lung and lymphatic vessels, express intermediate/high level of the molecule [255, 274-277]. In accordance with previous reports, gp38 was found to be expressed on epithelial (EPCAM+) cells in resting salivary glands by histology. However, enrichment of gp38+EPCAM-CD31- cells within the inflamed salivary glands was observed as soon as inflammation was established at day 5 p.c. This population of gp38+EPCAM-CD31- cells was observed mainly within the foci. Further histological characterization also showed acquisition of other lymphoid stromal cell markers such as ICAM, VCAM, ER-TR7 on these cells. This data supports the classification of gp38+ cells within the aggregates as lymphoid like stroma. Moreover, an increase of gp38 expression, in relationship with the size of the lymphoid aggregates, was also observed, and which is a clear indication of the cross-talk between haematopoietic and stromal cell compartment.

FACS analysis of collagenase digested salivary gland tissue demonstrate that the earliest phases of TLO formation are characterized by the differentiation of a gp38+ (non-hematopoietic, non-endothelial and non-epithelial) stromal cell component that progressively acquires lymphoid associated markers (ICAM-1, VCAM-1, gp38) and precedes lymphocyte accumulation and LTβ up-regulation within the tissue. This is followed by a rapid expansion and maturation phase of gp38+ fibroblasts that coincides with increased influx of lymphocytes and LT expression. During this period an increase in gp38+ stromal cell numbers and up-regulation of lymphoid chemokines and cytokines expression is observed in the stromal cells.

This is in agreement with reports on lymphoid stromal cells during organogenesis or immune response. Peduto et al, has also reported that the induction of gp38+ cells in the LN anlage precedes LTi arrival or LTβR signalling [226]. Furthermore, Benezech et al., demonstrated that early maturation of the embryonic mesenchyme into lymphoid tissue stromal organizer cells requires a dual step. Initial expression of ICAM-1 and VCAM-1 at intermediate levels, a process that is lymphotoxin β (LTβ) independent and a second stage, in which small aggregates of RORγt dependent lymphoid tissue inducer cells (LTi) [46] provide the LTβR+ mesenchyme with LTβ, favouring integrin up-regulation and stabilization of the aggregates [66]. This is followed by secretion of CXCL13, CCL21, CCL19 and CXCL12, that drive leukocyte recruitment, inducing further stromal cell maturation and establishment of the anlagen [278, 279]. In adult LNs, during an immune response, FRCs are rapidly activated within hours after the onset of inflammation and is independent of lymphocytes and LTβ. Of notice, a strong increase in gp38 expression on FRC was detected within few hours post-infection in these LNs but no change in transcript levels of IL-7, CC19 and CCL21 was observed [280].

Collectively, using this mouse model of TLO formation, we have demonstrated pathogenic transition of tissue stromal cells during the establishment of TLOs. We have shown that tissue fibroblasts acquire markers such as gp38, ICAM-1, VCAM-1, RANK-L, MadCAM-1 and LTβR and are able to respond to LTβ stimulation, up-regulating CXCL13, CCL19, IL7 and BAFF. This population of (EPCAM-CD45-) CD31-gp38+ cells recapitulates phenotypically and functionally the population of fibroblastic reticular cells (FRC) found in the lymph node T-cell zone. However, as these stromal cells also share features with follicular dendritic cells (FDC) and marginal zone reticular cells (MRC) [6], we have referred to them as lymphoid-like stromal cells (LLSc).

Our observations using this model suggests that the acquisition of LLSc can be split into three distinct but overlapping phases; (i) induction phase (day 0-2-p.c.), (ii) expansion phase (day 2-5 p.c.) and (iii) maturation/maintenance phase (day 5-15 p.c.). The next three

chapters will explore the signals that regulate these different phases of stromal cell activation.

.

Chapter 4

Unexpected role of IL-13 and IL-4 in regulating tissue-resident stromal cells in the induction phase of TLO formation

Introduction

The previous chapter clearly demonstrated that during TLO formation, otherwise quiescent, tissue resident stromal cells undergo dramatic changes, which enable them to acquire stromal lymphoid features and functions which could contribute to regulate the formation and maintenance of TLOs. However, little is known about the cell/s and signalling pathway/s involved in the transition of normal resident mesenchyme stromal cells towards a lymphoid like/pathological phenotype. A role for IL17 has been suggested in the context of stromal cell activation in a neonatal model of TLO formation in the lung [214]. In this study IL-17 was demonstrated to induce the expression of lymphoid chemokines in isolated pulmonary fibroblasts. However, the inability to reproduce this model in adult mice has questioned the role of IL17 in post-natal TLO formation, where normal bacterial flora inhabit the mucosal target site [281]. Fleige *et al*., reported normal iBALT development in *il17ko* mice upon intra-nasal challenge with replication-deficient poxvirus modified vaccinia virus ankara (MVA) [282]. Further data on the role of IL17 in TLO formation has been provided in an elegant study [283] from Peters *et al*., which established the requirement of gp38+ Th17 cells for EAE development in the brain. In our model, LLSc expansion precedes T cell infiltration, suggesting that Th17 lymphocytes are not involved in early LLSc induction. Despite the controversy, these findings suggest a new and fascinating paradigm of how ectopic organogenesis can be driven by an inflammatory cytokine as opposed to lymphoid cytokines, such as LT, which is the central cytokine in secondary lymphoid organogenesis.

Preliminary data, generated by our collaborator M. Coles in York, revealed that when human adipocyte derived stromal cells (ADSCs) are stimulated with IL-4Rα agonist cytokines IL-4 or IL-13, a significant increase in lymphoid stromal cell markers gp38, ICAM and VCAM was observed as compared to classical TNF/LTβR agonist stimulation. This suggested that IL4-R

signalling in adult mesenchyme has a role in lymphoid stroma specification (Mark Coles, Personal communication). Recent work has also shown that type 2 cytokine activity is able to modulate mesenchyme differentiation in muscle or adipose tissue upon injury [284]. Two different forms of IL4R have been documented, classical and alternative. Classical IL4R is composed of IL4α and IL-2Rγ chains and is predominantly expressed by hematopoietic cells, whereas the alternative form of the IL4R consists of IL4Rα and IL13Rα and is primarily expressed by non-hematopoietic cells, such as human skin and lung fibroblasts, as well as non-hematopoietic cancer cell lines such as A431, PA-1 and HT-29 [285-288]. IL-13Rα1 has been shown to be expressed on B cells, especially GC B cells and peritoneal macrophages in mice [289].

IL4Rα staining has been reported on human LN FRC networks [290]. Moreover, expression of IL-13Rα1 has been described on follicular dendritic networks (FDCs) in murine LNs and is suggested to be involved in increased production of IL-6 from FDCs, which is important for terminal differentiation of GC B cells [289]. While there is no reported function of IL-4 and IL-13 in conventional secondary lymphoid organogenesis, these cytokines are able to trigger expression of the adhesion molecules VCAM-1 and ICAM-1 in human lung fibroblasts [287]. These data suggest a fascinating possibility that, during inflammation, expression of IL-4Rα targeting cytokines might be involved in stromal cell reprogramming to a lymphoid-like phenotype. We therefore explored whether the IL-4/IL-13 axis might play a role in the induction phase of TLO formation.

Results

4.1 Direct administration of IL-4Rα signalling cytokines regulates LLSc induction in salivary glands

To evaluate in vivo the effect of IL-13 and IL-4 directly on stromal cell activation, recombinant (r) cytokine IL-13, IL-4 or TNFα+LTβR agonist were cannulated into the salivary glands. A 30% increase ($p<0.001$) in the LLSc component was observed in the rIL-13 cannulated salivary glands when compared to PBS cannulated salivary glands **(Figure 4.1A-B)**. Increase in the LLSc by 20% ($p<0.05$) and 15% ($p<0.05$) were observed when rIL-4 and rTNFα+LTβR agonist were directly administered into salivary glands respectively **(Figure 4.1A-B)**. Furthermore, MFI data exhibited a greater increase in the gp38 expression on LLSc when salivary glands were cannulated with rIL-13 as compared to PBS ($p<0.001$). An increase in gp38 expression was also observed in rIL-4 and rTNFα+LTβR agonist cannulated salivary gland but it was lower ($p>0.05$) to that detected on LLSc in rIL13 treated glands **(Figure 4.1C)**. When ICAM-1 and VCAM-1 expression was examined in the rIL-13, rIL-4, rTNFα+LTβR agonist and PBS treated salivary glands, we observed induction of 11% ($p<0.01$), 5% ($p<0.01$), 6% ($p<0.01$) and 1% of ICAM-1^{hi}VCAM-1^{hi} cells **(Figure 4.1D)**. The percentage of ICAM-1^{int}VCAM-1^{int} cells **(Figure 4.1E)** was 55% ($p>0.01$), 43.1%, 50% ($p>0.05$) and 32% in the rIL-13, rIL-4, and rTNFα+LTβR agonist and PBS cannulated mice respectively. The induction of ICAM-1 and VCAM-1 was significantly higher ($p>0.05$) in the rIL-13 treated glands compared to rIL-4 and rTNFα+LTβR agonist treated salivary glands **(Figure 4.1D-E)**.

This data clearly indicates a role for IL-4R signaling, mainly via IL-13 and only partially by IL-4 stimulation, in induction of lymphoid stroma *in vivo*.

Figure 4.1

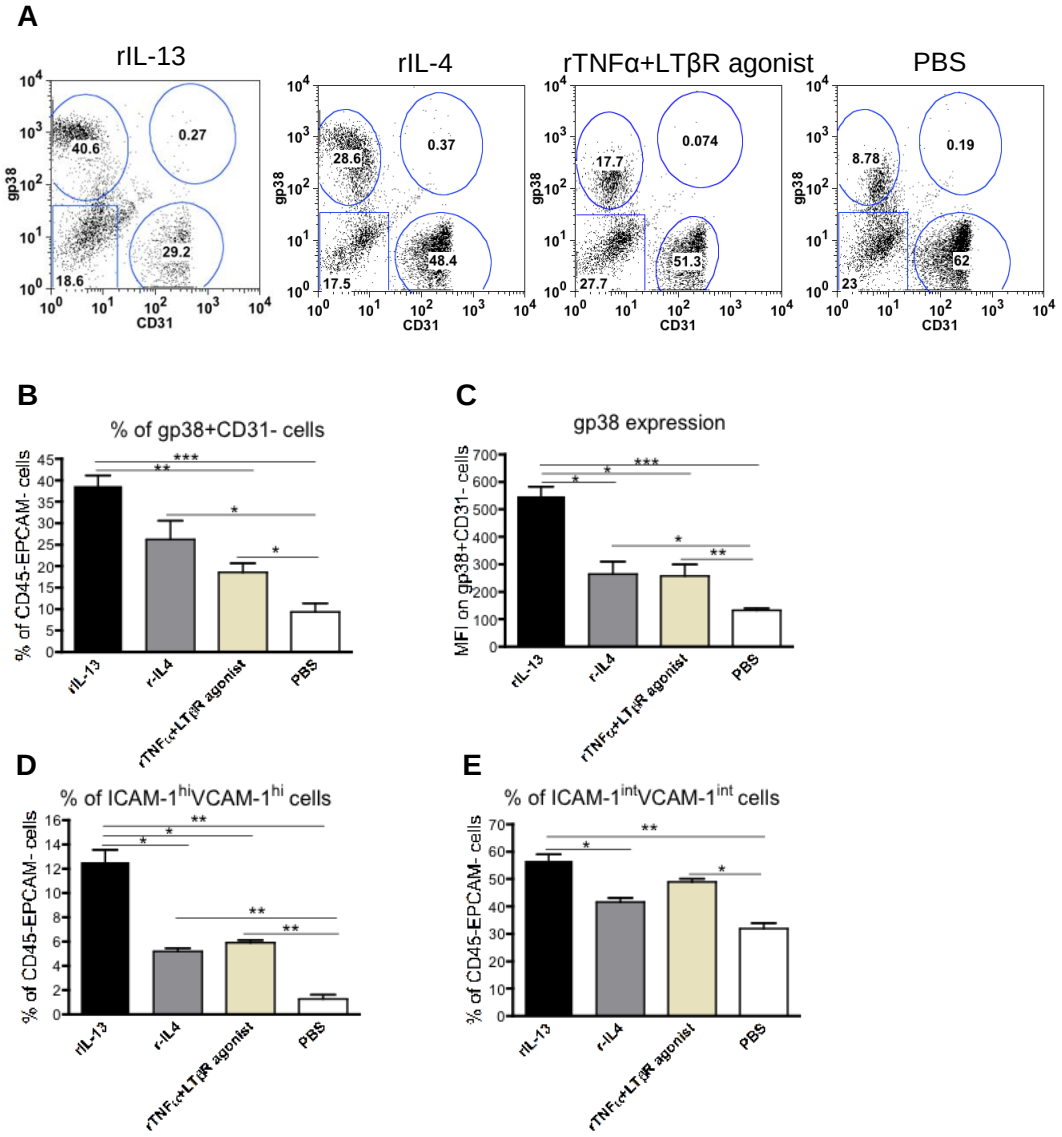

Figure 4.1 Direct administration of IL-4Rα signaling cytokines regulates LLSc induction in salivary glands. WT mice salivary glands were directly cannulated with IL13, IL4 recombinant cytokine or recombinant TNFα +LTβR agonist (rIL13, rIL4 or rTNFα +LTβR agonist) or PBS and analysed at day 2 p.c. Representative dot plots showing expansion of the epcam-cd45-component post treatment with rIL13, rIL4, TNFα +LTβR agonist or PBS. Graphs summarising flow cytometry results, demonstrating increased frequency of the epcam-cd45-cd31-gp38+ cells **(B)** and increased gp38 expression (shown as MFI values) on epcam-cd45-cd31-gp38+ cells **(C)** in the recombinant *il13*, *il4 or* TNFα +LTβR agonist cannulated samples compared to recombinant PBS control. *, $p < 0.05$; ***, $p < 0.001$; versus *PBS* cannulated mice. Data are representative of two experiments (two to three mice per group). Graphs summarising percentage of VCAM-1^{hi}ICAM-1^{hi} cells **(D)** and VCAM-1^{int}ICAM-1^{int} cells (**E**) obtained by flow cytometry in the recombinant *il13, il4 or* TNFα +LTβR agonist cannulated samples compared to recombinant PBS control. Data is representative mean of two independent experiments (two to three mice per group); * p<0.0.5; **, p<0.01.

4.2 LLSc, DN stromal cells and epithelial cells express IL4R

The next important question was to determine which stromal cell subsets are capable of responding directly to IL4R signaling, both in resting and cannulated salivary glands. In order to asses this, IL4Rα and IL13Rα gene expression was studied on isolated LLSc, DN stromal cells and epithelial cells. The mRNA data showed that LLSc and epithelial cells express higher transcript levels of IL-4Rα **(Figure 4.2A)** and IL13Rα **(Figure 4.2B)** at day 0 when compared to DN stromal cells. A further increase was observed in the expression of IL-4R chains on LLSc and epithelial cells post-cannulation, particularly day 2 p.c. **(Figure 4.2A-B)**. FACs analysis for IL-4Rα was performed to analyze the protein expression of the receptor on non-hematopoietic cells in resting salivary glands **(Figure 4.2C)**. Salivary glands from il4rαko were also stained to confirm specificity of the antibody. No staining for IL4Rα was observed in the ko mice **(Figure 4.2D)**. All three CD45- components, LLSc, DN and epithelial cells, expressed the receptor at day 0, however at day 2 p.c. a 4.5 fold increase in the IL4Rα+LLSc ($p>0.01$) and ~2–fold increase in IL4Rα+EPCAM+ (epithelial) cells was observed, whereas no increase was identified in IL4Rα+DN cells **(Figure 4.2E)**.

Overall, this data suggested that the non-hematopoietic cells in salivary gland have the machinery to respond to an IL-4R signal.

Figure 4.2

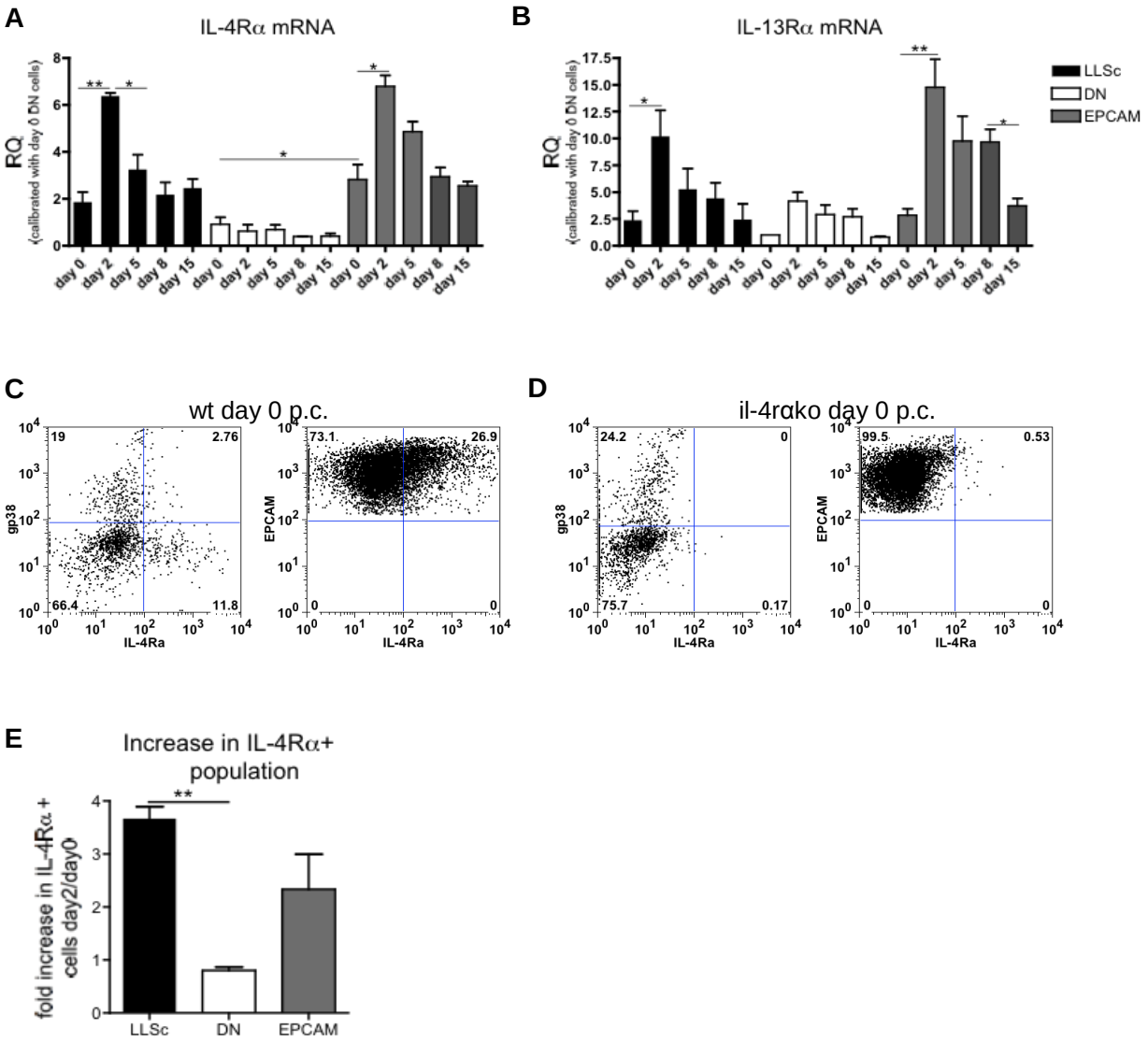

Figure 4.2 LLSc, DN stromal cells and epithelial cells express IL4R. IL4Rα transcripts **(A)** and IL-13Rα **(B)** on FACS sorted gp38+CD31-LLSc (black bars) in comparison to gp38-CD31- double negative cells (DN, white bars) and CD45-EPCAM+ (epithelial) cells (grey bars). Transcripts were assessed by quantitative RT-PCR and normalized to housekeeping gene β-actin. Relative quantitation (RQ) calculated with calibrator day 0 DN cells. Data expressed as mean ± s.e.m of two independent experiments with two-three mice per group. *, $p<0.05$; **, $p<0.01$ unpaired t test, comparing LLSc with DN at each time point. Representative dot plots showing flow cytometry for IL-4Rα+ cells in the CD45-EPCAM+ (epithelial) cells and CD45-EPCAM-CD31- stromal component component at day 0 p.c. salivary glands in wt **(C)** and *il4rαko* **(D)**. Graph representing flow cytometry data for IL4Rα expression **(E)** on LLSc (black bars), DN (white bars) cells and EPCAM+ (epithelial) cells (grey bar) from wt mice showing selective expansion of IL4Rα+gp38+ cells at day 2 p.c. as compared to day 0. Data representative of three different experiments with atleast two mice per group, expressed as mean ± s.e.m **, $p<0.01$.

4.3 IL-4 Receptor engagement is required for LLSc induction

To investigate whether IL-4Rα is involved in LLSc induction and formation, the salivary glands of *il4rαko* and *wt* mice were cannulated and the dynamic of LLSc was examined in these mice. As expected, wt mice showed an increase of nearly 15% in the LLSc component at day 2 whereas *il4rαko* were unable to increase the LLSc. The percentage of LLSc detected at day 2 in the *il4rαko* mice was analogous to the small population of LLSc generally observed at day 0. This significant defect ($p<0.01$) in LLSc induction was maintained until day 5. Surprisingly, it was restored from day 8 onwards **(Fig 4.3A-B)**. A defect in LLSc induction was further confirmed by failure of *il4rαko* mice to form ICAM-1^{high}VCAM-1^{high} cells and reduction in ICAM-1^{int}VCAM-1^{int} stromal cells compared to *wt* mice. Salivary glands of day 2 p.c. *il4rαko* showed baseline percentage ~1.5% of ICAM-1^{high}VAM-1^{high} ($p<0.01$) whereas wt mice displayed ~8% of these cells in the CD45-EPCAM-CD31- stromal compartment. In addition, a decrease from 56.2% of ICAM-1^{int}VCAM-1^{int} stromal cells in wt mice to 44.1% in *il4rαko* was observed at day 2 p.c. **(Fig 4.3C-D)**.

In order to asses, if the decrease in the LLSc that was observed in the *il4rαko* mice was due to their inability to proliferate, we performed BrdU and Ki67 staining on the LLSc from *il4rαko* and *wt* mice. The *il4rαko* mice showed a normal increase in proliferation at day 2, ~20% LLSc were BrdU+ and ~12% were Ki67+ in contrast to ~15% BrDU+ and ~8% Ki67+ LLSc in *wt* mice. The proliferation status of the LLSc in *il4rαko* mice was comparable to that of *wt* mice at all other time points **(Fig 4.3E-F)**. This data suggested that IL4Rα engagement is not crucial for the LLSc proliferation but clearly important for the induction of LLSc at the site of inflammation.

Figure 4.3

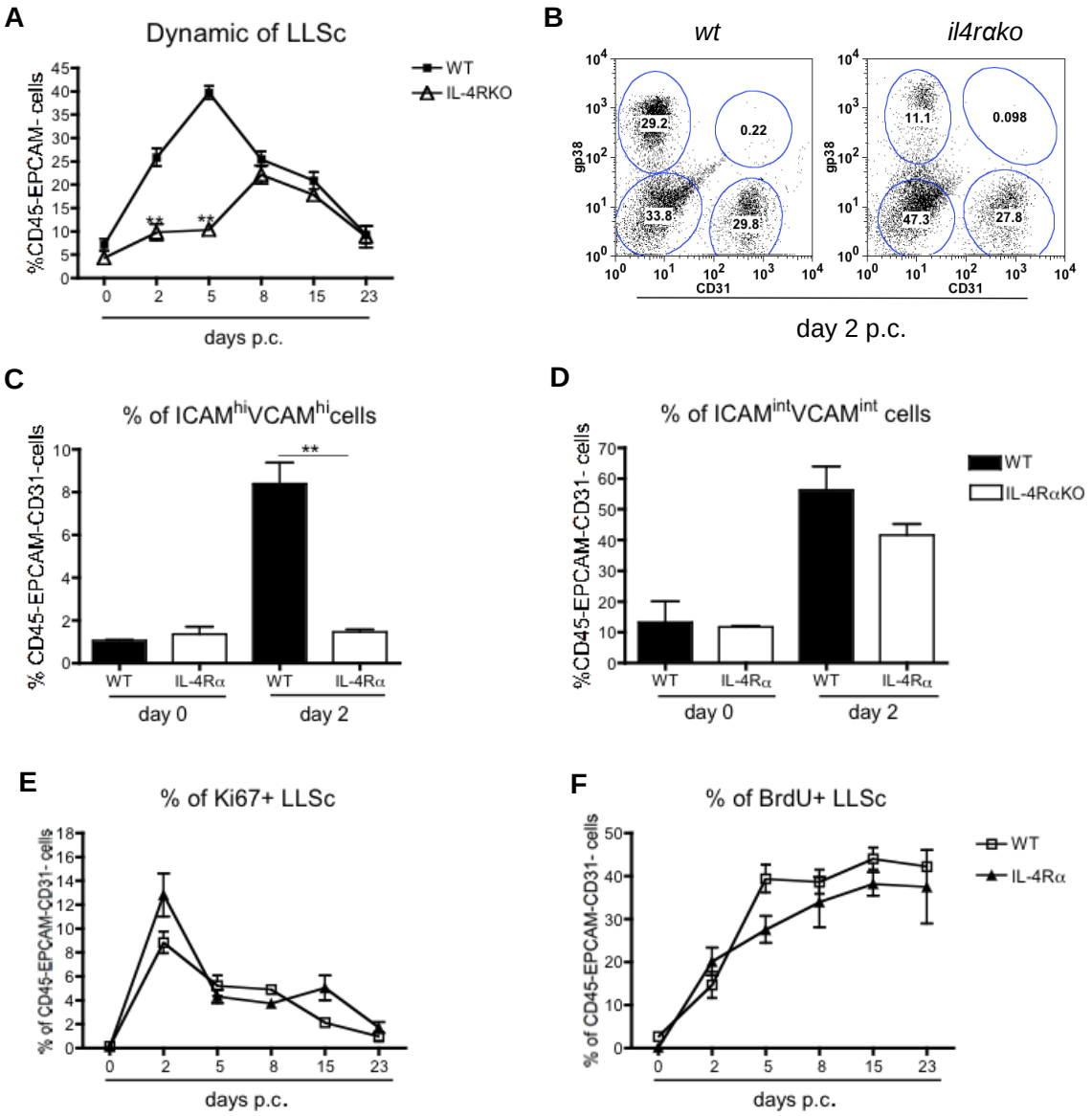

Figure 4.3 IL-4 Receptor engagement is required for LLSc induction. *A*, Dynamic of LLSc expansion during the inflammatory process determined by flow cytometry (percentage of gp38+CD31- population in the CD45-EPCAM- component) from infected *wt* (black squares)*and il4rako* (open triangles) mice at 0, day 2, day 5, day 8, day 15, day 23 p.c. Data is representative of two-three independent experiments with atleast two mice per group. **, p<0.01, unpaired t test, comparing *ko* LLSc population at each time point with corresponding *wt* LLSc population**. B,** Representative dot plots showing flow cytometry for percentage of gp38+CD31- population in the CD45-EPCAM- component from day 2 p.c. salivary glands in wt and *il4rako*. **C-D**, Flow cytometry of VCAM-1 and ICAM-1 expression in CD45-EPCAM-cells from salivary glands of *wt* and *il4rako* mice. The graphs show percentage of VCAM-1^{hi} ICAM-1^{hi} cells **(C)** and VCAM-1^{int} ICAM-1^{int} cells **(D)** obtained by flow cytometry on day 0 and day 2 p.c. salivary glands from *il4rako* mice (white bars) in comparison to wt mice (black bars). Data is representative mean of two independent experiments; **, p<0.01. **E-F**, Flow cytometry to show dynamic of Ki67+ LLSc **(E)** and BrDU+ LLSc **(F)** in wt (open squares) and *il4rako* (black triangles) mice from day 2, day 5, day 8, day 15 and day 23 p.c. salivary glands. . ∗, p<0.05; ∗∗, p<0.01, versus virus cannulated wt mice. Data are representative of two to three experiments with atleast two mice per group.

4.4 IL-4 signalling via IL-4R is not fundamental for LLSc induction but critical for its maintenance

To ascertain the role of IL-4 in induction of LLSc via IL4Rα engagement, *il4ko* mice salivary glands were cannulated and FACS analysis for the LLSc was performed in comparison to *wt* mice. The *il4ko* showed intact LLSc induction until day 5. However, at day 8 and day 15 a significant reduction ($p<0.05$) of ~15% was observed in the LLSc percentage in *il4ko* compared to *wt* mice **(Figure 4.4A-B)**. This data indicates that IL-13 and not IL-4 is responsible for the early induction defect observed in the *il4rαko* mice. Conversely, IL-4 appears to play a role in maintenance of LLSc.

The involvement of IL-13 and not IL-4 in induction of LLSc was also confirmed by PCR, performed to detect IL-4 and IL-13 gene expression in the whole salivary gland at all time-points post-cannulation. Significant IL-13 mRNA level was detected as early as 3 hours p.c. ($p<0.05$) whereas mRNA for IL-4 was detected ($p<0.01$-0.05) only from day 5 onwards **(Figure 4.4C-D)**.

Figure 4.4

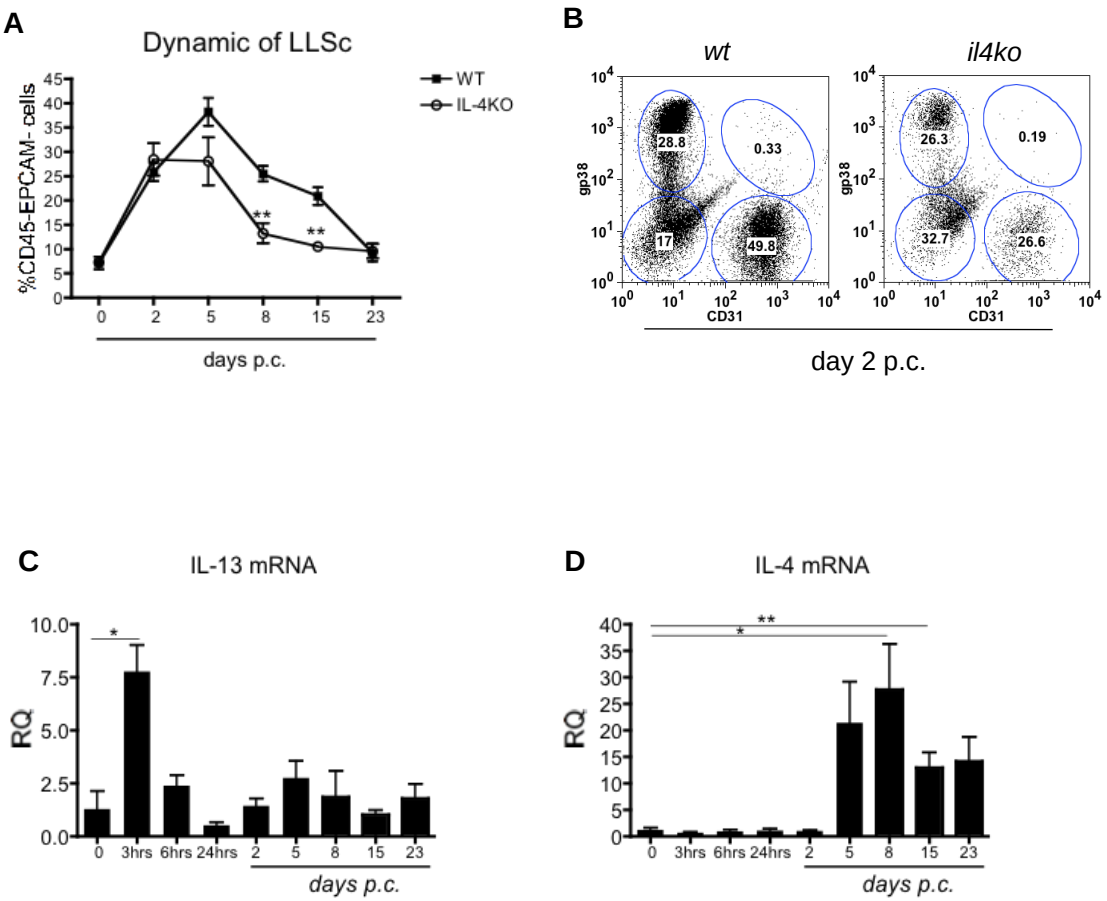

Figure 4.4 IL-4 signalling via IL-4R is not fundamental for LLSc induction but critical for its maintenance. Dynamic of LLSc expansion **(A)** during the inflammatory process determined by flow cytometry (percentage of gp38+CD31- population in the CD45-EPCAM- component) from infected *wt* (black squares) *and il4ko* (open circles) mice at 0, day 2, day 5, day 8, day 15, day 23 p.c. Data is representative mean of five independent experiments. **, $p < 0.01$, unpaired t test, comparing *ko* LLSc population at each time point with corresponding *wt* LLSc population**.** Representative dot plots **(B)** showing flow cytometry for percentage of gp38+CD31- population in the CD45-EPCAM- component from day 2 p.c. salivary glands in wt and *il4ko*. **C-D** Quantitative RT-PCR analysis of mRNA transcript for IL-13 **(C)** and IL-4 **(D)** in *wt* mice at day 0, 3hours, 6 hours, 24 hours, day 2, 5, 8, 15 and 23 post cannulation (p.c.). Transcripts were normalized to housekeeping gene β-actin. The relative expression values were calibrated to day 0 p.c. salivary gland values. Data are representative of three experiments with two to three mice analysed per group.

4.5 LLSc induction during inflammation is dependent on IL-13

To validate our hypothesis that IL-13 is crucial for LLSc induction, we cannulated the salivary glands of *il13ko* mice. *il13ko* mice displayed exactly the same phenotype **(Figure 4.5A-B)** in LLSc induction that was observed in cannulated salivary glands of the *il4rαko* mice. The percentage of LLSc at day 2 **(Figure 4.5B)** and day 5 showed no increase, as compared to *wt* salivary glands ($p<0.01$) where a progressive increase in this population was observed. Interestingly, an increase in the percentage of LLSc was observed from day 8 onwards, **(Figure 4.5A)** similar to *il4rαko* mice. Overall, these results establish the central role of IL-13 signalling via IL-4Rα in early induction of lymphoid like stromal cells during TLO formation.

Figure 4.5

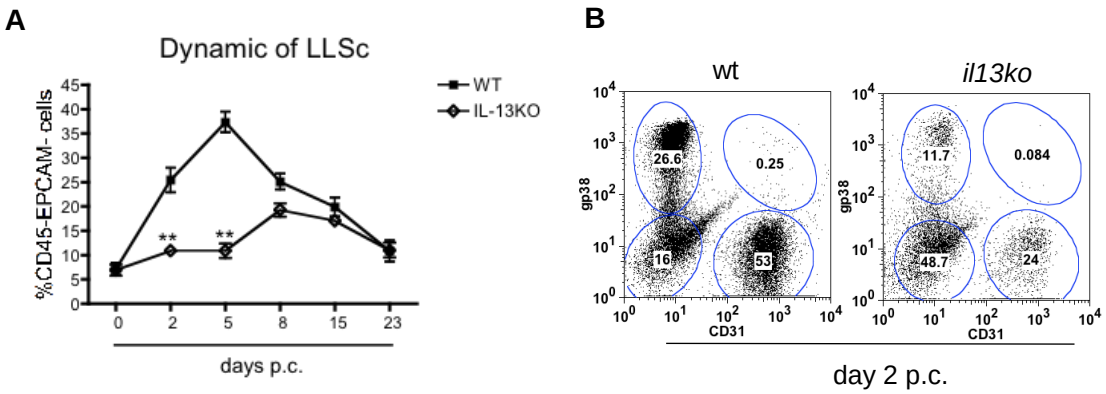

Figure 4.5 LLSc induction during inflammation is dependent on IL-13. Dynamic of LLSc expansion **(A)** during the inflammatory process determined by flow cytometry (percentage of gp38+CD31- population in the CD45-EPCAM- component) from infected *wt* (black squares) and *il13ko*(open triangles) mice at 0, day 2, day 5, day 8, day 15, day 23 p.c. Data presented as means of five independent experiments. **, $p<0.01$, unpaired t test, comparing *ko* LLSc population at each time point with corresponding *wt* LLSc population**.** Representative dot plots **(B)** showing flow cytometry for percentage of gp38+CD31- population in the CD45-EPCAM- component from day 2 p.c. salivary glands in wt and *il13ko*.

4.6 Different leukocyte cell subpopulations are responsible for IL13 production in inflamed salivary glands

In order to investigate the cellular source of IL13 in the inflamed mouse salivary glands we examined leukocytes from digested salivary glands at 3 hours, day 2 and day 5 p.c. A large number of IL13 producing cells were found at 2 hours p.c. **(Figure 4.6A-B)**. We found that the largest source of IL13 production at 3 hours p.c. was mainly innate lymphoid cells (ILCs). By day 5 p.c. this was mostly produced by T lymphocytes. Other cell populations responsible for early IL13 production were CD11b+Gr1+ cells, CD11c+ cells and CD3+CD11c+ cells **(Figure 4.6C)**.

Figure 4.6

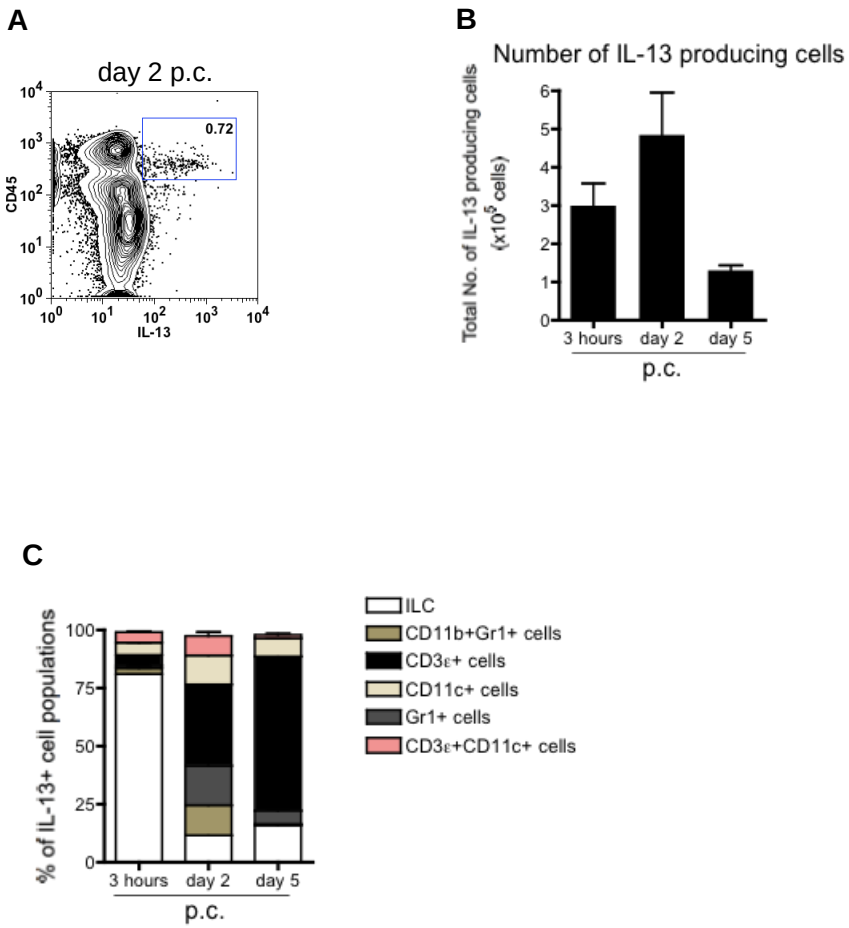

Figure 4.6 Different leukocyte cell subpopulations are responsible for IL13 production in inflamed salivary glands. Representative dot plot **(A)** showing percentage of CD45+ IL13 producing cells at day 2 p.c. Graphs showing absolute number of IL13 expressing cells **(B)** within cannulated salivary glands at 3hours, day 2 and day 5 p.c. Graph summarizing the relative distribution of IL-13 producing cells at 3 hours , day 2 and day 5 p.c. **(C)**. Data are representative of two different experiments with two mice per experiment.

4.7 IL-13 from both bone-marrow derived hematopoietic cells and tissue resident stromal cells contributes to the induction of LLSc

Studies in asthma biology have demonstrated that in pathological conditions IL13 can be produced by non-hematopoietic cells such as lung epithelial cells [291]. To better understand the role of bone-marrow versus non bone-marrow derived IL-13 producing cells in induction of LLSc, salivary gland cannulation was performed on bone-marrow chimeras with bone-marrow from *wt* and *il13gfp/gfp* mice, in which, in place of il13 gene, gfp gene had been knocked in (details of mice in chapter 3). Unexpectedly, the FACS analysis of LLSc in the cannulated mice with il13ko bone-marrow **(Figure 4.7.1A-B)** showed no defect in the induction of LLSc as observed in il4rko and il13ko mice. Immunofluorescence for detection of gfp+ cells demonstrated, as expected, presence of cd45+ il13gfp+ cells in the cannulated salivary glands of mice with il13gfp bone-marrow **(Figure 4.7.1C)**.

This observation led us to the question whether the early expression of IL-13, observed early in cannulated salivary glands, was produced by tissue resident non-hematopoietic cells. FACs analysis for IL-13 intracellular cytokine production was performed on single cell suspension from digested salivary gland stromal cells. In addition, PCR for IL-13 gene expression was performed on isolated salivary gland stromal cell subsets. As expected, tissue resident epithelial (EPCAM+) cells showed intracellular production of IL13, but interestingly the CD45-EPCAM- stromal cells also showed IL-13 production **(Figure 4.7.2A-B)**. This data was confirmed by PCR epithelial and CD45-EPCAM- stromal cells, where up-regulation in IL13 mRNA was detected **(Figure 4.7.2C)**.

Altogether these data suggests a significant role of non-hematopoietic cells in the production of IL13 during TLO formation.

Figure 4.7.1

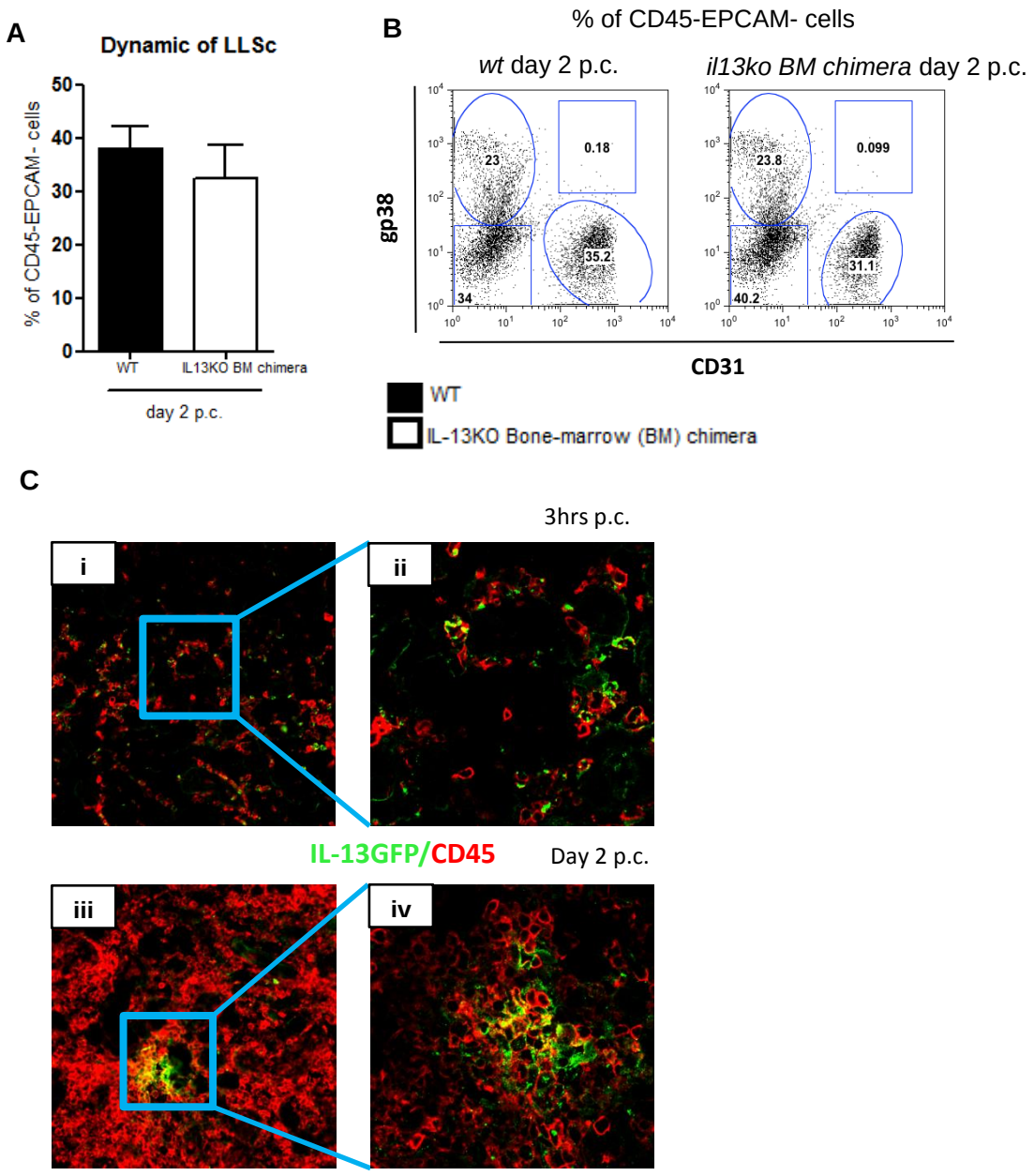

Figure 4.7.1 IL-13 from both bone-marrow derived hematopoietic cells and stromal cells contributes to the induction of LLSc. Graph **(A)** showing no significant differences in the dynamic of LLSc expansion obtained by flow cytometry on day 2 p.c. infected *wt (black bars)* and *il13ko* bone-marrow chimera *(white bars)* salivary glands. Representative dot plots **(B)** showing flow cytometry for percentage of gp38+CD31- population in the CD45-EPCAM- component from day 2 p.c. salivary glands in *wt* and *il13ko* bone-marrow chimera. Representative microphotograph **(C)** showing induction of *il13* expression in salivary gland upon inflammation in *il13gfp* bone-marrow chimera mice salivary glands (3 hours **(Ci-ii)** and day 2 **(Ciii-iv)** p.c.) probed with anti-gfp (green) and CD45 (red). Original magnification 10X (**Ci-iii)** and 63X **(Cii-iv)**.

Figure 4.7.2

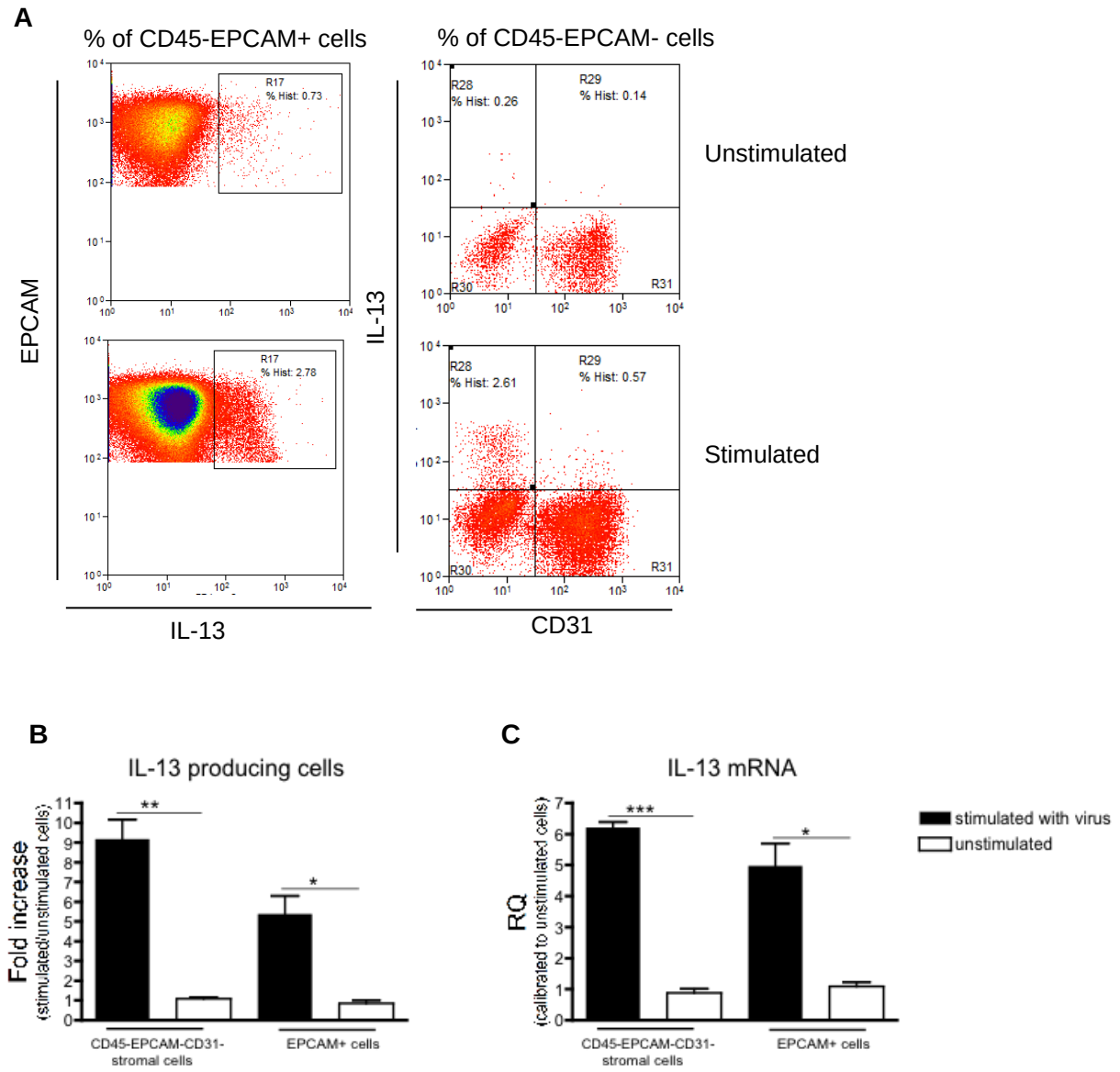

Figure 4.7.2 IL-13 production by from tissue resident stromal cells. Dot plots (**A**) showing flow cytometry acquisition of *il13* intracellular expression in CD45-CD31-EPCAM+ and CD45-CD31-EPCAM- cell components from *in-vitro* virus stimulated or unstimulated digested salivary gland cells for 3 hours. Graphs summarising **(B)** flow cytometry results, showing fold-increase in IL-13 intracellular expression in the stimulated (black bars) CD45-CD31-EPCAM- stromal cells and EPCAM+ cells as compared to their corresponding unstimulated (white bars) cellular components and **(C)** summarizes transcripts encoding for IL-13 gene quantified by qRT-PCR and normalized to housekeeping gene β-actin in sorted CD45-CD31-EPCAM- and EPCAM+ cells (relative quantitation to IL-13 mRNA in unstimulated population. *, p<0.05; **, p< 0.01; ***, p<0.001. Data are representative of three independent experiments.

4.8 Lack of IL-4Rα engagement results in reduced but not diminished TLO formation

In order to understand the consequence of the early defect observed in the LLSc induction on LLSc maturation and hence their ability to support TLO formation, the expression of LLSc derived lymphoid chemokines **(Figure 4.8.1A-B)** were studied in the cannulated salivary gland of *il4rαko.* Expectedly, a ten-fold and nearly thirty-fold decrease was observed in the CXCL13 gene expression within *il4rαko* mice salivary glands at day 5 and day 8 respectively, as compared to wt mice. Furthermore, a severe deficiency was also detected in up-regulation of CCL19 transcript in the il4rko mice at day 5 ($p<0.001$) and day 8 ($p<0.01$). Interestingly, normal expression in these genes was witnessed at day 15 when compared to wt mice, and was further confirmed by immunofluorescence **(Figure 4.8.2A)**. This increase in lymphoid chemokines appeared to be due to the expansion in LLSc from day 8 onwards (shown in section 5.1).

To ascertain the importance of IL-4Ra signal in TLO formation, the TLO were investigated in cannulated salivary glands of *il4rαko* mice. These animals showed defective CCR7+ and CXCR5+ cell accumulation at day 5 and day 8 **(Figure 4.8.1C-D)**, though an increase in CXCR5+ cells was witnessed at day 15, but not CCR7+ cells. The B/T cell ratio increased at day 15 confirming increased recruitment of B cells **(Figure 4.8.2B)**. Moreover, the average size of lymphoid aggregates in *il4rαko* increased from $4x10^4 \mu m^2$ at day8 to $8x10^4 \mu m^2$ at day15 **(Figure 4.8.2C)**. Nevertheless, B/T cell ratio observed in the salivary glands of il4rko mice was still significantly lower ($p<0.05$) to wt mice, and the lymphoid aggregates were not only lesser but significantly smaller ($p<0.05$) when compared to lymphoid aggregates present in wt mice at day 15 **(Figure 4.8.2B-C)**. Interestingly, the total lymphoid area was significantly lower in il4rko mice, ~ 4% total lymphoid aggregate area was observed in il4rko mice compared to ~10% in wt mice at day 8 **(Figure 4.8.2D)**. Furthermore, less than 10% segregated aggregates were found in the inflamed salivary glands of *il4rαko* mice whereas 40-50% aggregates exhibited segregation in wt mice **(Figure 4.8.2E)**. Germinal centres in TLO are known to express AID, which is critical for their functionality and leads to local

production of antibodies. The *il4rako* displayed a significant decrease of nearly hundred and fifty-fold in AICDA transcript expression at week 3 post cannulation **(Figure 4.8.2F)**.

Figure 4.8.1

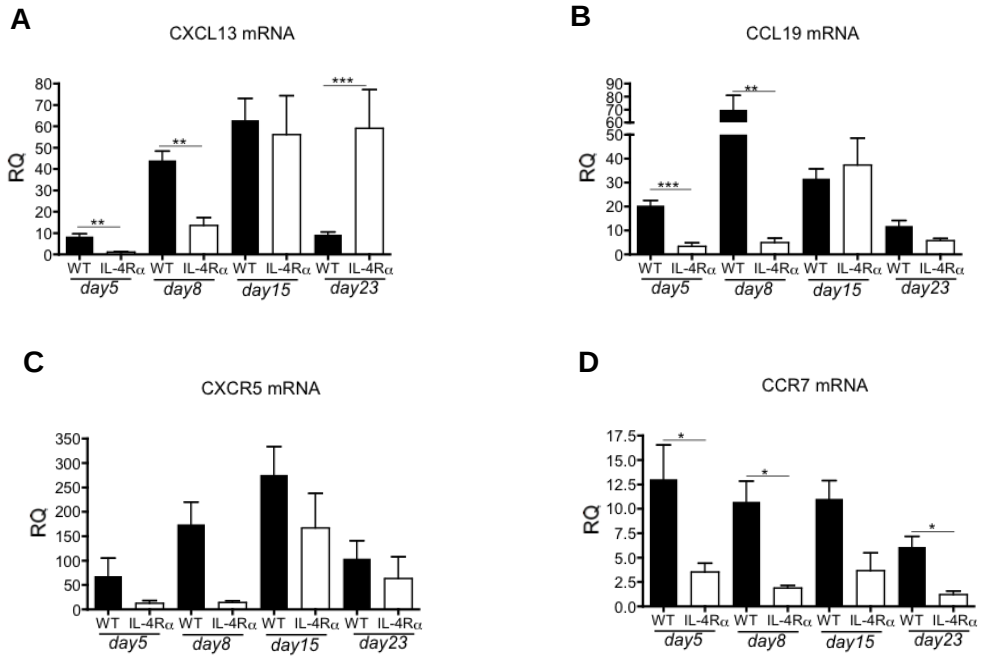

Figure 4.8.1 Lymphoid chemokines and their cognate receptor expression in *il4rαko* mice. A-D, Diagrams representing qRT-PCR analysis of the mRNA obtained from salivary glands at day 5, 8, 15 and 23 p.c. showing lymphoid chemokines (CXCL13 and CCL19) and their cognate receptors (CXCR5 and CCR7) in *il4rαko* mice (white bars) in comparison to their *wt* counterparts (black bars). CXCL13 and CCL19 mRNA transcripts were normalized to PDGFRβ mRNA and CXCR5 and CCR7 mRNA transcripts were normalized to β-actin mRNA. Results are presented as relative quantitation (RQ) values calculated with calibrator day 0 salivary glands *, $p<0.05$; **, $p<0.01$ versus virus cannulated *wt* mice. Data are representative of two replicates (3-4 infected mice per group).

Figure 4.8.2

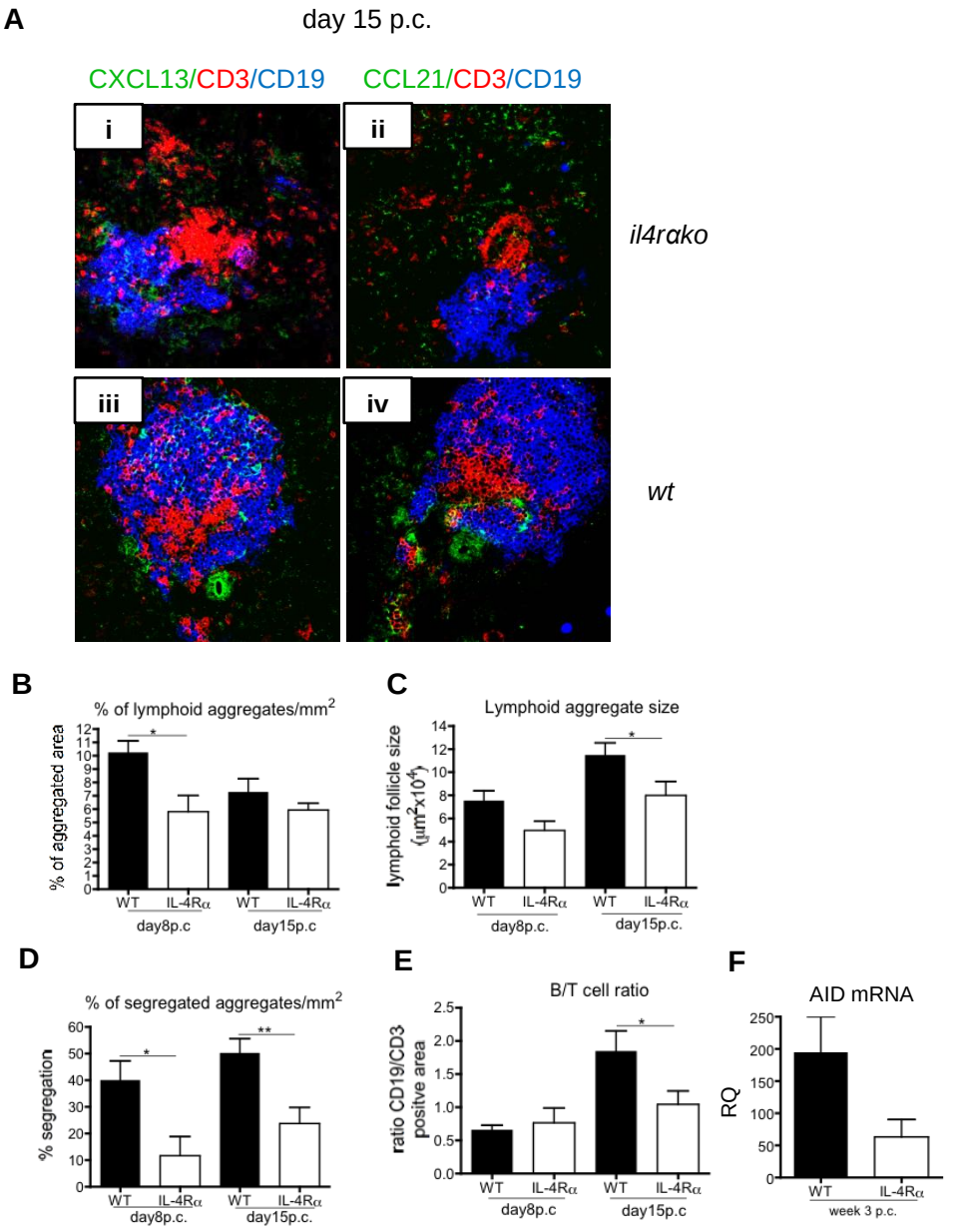

4.8.2 Lack of IL-4Rα engagement results in reduced but not diminished TLO formation. Microphotograph of lymphoid aggregates **(A)** from infected salivary glands (day 15 pc.) from *wt* **(Aiii-iv***)* and *il4rαko* **(Ai-ii)** mice stained for CD3 (red), CD19 (blue) and either CXCL13 (green in **i and ii**) or CCL21 (green in **iii and iv**). Salivary glands from *wt and il4rαko* day 8 and 15 p.c. were examined by immunofluorescence for CD3 and CD19. **B-E**, Graphs representing % of total lymphoid aggregate area **(B),** lymphoid aggregate size **(C)**, % of segregated aggregates **(D)** and ratio between the area covered by CD19+ B cells and CD3+ T cells **(E)** at day 8 and day 15 p.c. for *wt* (black bars) and *il4rαko* (white bars) mice. Data is representative of two different experiments with two to three mice per group, mean ± s.e.m. *, $p < 0.05$, unpaired t test, comparing *il4rαko* to *wt* mice. **(F)**, Transcripts encoding for AID gene (normalized to housekeeping gene β-actin), in week 3 p.c. salivary glands from *wt* and *il4rαko* mice, were quantified and expressed as RQ values relative to day 0 p.c. AID mRNA. Data shown as mean ± s.e.m. of three independent experiments.

4.9 Absence of IL13 results in reduced but not diminished TLO formation

In order to confirm that the defect observed in *il4rαko* mice in terms of LLSc-derived lymphoid chemokines and TLO formation was due to inability of IL-13 to signal via the receptor, we analysed the cannulated salivary glands of *il13ko.* Similar to *il4rαko* mice, reduced expression was detected in expression of CCL19 mRNA ($p<0.05$) in the *il13ko* mice at day 5 and day 8 p.c. No difference was detected in CXCL13 mRNA levels in *il13ko* mice as compared to *wt* mice at day 5 and day 8 p.c. However, significantly increased expression in CXCL13 and CCL19 genes *was* witnessed at day 15 when compared to wt mice **(Figure 4.9.1A-B)**. Expression of lymphoid chemokines in cannulated salivary glands of *il13ko* was further confirmed by immunofluorescence **(Figure 4.9.2A)**.

Analogous to *il4rko*, *il13ko* mice also showed defective CCR7+ and CXCR5+ cell accumulation at day 5 and day 8 **(Figure 4.9.1C-D)**, though an increase in CXCR5+ and CCR7+ cells was witnessed at day 15 p.c. in these mice. Expectedly, the total lymphoid area was significantly lower in *il13ko* mice at day 8 but not at day 15 p.c. **(Figure 4.9.2B)**. Moreover, the size of lymphoid follicles and B/T cell ratio within lymphoid follicles showed an increase between day 8 and day15 p.c. **(Figure 4.9.2C-D)**. Nevertheless, lymphoid follicle size and B/T cell ratio observed in the salivary glands of *il13ko* mice were always lower than wt mice **(Figure 4.9.2C-D)**. Furthermore, lymphoid aggregates found in inflamed salivary glands of *il13ko* exhibited lower segregation when compared to aggregates in *wt* mice **(Figure 4.9.2E)**. The *il13ko* also displayed a significant decrease of nearly hundred and fifty-fold in AID transcript expression at week 3 post cannulation **(Figure 4.9.2F)**.

Figure 4.9.1

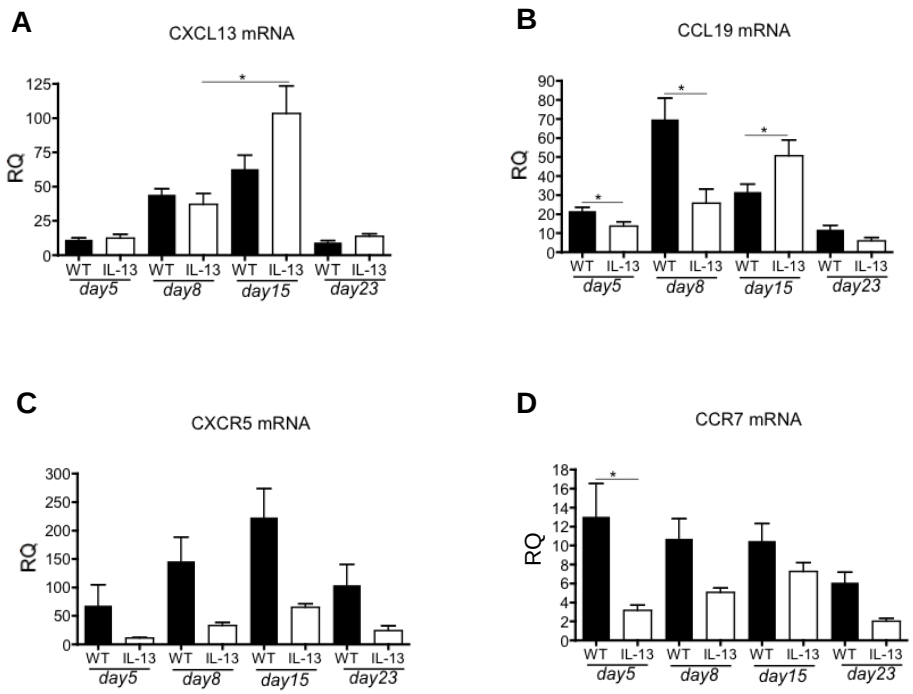

Figure 4.9.1 A-D, Lymphoid chemokines and their cognate receptor expression in *il13ko* mice. Diagrams representing qRT-PCR analysis of the mRNA obtained from salivary glands at day 5, 8, 15 and 23 p.c. showing lymphoid chemokines (CXCL13 and CCL19) and their cognate receptors (CXCR5 and CCR7) in *il13ko* mice (white bars) in comparison to their *wt* counterparts (black bars). CXCL13 and CCL19 mRNA transcripts were normalized to PDGFRβ mRNA and CXCR5 and CCR7 mRNA transcripts were normalized to β-actin mRNA. Results are presented as relative quantitation (RQ) values calculated with calibrator day 0 salivary glands *, $p<0.05$ versus virus cannulated *wt* mice. Data are representative of two replicates (3-4 infected mice per group).

Figure 4.9.2

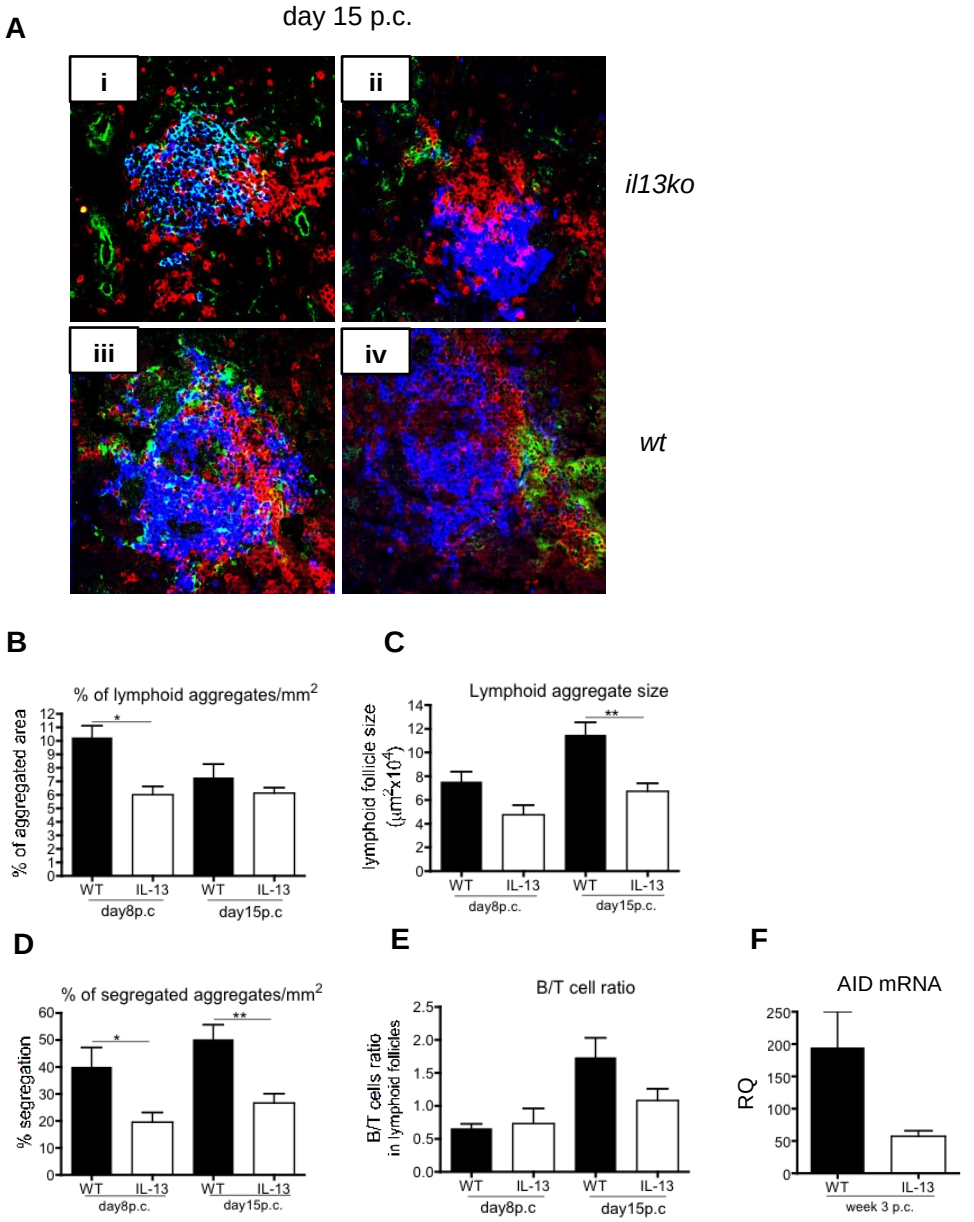

Figure 4.9.2 Absence of IL13 engagement results in reduced but not diminished TLO formation. Microphotograph of lymphoid aggregates **(A)** from infected salivary glands (day 15 pc.) from *wt* **(Aiii-iv***)* and *il13ko* **(Ai-ii)** mice stained for CD3 (red), CD19 (blue) and either CXCL13 (green in **i and ii**) or CCL21 (green in **iii and iv**). Salivary glands from *wt and il13ko* day 8 and 15 p.c. were examined by immunofluorescence for CD3 and CD19. **B-E**, Graphs representing % of total lymphoid aggregate area **(B),** lymphoid aggregate size **(C)**, % of segregated aggregates **(D)** and ratio between the area covered by CD19+ B cells and CD3+ T cells **(E)** at day 8 and day 15 p.c. for *wt* (black bars) and *il13ko* (white bars) mice. Data is representative of two different experiments with two to three mice per group, mean ± s.e.m. *, $p<0.05$, unpaired t test, comparing *il13ko* to *wt* mice. **(F)**, Transcripts encoding for AID gene (normalized to housekeeping gene β-actin), in week 3 p.c. salivary glands from *wt* and *il13ko* mice, were quantified and expressed as RQ values relative to day 0 p.c. AID mRNA. Data shown as mean ± s.e.m. of three independent experiments.

4.10 Absence of IL-4 results in defective TLO formation

Detailed analysis of TLO and TLO-associated genes in salivary glands of *il-4ko* mice demonstrated an unpredicted phenotype.

Quantitative PCR for lymphoid chemokines demonstrated a eighty-fold increase ($p<0.01$-0.001) in CXCL13mRNA within salivary glands of *il4ko* mice at day 5 and day 8 p.c. compared to a ten-fold and forty-fold increase in CXCL13 transcript levels observed in *wt* mice salivary glands at day 5 and day 8 p.c. respectively **(Figure 4.10.1A)**. Similarly, CCL19 gene expression was increased by nearly thirty fold ($p<0.05$) in il4ko mice as compared to *wt* mice at day 5 p.c. **(Figure 4.10.1B)**. *il4ko* mice exhibited a failure to maintain the lymphoid chemokine expression, and CCL19mRNA ($p<0.01$-0.001) level was reduced from day 8 p.c. onwards ($p<0.01$-0.001) and CXCL13 ($p<0.05$) at day 15 p.c. **(Figure 4.10.1A-B)**. Histological examination for CXCL13 and CCL21, presented a severe reduction in expression of these lymphoid chemokines **(Figure 4.10.1E)**. mRNA detection for both CXCR5 and CCR7 revealed considerably reduced expression for these genes from day 5 onwards **(Figure 4.10.1C-D)**. Even though, early expression of both CCL19 and CXCL13 was intact in the *il4ko* mice, they displayed inadequacy to recruit CXCR5+ and CCR7+ cells. Histological analysis of lymphoid aggregates confirmed this observation, and the total lymphoid area **(Figure 4.10.2A)** and percentage of segregated aggregates **(Figure 4.10.2B)** were significantly lower in *il4ko* mice compared to in *wt* mice at day 8 and day 15. Furthermore, fewer and significantly smaller size aggregates **(Figure 4.10.2C),** with lower B/T cell ratio **(Figure 4.10.2D)** were found in *il4ko* mice. As expected, marked suppression of AID mRNA transcripts was observed in treated mice **(Figure 4.10.2E)**.

Figure 4.10.1

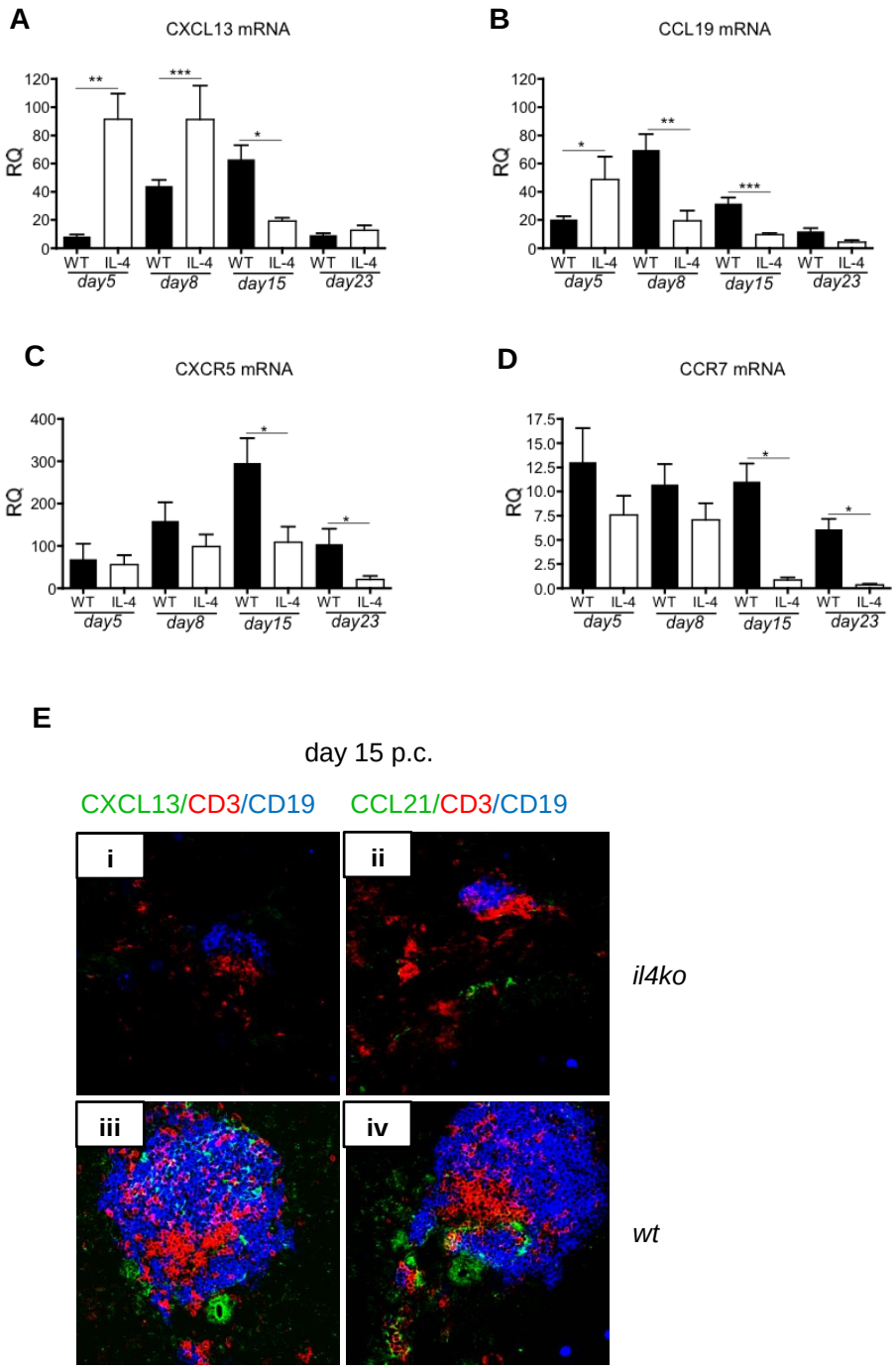

Figure 4.10.1 Lymphoid chemokines and their cognate receptor expression in *il4ko* mice. A-D, Diagrams representing qRT-PCR analysis of the mRNA obtained from salivary glands at day 5, 8, 15 and 23 p.c. showing lymphoid chemokines (CXCL13 and CCL19) and their cognate receptors (CXCR5 and CCR7) in *il4ko* mice (white bars) in comparison to their *wt* counterparts (black bars). CXCL13 and CCL19 mRNA transcripts were normalized to PDGFRβ mRNA and CXCR5 and CCR7 mRNA transcripts were normalized to β-actin mRNA. Results are presented as relative quantitation (RQ) values calculated with calibrator day 0 salivary gland *, $p<0.05$; **, $p<0.01$ versus virus cannulated *wt* mice. Data are representative of two replicates (3-4 infected mice per group). Microphotograph of lymphoid aggregates **(E)** from infected salivary glands (day 15 p.c.) from *wt* **(Eiii-iv***)* and *il-4ko* **(Ei-ii)** mice stained for CD3 (red), CD19 blue) and either CXCL13 (green in **i and ii**) or CCL21 (green in **iii and iv**).

Figure 4.10.2

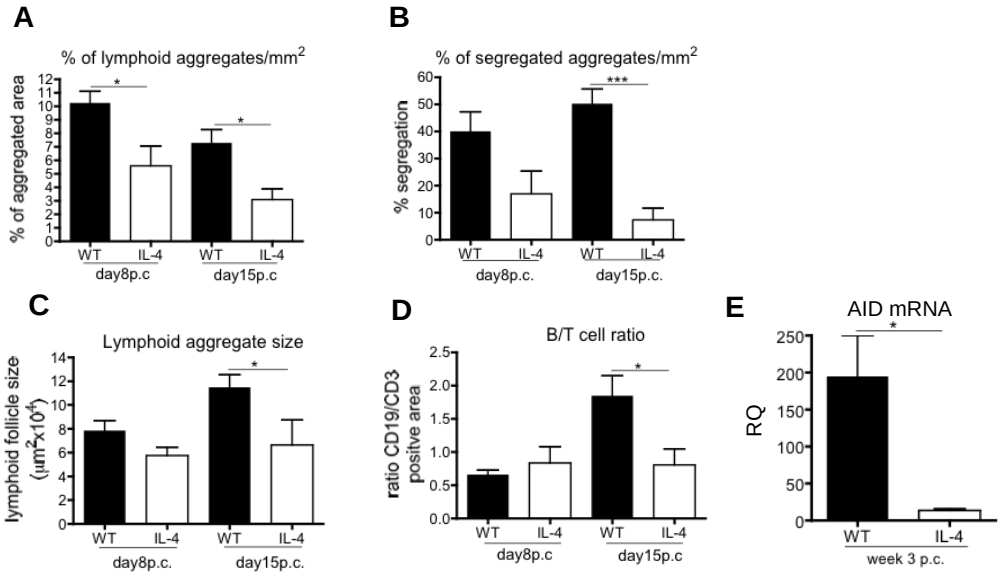

Figure 4.10.2 Absence of IL-4 results in defective TLO formation. Salivary glands from *wt and il4ko* day 8 and 15 p.c. were examined by immunofluorescence for CD3 and CD19. **A-D**, Graphs representing % of total lymphoid aggregate area **(A),** % of segregated aggregates **(B)**, lymphoid aggregate size **(C)** and ratio between the area covered by CD19+ B cells and CD3+ T cells **(D)** at day 8 and day 15 p.c. for *wt* (black bars) and *il4ko* (white bars) mice. Data is representative of two different experiments with two to three mice per group, mean ± s.e.m. *, $p<0.05$, unpaired t test, comparing *il4ko* to *wt* mice. **(E)**, Transcripts encoding for AID gene (normalized to housekeeping gene β-actin), in week 3 p.c. salivary glands from *wt* and *il4ko* mice, were quantified and expressed as RQ values relative to day 0 p.c. AID mRNA. Data shown as mean ± s.e.m. of three independent experiments.

Discussion

This chapter illustrates a previously unappreciated role for IL-4R signaling, mediated by IL-13, in the induction of quiescent tissue-resident stromal cells towards lymphoid-like stromal cells during inflammation. This was an exciting finding, as IL-13 (and IL-4) is known to drive Th2 type immune responses, which are also associated with allergy, asthma, gastrointestinal nemadote infections and fibrosis [292-295], but they have not previously been implicated to have a role in lymphoid stromal cell activation and differentiation during inflammation.

Activated stromal cells have been shown to have the ability to initiate TLO formation in transplantation studies [212, 224]. Nonetheless, the specific signals that could lead to stromal cell activation during TLO formation are still obscure [296]. Most of our current knowledge about signals regulating TLO formation is dependent upon transgenic mice over-expressing lymphoid molecules such as TNFα, LTα, LTα/LTβ, CXCL13 and CCL21 in ectopic sites [4, 157, 158, 165, 169, 173, 174, 227, 232]. Even though these models have provided important insights into TLO development, they lack the pathophysiological complexity that underpins *in vivo* generation of TLOs destruction [166-168]. Some recent studies have suggested a role for inflammatory effector cytokines in the initiation of stromal cell activation during inflammation [214, 230].

While conducting experiments to identify cytokines involved in the regulation of lymphoid stroma, our collaborator, Mark Coles identified that treatment of mesenchymal adipose-derived stem cells (ADSC), with either interleukin 4 (IL-4) or interleukin 13 (IL-13) in conjunction with LT and TNF, significantly induced expression of gp38, ICAM and VCAM. Doucet *et al*., in 1998 have demonstrated that the effect of IL-4 and IL-13 on fibroblasts is mediated by type 2 IL-4 receptor composed of IL-4Rα and IL-13Rα chains and not by type 1 that is composed of IL-4Rα and IL-2Rγ chains [287].

Studies have shown that IL-4 can signal via type 1 and type 2 IL-4R whereas IL-13 only uses type 2 IL-4 receptor. Type 1 IL-4R expression is mainly confined to hematopoietic cells

whereas type 2 IL-4R receptor is majorly found on non-hematopoietic cells such as epithelial cells, fibroblasts [285-288] . In fact, IL-13Rα expression has been documented to be expressed on non-inflamed gut epithelium and myofibroblasts [295, 297]. Additionally, in Crohn's disease and ulcerative colitis, increased expression IL-13Rα has been observed [295, 298]. We detected IL4Rα and IL13Rα expression on salivary gland CD45-EPCAM- stromal cells and epithelial cells in resting conditions. However, upon inflammation, LLSc further up-regulate the expression of these receptors. Inflammatory cytokines such as TNFα have been demonstrated to induce up-regulation of IL-4R on fibroblasts [289]. In our model TNFα production is observed very early in inflammatory process, potentially representing a signal that might promote further expression of IL-4R chain on LLSc. Moreover, IL-13 has been shown to promote its own receptor expression [293, 295].

These observations prompted our *in vivo* studies in which we demonstrated that administration of recombinant IL-13, in absence of virus, to wild-type mice salivary gland was sufficient to induce lymphoid stromal cell activation. Interestingly, the induction of the lymphoid phenotype was less efficient when recombinant IL-4 or TNFα and LTβR agonist were administered to salivary glands. Of note, there was no significant difference observed between the expression of gp38, ICAM and VCAM on the CD45-EPCAM-CD31- stromal compartment in recombinant IL-4 and TNFα plus LTβR agonist cannulated salivary glands. Overall, this data suggested that IL-13 is a more potent inducer of the stromal cell transition to a lymphoid phenotype than IL-4, and even classical lymphoid cytokines such as LT and TNF [4, 16].

Intriguingly, Raza *et al*., during their analysis of synovial fluid cytokine profiles in rheumatoid arthritis patients at different stages, found that IL-13 was transiently detected in early rheumatoid arthritis patients but not patients with established rheumatoid arthritis. Moreover, early rheumatoid arthritis patients with significantly increased levels of IL-13 went on to develop established autoantibody positive rheumatoid arthritis. This data indicates a pathological role for IL-13 early in inflammation [299]. IL-13 has also been implicated in

inducing fibroblast proliferation and differentiation during fibrosis in Th2 mediated diseases such as schistosomiasis [300].

We hypothesised that IL-4R signalling might play a role in regulating early transition of normal resident stromal cells towards a lymphoid like/pathological phenotype. In order to test this hypothesis, salivary glands of C57BL/6 mice wild type and knockout mice (IL-4Rα, IL-4, IL-13) were cannulated and analysed for LLSc induction and TLO formation. We observed a significantly reduced percentage of gp38+LLSc in *il4rαko* and *il13ko* mice at day 2 p.c. as compared to wild-type mice. Moreover, *il4rαko* and *il13ko* mice exhibited failure to up-regulate the expression of other stromal cell markers such as ICAM-1 and VCAM-1.

Our results from Ki67 and BrDU staining on LLSc confirmed that the defect observed in the lymphoid stroma (LLSc), of *il4rαko* and *il13ko*, was not due the inability of LLSc to proliferate. Other studies have shown that IL-13 can prevent apoptosis of tumour cells and activated fibroblasts during inflammatory and fibrotic diseases [293, 295, 301-304] and this proposed anti-apoptotic role of IL-13 cannot be ruled out with the present set of data.

In our model, IL-13 is produced in significant quantities by CD4+Th2 cells [305]. However, innate immune cells such NK cell, NKT cells and CD11b+ myeloid cells including eosinophils, basophils and mast cells, have also been reported to produce IL-13 [293, 295]. Group 2 innate lymphoid cells (ILC) subset has been shown to produce canonical Th-2 cytokines IL-13 and IL-5 in response to epithelial cell–derived cytokines IL-25, IL-33, that are themselves released in response to inflammation and infection [306]. Group 2 ILC cells have also been shown to mediate allergic lung inflammation [307, 308]. ILCs require IL-7Ra signalling for their development and maintenance. Thus, they are broadly identified as lineage negative IL-7Rα positive cells [306]. FACs analysis identified ILC as the major source of IL-13 at 3 hours p.c. We have demonstrated that virus infects the epithelial cells [237] and thus one can speculate that epithelial derived cytokines IL-25/IL-33 are produced which stimulate the ILC (already shown in previous chapter to be present in resting salivary glands) to produce IL-13.

However, at day 2, various IL-13 producing cell types were observed which included granulocytes, ILC and T cells. Though, at day 5, the majority of IL-13 was produced by T cells, which coincides increased IL-4 expression detected in cannulated salivary glands. It has been previously shown that IL-4 is required for priming and differentiation of CD4+ Th-2 cells, thus production of IL-13 from T cells is dependent on IL-4.

Cannulated salivary glands of bone-marrow chimera mice reconstituted with il13ko hematopoietic cells demonstrated intact LLSc induction, clearly suggesting that non-hematopoietic cells were sufficient to produce IL-13 upon inflammation and activate lymphoid stroma induction. Accordingly, epithelial cell have been implicated to be the chief source of IL-13 during airway inflammation [291]. Moreover, microarray analysis of thymic epithelial cells (TECs) revealed significantly up-regulated IL-13 expression in these cells (Immgene). We identified epithelial cells and also CD45-EPCAM-CD31- stromal cells as the major source of IL13, after adenovirus infection. This suggests that tissue-resident stromal cells (epithelial cells and fibroblasts) provide the first signal in lymphoid stromal cell activation in response to inflammatory stimuli.

Detailed analysis of LLSc and TLO-associated features, and lymphoid genes in *il4ko* mice, revealed a defect in maintenance of LLSc and production of lymphoid chemokines and cytokines from day 8 onwards. In agreement with this data, significant decrease was observed in the size of lymphoid aggregates and B/T cell ratio in the salivary glands of these mice. However, these results in *il4ko* are under further investigation as these observations were not replicated in *il4rαko,* which would be expected, since IL4Rα subunit is common to both type1 and type 2 IL-4R and is utilized by IL-4 to mediate its biologic functions. Such discrepancy has been observed in experimental mouse model of autoimmune diabetes, where IL-4 administration has been reported to play a protecting role [309]. Conversely, another study reported that lack of IL-4Rα protected the mice against the induction of diabetes in a spontaneous mouse model . One speculation for our finding is that IL-4 mainly mediates its function on immune cells whereas IL-13 mediates its effect mainly on stromal

cells. Because immune cells express IL-4Rα and yc chain, there is a possibility that in the absence of IL4Rα, its function is probably transferred to the gamma chain of the IL-2 receptor complex, as suggested by Wang *et al*., in 1996 [310].

In agreement with our data, both *in vitro* and *in vivo*, we propose that IL-13 signalling through the IL-4Rα is critical for induction of lymphoid stromal cells. However, data in this chapter indicates that there are other signals operating during the initial phases of TLO formation which seem to compensate for the early defect observed in the absence of IL13/IL4Rα signalling axis.

Chapter 5

IL22 regulates antibody-mediated autoimmunity by inducing lymphoid like stromal cell proliferation in TLOs

Introduction

IL22 is a member of IL-10 cytokine family, and it signals via a heterodimeric receptor consisting of IL-22Rα and IL-10Rβ [311-313]; the expression of IL-22R is largely confined to non-hematopoietic cells [314]. Keratinocytes, colonic epithelial cells and hepatocytes are well established IL-22- target cells in literature [313]. IL22 is a paradoxical cytokine. It has been shown to be involved in tissue homeostasis and wound healing at barrier surfaces [315] and has also recently been shown to regulate thymic regeneration, following tissue damage [316]. During infection with C.rodentium, IL-22 has been demonstrated to help maintain normal architecture of colonic patches and most interestingly sustain the number of ILFs [317]. In addition to promoting tissue repair via induction of epithelial cell proliferation and survival, it has also been implicated in the development of skin pathology [318] as well as epithelial tumors in the gut [319]. Furthermore, IL-22 has been shown to induce podoplanin (gp38) expression on epidermal keratinocytes that are associated with wound and psoriatic hyper-proliferative epidermis [320]. An association between IL22 expression and autoimmune conditions has also been suggested [321, 322]. IL-22R1 expression has been reported by Ikeuchi et al., on synovial fibroblasts derived from RA patients (RASF). Authors further demonstrated that IL-22, promoted proliferation and chemokine production of synovial fibroblasts [323]. Moreover, IL-22 stimulated lung fibroblasts have been shown to up-regulate lymphoid chemokine expression, particularly CXCL13 [324]. In SS, serum levels of IL22 correlate with clinical manifestations of the disease, including autoantibody production [325].

Moreover, IL-22 has been associated with IL-17 in various inflammatory diseases, and in some disease conditions such as psoriasis it has been demonstrated to be required for IL-17 mediated pathology [326]. In *il22ko* mice, CIA was shown to be less severe due to decreased germinal centre formation, plasma cell formation and IgG2a antibody production, suggesting

a pathogenic role for IL-22 in B cell autoimmunity. The authors confirmed that *il22ko* did not have defect in IL-17 production and thus the reduction in arthritis was due to absence of IL-22 and not IL-17 [19]. Th17 cells have been thought to be the major producers of IL-22. However, it is now known that IL-22 can also be produced by a novel CD4+ T cell subset, Th22 cells as well as NK cells and ILC [306, 313]. In fact, IL-22+IL-17-CD4+T cells have been reported in patients with rheumatoid arthritis and active SLE [327, 328].

Taken together, these studies provided a rationale to examine if IL-22 plays any role in regulating LLSc within TLOs and in particular whether IL-22 might be responsible for the proliferation phase, observed in our model after IL-13 induction of LLSc.

Results

5.1 IL22 is expressed early in salivary gland inflammation and T cells are the major cellular source of IL22 in inflamed salivary glands

In order to explore a potential role of IL22 in driving transition from constitutive fibroblastic stroma to "lymphoid like stroma", and the subsequent formation of TLOs, quantitative analysis of total salivary gland mRNA was used to identify the temporal expression of IL22 in cannulated salivary glands. IL22 was significantly up regulated as early as 3 hours p.c. (~6000 fold increase was detected in comparison to day 0 p.c. salivary gland), and a second peak of 1000 fold increase in IL22 mRNA transcript levels was detected at day 5 p.c. **(Figure 5.1A)**.

We next investigated the cellular source of IL22 in single cell suspensions from cannulated salivary glands at different time-points p.c. (3 hours, day 2 and day 5 p.c.) **(Figure 5.1B-D)**. The highest numbers of IL22 producing cells were found within the CD45+ cell population by 3 hour p.c. **(Figure 5.1B)**. The largest source of IL22 was T cells at all time-points examined **(Figure 5.1C)**. While at 3 hours p.c. IL22 production was mainly derived from γδ T cells (~80% of the IL22+ cells were γδ T cells **(Figure 5.1C-D)**), by day 5 p.c. 85% of IL22 producing cells were αβ T lymphocytes **(Figure 5.1C-D)**. Other leukocyte populations, responsible for early IL22 production, were innate lymphoid cells (ILCs) and natural killer cells (NK). At 3 hours and day 2 p.c. ILC represented ~20-30% of the IL22+ cells in the cannulated glands. In addition, at day 2 p.c. ~20% of IL-22+CD45+ cells were NK cells **(Figure 5.1C)**.

Figure 5.1

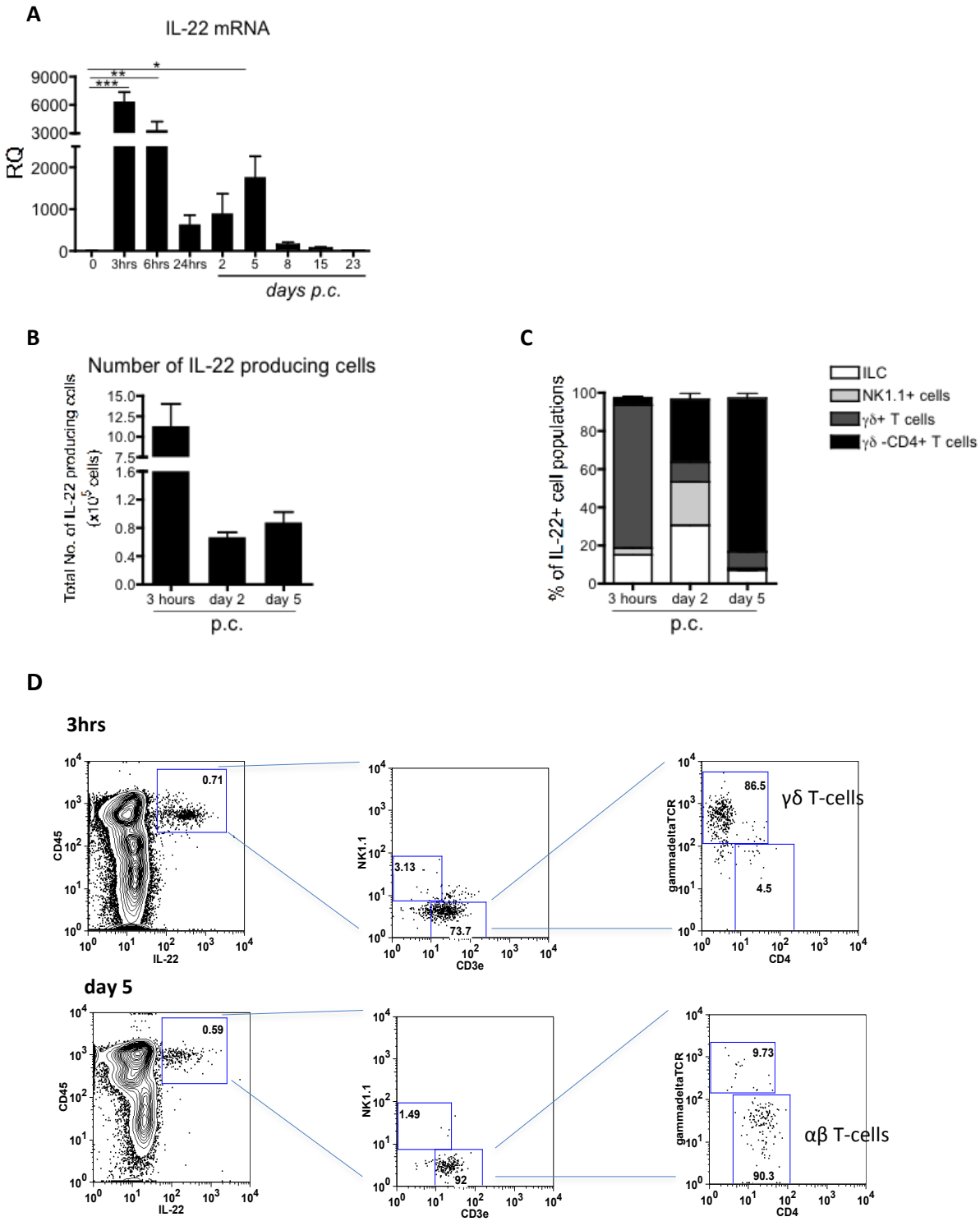

Figure 5.1 IL22 is expressed early in salivary gland inflammation and T cells are the major cellular source of IL22 in inflamed salivary glands. Quantitative RT-PCR analysis of mRNA transcripts for il22 **(A)** in *wt* mice at various time points post-cannulation (p.c.). Transcripts were normalized to β-actin. The relative expression values were calibrated to day 0 p.c. salivary gland values. * $p < 0.05$; ** $p < 0.01$; *** $p < 0.001$ versus day 0. Data are representative of three to four experiments with two to three mice analysed per group. **(B)** Graphs showing absolute number of IL22 expressing cells contained within the digested CD45+ leukocyte population from cannulated salivary glands at 3h, day 2 and day 5 p.c. **(C)** Graph summarizing the relative distribution of IL22 producing cells in the CD45+ leukocyte population at 3h, day 2 and day 5 p.c. **(D)** Representative dot plots identifying IL22 producing cells at 3 hours and day 5 p.c. in the γδ+ T cell population at 3h and in the αβ+T cells at day 5 p.c. Data are representative of two different experiments with three mice per experiment.

5.2 Lack of IL22 results in abortive TLO formation and suppression of autoantibody production

IL22 and IL22 producing cells have been reported in salivary glands of patients with SS. Furthermore, IL22 serum level in SS patients has been shown to correlate with clinical manifestations of the disease and autoantibody production. However, the mechanistic contribution of IL22 to TLO development and autoantibody production remains unknown. In order to investigate the role of IL22 in TLO formation, salivary glands of *il22ko* mice were cannulated with adenovirus and compared to *wt* controls. Detailed histological analysis of lymphoid aggregates at day 8 and day 15 p.c. was performed for *il22ko* versus *wt* mice **(Figure 5.2.1A-F)**. Interestingly, the fraction lymphoid area was significantly lower in *il22ko* mice as compared to the wt. Indeed, less than 4% total lymphoid aggregate area was observed in *il22ko* mice compared to ~10% and 8% in *wt* mice at day 8 and day 15 p.c. respectively **(Figure 5.2.1B).** *il22ko* mice showed abortive follicle formation with the generation of small T-cell aggregates and defective B-cell accumulation at day 8 and 15 p.c. reflected by reduced lymphoid follicle size (4-5um^{2}x10^4 in *il22ko* versus 7.5-11 um^{2}x10^4 in *wt* mice **(Figure 5.2.1C)** and lower B/T cell ratio (ratio of CD19/CD3 positive area was less than 0.25 and 1 at day 8 and day 15 respectively compared to a ratio of 0.6 at day 8 and ratio of 2 at day 15 in *wt* mice **(Figure 5.2.1D)**. Less than 10% segregated aggregates were found in the inflamed salivary glands of il22ko mice, whereas 40-50% aggregates exhibited segregation in *wt* mice **(Figure 5.2.1E).** A significant decrease in AID transcript expression was observed in the salivary glands of *il22ko* at week 3 post cannulation **(Figure 5.2.1F)**, which coincided with a marked suppression of ANA autoantibody production as compared to *wt* mice **(Figure 5.2.2A-B)**.

Figure 5.2.1

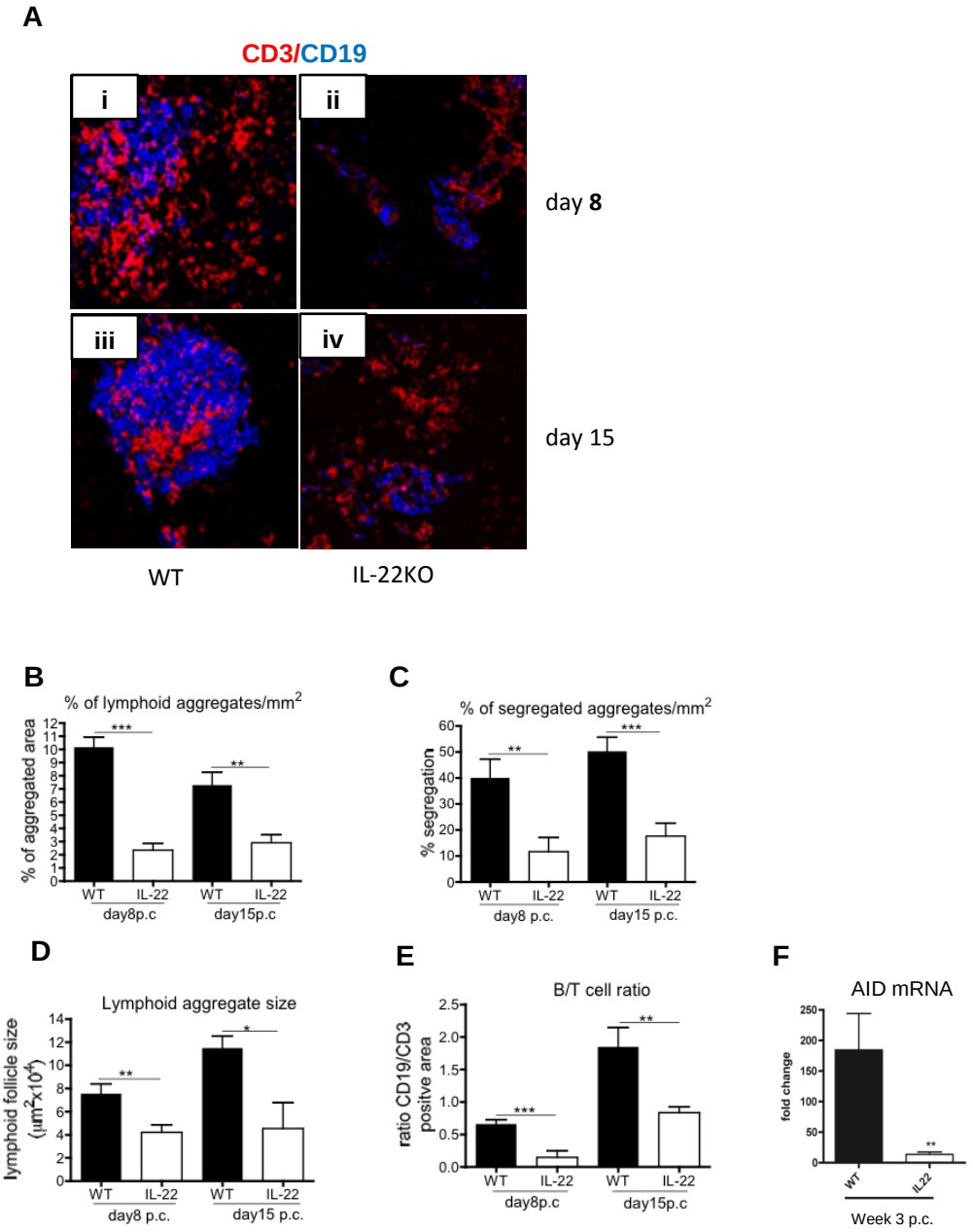

Figure 5.2.1 Lack of IL22 results in abortive TLO formation. Microphotograph of lymphoid aggregates **(A)** from infected *wt* **(Ai-iii)** and *il22ko* **(Aii-iv)** mice salivary glands at day 8 **(Ai-ii)** and day 15 **(Aiii-iv)** p.c**.** stained for CD3 (red) and CD19 (blue). % of total lymphoid aggregate area **(B)** and % of segregated aggregates **(C)** at day 8 and day 15 p.c. for *wt* (black bars) and *il22ko* (white bars) mice. Lymphoid aggregate size **(D)** at day 8 and day 15 p.c. for *wt* (black bars) and *il22ko* (white bars) mice. Ratio between the area covered by CD19+ B cells and CD3+ T cells **(E)** at day 8 and 15 p.c. for *wt* (black bars) and *il22ko* (white bars) mice. Data is representative of two different experiments with two to three mice per group, mean ± s.e.m. **, $p < 0.01$; ***$p<0.001$ unpaired t test, comparing *il22ko* to *wt* mice. **(F)**, Transcripts encoding for aicda gene (normalized to housekeeping gene β-actin), in week 3 p.c. salivary glands from *wt* and *il22ko* mice, were quantified and expressed as RQ values relative to day 0 p.c. AID mRNA. Data shown as mean ± s.e.m. of three independent experiments.

Figure 5.2.2

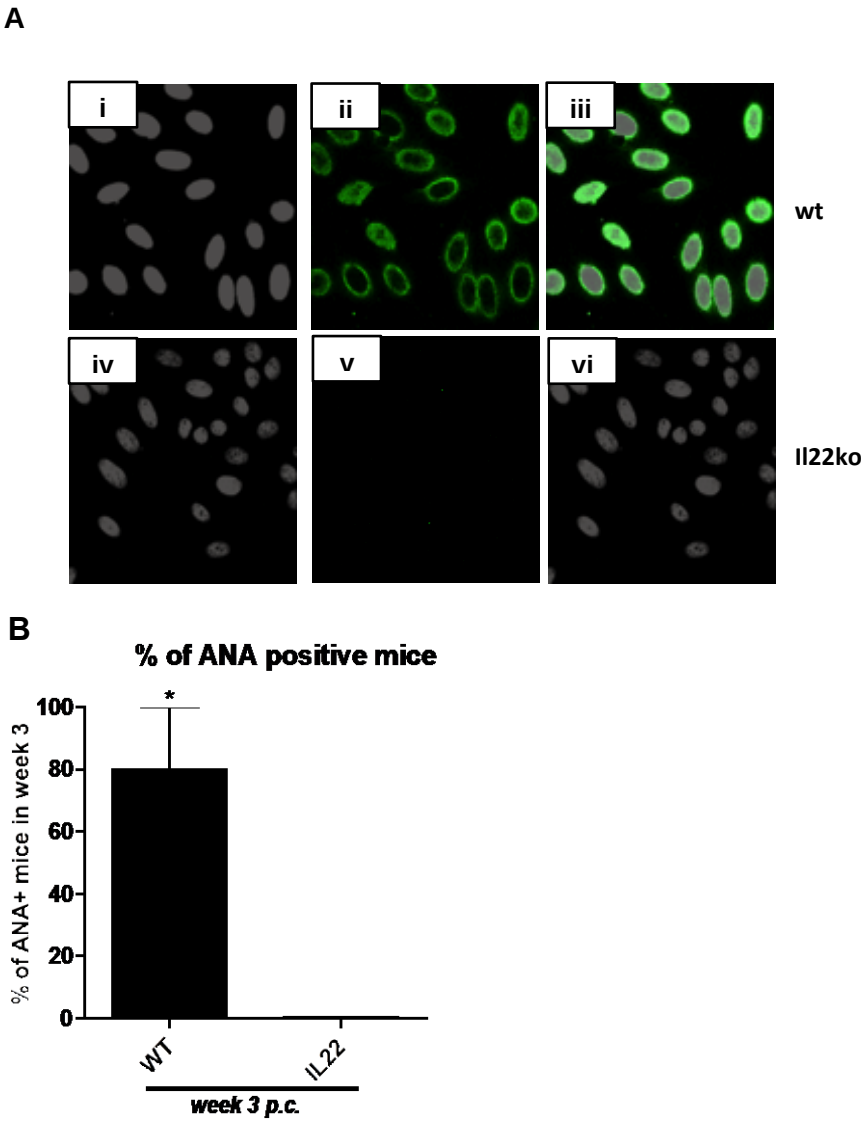

Figure 5.2.2 Lack of IL22 results in suppression of autoantibody production. Representative microphotographs of immunofluorescence detection of ANA **(Ai-vi)** using Hep2 cells as a substrate demonstrating strong nuclear reactivity in sera of day 23 p.c. *wt* **(Ai-iii)** mice, but not in *il22ko* **(Aiv-vi)** mice (nuclear staining in grey, ANA reactivity in green)(serum dilution 1:80). Original magnification 40X. **(B)** Detection of ANA reactivity in *wt* mice compared to *il22ko* mice. * $p < 0.05$ *wt* versus day 23 p.c *il22ko* mice. Data are representative of two experiments with five cannulated mice (biological replicates expressed as percentage of mice positive for ANA at 1:80 dilution or more, mean ± s.e.m.)**.**

5.3 Abortive TLO formation observed in il22ko mice can be attributed to the deficiency in the lymphoid chemokines and cytokine production in these mice.

Further examination of the cannulated *il22ko* mice revealed significantly decreased production of the B-cell recruiting chemokine CXCL13 at all time-points compared to their wt counterparts. Nearly 5-fold, 35-fold and 55-fold difference was observed in the cxcl13 transcript levels between *il22ko* and *wt* mice at day 5, day 8 and day 15 p.c. respectively **(Figure 5.3B)**. Reduced CXCL13 expression in the *il22ko* salivary glands was confirmed by IF **(Figure 5.3Ai-ii)**. *il22ko* additionally exhibited a defect in B cell survival factor BAFF mRNA up-regulation **(Figure 5.2C)**. Moreover, a significant decrease of 15-fold, 55-fold and 20-fold in the T-cell associated chemokine CCL19 was also observed in *il22ko* as compared to wt salivary glands at day 5, day 8 and day 15 p.c. respectively **(Figure 5.3D)**. To further support the lymphoid chemokine expression and aggregate histological data, q-PCR analysis for CXCR5 and CCR7 mRNA also showed a significantly lower transcript levels when compared to *wt* mice **(Figure 5.3D-E)**. Finally, a substantial reduction in LTβ mRNA in the *il22ko* mice was observed which was most likely due to defective recruitment of LTβ expressing lymphocytes **(Figure 5.3F)**. Altogether, the data indicated defective recruitment and ability of lymphocytes to organize and form TLO within cannulated salivary glands in the absence of IL22.

Figure 5.3

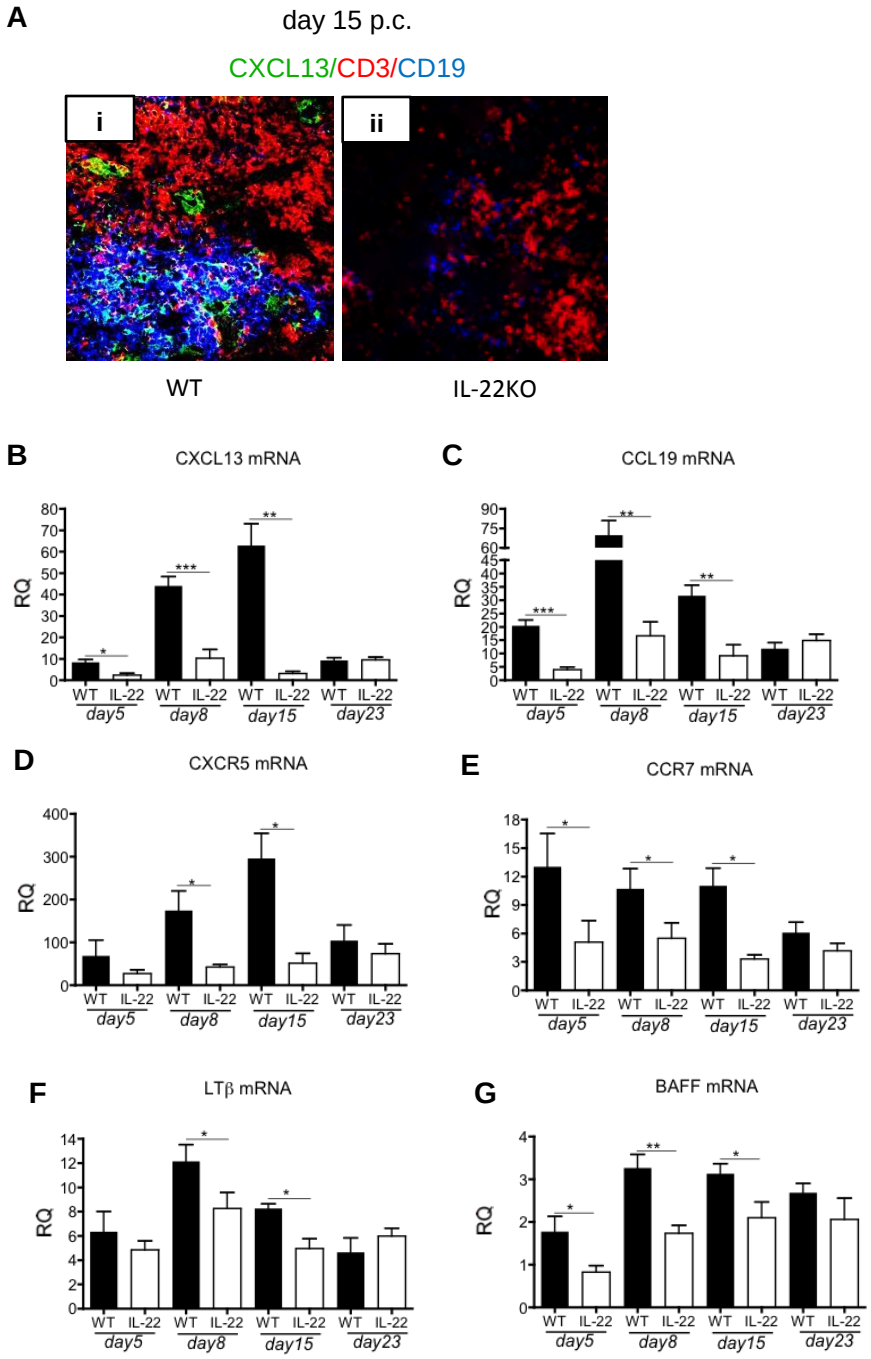

Figure 5.3 Abortive TLO formation observed in *il22ko* mice can be attributed to the deficiency in the lymphoid chemokines and cytokine production in these mice. Microphotograph of lymphoid aggregate **(A)** from infected salivary glands (day 15 p.c.) from *wt* **(Ai)** and *il22rako* **(Aii)** mice stained for CD3 (red), CD19 (blue) and CXCL13 (green). Quantitative PCR analysis of CXCL13 **(B)**. CCL19 **(C)**, CXCR5 **(D)**, CCR7 **(E)** and LTβ **(F)** and BAFF **(G)** mRNA obtained from salivary glands at day 5, 8, 15 and 23 p.c. Expression of these genes is shown for *il22rako* mice (white bars) compared to their *wt* counterparts (black bars); CXCL13, CCL19 and BAFF mRNA transcripts were normalized to PDGFRβ mRNA. CXCR5, CCR7 and LTβ mRNA transcripts were normalized to β-actin mRNA. Results are presented as relative quantitation (RQ) values calculated with calibrator day 0 salivary gland * $p < 0.05$; ** $p < 0.01$. Data are representative as mean ± s.e.m. of three independent experiments with three to four mice per group.

5.4 IL22 Receptor engagement is required for LLSc proliferation

Since analysis of LLSc in chapter 1 had shown that these cells were responsible for the production of lymphoid chemokines and cytokines in the salivary gland inflammation model, it was postulated that the defect in TLO formation observed in the *il22ko* might be due to an effect on LLSc maturation or expansion.

First, to investigate whether IL22 exerted its effect directly on LLSc, the expression of IL22rα on the LLSc was examined. FACS analysis performed on digested tissue revealed that IL22Rα was expressed, both on gp38+LLSc and on the gp38-CD31-EPCAM-CD45- stroma in non-stimulated tissue **(Figure 5.4.1A)**. Five days p.c. the percentage of IL22Rα+ expression increased in the LLSc, but not in the gp38-CD31-EpCAM-CD45- cells ($p<0.01$), suggesting preferential up-regulation of IL22rα in this population **(Figure 5.4.1A-B)**. The specificity of the IL22Rα staining was confirmed by staining the digested salivary glands of *il22rαko* mice, both at day 0 and day 5 p.c **(Figure 5.4.1A)**. The up-regulation of IL22Rα was further confirmed at mRNA level in the LLSc. As expected, IL-22Rα expression was also observed in the EPCAM+ epithelial cells **(Figure 5.4.1C)**. Analysis of cell proliferation, comparing IL22Rα+ and IL22Rα- cells within the LLSc and double negative (gp38-CD31-EPCAM-CD45-) populations, showed a significant proliferative advantage ($p<0.01$) for IL22Rα+LLSc as compared to IL22Rα-LLSc **(Figure 5.4.1D)**.

In order to further examine the formation of LLSc in the salivary glands of both Il22ko and Il22rako, as compared wt mice, these mice were cannulated with replication deficient adenovirus, and FACs analysis of the lymphoid stromal cell compartment was performed **(Figure 5.4.2A-B)**. The *il22ko* and *il22rαko* mice exhibited an intact activation of LLSc up to day 2 p.c., confirmed by a ~20% increase in percentage of LLSc observed in these ko mice, similar to wt mice. However, the wt mice at day 5 ($p<0.05$) showed further increase of nearly 20% in the LLSc component, whereas both the il22ko and *il22rαko* demonstrated failure to expand the LLSc at day 5. This significant decrease in LLSc was further maintained at day 8

(p<0.01-0.001) and day 15 (p<0.01) p.c., with nearly 10% difference observed in the wt compared to *il22ko* and *il22rako* at these time points **(Figure 5.4.2A-B)**.

In order to assess the proliferative status of LLSc in absence of il22 signal, BrdU and Ki67 staining was performed on the LLSc from *il22rako ko* and wt mice. Interestingly, the *il22rako* mice showed decreased proliferation at day 5 (~10% LLSc were BrdU+ and ~2.5% were Ki67+ in contrast to ~40% BrDU+ and ~8% Ki67+ LLSc in wt mice). BrdU staining on LLSc at other time-points revealed the reduced proliferative ability of the LLSc in *il22rako* mice at all other time points as well. A moderate increase in Ki67+ LLSc was observed at day 15 p.c. **(Figure 5.4.2C-D)**.

Overall, this data suggests that IL22Rα engagement is crucial for the LLSc proliferation but not required for LLSc induction at the sites of TLO formation.

Figure 5.4.1

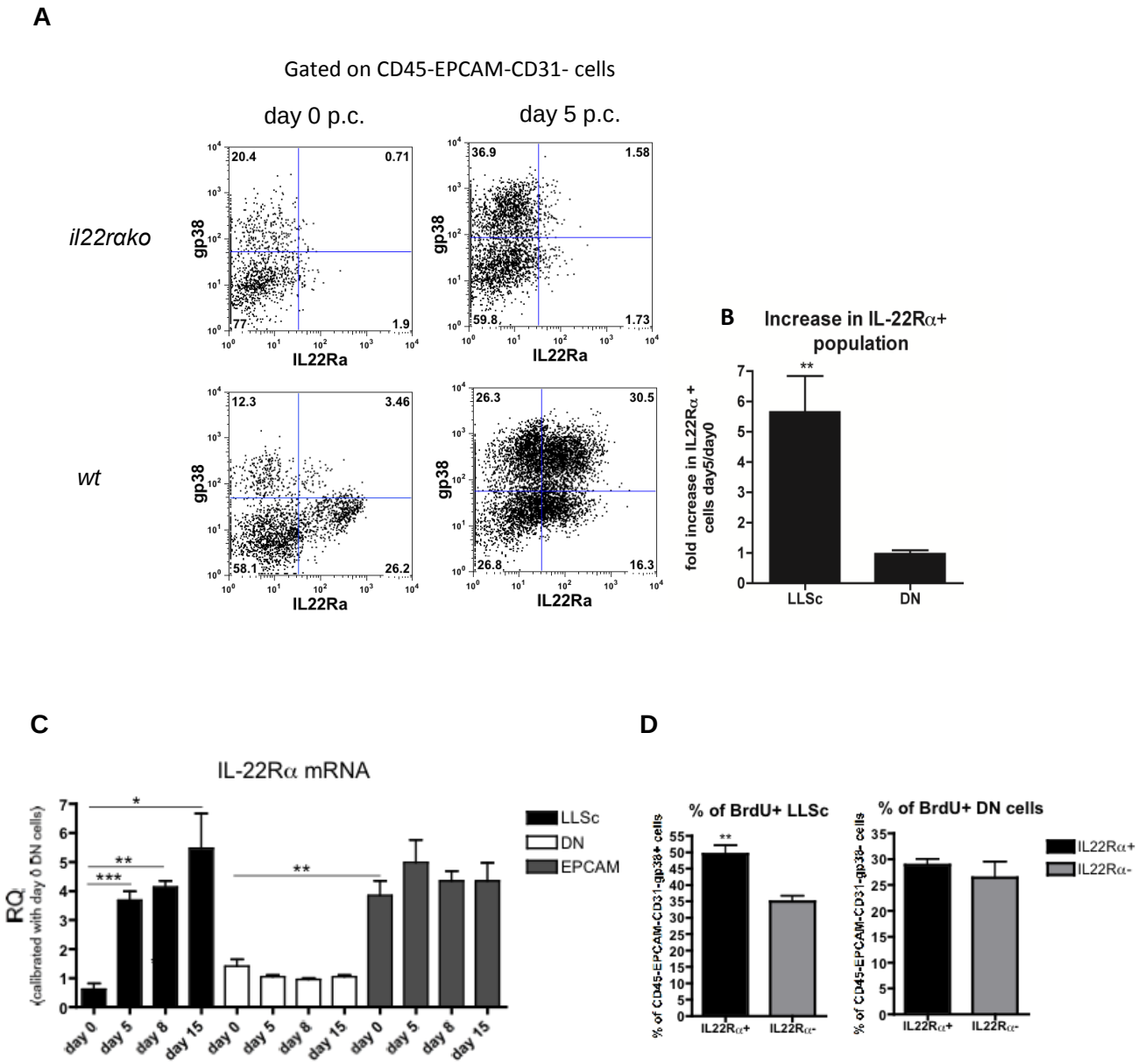

Figure 5.4.1 IL22 Receptor engagement is required for LLSc proliferation. Representative dot plots showing flow cytometry for IL-22Rα+ cells in the CD45-EPCAM-CD31- gp38+ and gp38- stromal component at day 5 p.c. salivary glands in *il22rako* and *wt mice* **(A)**. FACS analysis of the fold increase in IL22rα+ expressing cells **(B)** within CD45-EPCAM-CD31-gp38+ cells and CD45-EPCAM-CD31-gp38- cells at day 5 p.c. as compared to day 0. Data representative of two different experiments with two mice per group, expressed as mean ± s.e.m ** $p < 0.01$. IL22Rα transcripts **(C)** on FACS sorted gp38+CD31-LLSc (black bars) in comparison to gp38-CD31- double negative cells (DN, white bars) and CD45-EPCAM+ (epithelial) cells (grey bars). Transcripts were assessed by quantitative RT-PCR and normalized to housekeeping gene β-actin. Relative quantitation (RQ) calculated with calibrator day 0 DN cells. Data expressed as mean ± s.e.m. of two independent experiments with three mice per group. *, $p<0.05$; **, $p<0.01$; *** $p<0.001$ unpaired t test, comparing LLSc with DN at each time point. BrdU **(D)** incorporation in IL22Rα+ (black bars) and IL22Rα- (grey bars) cells within CD45-EPCAM-CD31-gp38+ (LLSc) and CD45-EPCAM-CD31-gp38- (DN) cell populations at day 5 p.c. Graph representative of two different experiments with three mice per group. Data expressed as mean ± s.e.m ** $p<0.01$.

Figure 5.4.2

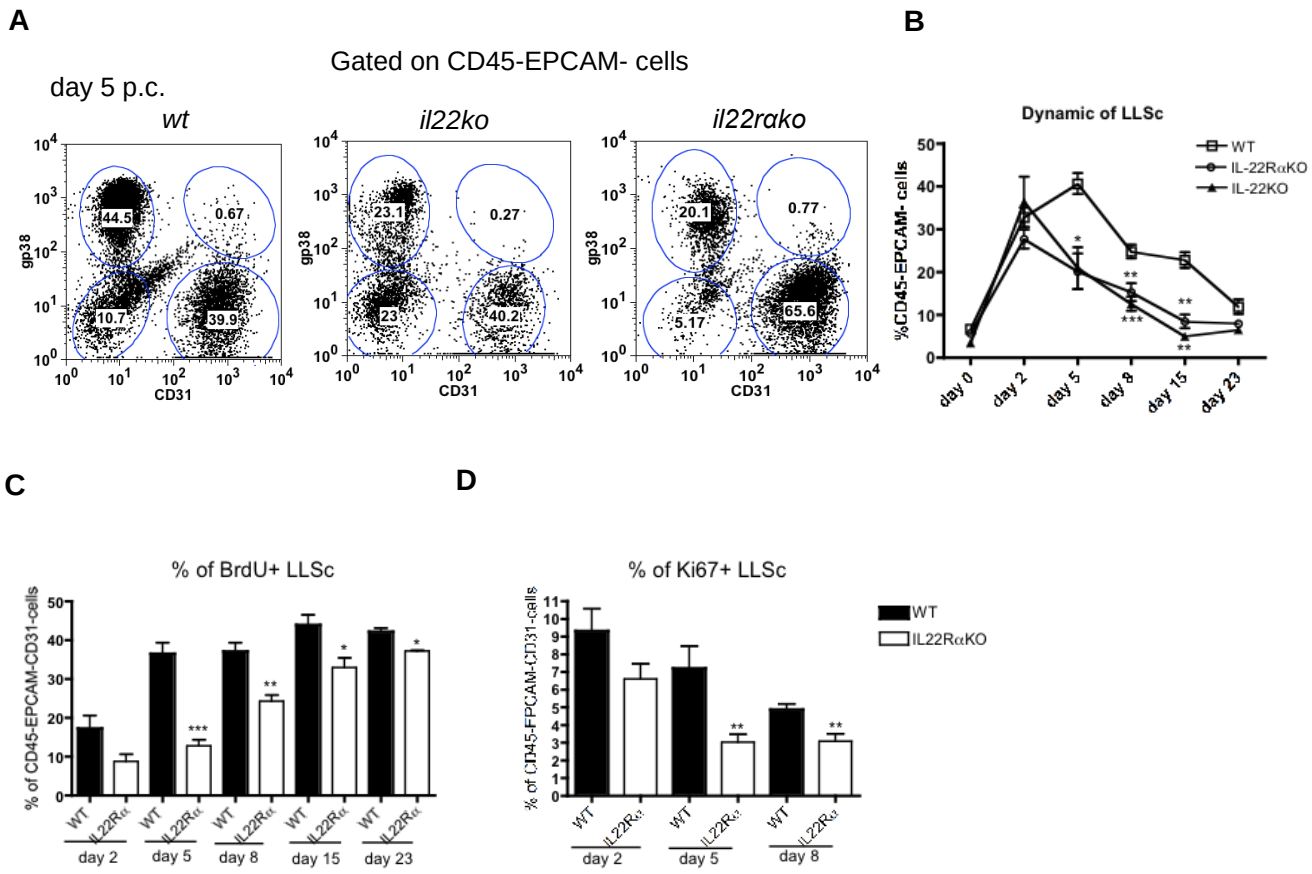

Figure 5.4.2 *il22ko* and *il22rako* exhibit defective LLSc expansion. FACS histogram representing **(A)** LLSc expansion in *il22ko* and *il22rako* compared to *wt* mice at day 5 p.c. Graph summarising **(B)** the FACS data, *il22rako* (open circles), *il22ko* (open triangles) and *wt* mice (open squares). Data are presented as mean ± s.e.m. of three independent experiments with at least two mice for each experiment. * p<0.05; ** p<0.01, *** p<0.001, unpaired t test. Graph summarizing flow cytometry data of BrdU incorporation **(C)** and Ki67+ **(D)** in LLSc from *wt* (black bars) and *il22ra*ko (white bars) mice from day 2, 5, 8, 15 and day 23 p.c. * p<0.05; ** p<0.01, *** p<0.001 versus cannulated *wt* mice. Data presented as mean ± s.e.m. of three independent experiments with at least three mice for each experiment.

5.5 IL22 administration up-regulates IL-22Rα expression and regulates LLSc proliferation

To confirm whether IL22 alone was responsible for the induction of LLSc proliferation, IL22 recombinant protein or PBS was directly cannulated into the salivary glands of *wt* mice in the absence of virus.

A 30% increase ($p<0.05$) in the LLSc component was observed in the recombinant (r) IL-22 **(Figure 5.5.1A and C)** cannulated salivary glands when compared to PBS cannulated salivary glands. As expected nearly 30% of LLSc were positive for Ki67 in rIL22 ($p<0.001$) cannulated salivary glands compared to 1% of Ki67+ LLSc in PBS cannulated salivary glands **(Figure 5.5.1A and D)**. Further analysis of LLSc and DN cells in rIL22 cannulated mice, showed an increased proliferative ability of the LLSc ($p<0.001$) compared to DNs **(Figure 5.5.1E).** IL22 is known to induce cell proliferation via the phosphorylation of Akt and mTOR activation [329]. Hence, IL22rα activity in LLSc was confirmed by showing increased phosphorylated Akt in LLSc compared to DN cells in rIL22 cannulated glands and LLSc from PBS cannulated salivary glands **(Figure 5.5.1B)**. MFI data exhibited almost three fold increase ($p<0.001$) in the gp38 expression on LLSc when salivary glands were cannulated with rIL-22 as compared to PBS **(Figure 5.5.1F)**.

IL22 administration, but not PBS, demonstrated the ability of IL-22 to induce up-regulation of IL22Rα on the LLSc, four-fold increase in IL22Rα expression was observed in LLSc compared to DN cells **(Figure 5.5.2A-B)**.

Figure 5.5.1

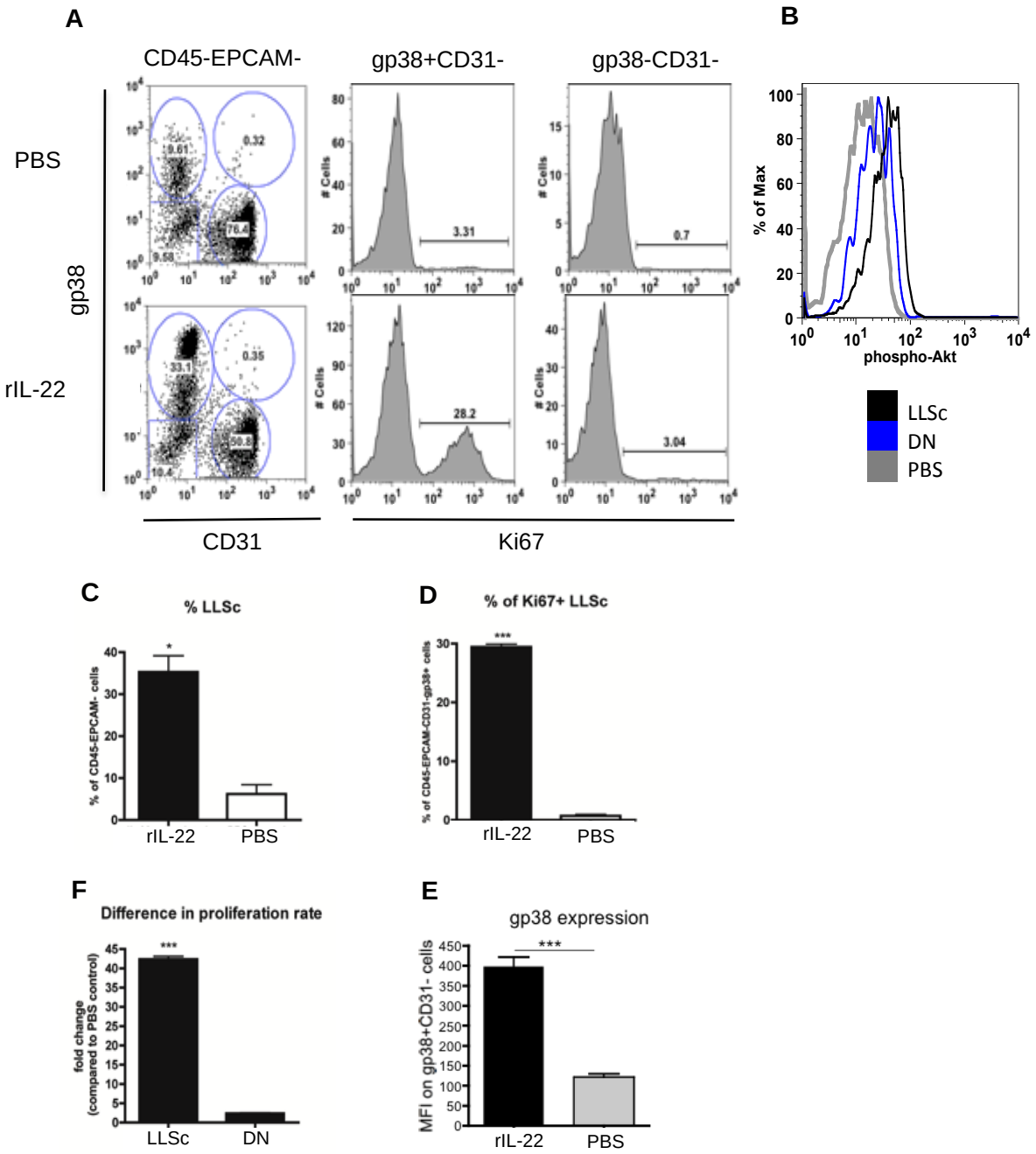

Figure 5.5.1 Direct IL22 administration induces LLSc proliferation. *wt* mice salivary glands were directly cannulated with IL22 recombinant cytokine (rIL22) or PBS and analysed at day 2 p.c. Representative dot plots **(A)** showing expansion of the CD45-EpCAM- CD31- gp38+ cells post treatment with IL22 or PBS. Histogram showing increased phosphorylation of AKT **(B)** at day 2 p.c. in CD45-EpCAM-CD31-gp38+ cells as compared to CD45-EpCAM-CD31-gp38- cells taken from salivary glands stimulated with IL22 (black and blue lines) compared to PBS (grey line). Proliferation was assessed by Ki67 staining for CD45-EpCAM-CD31-gp38+ and CD45-EpCAM- CD31-gp38- stromal cells. Graph summarizing the flow cytometry data showing a significant increase in the percentage of CD45-EpCAM-gp38+CD31- **(C)** and percentage of Ki67+ cells **(D)** within CD45-EpCAM-CD31-gp38+ cell population and the difference in proliferation rate **(E)** between CD45-EpCAM-CD31-gp38+ and CD45-EpCAM-CD31-gp38- cells and increased gp38 expression (shown as MFI values) on CD45-EpCAM-CD31-gp38+ cells **(F)** in IL22 treated mice (day 2 p.c.)**.** Data are presented as mean ± s.e.m. of three independent experiments two mice per group * $p<0.05$; *** $p < 0.001$.

Figure 5.5.2

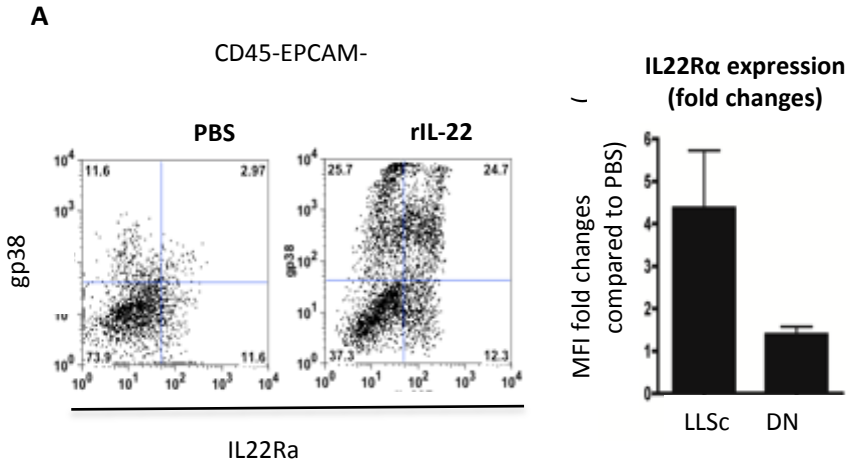

Figure 5.5.2 IL22 administration up-regulates IL-22Rα expression. *wt* mice salivary glands were directly cannulated with IL22 recombinant protein (rIL22) or PBS and analysed at day 2 p.c. Flow cytometry for IL22rα expression on CD45-EpCAM-CD31- cells from PBS and recombinant IL22 cannulated mice. Graph representing the FACS data for the fold increase in IL22rα+ expressing cells within CD45-EPCAM-CD31-gp38+ cells and CD45-EPCAM-CD31-gp38- cells in IL22 treated mice as compared to day PBS treated mice. Data are presentated as mean ± s.e.m. of three independent experiments two mice per group.

5.6 IL22Rα engagement on LLSc up-regulates lymphoid chemokines and cytokines

Given the severe impairment observed in expression of lymphoid chemokine and cytokines in *il-22ko* mice and the suggestion in literature that IL-22 can directly up-regulate CXCL13 expression in lung fibroblasts [324], we hypothesized that IL-22 not only promotes expansion of LLSc but also supports their production of lymphoid chemokines and cytokines. To test this hypothesis, LLSc were isolated from salivary glands of mice, cultured *in vitro* for 24 hours with rIL22, rTNFα+LTβR agonist, rIL22+rTNFα+LTβR agonist or PBS and analyzed for the expression of CXCL13 **(Figure 5.6A)**, CCL19 **(Figure 5.6B)** and BAFF **(Figure 5.6C)** by quantitative PCR. As expected, treatment with TNFα+LTβR agonist promoted increased expression ($p<0.05$) of CXCL13, CCL19 and BAFF, but a significant up-regulation in these genes, and in particular, CXCL13 ($p<0.05$) was also observed in LLSc treated with only rIL22. Combined treatment with rIL22+rTNFα+LTβR agonist increased the expression of CXCL13 ($p<0.01$), CCL19 and BAFF ($p<0.01$) above the levels observed with the single cytokines.

Figure 5.6

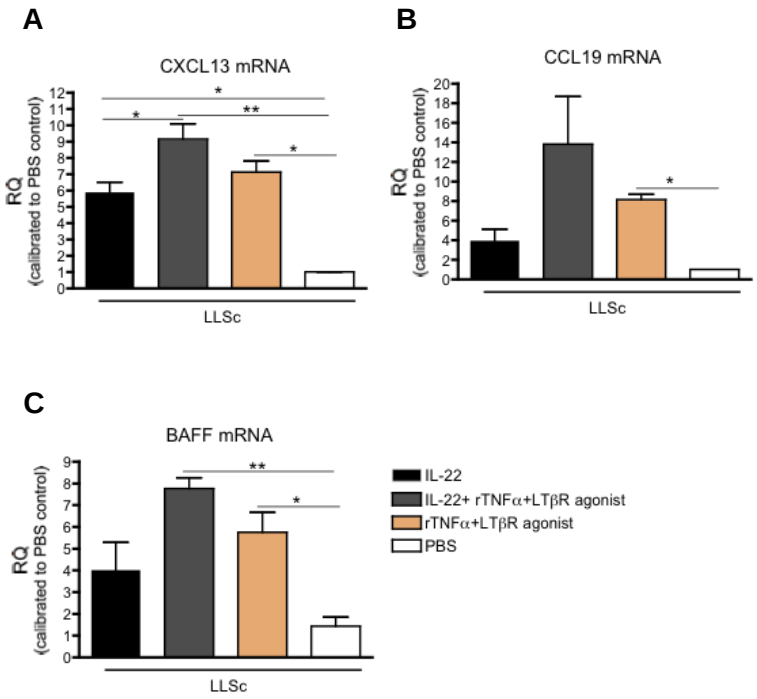

Figure 5.6 IL22Rα engagement on LLSc up-regulates lymphoid chemokines and cytokines. Quantitative PCR analysis of CXCL13 **(A)** CCL19 **(B)** and BAFF **(C)** mRNA obtained from LLSc stimulated with recombinant cytokines; IL-22 (black bars), IL-22+TNFα+LTβR agonist (grey bars), TNFα+LTβR agonist (light brown bars) or PBS (white bars). CXCL13, CCL19 and BAFF mRNA transcripts were normalized to β-actin mRNA. Results are presented as relative quantitation (RQ) values calculated with calibrator day 0 salivary gland * $p < 0.05$; ** $p < 0.01$. Data are representative as mean ± s.e.m. of three independent experiments with three to four mice per group.

5.7 Therapeutic IL22 blockade inhibits stromal cell proliferation and abolishes autoantibody production

In order to explore therapeutic consequences of our findings in *il22ko* mice, cannulated mice were treated with blocking anti-IL22 antibody starting at either day 2 or day 8 p.c. IF analysis revealed defective lymphoid aggregate formation in IL-22 blocking antibody treated mice compared to untreated mice, both in terms of TLOs size **(Figure 5.7.1A-B)** and B/T-cell organization **(Figure 5.7.1A and C).** This impairment was more pronounced if mice were treated from day 2 p.c. compared to day 8 p.c. **(Figure 5.7.1A-C)**. Quantitative RT-PCR analysis of the salivary glands from treated mice showed significant reduction in the production of cxcl13, ccl19 and baff, as observed in the *il22ko* mice **(Figure 5.7.1D-F)**. This was accompanied by a significant defect in the expansion and proliferation of the LLSc in the treated mice **(Figure 5.7.1G-H)**. Marked suppression of aicda mRNA transcripts was also observed in mice treated with IL-22, blocking antibody **(Figure 5.7.2A)** that coincided with a significant decrease in ANA autoantibody production **(Figure 5.7.2B-C)**.

Figure 5.7.1

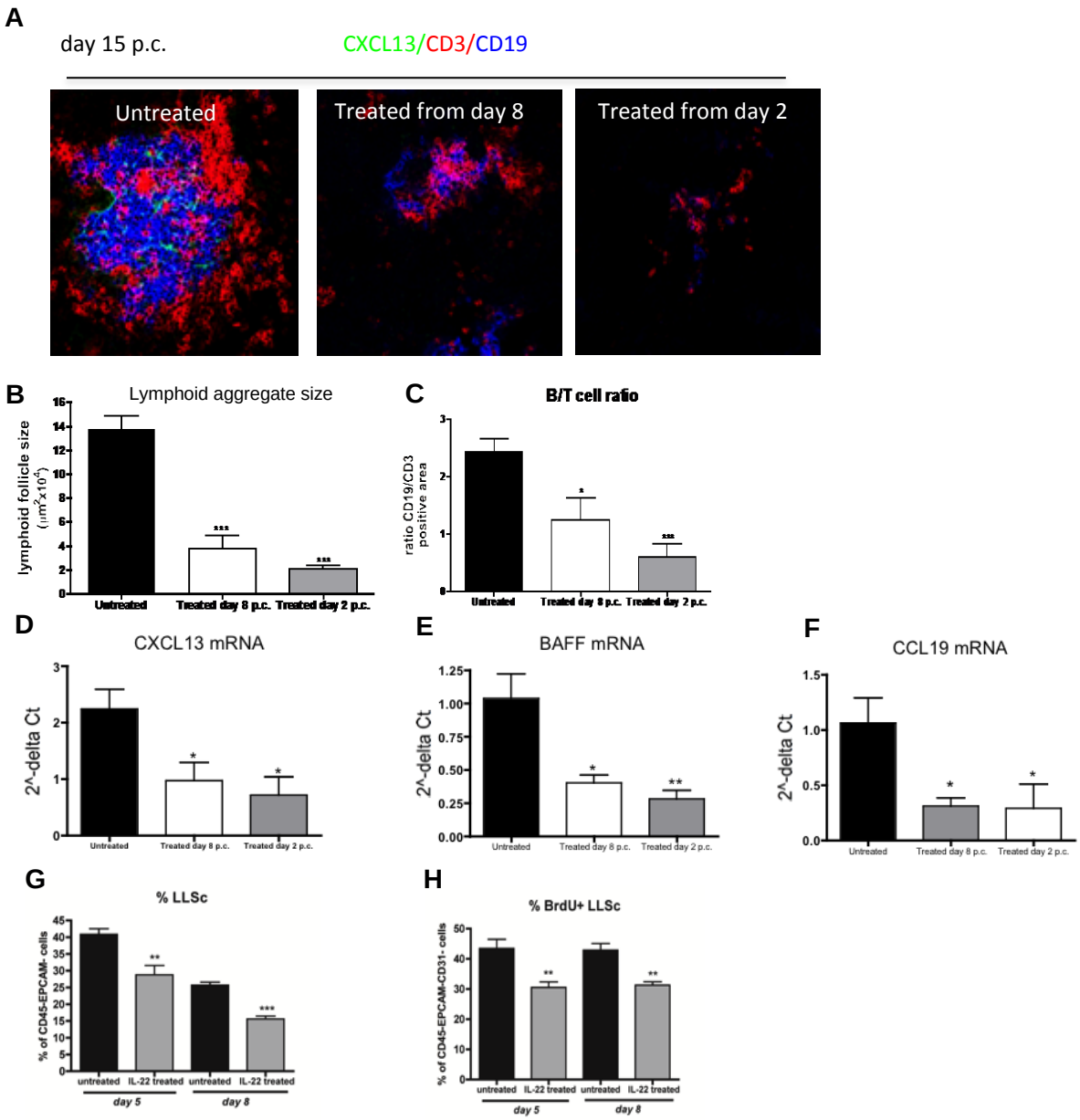

Figure 5.7.1 Therapeutic IL22 blockade inhibits stromal cell proliferation. Cannulated wt mice were treated with IL22 blocking antibody every three days from day 2 p.c. or every three days from day 8 p.c. Microphotographs of lymphocytic aggregates **(A)** from wt cannulated salivary glands from untreated mice and mice treated with anti IL22 blocking agent from day 8 or day 2 p.c. analysed at day 15 p.c. for CD3 (red), CD19 (blue) and CXCL13 (green). Original magnification 25X. Lymphoid aggregate **(B)** for untreated mice (black bars) compared to mice treated from day 8 p.c. (white bars) and mice treated from day 2 p.c. (grey bars) for aggregates at day 15 p.c. *** $p < 0.001$. The ratio between the area covered by CD19+ B cells and CD3+ T cells **(C)** at day 15 p.c. for untreated (black bars) vs. treated from day 8 p.c. (white bars) and treated from day 2 p.c. (grey bars) mice. Data are represented as mean ± s.e.m. of two independent experiments with two to three mice per group. * $p < 0.05$; *** $p < 0.001$, unpaired t test between each group. Quantitative PCR analysis for cxcl13 mRNA **(D),** ccl19 mRNA **(E) and** baff mRNA **(F)** obtained from salivary glands at day 15 p.c. is shown for *wt* cannulated untreated mice (black bars) and mice treated with IL22 blocking antibodies from day 8 p.c. (white bars) and day 2 p.c. (grey bars). cxcl13 mRNA transcripts were normalized to pdgfrβ mRNA and results are presented as relative quantitation (RQ) values calculated with calibrator day 0 untreated salivary glands ** $p < 0.01$; *** $p < 0.001$ versus untreated cannulated salivary gland. Data are presented as mean ± s.e.m. of two independent experiments with two to three mice per group. Percentage of LLSc **(G)** in mice treated with IL22 blocking antibody from day 2 p.c. (grey bars) as compared to untreated controls at day 5 and 8 p.c. (black bars). Graph showing flow cytometry data for percentage of BrdU+ cells within LLSc **(H)** cells in mice treated with IL22 blocking antibody from day 2 p.c. (grey bars) as compared to untreated controls at day 5 and 8 p.c. (black bars). Data representative of two experiments with two to three mice per group, Data are expressed as mean ± s.e.m. ** $p < 0.01$, *** $p < 0.001$ versus untreated WT mice.

Figure 5.7.2

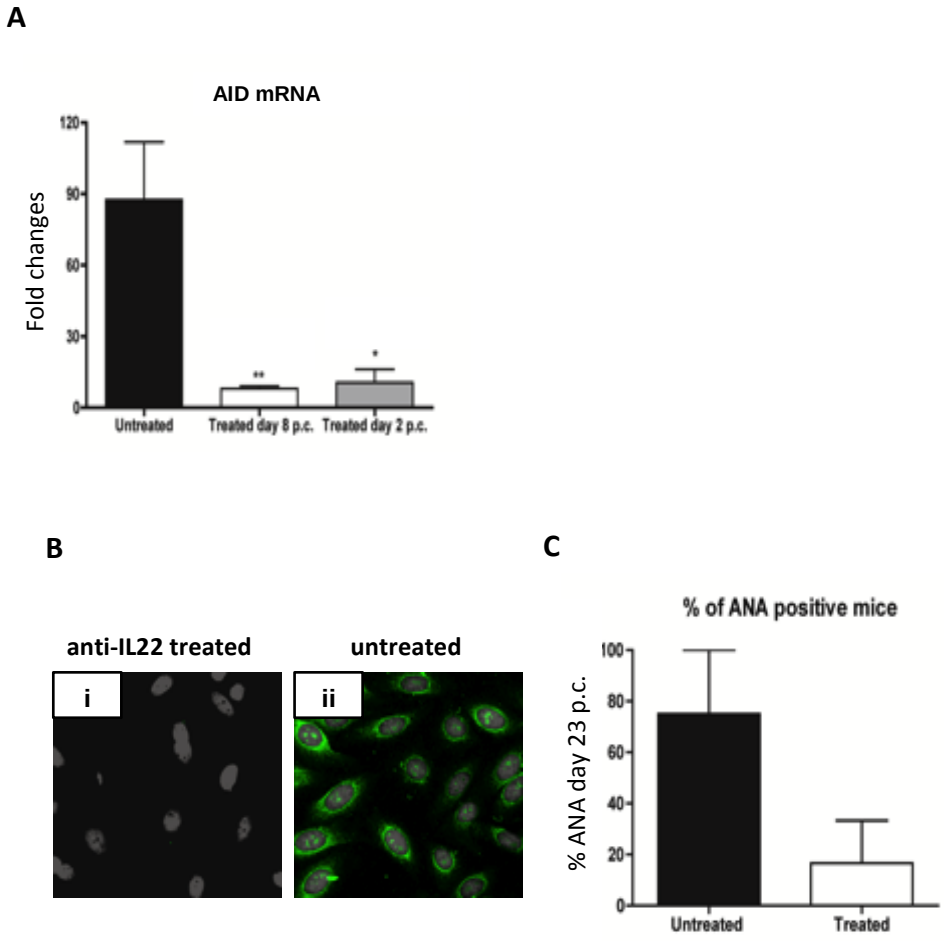

Figure 5.7.2 Therapeutic IL22 blockade abolishes autoantibody production. Quantitative PCR analysis for aicda mRNA **(A)** obtained from salivary glands at day 23 pc., for *wt* cannulated untreated mice (black bars) and mice treated with IL22 blocking antibodies from day 8 p.c. (white bars) and day 2 p.c. (grey bars). Results are presented as RQ value as compared to day 0 resting salivary glands. * $p < 0.05$; ** $p < 0.01$. Data are presented as mean ± s.e.m. of two independent experiments with two to three mice per group. **(B)** Representative microphotographs of immunofluorescent detection of ANA on Hep2 cells showing nuclear reactivity in sera of day 23 p.c. untreated *wt* mice, **(Bi)** and loss of ANA antibody in the anti-IL22 treated mice **(Bii)** from day 2 p.c. at day 23 p.c (nuclear staining in grey, ANA reactivity in green)(dilution 1:80). Original magnification 40X. **(C)** Graph summarizing ANA reactivity in treated vs. untreated mice at day 23 p.c. Data are representative of two experiments with four cannulated mice (biological replicates expressed as percentage of mice positive for ANA at 1:80 dilution or more, mean ± s.e.m.)**.**

Discussion

IL22 regulates mucosal homeostasis and promotes epithelial repair following tissue damage [330, 331]. Recently, implicated in malignant epithelial cell proliferation [319], the role of IL22 in chronic inflammation remains enigmatic. Studies in humans have detected IL22 mRNA in salivary glands of patients with SS [332], and in this disease, elevated serum levels of IL22 correlate with disease parameters, including hyper-gammaglobulinemia and autoantibody production [325]. These clinical observations suggest a role for IL-22 in TLO-associated inflammatory diseases such as SS. This chapter documents data on IL22 and its role in regulating stromal cell proliferation during TLO formation in our model of salivary gland inflammation.

Similar to IL-13, increased expression of IL22 was found to occur within hours of salivary gland cannulation, with different cell populations involved in IL22 production. Various immune cell populations particularly T cells, NK cells and innate lymphoid cells belonging to the LTi family have been reported to produce IL-22 [322]. In the earliest phases, $\gamma\delta$ T cells represent the major source of IL22, although other cell types such as innate lymphoid cells (ILC) and natural killer cells (NK) also contributed to the production of this cytokine. By day 5, newly recruited $\alpha\beta$ T cells were primarily responsible for the second wave of IL22 expression.

Recently, IL22Rα expression has been observed in a population of non-epithelial stromal cells isolated from rheumatoid arthritis synovial tissue [329]. Similarly, in our model, IL-22Rα was detected on the LLSc and shown to play a non-redundant role in the proliferation of gp38+IL22Rα+ LLSc via AKT phosphorylation. Several cytokines such as TNFα or IFNα have associated with up-regulation of IL-22Rα on epithelial cells and keratinocytes [333, 334]. TNFα expression is detected early in inflammation in our model and therefore could be possibly involved in IL-22Rα up-regulation that we observe. A role for IFN cannot be ruled out as this family of cytokines are expressed early as a first line of defence during adenovirus virus infection [17, 19].

We also showed that IL22 expression is able to induce up-regulation of IL22Rα on LLSc, thus establishing an amplificatory loop, which provides a feed forward proliferative advantage to this cellular component. We demonstrated that CXCL13, CCL19 and BAFF expression can be directly regulated by IL22Rα engagement as previously shown *in vitro* [324]. It has been elegantly demonstrated that CXCL13 expression is necessary and sufficient for the establishment of lymphoid follicles [36, 169] and for the regulation of functional germinal centres [335]. We propose that the impairment of CXCL13 and BAFF production, due to poor expansion and activation of LLSc, as observed in the *il22ko* and *il22rako*, is most likely responsible for the impaired B cell accumulation, aberrant follicle formation and lack of autoantibody production observed.

There is convincing evidence that AID expression, on locally activated B cells within TLOs, supports class switch recombination and somatic hypermutation, thus sustaining affinity maturation of autoreactive B cells to tissue autoantigens [194, 233]. In this study we showed that IL22-driven LLSc expansion is critical for the establishment of TLO and tightly associated with the development of ANA antibodies. It has recently been shown that exposure of salivary gland epithelial cells to anti Ro/SSA and La/SSB antibodies is able to induce IL22 production [336]. In agreement with these *in vitro* observations, there is evidence that B cell depletion, following treatment with Rituximab, decreased expression of IL22 in the salivary glands [337]. This strongly suggests the possibility of a feed forward loop established between IL22 expression, survival of autoreactive B cells and autoantibody production. Such an amplificatory loop may also be relevant to the well-known, but poorly understood association between Sjogren's syndrome and the predisposition to B cell mucosal associated lymphoma [231], where an increase in IL22 production might play a role.

Therapeutic blockade of IL22 using function blocking antibodies is sufficient to impair TLO formation and abolish autoantibody production. This effect, phenocopies observations in the *il22*-/- and *il22r*α-/- mice, is also mediated by decreased LLSc proliferation, which leads to

decreased CXCL13 and BAFF expression as well as defective B lymphocyte accumulation in the salivary glands.

Overall, these observations indicate a functional connection between the expression of IL22, the proliferation of pathogenic stroma and the production of autoantibody that provides a new therapeutic option, and suggests an important role for IL22 in humoral responses at sites of inflammation.

Chapter 6

Maturation of lymphoid stromal cells to support TLO formation is dependent on lymphocytes and LTβR signalling

Introduction

Ltαko, ltβko and *ltβrko* mice lack LNs, underpinning the prime position of LTβR and its ligand in lymph node formation [11, 56, 117, 118]. Similarly, absence of lymphotoxin, expressing lymphoid tissue inducer cells (LTi), as in the *rorγtko* or *id2ko* mice, results in complete lack of lymph nodes, highlighting the absolute necessity of LTi cell-derived signals in secondary lymphoid organogenesis [11, 42, 48, 56, 338]. During development, LN formation is critically dependent on the interaction between LTβR expressed on mesenchymal cells (stromal organizer cells) and LTα1β2 produced by CD3-CD4+RORγ+ hematopoietic cells (LTi cells). The LTβR triggering subsequently leads to the production of chemokines, such as CXCL13, CCL19, CCL21 and CXCL12, and up-regulation of stromal adhesion molecules VCAM-1 and ICAM-1 expression. This results in accumulation of more haematopoietic cells, including T cells and B cells, resulting in an amplificatory loop. During this phase, organizer cells further differentiate to various lymphoid stromal cell subsets that organize lymphocytes into distinct T cell zones and B cell follicles. Moreover, sustained LT expression is also crucial for maintenance of lymphoid architecture in adult LNs [11, 16, 56, 117, 118].

Evidence over the last few years has highlighted the role of lymphoid cytokines and lymphoid cells in supporting TLO formation [4, 12-14]. Most of the data, supporting the role of LT/LTβR involvement in TLO has come from transgenic models, overexpressing LT and its downstream products such as lymphoid chemokines or circumstantial evidence from human diseases where these molecules have been detected in patient tissues harboring TLO. However, transgenic models lack the complexity of a pathophysiological process and human studies just give us a snapshot of the dynamic inflammatory disease process.

Data presented in the previous chapters and in the recent literature clearly demonstrates that TLO formation can be initiated by inflammatory effector cytokines and does not necessarily requires the LTβR pathway, suggesting that SLO and TLO may use different pathways for their development [214, 230, 281, 339]. Nevertheless, blocking of LTβR has been shown to be beneficial in some established models of autoimmunity [257, 340, 341], supporting their crucial role in inflammatory disease. Therefore, the exact role that LT/LTβR interaction plays during TLO formation and maturation needs to be formally addressed.

The identity of inducer cells, that provide LT during the development of TLO during inflammation, is still in debate. The literature is divided among adult LTi cells or lymphocytes [12-14]. In this chapter we used the adenoviral infected salivary glands mouse model of TLO formation to dissect the role of LT/LTβR axis in ectopic lymphoneogenesis and also aimed to identify the TLO-inducer cell.

Results

6.1 Lack of LTβR signalling impairs full lymphoid conversion of LLSc

In order to examine the role of LTβR in TLO formation and maturation, we cannulated the salivary glands of *ltβrko* mice. The development of TLOs was followed to evaluate the timing of T and B cell populations as well as the compartmentalization and expression of lymphoid chemokines. Even though, lymphoid cell infiltration was observed within the salivary glands of *ltβrko*, the total lymphoid area was significantly lower in *ltβrko* mice ($p<0.01$), only ~3-4% of total lymphoid aggregate area was observed in these mice compared to 8-10% in wt mice at day 8 and day 15 p.c. **(Figure 6.1.1A-B)**. Accordingly, the size of the lymphoid follicles **(Figure 6.1.1D)** was smaller at day 8 p.c., and this difference in size became significant at day 15 p.c. ($p<0.05$) when compared to lymphoid follicles formed in the *wt* mice. Moreover, the lymphoid aggregates did not show clear segregation between the T and B cell area in *ltβrko* mice **(Figure 6.1.1C)**. In addition, the B/T cell ratio **(Figure 6.1.1E)** in *ltβrko* mice was significantly lower at day 8 and 15 p.c. ($p<0.05$) as compared to *wt* mice. In line with these observations, a significant decrease in AID mRNA expression was detected at week 3 p.c in the *ltβrko* mice salivary glands as compared to salivary glands of wt mice **(Figure 6.1.1F)**

Expression of the lymphoid chemokines (CXCL13 and CCL19) was evaluated by quantitative PCR analysis of salivary gland tissue from *ltβrko* and compared to wt mice. Expression of CXCL13 was drastically reduced in the *ko* mice at day 5 ($p<0.05$), day 8 ($p<0.001$) and day 15 ($p<0.001$) p.c. **(Figure 6.1.2A)**. Of interest, the immunofluorescence analysis also showed a significant reduction in the expression of CXCL13 in cannulated salivary glands of *ltβrko* mice as compared to *wt* controls **(Figure 6.1.1Ai and iii)**. CCL19 mRNA **(Figure 6.1.2B)** expression was intact at day 5 p.c. in the *ltβrko* mice but showed significant decline at day 8 ($p<0.01$) and day 15 ($p<0.001$) p.c. This decrease in chemokines correlated with CXCR5 and CCR7 mRNA expression **(Figure 6.1.2C-D)**. Finally, gene expression analysis revealed a significant reduction in the BAFF and IL7 transcript levels in *ltβrko* infected mice **(Figure 6.1.2E-F)**. Overall, these results indicate a defect in full TLO maturation in *ltβrko* mice.

Figure 6.1.1

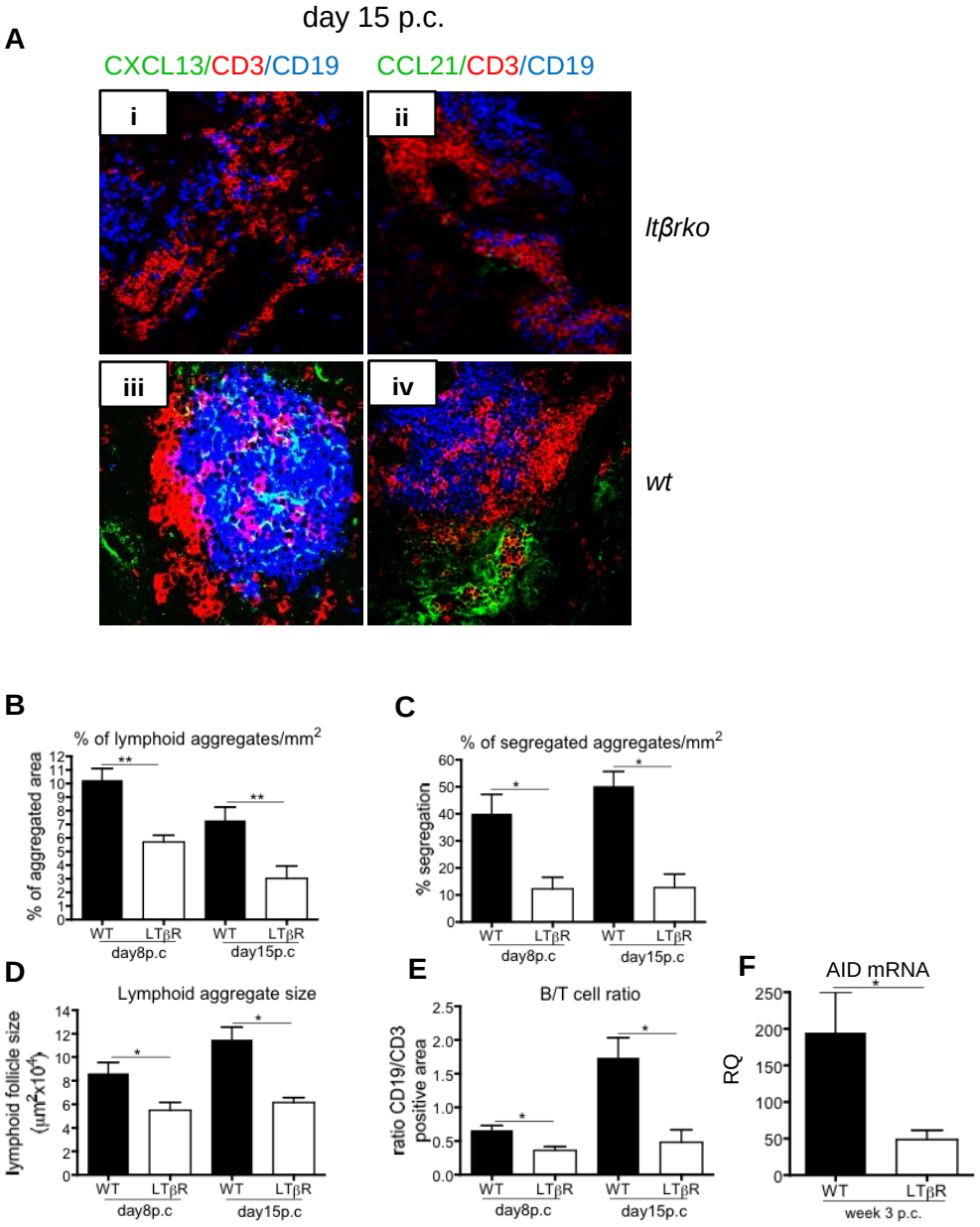

Figure 6.1.1 Absence of LTβR signalling prevents formation and maintenance of fully mature TLOs. Microphotograph of lymphoid aggregates **(A)** from infected salivary glands (day 15 pc.) from *wt* **(Aiii-iv***)* and *ltβrko* **(Ai-ii)** mice stained for CD3 (red), CD19 (blue) and either CXCL13 (green in **i and ii**) or CCL21 (green in **iii and iv**). Salivary glands from *wt and ltβrko* day 8 and 15 p.c. were examined by immunofluorescence for CD3 and CD19. **B-E**, Graphs representing % of total lymphoid aggregate area **(B),** % of segregated aggregates **(C)**, lymphoid aggregate size **(D)** and ratio between the area covered by CD19+ B cells and CD3+ T cells **(E)** at day 8 and day 15 p.c. for *wt* (black bars) and *ltβrko* (white bars) mice. Data is representative of two different experiments with two to three mice per group, mean ± s.e.m. *, p<0.05, unpaired t test, comparing *ltβrko* to *wt* mice. **(F)**, Transcripts encoding for AID gene (normalized to housekeeping gene β-actin), in week 3 p.c. salivary glands from *wt* and *ltβrko* mice, were quantified and expressed as RQ values relative to day 0 p.c. AID mRNA. Data shown as mean ± s.e.m. of three independent experiments.

Figure 6.1.2

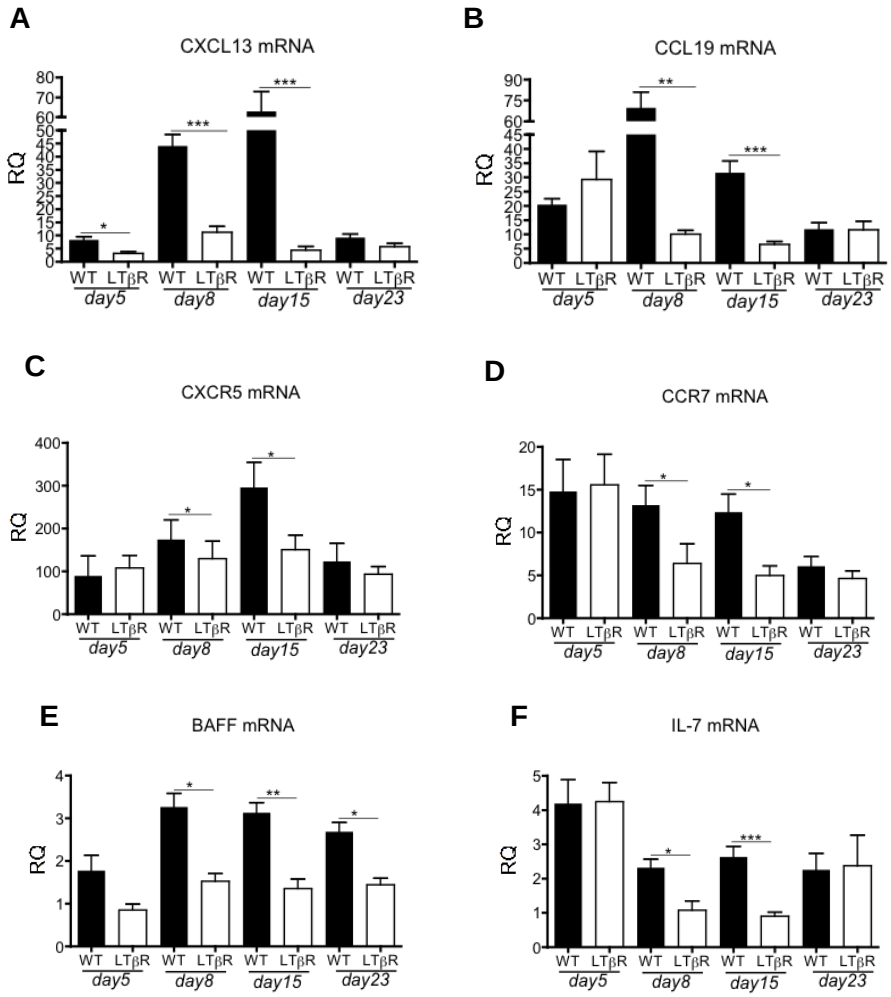

Figure 6.1.2 Lack of LTβR impairs production of TLO-associated genes. Quantitative PCR analysis of CXCL13 **(A)** CCL19 **(B)**, CXCR5 **(C)**, CCR7 **(D)**, BAFF **(E)** and IL-7 **(F)** mRNA obtained from salivary glands at day 5, 8, 15 and 23 p.c. Expression of these genes is shown for *ltβrko* mice (white bars) compared to their *wt* counterparts (black bars); CXCL13, CCL19, BAFF and IL-7 mRNA transcripts were normalized to PDGFRβ mRNA and CXCR5 and CCR7 mRNA transcripts were normalized to β-actin mRNA. Results are presented as relative quantitation (RQ) values calculated with calibrator day 0 salivary gland * $p<0.05$; ** $p<0.01$; *** $p<0.001$. Data are representative as mean ± s.e.m. of three independent experiments with three to four mice per group.

6.2 LLSc induction and expansion is not dependent on LTβR signalling

Interestingly, LLSc induction and proliferation was not affected in *ltβrko* mice, and a significant decrease in LLSc was only observed from day 15 p.c. **(Fig 6.2A-D)**. Furthermore, analysis of the LLSc phenotype in *ko* showed no significant differences as compared to *wt* mice in terms of percentage of ICAM-1^{int}/VCAM-1^{int} andICAM-1^{high}/VCAM-1^{high+} cell at day 5 p.c. **(Fig 6.2E-F)**. However, the analysis for ICAM-1 and VCAM-1 on LLSc at day 15 p.c. showed a lower percentage of ICAM-1^{int}/VCAM-1^{int} and ICAM-1^{high}/VCAM-1^{high+} cell **(Fig 6.2E-F)**. Moreover, reduced proliferation was observed in the LLSc compartment at day 8 p.c. demonstrated by Ki67 staining in the *ltβrko* mice **(Fig 6.2C)**.

Overall, this data indicated that even though LLSc induction and proliferation was not reliant on LTβR signalling during the early stages of stromal cell activation, but maintenance of LLSc phenotype and subsequent expansion was dependent on LTβR signalling at later stages of the inflammatory process **(Fig 6.2D-E)**.

Figure 6.2

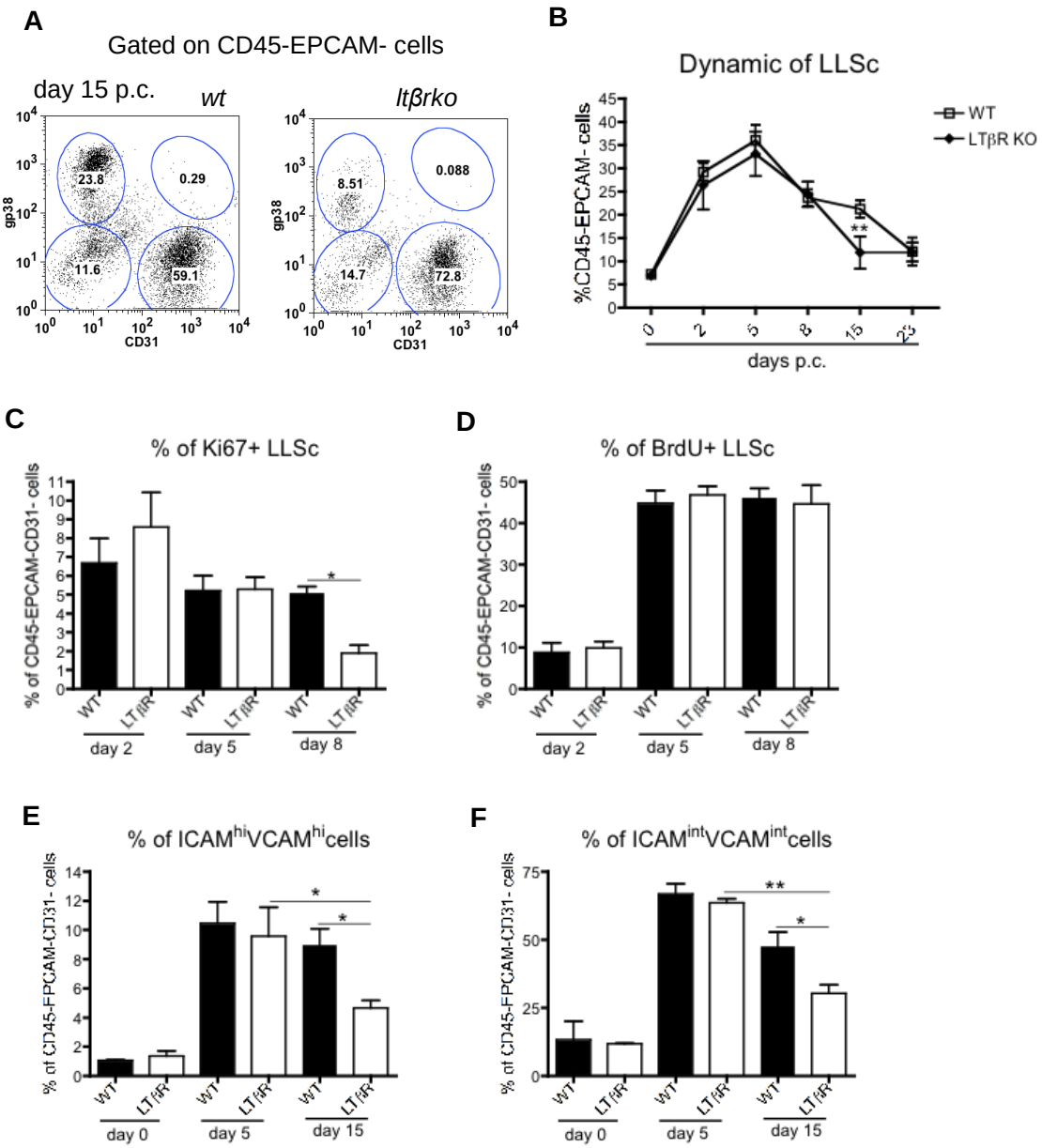

Figure 6.2 LLSc induction and expansion are not dependent on LTβR signalling. Representative dot plots **(A)** showing flow cytometry for percentage of gp38+CD31- population in the CD45-EPCAM- component from day 15 p.c. salivary glands in wt and *ltβrko.* Dynamic of LLSc expansion **(B)** during the inflammatory process determined by flow cytometry (percentage of gp38+CD31- population in the CD45-EPCAM- component) from infected *wt* (black squares)*and ltβrko* (open triangles) mice at 0, day 2, day 5, day 8, day 15, day 23 p.c. Data presented as means of five independent experiments. **, p < 0.01, unpaired t test, comparing *ko* LLSc population at each time point with corresponding *wt* LLSc population**. C-D**, Flow cytometry to show dynamic of Ki67+ LLSc **(C)** and BrDU+ LLSc **(D)** in wt (open squares) and *ltβrko* (black triangles) mice from day 2, day 5 and day 8 p.c. salivary glands. ∗, *p*<0.05 versus virus cannulated wt mice. Data are representative of two to three experiments with three to four mice per group. **E-F**, Flow cytometry of VCAM-1 and ICAM-1 expression in CD45-EPCAM- cells from salivary glands of *wt* and *ltβrko* mice. The graphs show percentage of VCAM-1^{hi} ICAM-1^{hi} cells **(E)** and VCAM-1^{int} ICAM-1^{int} cells **(F)** obtained by flow cytometry on day 0, day 2 and day 15 p.c. salivary glands from *ltβrko* mice (white bars) in comparison to wt mice (black bars). Data presented as means of two independent experiments ∗, *p*<0.05; **, p<0.01.

6.3 RORγ+ cells are redundant for LLSc generation and TLO formation

In *wt* cannulated animals RORγt+ adultLTi (CD3-CD4+IL-7Rα+RORγt+) were first detected at day 15 p.c. **(Figure 6.3.1A)** where they were mainly confined to the periphery of the aggregates, suggesting that RORγt+ cells are unlikely to play a role in the early phases of stromal cell activation. To confirm these observations, we cannulated the salivary glands of adult *rorγko* mice. Aggregates formed normally in these animals with no significant difference in terms of size, organization and chemokine expression when compared to wt mice **(Figure 6.3.2A-E)**. Accordingly, AID expression did not show any significant difference when compared to wt mice **(Figure 6.3.2F)**. Evaluation of lymphoid chemokines CXCL13 and CCL19, and their cognate receptor expression in salivary glands of cannulated *rorγko* mice, also revealed normal transcript levels at day 5 and day 8 p.c. However, a small but significant decline was observed at day 15 p.c. in mRNA expression of lymphoid chemokines **(Figure 6.3.3A-D)**. mRNA expression of other lymphoid cytokine genes **(Figure 6.3.3E-H)** including BAFF, IL-7, LTα and LTβ was also found to be comparable to *wt* mice, though LTβ expression showed a 2-fold decrease at day 15 p.c.

Induction and proliferation of the LLSc was maintained in *rorγko* mice up to day 15 p.c. when a decrease in LLSc number was observed **(Figure 6.3.4A-C)**. Normal lymphoid stromal cell differentiation was also demonstrated by ICAM-1 and VCAM-1 staining that showed no significant difference in the percentage of ICAM-1^{int}/VCAM-1^{int} andICAM-1^{high}/VCAM-1^{high+} cell at both at day 5 and day 15 p.c. in *rorγko* and wt mice **(Figure 6.3.4D-E)**. These findings suggest that at sites of TLO formation, stromal cells acquire a lymphoid-like phenotype, independent of RORγt signals and that TLO formation and maturation is largely independent of RORγt+ cells.

Figure 6.3.1

A

day 15 p.c.

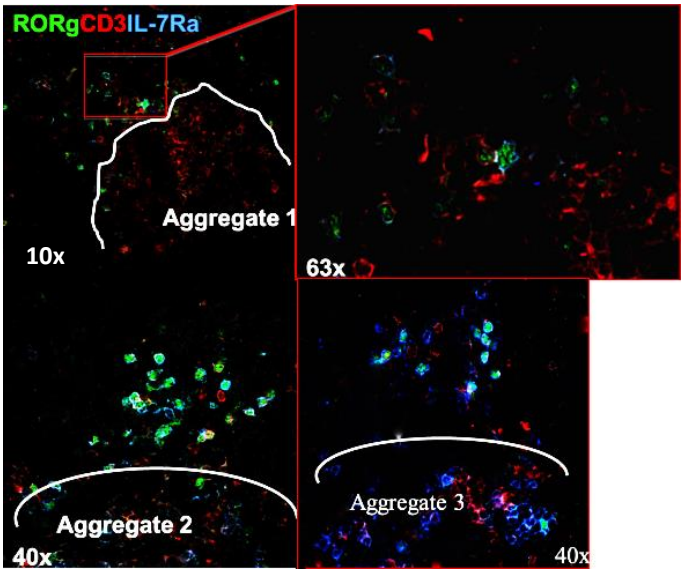

Figure 6.3.1 RORγt+ cells are observed late in inflammation. Microphotograph *RORγt+ cells* in infected *wt* salivary glands at day 15 p.c. for CD3 (red), IL-7Rα (blue) and *RORγt* (green).

Figure 6.3.2

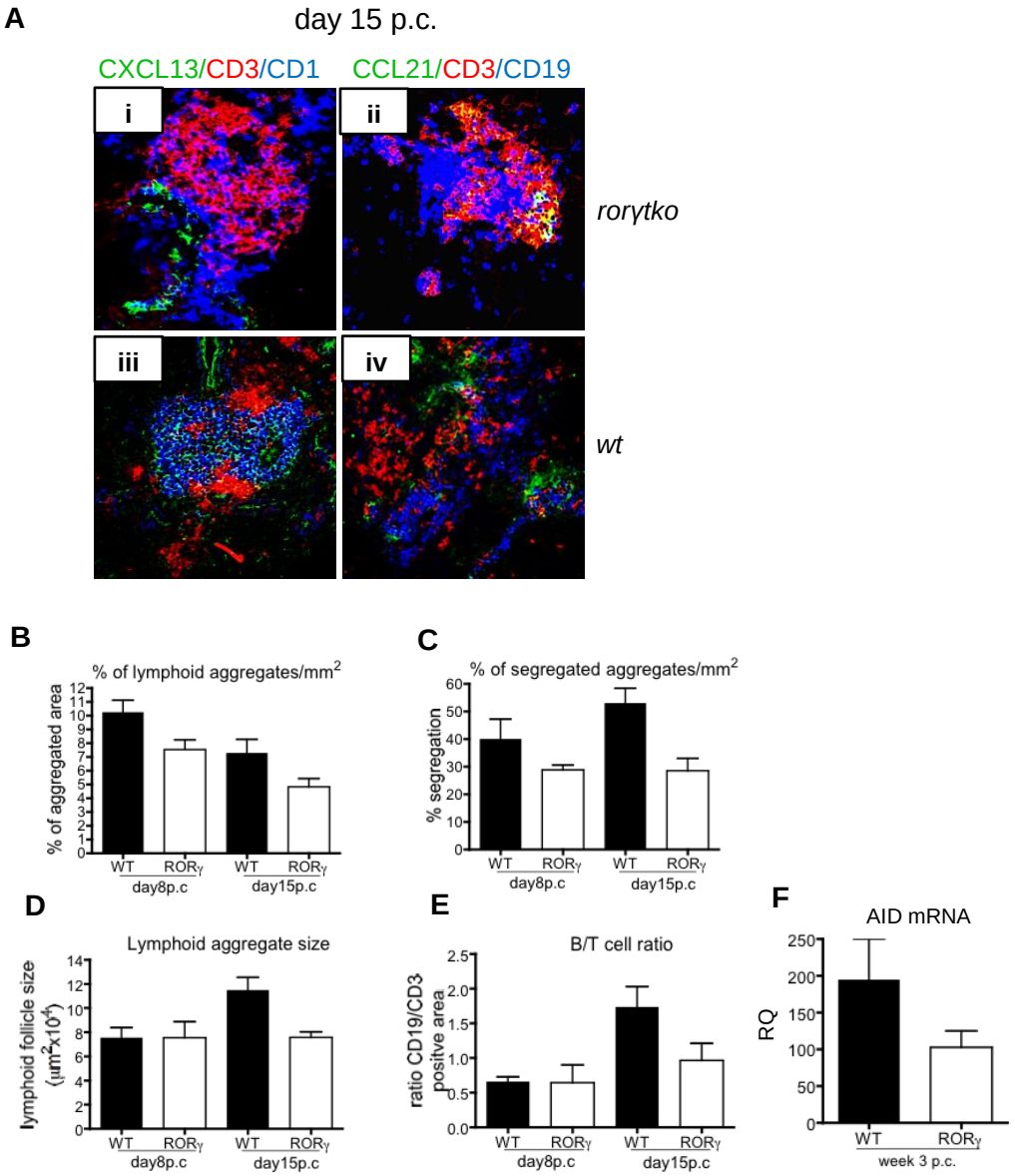

6.3.2 RORγt+ cells are indispensable for formation of mature TLOs. Microphotograph of lymphoid aggregates **(A)** from infected salivary glands (day 15 pc.) from *wt* **(Aiii-iv***)* and *rorγko* **(Ai-ii)** mice stained for CD3 (red), CD19 (blue) and either CXCL13 (green in **i and ii**) or CCL21 (green in **iii and iv**). Salivary glands from *wt and rorγko* day 8 and 15 p.c. were examined by immunofluorescence for CD3 and CD19. **B-E**, Graphs representing % of total lymphoid aggregate area **(B),** % of segregated aggregates **(C)**, lymphoid aggregate size **(D)** and ratio between the area covered by CD19+ B cells and CD3+ T cells **(E)** at day 8 and day 15 p.c. for *wt* (black bars) and *rorγko* (white bars) mice. Data is representative of two different experiments with two to three mice per group, mean ± s.e.m. *, $p<0.05$, unpaired t test, comparing *rorγko* to *wt* mice. **(F)**, Transcripts encoding for AID gene (normalized to housekeeping gene β-actin), in week 3 p.c. salivary glands from *wt* and *rorγko* mice, were quantified and expressed as RQ values relative to day 0 p.c. AID mRNA. Data shown as mean ± s.e.m. of three independent experiments.

Figure 6.3.3

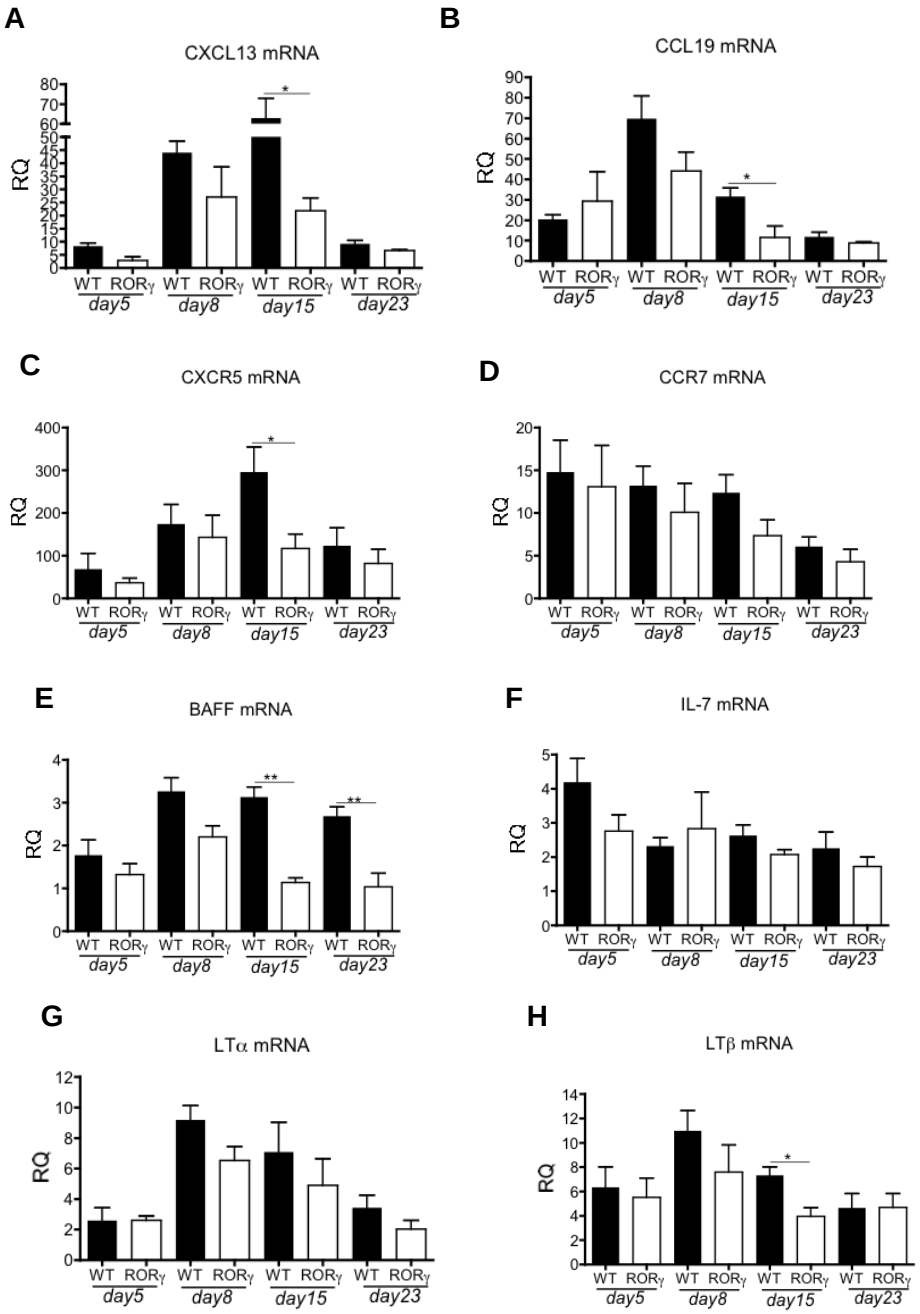

Figure 6.3.3 Expression of TLO-associated genes is intact in *rorγtko* mice. Quantitative PCR analysis of CXCL13 **(A)** CCL19 **(B)**, CXCR5 **(C)**, CCR7 **(D)**, BAFF **(E),** IL-7 **(F),** LTα **(G)** and LTβ **(H)** mRNA obtained from salivary glands at day 5, 8, 15 and 23 p.c. Expression of these genes is shown for *rorγtko* mice (white bars) compared to their *wt* counterparts (black bars); CXCL13, CCL19, BAFF and IL-7 mRNA transcripts were normalized to PDGFRβ mRNA and CXCR5, CCR7, LTα and LTβ mRNA transcripts were normalized to β-actin mRNA. Results are presented as relative quantitation (RQ) values calculated with calibrator day 0 salivary gland * $p<0.05$; ** $p< 0.01$. Data are representative as mean ± s.e.m. of three independent experiments with three to four mice per group.

Figure 6.3.4

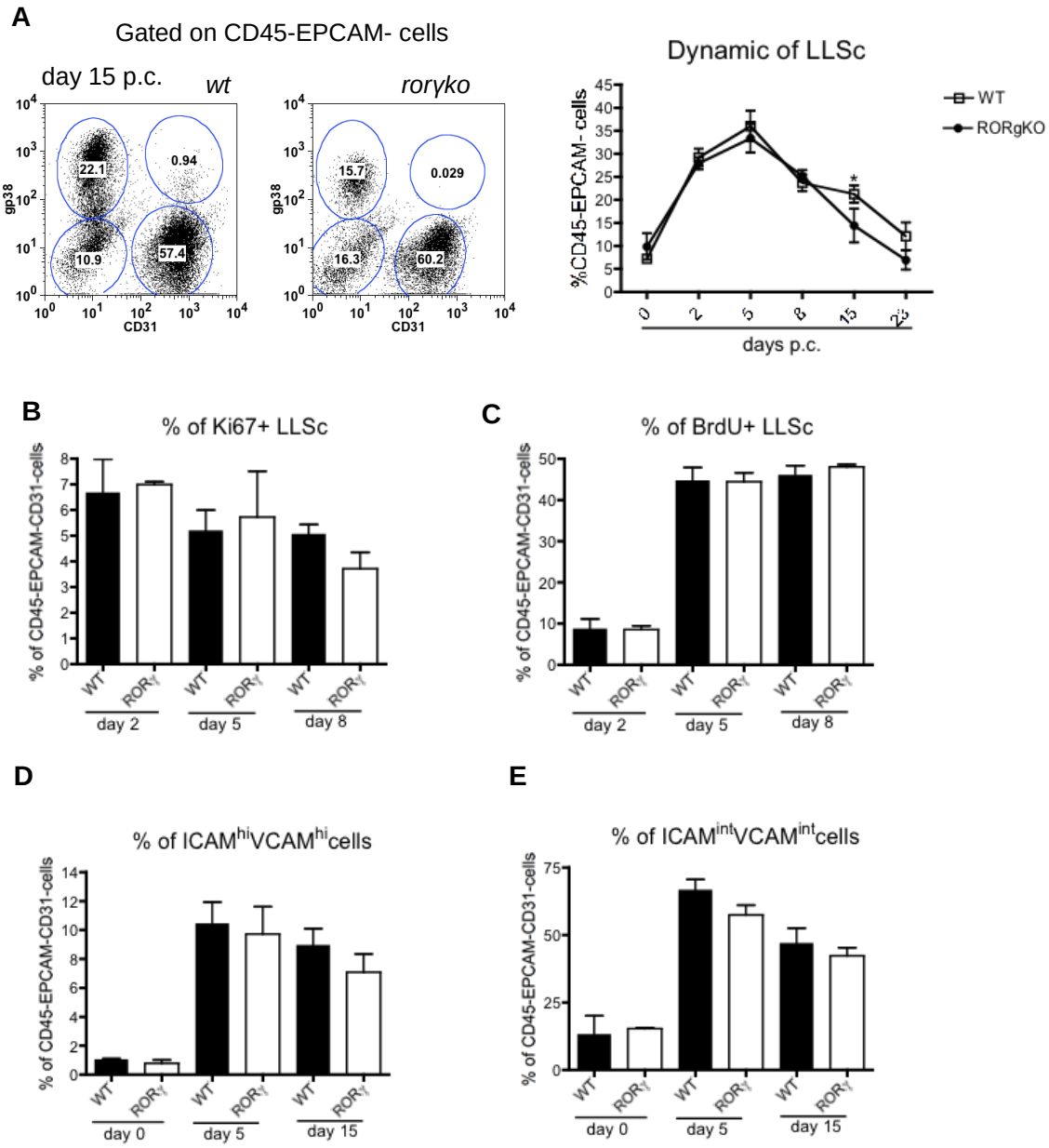

Figure 6.3.4 RORγt is redundant for generation of LLSc during TLO formation. Representative dot plots **(A)** showing flow cytometry for percentage of gp38+CD31- population in the CD45-EPCAM- component from day 15 p.c. salivary glands in wt and *rorγtko .* Dynamic of LLSc expansion **(B)** during the inflammatory process determined by flow cytometry (percentage of gp38+CD31- population in the CD45-EPCAM- component) from infected *wt* (black squares)*and rorγtko* (open triangles) mice at 0, day 2, day 5, day 8, day 15, day 23 p.c. Data presented as means of three independent experiments. *, $p < 0.05$, unpaired t test, comparing *ko* LLSc population at each time point with corresponding *wt* LLSc population**. C-D**, Flow cytometry to show dynamic of Ki67+ LLSc **(C)** and BrDU+ LLSc **(D)** in *wt* (white bars) and *rorγtko* (black bars) mice from day 2, day 5 and day 8 p.c. salivary glands. Data are representative of two to three experiments with three to four mice per group. **E-F**, Flow cytometry of VCAM-1 and ICAM-1 expression in CD45-EPCAM- cells from salivary glands of wt and *rorγtko* mice. The graphs show percentage of VCAM-1^{hi} ICAM-1^{hi} cells **(E)** and VCAM-1^{int} ICAM-1^{int} cells **(F)** obtained by flow cytometry on day 0, day 2 and day 15 p.c. salivary glands from *rorγtko* mice (white bars) in comparison to wt mice (black bars). Data presented as means of two independent experiments.

6.4 Lack of lymphocytes impairs chemokine and cytokine production during TLO formation

Lymphocytes have been shown to produce lymphotoxin [342]. In order to ascertain the role of lymphocytes in TLO formation and maintenance, we cannulated *ragko* mice. These mice are deficient in T and B lymphocytes and thus lack the ability to mount an adaptive immune response. This mouse provides us with a powerful tool to investigate the role of innate and adaptive immune factors in regulation of stromal cell activation and function during tertiary lymphoid structure formation.

The percentage of LLSc at day 2 p.c. in *ragko* mice was similar to that observed in *wt* mice. However, the LLSc failed to increase in *ragko* mice from day 5 p.c. onwards. A significant difference of ~10% was detected at day 5 p.c. ($p<0.05$), a further reduction of 10% and 12% was noticed at day 8 p.c. ($p<0.01$) and day 15 p.c. ($p<0.01$) in the gp38+ stromal cells of *ragko* mice in comparison to percentage of LLSc acquired on these days in the wt mice **(Figure 6.4.1A-B)**. In addition, FACS analysis for ICAM-1 and VCAM-1 expression **(Figure 6.4.1C-D)** on *ragko* cannulated salivary gland CD45-EPCAM-CD31- cells showed a lower percentage of ICAM-1^{int}/VCAM-1^{int} and ICAM-1^{high}/VCAM-1^{high} cells at day 5 p.c. and the decrease was significant at day 15 p.c. when compared to salivary glands from *wt* mice. Hence, this data clearly suggests towards importance of the lymphocytes to sustain lymphoid stromal cell activation.

Interestingly, salivary glands of cannulated *ragko* mice failed to up-regulate lymphoid chemokine (CXCL13 and CCL19) expression at all time-points (day 5 p.c. $p<0.01$-0.001; day 8 p.c. $p<0.001$; day 15 p.c. $p<0.01$; day 23 p.c. $p<0.05$ when compared with lymphoid chemokine expression in cannulated salivary glands of *wt* mice **(Figure 6.4.2A-B)**. Significant reduction was also observed in the IL-7 and BAFF **(Figure 6.4.2C-D)** transcript levels from day 5 p.c. and day 8 p.c. onwards respectively ($p<0.05$). Additionally, expression of both LTα and LTβ mRNA **(Figure 6.4.2E-F)** was absent in *ragko* mice, clearly indicating that lymphocytes are the main source of lymphotoxin during TLO formation.

Overall, these results revealed an indispensable role for lymphocytes in the maintenance and maturation of lymphoid stromal cell within TLO and provide data that lymphocytes primarily provide the lymphotoxin signals during TLO formation.

Figure 6.4.1

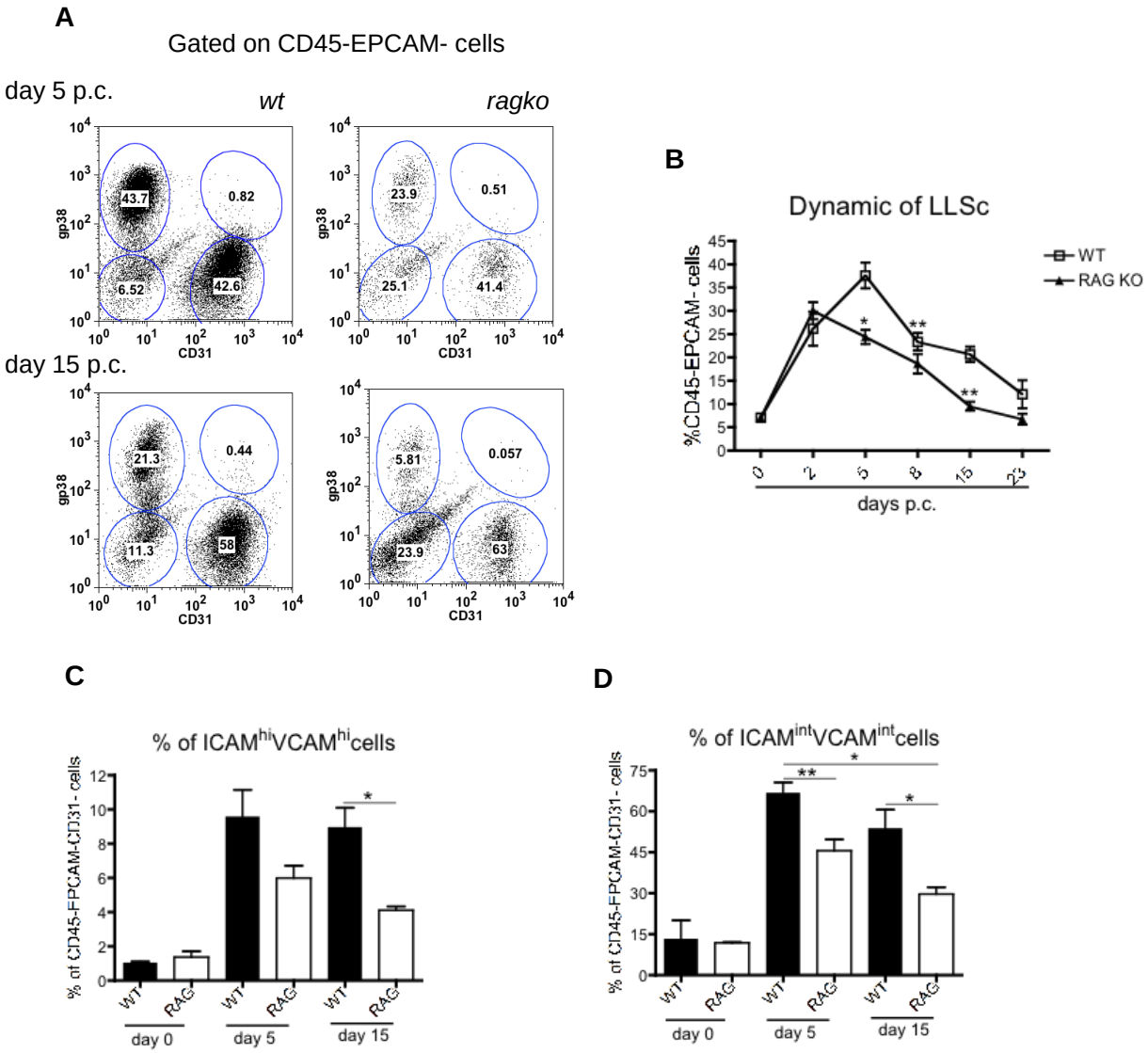

Figure 6.4.1 *ragko* mice exhibit failure to maintain induction and expansion of LLSc. Representative dot plots **(A)** showing flow cytometry for percentage of gp38+CD31- population in the CD45-EPCAM- component from day 15 p.c. salivary glands in wt and *ragko.* **(B)** Dynamic of LLSc expansion during the inflammatory process determined by flow cytometry (percentage of gp38+CD31- population in the CD45-EPCAM- component) from infected *wt* (black squares) *and ragko* (open triangles) mice at 0, day 2, day 5, day 8, day 15, day 23 p.c. Data presented as means of three independent experiments with two mice per group. ∗, $p<0.05$; **, $p<0.01$ unpaired t test, comparing *ko* LLSc population at each time point with corresponding *wt* LLSc population. **C-D**, Flow cytometry of VCAM-1 and ICAM-1 expression in CD45-EPCAM- cells from salivary glands of wt and *ragko* mice. The graphs show percentage of VCAM-1^{hi} ICAM-1^{hi} cells **(C)** and VCAM-1^{int} ICAM-1^{int} cells **(D)** obtained by flow cytometry on day 0, day 5 and day 15 p.c. salivary glands from *ragko* mice (white bars) in comparison to wt mice (black bars). Data presented as means of two independent experiments *, $p<0.05$; **, $p<0.01$.

.

Figure 6.4.2

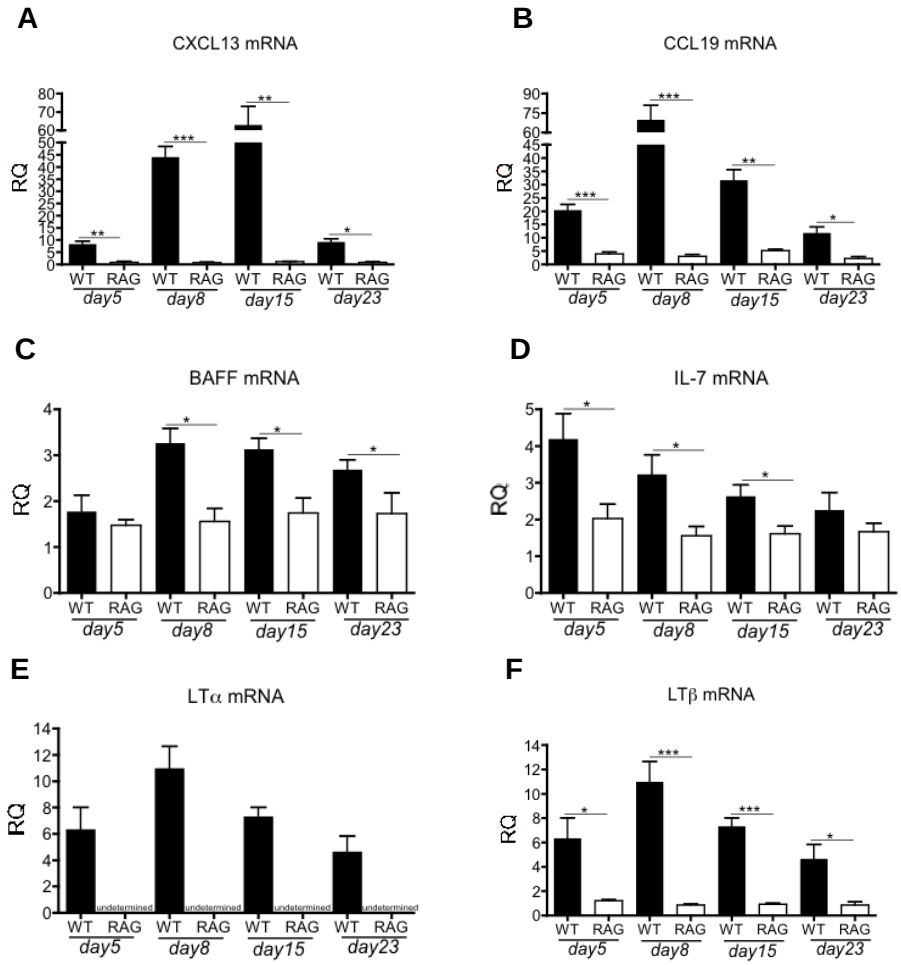

Figure 6.4.2 Lack of lymphocytes severely impairs production lymphoid chemokines and cytokines during TLO development. Quantitative PCR analysis of CXCL13 **(A)** CCL19 **(B)**, BAFF **(C),** IL-7 **(D),** LTα **(E)** and LTβ **(F)** mRNA obtained from salivary glands at day 5, 8, 15 and 23 p.c. Expression of these genes is shown for *ragko* mice (white bars) compared to their *wt* counterparts (black bars); CXCL13, CCL119, BAFF and IL-7 mRNA transcripts were normalized to PDGFRβ mRNA and LTα and LTβ mRNA transcripts were normalized to β-actin mRNA. Results are presented as relative quantitation (RQ) values calculated with calibrator day 0 salivary gland * p<0.05; ** p<0.01; *** p<0.001. Data are representative as mean ± s.e.m. of two independent experiments with two to three mice per group.

.

6.5 T-cells are the central player in stromal cell maturation during TLO formation

In order to determine if both T and B cells or only T or B cell population was instrumental in the defect observed in the *ragko* mice, the *cd3ε*^{tg26} (deficient in T cells) and *B-cellko* (deficient in B cells) mice were cannulated.

In agreement with *ragko* data on LLSc, both the *cd3ε*^{tg26} **(Figure 6.5.1A)** and *B-cellko* **(Figure 6.5.1B)** mice displayed normal induction of the LLSc at day 2 p.c. The percentage of LLSc showed a significant decrease of nearly 10% at day 5 p.c. in *cd3ε*^{tg26} ($p<0.05$ in contrast to *wt* day 5 p.c.), the defect in LLSc number was maintained at day 8 ($p<0.05$) and day 15 p.c. ($p<0.05$). No decrease in gp38+ lymphoid stromal cells was observed in the *B-cellko* mice at day 5. However, a small yet significant decrease in percentage of LLSc was noticed at day 8 ($p<0.05$) and day 15 ($p<0.05$) within the salivary glands of *B-cellko* mice in comparison to *wt* mice. The analysis of LLSc in *cd3ε*^{tg26} and *B-cellko* suggested that the deficiency noted in the *ragko* mice at day 5 p.c. is T cell dependent. Even though the maintenance of LLSc at day 8 and day 15 p.c. is centrally dependent on T cells, a further defect within the lymphoid stromal cells is augmented in absence of B cells, hence a more severe phenotype was observed in the *ragko* mice compared to T and B cell deficient mice on their own.

Quantitative PCR analysis for lymphoid chemokines revealed that up-regulation of both CCL19 mRNA **(Figure 6.5.1C)** and CXCL13 mRNA **(Figure 6.5.1E)** was absent ($p<0.05$-0.001) in salivary glands of *cd3ε*^{tg26} mice at all time-points. In contrast the *B-cellko* displayed normal expression CCL19 **(Figure 6.5.1D)** at day 5 and day 8 p.c. but significant decrease of thirty-fold ($p<0.01$) and fifty-fold ($p<0.05$) was observed in CXCL13 mRNA **(Figure 6.5.1F)** levels at day 8 and day 15 p.c. respectively. BAFF transcript **(Figure 6.5.2A)** levels were decreased in *B-cellko* and *cd3ε*^{tg26} mice **(Figure 6.5.2B)** from day 8 p.c. onwards ($p<0.05$). IL-7 mRNA expression **(Figure 6.5.2C-D)** was normal in absence of B cells (*B-cellko*). T cell deficiency (*cd3ε*^{tg26}) resulted in a three-fold decrease at day 5 p.c. ($p<0.01$), and nearly two-

fold decrease in IL-7mRNA levels at day 8 ($p<0.01$) and day 15 p.c. ($p<0.05$). Transcript level of LTα and LTβ **(Figure 6.5.2E-H)** were also examined in these KO mice. The results exhibited baseline expression of both lymphotoxin molecules in *cd3ε*^{tg26} mice at all time-points ($p<0.05$-0.001) as compared to wt mice. The expression of LTβ was severely affected in the salivary glands of *B-cellko* mice ($p<0.05$-0.001), though *B-cellko* salivary glands showed higher expression of LTβ mRNA than salivary glands of *cd3ε*^{tg26} mice.

T cell deficiency resulted in a lack of up-regulation to inflammatory cytokines IL-22 and IL-4, which further explains the collapse in the lymphoid stromal cells in *ragko* and *cd3ε*^{tg26} **(Figure 6.5.3A-D)** .

Overall, this data indicates that LLSc maturation and local expression of lymphoid genes is more severely impaired in T cell deficient mice than B cell deficient mice.

Figure 6.5.1

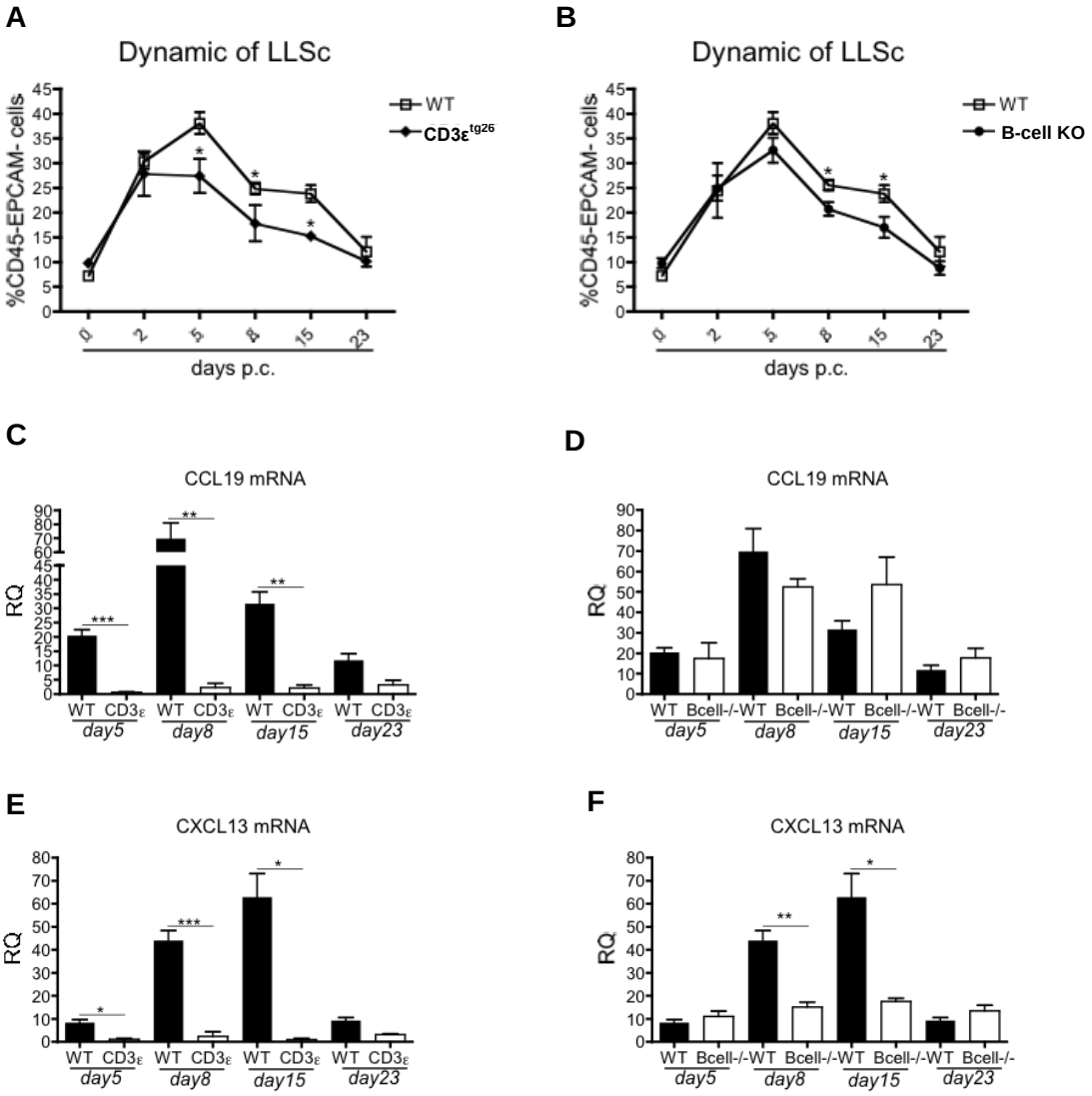

Figure 6.5.1 T cells are the central players in stromal cell maturation within TLOs. Dynamic of LLSc expansion during the inflammatory process determined by flow cytometry (percentage of gp38+CD31- population in the CD45-EPCAM- component) from infected *wt* (black squares) and *cd3ε*^{tg26} **(A)** or *B-cellko* mice **(B)** (open squares) mice at day 0, day 2, day 5, day 8, day 15, day 23 p.c. Data presented as means of two independent experiments with atleast two mice per group. ∗, $p < 0.05$ unpaired t test, comparing *ko* LLSc population at each time point with corresponding *wt* LLSc population**.** Quantitative PCR analysis of CCL19 **(C-D)** CXCL13 **(E-F)** mRNA obtained from salivary glands at day 5, 8, 15 and 23 p.c. Expression of these genes is shown for *cd3ε*^{tg26} **(C and E)** and *B-cellko* **(D and F)**, *cd3ε*^{tg26} or *B-cellko* mice (white bars) compared to their *wt* counterparts (black bars); CXCL13 and CCL19 mRNA transcripts were normalized to PDGFRβ mRNA. Results are presented as relative quantitation (RQ) values calculated with calibrator day 0 salivary gland * $p<0.05$; ** $p<0.01$; *** $p<0.001$. Data are representative as mean ± s.e.m. of two independent experiments with two to three mice per group.

Figure 6.5.2

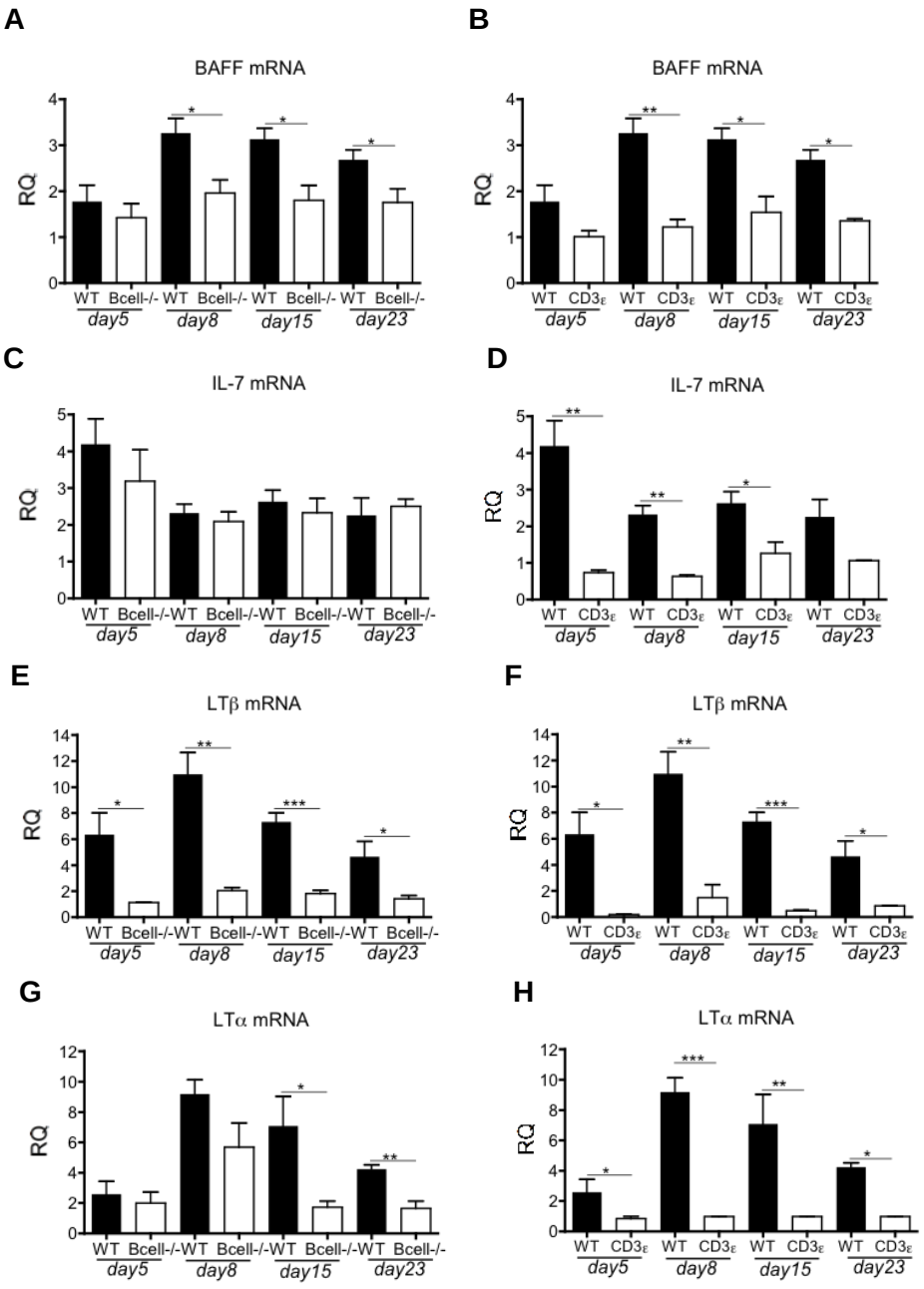

Figure 6.5.2 T cell deficient mice exhibit greater defect than B cell deficient mice in up-regulating expression of lymphoid cytokines. Quantitative PCR analysis of BAFF **(A-B),** IL-7 **(C-D),** LTβ **(E-F)** and LTα **(G-H)** mRNA obtained from salivary glands at day 5, 8, 15 and 23 p.c. Expression of these genes is shown for *B-cellko* **(A,C,E and G)** *and cd3ε*^{tg26} **(B, D, F and H)**, *cd3ε*^{tg26} *or B-cellko* mice (white bars) compared to their *wt* counterparts (black bars); BAFF and IL-7 mRNA transcripts were normalized to PDGFRβ mRNA and LTα and LTβ mRNA transcripts were normalized to β-actin mRNA. Results are presented as relative quantitation (RQ) values calculated with calibrator day 0 salivary gland * $p<0.05$; ** $p<0.01$; *** $p<0.001$. Data are representative as mean ± s.e.m. of two independent experiments with two to three mice per group.

Figure 6.5.3

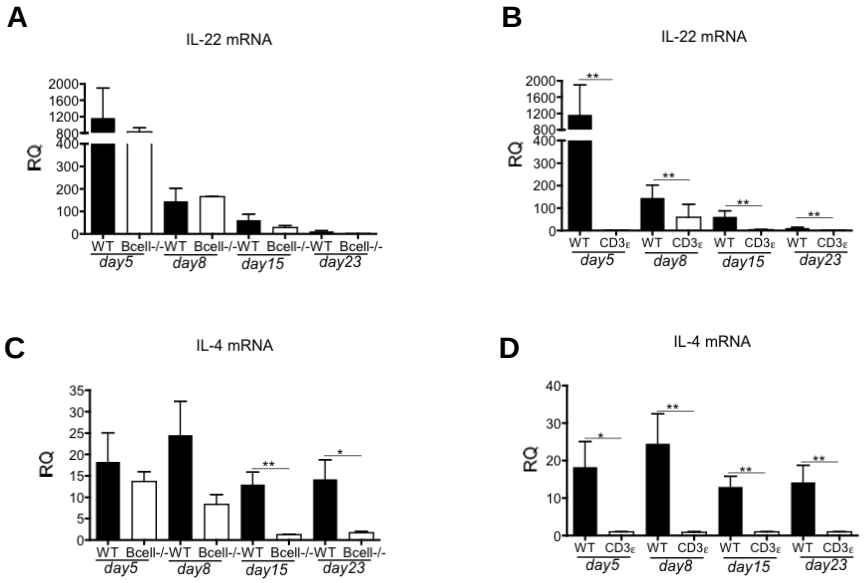

Figure 6.5.3 Expression profiles of effector cytokines in *cd3ε^{tg26}* and *b-cellko* mice. Quantitative PCR analysis of IL-22 **(A-B)** and IL-4 **(C-D)** mRNA obtained from salivary glands at day 5, 8, 15 and 23 p.c. Expression of these genes is shown for *B-cellko* **(A and C)** *and cd3ε^{tg26}* **(B and D)**, *cd3ε^{tg26}* or *B-cellko* mice (white bars) compared to their *wt* counterparts (black bars); mRNA transcripts were normalized to β-actin mRNA. Results are presented as relative quantitation (RQ) values calculated with calibrator day 0 salivary gland * $p<0.05$; ** $p<0.01$; *** $p<0.001$. Data are representative as mean ± s.e.m. of two independent experiments with two to three mice per group.

Discussion

During secondary lymphoid organogenesis, LTβR signaling is necessary for maturation of mesenchymal-derived gp38+ICAM-1^{high}VCAM-1^{high} lymphoid organizer cells (LTo), including adhesion molecule up-regulation, production of lymphoid chemokines and cytokines [66, 75]. Moreover, LT signals are crucial for proliferation and survival of LTo within the LN anlage [60]. Over the past few years, studies have highlighted an LTβR independent stage of stromal activation during LN development [60, 66, 67, 75, 83, 142, 226]. Peduto *et al*., have shown that gp38 can be induced on LN stromal cells independent of LTβR. Similarly, other studies have also documented that the priming of mesenchymal precursor cells is independent of lymphotoxin. However, all these studies have emphasized the critical role of LTβR in providing the final maturation stimulus for LN stromal cells [60, 66].

There is recent data in adult LNs, where there is an LTαβ independent phase of lymphoid stromal cell FRC activation during an immune response. However, the maintenance of FRC expansion and function was mediated by LTβR and its ligands [280]. Similarly, Chai *et al*, [60, 66] have demonstrated that LTβR signaling is central to full maturation of FRC, and hence their immune-stimulatory capacity during an immune response [142].

Interestingly, early LLSc induction and proliferation is not affected in *ltβr-/-* in our mouse model. Analysis of the LLSc phenotype at day 5 p.c. in *ltβr-/-* mice showed no significant differences as compared to wt mice in terms of percentage of ICAM-1^{int}/VCAM-1^{int} andICAM-1^{high}/VCAM-1^{high+} cells. Nonetheless, mRNA and immunofluorescence analysis showed significant reduction, especially from day 8 p.c., in the expression of CXCL13, CCL21, CCL19, BAFF and IL7 in ltβrko infected mice as compared to *wt c*ontrols. Accordingly, lymphoid aggregates formed within the salivary glands of *ltβr-/-* were characterized by smaller size and partial T and B cell organization at day 8 and day 15 p.c. Moreover, *ltβr-/-* exhibited a defect in proliferation at day 8 p.c. and a significant decrease in ICAM-1^{int}/VCAM-1^{int} and ICAM-1^{high}/VCAM-1^{high+} LLSc at day 15 p.c. Thus, in cognizance with above mentioned studies, we also demonstrated that LTβR is not required for the early acquisition

of a lymphoid-like phenotype by stromal cells during TLO formation within the inflamed salivary gland. LTβ/LTβR interaction is, however, required for the full maturation and maintenance of LLSc to a functional lymphoid phenotype, because lack of LTβ/LTβR signal affects the subsequent secretion of lymphoid chemokine and cytokines in these cells.

The early expression of lymphoid chemokines and presence of lymphocytes can be explained by our findings in chapter 5 where we demonstrated that the cytokine IL-22 has the capability to induce chemokines and cytokines in the LLSc. Moreover, LLSc also express TNFR1 (shown in chapter 3) and therefore can respond to LTα3, which has also been shown to induce chemokines in lymphoid stromal cells [157, 158, 186].

CD3-CD4+IL-7rα+RORγt+ lymphoid tissue inducer (LTi) cells represent the first source of LTβ in the LN anlagen. This signal is necessary for LTβR-mediated stromal cell maturation during lymphoid organogenesis [97]. The application of our model to *rorγt-/-* mice provided a useful tool to interrogate the role of adult LTi in TLO maturation. We found that adult RORγt+ LTi are recruited late in the formation of TLOs, well after LLSc become activated and proliferate. In addition, *rorγt-/-* mice had preserved induction and proliferation of the LLSc with normal TLO formation. Our findings are further supported by studies in other models in which *id2-/-* or *rorγt-/-* mice, which lack LTi cells, when infected with influenza virus or exposed to LPS. These mice develop normal iBALT structures in the lung [76, 214, 215]. Similarly, another study demonstrated development of TLOs in colon of *rorγt-/-* mice [216]. However, in our model we observed a decrease in the LLSc and CXCL13 production at day 15 p.c. A small, though non-significant decrease in TLO size and organization was also identified.

In the spleen LTi have been demonstrated to be essential for T/B cell segregation and follicle size [343]. One cannot rule out the possibility that LTi can have a role in maintenance of TLOs, because our mouse model is a resolving model of TLO formation and will be an interesting question to address in a pathophysiological mouse model of persistent TLO

formation. In fact, there are some human TLOs, such as those seen in idiopathic pulmonary arterial hypertension (IPAH), where RORc+CD4-cKit+ LTi have been detected [12]. However, our observations suggest that LTi are not required for the formation of TLOs at least in our model.

We found that lymphocytes and in particular T cells are necessary for the expansion and maturation of stromal cells and hence TLO formation. In fact, even during lymph node organogenesis the stromal activation phase occurs independently of lymphocytes but formation and maintenance of the mature LN has been demonstrated to be dependent on T and NK cells [27]. Moreover, lymphocytes are critical in adult SLOs for maintenance of lymphoid structures using LT/chemokine axis positive feedback loop. In adult SLOs, lymphocyte derived lymphotoxin promotes expression of CXCL13, CCL21 and CCL19 by stromal cells [115]. This regulates steady state homing and correct positioning of T and B cells, and also plays a role in maintenance of LTαβ expression on lymphocytes, thereby sustaining the positive feedback loop to maintain the structure and function of SLOs [16, 36, 115-117]. Evidence suggests that the maintenance of homeostatic lymphoid chemokine expression and FDCs in B cell follicles is dependent on LTαβ and TNFα expression on mature B cells [16, 108, 118]. However, normal levels of chemokines, and B cell follicles with FDCs were detected in the LNs of mice that lack LTβ, specifically on B cells. Hence, in this case, it was been shown that LTαβ-expressing T lymphocytes are sufficient to maintain LN structure and function [16, 119, 120]. Altogether, this data indicates that expression of LTαβ by both T and B lymphocytes is necessary for appropriate conservation of lymphoid architecture in adult SLOs.

It has been widely suggested that lymphocytes analogous to their function in adult SLOs can substitute for the inductive function of LTi cells within TLOs, particularly when they are activated [108, 111, 119, 120, 212, 342, 344]. CD4+ T cells have been shown to be crucial for development of TLO in the thyroid [217]. Moreover, in NOD mice LIGHT expressed on T cells has been demonstrated to be essential for formation and maintenance of TLO

structures. A similar role for LTα expressing T cells has been documented in mice model of colitis [116, 235, 341]. T cells are not only an important source of LTαβ but also of inflammatory cytokines IL-22 and IL-4 which have been demonstrated to be important for LLSc expansion and maintenance in chapters 4 and 5. This could possibly explain why the defect observed in LLSc maturation and maintenance is more severe in *cd3εko* mice than *ltβrko* mice.

In agreement with our results, T cells have been identified to have a higher tendency to activate mesenchymal stromal cells to express both CCL19 and CXCL13, whereas B cells only induce CXCL13 expression when co-cultured with stromal cells (Mark Coles, unpublished data). When both B and T lymphocytes were added together, the production of CXCL13 significantly increased above the level induced by T lymphocytes alone, an effect which was not seen when the expression of either CCL19 or CCL21 was determined. This suggests that T lymphocytes could indirectly attract B lymphocytes into a site of inflammation by inducing stromal cells to express CXCL13 and this is exacerbated by a positive feedback loop as B lymphocytes begin to enter (Mark Coles, unpublished data). Thus, at later stages both T and B cells contribute to maintain the stromal cells in our model. This propensity of lymphocytes to instruct stromal cells to mature into lymphoid stromal cells requires the lymphocyte and stromal cell to be in physical contact, requires activation and crucial signalling within lymphocytes (Mark Coles, unpublished data), and these signals are currently under investigation in our lab.

It will also be interesting to see if maintenance of lymphoid phenotype and function of LLSc is completely taken over by B cells in a model of persistent TLO formation. This might explain why rituximab (anti-CD20) therapy has been proved to be efficacious in patients with TLO-associated chronic inflammatory diseases such as Sjogren's syndrome.

Chapter 7

Concluding Discussion

TLOs form *de novo* in the target tissues of many inflammatory diseases, such as in the inflamed salivary glands of Sjogren's syndrome patients, the joints of rheumatoid arthritis patients and the lungs of pulmonary infection or inflammation patients, [14]. TLO development is characterized by the progressive organization of T and B-lymphocytes, formation follicular dendritic cells networks and maturation of high endothelial venules [236, 345, 346]. There is accumulating evidence that naïve T cell priming and T cell epitope spreading can take place within TLOs [4, 161, 207]. This can contribute to the exacerbation of disease by activation of auto-reactive T cells due to presence of tissue auto-antigens at the site of TLOs, released by the destructive inflammatory process [4, 14]. Moreover, expression of AID, the enzyme that support class switch recombination and somatic hyper-mutation has been shown on activated B cells within these structures [194]. Therefore, TLOs seem to be able to sustain B-cell affinity maturation and production of autoantibodies [194, 233].

Autoantibodies are one of the major hallmarks of chronic autoimmune diseases and are highly predictive of disease severity [14, 347-349]. In some cases, autoantibodies have been demonstrated to directly provoke damage and in Sjogren's syndrome there are evidence that they can influence the gene expression profiles of epithelial cells to produce pro-inflammatory cytokines [350]. TLO formation has been also associated with disease persistence and malignant transformation [4, 13, 14, 18, 160, 194, 210, 211, 236]

Due to their pathogenic contribution to disease development and their correlation with more aggressive form of disease and development of malignancy there has been an increasing interest in targeting TLOs in clinical practice [14, 222]. Current treatments aimed to targeting leukocytes in autoimmune conditions have led to a dramatic change in the management of inflammatory diseases [222]. However, this approach does not result in a definitive cure and

even in patients that achieve clinical remission, relapse occur once the treatment is withdrawn [222]. This suggests the need to consider non-leukocyte targets.

Over the past few years, it has become increasingly evident that at site of chronic inflammation and in particular within TLOs, resident stromal cells can undergo functional changes, which enable them to modulate the formation, organization and maintenance of ectopic lymphoid structures [221, 222, 351, 352]. In this thesis, we have explored the crosstalk between tissue resident stromal cells and immune cells, that is mediated by cytokines and provide mechanistic insights into how TLO develops. Our results provide a framework for selection of new therapeutic strategies aimed at silencing TLO associated stroma and to treat autoimmune conditions.

The presence of stromal cells resembling lymphoid, stromal cells is well documented in many human chronic inflammatory diseases and mouse model of TLOs [76, 159, 160, 177-179, 185, 248, 249] . In 2009 Peduto *et al.* were the first to perform a direct comparison of lymphoid stromal cells with activated stromal cells at sites of inflammation in non-lymphoid organs [226]. Their findings suggested that during inflammation, tissue-resident stromal cells recapitulated features of lymphoid stromal cells [226]. gp38, a marker of lymph node stromal cells, was used to identify and isolate these inflammation-induced lymphoid stromal cells that acquired the capability to express genes, essential in lymphoid tissue genesis and in the recruitment and survival of leukocytes [226]. Strikingly, the early development of gp38+ stromal cells during inflammation was shown to be independent of LTβR and TNF signalling [226].

In 2011, Randall's group, using a mouse model of iBALT formation in the lungs of neonatal mic, provided evidence that pro-inflammatory cytokines such as IL-17 could initiate TLO formation [214]. This study demonstrated that iBALT formation did not require LTi and lymphotoxin mediated signals but it was dependent on IL-17 produced by CD4+ T cells [214]. Most striking finding in this study was that IL-17, not only demonstrated an ability to induce

expression of inflammatory chemokines such as CXCL10, CXCL11 and CXCL9, but it could also directly stimulate the expression of CXCL13 and CCL21 in stromal cells [214]. In the same year, study from Kuchroo's group also supported the role of effector cytokines such as IL-17 in initiating TLO formation [230].

Taken together these studies clearly indicated that acquisition of phenotypical and functional features of lymphoid stromal cells can occur in tissue-resident fibroblasts and challenged the current dogma that SLO and TLO development engage similar pathways and proposed probable role of proinflammatory cytokines in TLO development [353].

The conjecture that TLO formation follows the same cellular and molecular routes used by SLOs comes from structural and partly functional resemblance of TLOs to secondary lymphoid organs, and studies on transgenic mice over-expressing lymphoid cytokines (LT) and chemokines (CXCL13, CCL21) [12, 14, 158-160, 165, 169, 173, 174, 186, 227] in non-lymphoid organs resulting in TLO formation. These findings were further fuelled by evidence from human studies which suggested a strong correlation between the expression of lymphoid cytokines such as LTα, LTβ, CXCL13, CCL21 and TLO development [13, 14, 160, 179, 180, 183-186]. However, transgenic mice lack the pathophysiological complexity that underpins TLO formation during disease development.

A major limitation of studies in humans is that they only provide us with a snapshot of the inflammatory process whereas it is well-known that inflammation is dynamic process, characterized by different stages namely activation, maintenance and resolution or persistence [351, 352, 354-356]. For example, a study conducted by Raza *et al*., to study cytokine profiles of patients with RA at different stages of the diseases, clearly indicated differences in the inflammatory cytokine profiles of patients with early RA compared to established RA [299], further establishing the idea that inflammation is an actively changing process. Robust data for most chronic diseases is lacking and many diseases are diagnosed

at established stages when TLOs have already developed and this could possibly explain the overestimation of the capability of certain cytokines to drive TLO formation.

Nevertheless, lymphotoxin signalling has been demonstrated to be crucial for maintenance and organization of TLOs, as these lymphoid structures were highly disrupted in mice deficient in LT signalling or treated with anti-LTβR antibody [164, 193, 214, 257, 340, 341, 357]. These evidences are more in line with role of LT in maintenance and function of adult SLOs [117, 357, 358]. Due to the perplexity in the current literature regarding the signals regulating TLO formation, we decided to dissect these signals in our model of salivary gland inflammation. Stromal cells occupy the centre-stage in the process of SLO organogenesis, and also fundamental for SLOs to mount an effective immune response during adult life [6, 67, 126]. However, the role of stromal cells in TLOs establishment and pathology remains unclear. Therefore, our prime focus was to first examine stromal cell activation during TLO formation and then understand signal/s modulating their phenotype and function during inflammation and TLO formation.

Using a mouse model of TLO formation that mimics features of Sjogren's syndrome [237], we demonstrated that lymphoid-like stromal cell (LLSc) expansion occurs early during the development of TLOs. We have shown that LLSc acquire markers such as gp38, ICAM-1, VCAM-1, RANK-L, MadCAM-1 and LTβR and are able to respond to LTβ stimulation, up-regulating CXCL13, CCL19, IL7 and BAFF. We showed that the acquisition of these features is the result of a concerted process mediated by few cytokines, namely IL-13, IL-22, LT and IL-4 that play different roles at different stages of the inflammation process. Based on our findings, we recognized three phases of stromal cell activation which were named induction, expansion and maintenance phase (Figure 7.1).

We demonstrated that early after the inflammatory insult (in our case Adv infection) a significant increase in the expression of IL-13 occurs, mainly sustained by the resident stroma (both epithelial and non-epithelial/endothelial stromal cells). IL-4Rα/IL-13Rα

engagement on tissue stromal cells then initiates the induction phase, which results in over-expression of gp38 and adhesion molecules ICAM-1 and VCAM-1 on local non-epithelial non-endothelial stromal cells (fibroblasts) and transient expression of inflammatory chemokines including CXCL10, CXCL9 (M. Coles personal communication). These events cause the recruitment and retention of activated and memory effector T cells (which are known to express receptors such as CXCR3, specific for inflammatory chemokines) at the site of inflammation. During this period, resident γδT cells and incoming αβ T cells produce IL-22, which engages IL-22R on activated tissue gp38+ fibroblasts and induces their proliferation and also up-regulates early expression of lymphoid chemokines. This phenomenon contributes to the further recruitment of T as well as some B cells. Subsequently, LTα and LTβ production particularly by activated T cells engages LTβR and TNFR signalling on LLSc which further enhances production of chemokines (CCL19, CXCL13 and CCL21) and lymphocyte survival factors (IL-7 and BAFF) by LLSc. Besides, LTβR mediated signalling in LLSc further increases their proliferation. Overall, IL-22 and LT/TNF enable functional maturation of LLSc. Additionally, LTβR triggering promotes maintenance of phenotypical and functional features acquired by LLSc. Expansion of functionally mature LLSc allows attraction of more T cells (apart from activated and memory effector cells, recruitment of naïve T cells is also observed) as well as B cells that results in establishment of a positive feedback loop and development of lymphoid aggregates with progressively organized of T and B-lymphocytes, formation follicular dendritic cells networks and maturation of high endothelial venules. During this phase, IL-4 produced by T cell can enhance expression of LTαβ on naïve T cells [175], which aids in enhancing LTβR triggering. Additionally, lymphoid chemokines such as CXCL13 are also reported to enhance expression of LT on lymphocytes [13, 36] and could possibly aid in further reinforcing the LT/CK/lymphocytes amplificatory loop that allows maintenance of TLOs. Thus the main components of lymphoid tissue are formed within organs where lymphoid tissue is not usually found.

Of note, IL22 has been previously demonstrated to promote organization and maintenance of mature colonic patches and isolated lymphoid follicles during infection with C. rodentium of the gut [317]. In this study IL-22 function was implicated to be downstream of LTβR. In contrast, we have established in chapter 5 and 6 that IL22 is necessary and sufficient to induce the proliferation LLSc and is able to induce the early production lymphoid chemokines independent of LTβR signalling. Interestingly, while LTβ signalling is not required in these early phases, it is necessary for the late maintenance of the follicle and full conversion of the LLSc to a functional lymphoid phenotype since full TLO formation is abrogated in *ltβrko* mice.

In this study we also demonstrated that stromal activation can occur independently of RORγ+ cell. The application of our model to rorγko mice provided a useful tool, not only to interrogate the role of adult LTi but also of IL17 (since RORγ is master-regulator of Th17 cells) in TLO maturation. A role for IL17 has been suggested in the context of stromal cell activation in a neonatal model of TLO formation [214]. However, the inability to reproduce this model in adult mice has questioned the role of IL17 in post-natal TLO formation [282]. Further data on the role of IL17 in TLOs has been provided in a study [230] from Peters *et al*., which demonstrated the requirement of gp38+ Th17 cells for EAE development in the CNS. However, in our model, LLSc expansion precedes T cell infiltration, suggesting that Th17 lymphocytes are not involved in early LLSc expansion and proliferation. We demonstrated in chapter 6 that RORγ+ cells are not required for the LLSc generation and TLO formation, at least in this model. Therefore, role for RORγt+Th17 lymphocytes in LLSc differentiation and TLO formation in our model is highly unlikely. However, to formally rule out the possibility that IL-17 plays any role in our model, further work in *il17ko* will be required.

Overall, our data establishes a functional connection between the expression of pro-inflammatory cytokines (IL-13, IL-22, IL-4 and LT), the activation of pathogenic stroma and the development of TLOs which provides a rationale for new therapeutic options and suggests an important role for T lymphocytes in the expansion and maintenance of pathogenic stroma at sites of inflammation.

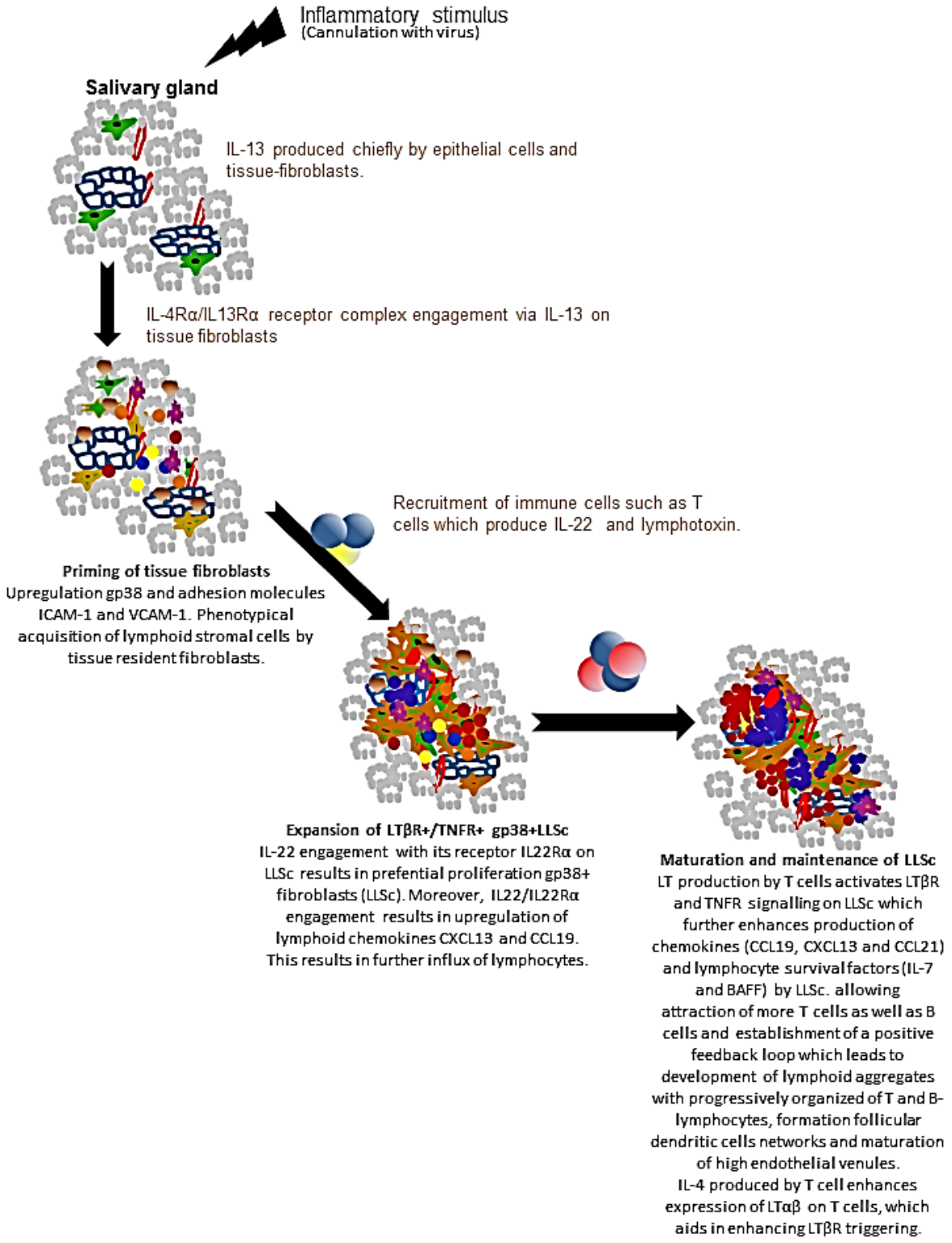

Figure 8.1 Illustration of the different phases (induction, expansion and maturation/maintenance) of stromal cell activation and the signals regulating each of these phase during TLO formation.

Future Work

Even though we demonstrate that stromal cells have the ability to respond directly to virus and inflammatory cytokines to undergo transition into pathogenic stroma, however we cannot exclude the contribution of other mechanisms that have been implicated in the generation of stromal cells during development, inflammation and fibrosis [222]. Fibroblasts are believed to arise from three distinct cellular origins: primary mesenchyme, local epithelial-mesenchymal transition (EMT) or bone marrow derived precursors. It is widely accepted that the majority of fibroblasts originate from primary mesenchymal cells and that upon appropriate stimulation these fibroblasts can proliferate to generate new fibroblasts [222, 359-363]. In fact, it has recently been suggested by Krautler *et al*. that non-lymphoid tissue has myofibroblast (perivascular) precursor cells that can give rise to FDC upon appropriate stimulation [147].

In the LN, gp38- subset of fibroblastic stromal cells have been shown to contain a population of α7+ perivascular cells which could serve as precursors of gp38+ FRC, as these two cell types share some common features [142, 296, 364]. In our model, we have observed a gp38- population of fibroblasts (termed DN cells), and demonstrated that these cells differ from LLSc, not only in their expression of lymphoid adhesion molecules ICAM-1 and VCAM-1 but also have significantly lower ability to produce lymphoid chemokines and lymphocyte survival factors. Nonetheless, these DN cells were shown to express receptors for the various cytokines that we studied.

Our experiments did not discriminate between the ability of DN and LLSc to respond to virus. Additionally, there is only a small population of gp38+ fibroblasts in resting salivary glands, and the substantial increase in this population within 48 hours cannot be attributed only to proliferation, since only 15% LLSc showed BrdU staining at this stage. Altogether, it is tempting to speculate that the gp38- tissue fibroblasts respond to inflammatory stimulation and up-regulate gp38 and therefore contribute to generation of pathogenic stroma. This could be tested by fate mapping experiments.

Intriguingly, increased gp38 expression has been reported on epithelial cells that are undergoing EMT, a process that involves down-regulation of epithelial markers, such as adhesion molecules like E-cadherin which allows transition of sessile epithelial cells into more motile mesenchymal cells [365]. We demonstrated that epithelial cells not only produce IL-13 upon virus infection but also express both IL-13Rα and IL-4Rα. Moreover IL-13 has been implicated in EMT during fibrosis [298]. Hence, using genetic lineage tracing and ablation systems, it will be very interesting to address in future whether LLSc in TLOs arise from distinct progenitors during an inflammatory process.

Another very important question for the future is to understand the function of gp38 acquisition by tissue stromal cells. gp38 expression has been detected on cancer – associated fibroblasts (CAFs) where it has been reported to promote plasma membrane extension and actin cytoskeleton rearrangement; thought to play an important role in tumor cell migration and metastais [365]. gp38 signalling have been demonstrated to have intrinsic effects on the proliferation and migration of cells expressing it [365, 366]. In fact, results presented in this thesis have also demonstrated that gp38+ fibroblasts exhibited higher proliferative ability than gp38- fibroblasts.

Impaired B and T cell segregation within the white pulp of the spleen correlates with a lack of gp38 expression on the T zone stroma, thus suggesting a role for gp38 in the separation of lymphocytes [365, 367]. In SLOs, gp38 is expressed on fibroblastic reticular cells (FRCs). FRCs together with reticular fibers (RFs) and fibrous extracellular matrix (ECM) bundles forms the highly diverse reticular network that serves as a scaffold to maintain the 3-D structure of these SLO and also forms an enclosed conduit structure through which molecules such as chemokines and antigens can be delivered within SLOs [1, 3]. It has recently been demonstrated that gp38+ER-TR7+ reticular networks found at the site of TLOs, are functional and can mediate transport of fluid and small molecular weight molecules, such as chemokines and antigens, analogous to FRC found in SLOs [213]. This proposes an interesting possibility of gp38+LLSc delivering antigen directly to TLOs.

gp38 has been shown to bind chemokines such as CCL21 and CCL19 via its negatively charged glycosaminoglycans on the surface of FRCs, which helps to actively direct the migration of lymphocytes between and within separate lymphoid tissue compartments [3, 126, 365, 368]. Moreover, gp38 has been shown to be important for motility of DCs along FRCs networks and this process is guided by engagement of gp38 by its receptor Clec-2 on LNs. Interestingly, a study has shown that gp38 expression is further up-regulated on LN FRCs within few hours of an immune response, suggesting that it acts as an activation marker [280]. This is line with evidence where gp38 was shown to be expressed by damaged keratinocytes during wounding [365]. Besides, another group recently demonstrated that LNs were unable to mount an appropriate immune response to virus insult in the absence of gp38 on FRC [142]. In spite of the large number of descriptive studies, little is understood about podoplanin's biological function. Currently, there are experiments undergoing in our lab to address the functional relevance of gp38 on tissue stromal cells during TLO formation, since *gp38ko* mice are embryonically lethal, we are using the conditional knockout $Pdpn^{loxp/loxp}Rosa26ERT2^{Cre/Cre}$ mice.

Lymphatic endothelial cells (LEC) and blood endothelial cells (BEC) are also a part of tissue stromal cells, and have been demonstrated to be important players of inflammation [222]. Striking changes in the lymphatic vasculature are associated with inflammation, which include acute and chronic infections, autoimmune diseases such as RA, Crohn's disease, wound healing, cancer, and transplant rejection [20, 21, 222]. Neo-lymphangiogenesis is a critical mechanism regulating changes in interstitial fluid. Deregulated activation of its cascade results in defective leukocyte drainage and persistence of the inflammatory process [222].

Similar to the fibroblasts and lymphatic vessels, blood vessels undergo remodelling during inflammation. Blood endothelium changes its structure and phenotype and participates in the inflammatory response, mainly through regulating leukocyte recruitment into the tissue [222]. Furthermore, expression of co-stimulatory molecules such as OX40, ICOSL, and CD2,

known to be important in the formation and activation of T cell memory, has been documented in activated human endothelial vessels [22, 222]. Additional endothelial phenotypical changes are observed in various chronic inflammatory diseases, such as Sjogren's syndrome, thyroiditis, RA [14, 179, 180, 182, 228]. The chronically inflamed organ acquires ectopic lymphoid-like structures with conversion of flat venular endothelial cells into tall and plump endothelial cells that very closely resemble the high endothelial venules (HEVs) found in the lymph nodes [222]. These ectopic HEVs also concomitantly express lymphoid chemokines CCL21 and mostly PNAd that allows large scale and at times misguided influx of CCR7+ memory T cells and potentially naïve cells into the inflamed tissue, leading to amplification and maintenance of chronic inflammation [222]. Moreover, endothelial cells are strongly implicated in LN development [74, 222].

The role of lymphatic and blood endothelial cells in TLO formation and maintenance, as well as signals regulating TLO-associated lymphangiogenesis and changes in the blood vascular bed have not been addressed in this thesis. The presence of lymphatic vessels and HEVs has been documented in inflamed salivary during TLO formation in our mouse model. Therefore, this model provides an exciting tool to address these questions in future.

References

1. Mueller, S.N. and R.N. Germain, *Stromal cell contributions to the homeostasis and functionality of the immune system.* Nature Reviews Immunology, 2010.
2. Malhotra, D., A.L. Fletcher, and S.J. Turley, *Stromal and hematopoietic cells in secondary lymphoid organs: partners in immunity.* Immunol Rev, 2013. **251**(1): p. 160-76.
3. Junt, T., E. Scandella, and B. Ludewig, *Form follows function: lymphoid tissue microarchitecture in antimicrobial immune defence.* Nat Rev Immunol, 2008. **8**(10): p. 764-75.
4. Drayton, D.L., et al., *Lymphoid organ development: from ontogeny to neogenesis.* Nature Immunology, 2006. **7**(4): p. 344-353.
5. Pabst, R., *Plasticity and heterogeneity of lymphoid organs.* Immunology Letters, 2007. **112**(1): p. 1-8.
6. Roozendaal, R. and R.E. Mebius, *Stromal Cell–Immune Cell Interactions.* Annual Review of Immunology, 2011. **29**(1): p. 23-43.
7. Fritz, J.H. and J.L. Gommerman, *Cytokine/Stromal Cell Networks and Lymphoid Tissue Environments.* Journal of Interferon & Cytokine Research, 2011. **31**(3): p. 277-289.
8. Anderson, G. and E.J. Jenkinson, *Lymphostromal interactions in thymic development and function.* Nat Rev Immunol, 2001. **1**(1): p. 31-40.
9. Auerbach, R., *Morphogenetic interactions in the development of the mouse thymus gland.* Dev Biol, 1960. **2**: p. 271-84.
10. Bockman, D.E. and M.L. Kirby, *Dependence of thymus development on derivatives of the neural crest.* Science, 1984. **223**(4635): p. 498-500.
11. Mebius, R.E., *Organogenesis of lymphoid tissues.* Nature Reviews Immunology, 2003. **3**(4): p. 292-303.
12. Neyt, K., et al., *Tertiary lymphoid organs in infection and autoimmunity.* Trends Immunol, 2012. **33**(6): p. 297-305.
13. Carragher, D.M., J. Rangel-Moreno, and T.D. Randall, *Ectopic lymphoid tissues and local immunity.* Semin Immunol, 2008. **20**(1): p. 26-42.
14. Aloisi, F. and R. Pujol-Borrell, *Lymphoid neogenesis in chronic inflammatory diseases.* Nat Rev Immunol, 2006. **6**(3): p. 205-17.
15. Ruddle, N.H. and E.M. Akirav, *Secondary lymphoid organs: responding to genetic and environmental cues in ontogeny and the immune response.* J Immunol, 2009. **183**(4): p. 2205-12.
16. Randall, T.D., D.M. Carragher, and J. Rangel-Moreno, *Development of secondary lymphoid organs.* Annu Rev Immunol, 2008. **26**: p. 627-50.
17. Fukuyama, S., et al., *Initiation of NALT organogenesis is independent of the IL-7R, LTbetaR, and NIK signaling pathways but requires the Id2 gene and CD3(-)CD4(+)CD45(+) cells.* Immunity, 2002. **17**(1): p. 31-40.
18. Banks, T.A., et al., *Lymphotoxin-alpha-deficient mice. Effects on secondary lymphoid organ development and humoral immune responsiveness.* J Immunol, 1995. **155**(4): p. 1685-93.
19. De Togni, P., et al., *Abnormal development of peripheral lymphoid organs in mice deficient in lymphotoxin.* Science, 1994. **264**(5159): p. 703-7.
20. Harmsen, A., et al., *Cutting edge: organogenesis of nasal-associated lymphoid tissue (NALT) occurs independently of lymphotoxin-alpha (LT alpha) and retinoic acid receptor-related orphan receptor-gamma, but the organization of NALT is LT alpha dependent.* J Immunol, 2002. **168**(3): p. 986-90.
21. Koni, P.A., et al., *Distinct roles in lymphoid organogenesis for lymphotoxins alpha and beta revealed in lymphotoxin beta-deficient mice.* Immunity, 1997. **6**(4): p. 491-500.
22. Futterer, A., et al., *The lymphotoxin beta receptor controls organogenesis and affinity maturation in peripheral lymphoid tissues.* Immunity, 1998. **9**(1): p. 59-70.

23. Scheu, S., et al., *Targeted disruption of LIGHT causes defects in costimulatory T cell activation and reveals cooperation with lymphotoxin beta in mesenteric lymph node genesis.* J Exp Med, 2002. **195**(12): p. 1613-24.
24. Miyawaki, S., et al., *A new mutation, aly, that induces a generalized lack of lymph nodes accompanied by immunodeficiency in mice.* Eur J Immunol, 1994. **24**(2): p. 429-34.
25. Adachi, S., et al., *Essential role of IL-7 receptor alpha in the formation of Peyer's patch anlage.* Int Immunol, 1998. **10**(1): p. 1-6.
26. Yoshida, H., et al., *Different cytokines induce surface lymphotoxin-alphabeta on IL-7 receptor-alpha cells that differentially engender lymph nodes and Peyer's patches.* Immunity, 2002. **17**(6): p. 823-33.
27. Coles, M.C., et al., *Role of T and NK cells and IL7/IL7r interactions during neonatal maturation of lymph nodes.* Proc Natl Acad Sci U S A, 2006. **103**(36): p. 13457-62.
28. Kim, D., et al., *Regulation of peripheral lymph node genesis by the tumor necrosis factor family member TRANCE.* J Exp Med, 2000. **192**(10): p. 1467-78.
29. Kong, Y.Y., et al., *OPGL is a key regulator of osteoclastogenesis, lymphocyte development and lymph-node organogenesis.* Nature, 1999. **397**(6717): p. 315-23.
30. Dougall, W.C., et al., *RANK is essential for osteoclast and lymph node development.* Genes Dev, 1999. **13**(18): p. 2412-24.
31. Naito, A., et al., *Severe osteopetrosis, defective interleukin-1 signalling and lymph node organogenesis in TRAF6-deficient mice.* Genes Cells, 1999. **4**(6): p. 353-62.
32. Eberl, G. and D.R. Littman, *The role of the nuclear hormone receptor RORgammat in the development of lymph nodes and Peyer's patches.* Immunol Rev, 2003. **195**: p. 81-90.
33. Sun, Z., et al., *Requirement for RORgamma in thymocyte survival and lymphoid organ development.* Science, 2000. **288**(5475): p. 2369-73.
34. Yokota, Y., et al., *Development of peripheral lymphoid organs and natural killer cells depends on the helix-loop-helix inhibitor Id2.* Nature, 1999. **397**(6721): p. 702-6.
35. Wang, J.H., et al., *Selective defects in the development of the fetal and adult lymphoid system in mice with an Ikaros null mutation.* Immunity, 1996. **5**(6): p. 537-49.
36. Ansel, K.M., et al., *A chemokine-driven positive feedback loop organizes lymphoid follicles.* Nature, 2000. **406**(6793): p. 309-14.
37. Luther, S.A., K.M. Ansel, and J.G. Cyster, *Overlapping roles of CXCL13, interleukin 7 receptor alpha, and CCR7 ligands in lymph node development.* J Exp Med, 2003. **197**(9): p. 1191-8.
38. Forster, R., et al., *A putative chemokine receptor, BLR1, directs B cell migration to defined lymphoid organs and specific anatomic compartments of the spleen.* Cell, 1996. **87**(6): p. 1037-47.
39. Forster, R., et al., *CCR7 coordinates the primary immune response by establishing functional microenvironments in secondary lymphoid organs.* Cell, 1999. **99**(1): p. 23-33.
40. Veiga-Fernandes, H., et al., *Tyrosine kinase receptor RET is a key regulator of Peyer's patch organogenesis.* Nature, 2007. **446**(7135): p. 547-51.
41. Honda, K., et al., *Molecular basis for hematopoietic/mesenchymal interaction during initiation of Peyer's patch organogenesis.* J Exp Med, 2001. **193**(5): p. 621-30.
42. Finke, D., *Fate and function of lymphoid tissue inducer cells.* Current Opinion in Immunology, 2005. **17**(2): p. 144-150.
43. Ferreira, M., R.G. Domingues, and H. Veiga-Fernandes, *Stroma cell priming in enteric lymphoid organ morphogenesis.* Frontiers in Immunology, 2012. **3**.
44. Coles, M. and H. Veiga-Fernandes, *Insight into lymphoid tissue morphogenesis.* Immunology Letters, 2013. **156**(1-2): p. 46-53.
45. Coles, M., D. Kioussis, and H. Veiga-Fernandes, *Cellular and Molecular Requirements in Lymph Node and Peyer's Patch Development.* 2010. **92**: p. 177-205.
46. Cupedo, T., G. Kraal, and R.E. Mebius, *The role of CD45+CD4+CD3- cells in lymphoid organ development.* Immunol Rev, 2002. **189**: p. 41-50.

47. Yoshida, H., et al., *IL-7 receptor alpha+ CD3(-) cells in the embryonic intestine induces the organizing center of Peyer's patches.* Int Immunol, 1999. **11**(5): p. 643-55.
48. Cherrier, M. and G. Eberl, *The development of LTi cells.* Current Opinion in Immunology, 2012. **24**(2): p. 178-183.
49. Kelly, K.A. and R. Scollay, *Seeding of neonatal lymph nodes by T cells and identification of a novel population of CD3-CD4+ cells.* Eur J Immunol, 1992. **22**(2): p. 329-34.
50. Mebius, R.E., P. Rennert, and I.L. Weissman, *Developing lymph nodes collect CD4+CD3- LTbeta+ cells that can differentiate to APC, NK cells, and follicular cells but not T or B cells.* Immunity, 1997. **7**(4): p. 493-504.
51. Adachi, S., et al., *Three distinctive steps in Peyer's patch formation of murine embryo.* Int Immunol, 1997. **9**(4): p. 507-14.
52. Yoshida, H., et al., *Expression of alpha(4)beta(7) integrin defines a distinct pathway of lymphoid progenitors committed to T cells, fetal intestinal lymphotoxin producer, NK, and dendritic cells.* J Immunol, 2001. **167**(5): p. 2511-21.
53. Mebius, R.E., et al., *The fetal liver counterpart of adult common lymphoid progenitors gives rise to all lymphoid lineages, CD45+CD4+CD3- cells, as well as macrophages.* J Immunol, 2001. **166**(11): p. 6593-601.
54. Georgopoulos, K., et al., *The Ikaros gene is required for the development of all lymphoid lineages.* Cell, 1994. **79**(1): p. 143-56.
55. Boos, M.D., et al., *Mature natural killer cell and lymphoid tissue-inducing cell development requires Id2-mediated suppression of E protein activity.* J Exp Med, 2007. **204**(5): p. 1119-30.
56. van de Pavert, S.A. and R.E. Mebius, *New insights into the development of lymphoid tissues.* Nat Rev Immunol, 2010. **10**(9): p. 664-74.
57. Cherrier, M., S. Sawa, and G. Eberl, *Notch, Id2, and RORgammat sequentially orchestrate the fetal development of lymphoid tissue inducer cells.* J Exp Med, 2012. **209**(4): p. 729-40.
58. Eberl, G., et al., *An essential function for the nuclear receptor RORgamma(t) in the generation of fetal lymphoid tissue inducer cells.* Nat Immunol, 2004. **5**(1): p. 64-73.
59. Vondenhoff, M.F., et al., *LT R Signaling Induces Cytokine Expression and Up-Regulates Lymphangiogenic Factors in Lymph Node Anlagen.* The Journal of Immunology, 2009. **182**(9): p. 5439-5445.
60. White, A., et al., *Lymphotoxin a-dependent and -independent signals regulate stromal organizer cell homeostasis during lymph node organogenesis.* Blood, 2007. **110**(6): p. 1950-1959.
61. Finke, D., et al., *CD4+CD3- cells induce Peyer's patch development: role of alpha4beta1 integrin activation by CXCR5.* Immunity, 2002. **17**(3): p. 363-73.
62. Meier, D., et al., *Ectopic lymphoid-organ development occurs through interleukin 7-mediated enhanced survival of lymphoid-tissue-inducer cells.* Immunity, 2007. **26**(5): p. 643-54.
63. Fukuyama, S. and H. Kiyono, *Neuroregulator RET initiates Peyer's-patch tissue genesis.* Immunity, 2007. **26**(4): p. 393-5.
64. Patel, A., et al., *Differential RET signaling pathways drive development of the enteric lymphoid and nervous systems.* Sci Signal, 2012. **5**(235): p. ra55.
65. Ferreira, M., R.G. Domingues, and H. Veiga-Fernandes, *Stroma cell priming in enteric lymphoid organ morphogenesis.* Front Immunol, 2012. **3**: p. 219.
66. Benezech, C., et al., *Ontogeny of stromal organizer cells during lymph node development.* J Immunol, 2010. **184**(8): p. 4521-30.
67. Brendolan, A. and J.H. Caamano, *Mesenchymal cell differentiation during lymph node organogenesis.* Front Immunol, 2012. **3**: p. 381.
68. Sabin, F.R., *The lymphatic system in human embryos, with a consideration of the morphology of the system as a whole.* American Journal of Anatomy, 1909. **9**(1): p. 43-91.
69. Sabin, F.R., *Symposium on the development and structure of the lymphatic system. III. Further evidence on the origin of the lymphatic endothelium from the endothelium of the blood vascular system.* The Anatomical Record, 1908. **2**(1-2): p. 46-55.

70. Sabin, F.R., *On the development of the superficial lymphatics in the skin of the pig.* American Journal of Anatomy, 1904. **3**(2): p. 183-195.
71. Sabin, F.R., *On the origin of the lymphatic system from the veins and the development of the lymph hearts and thoracic duct in the pig.* American Journal of Anatomy, 1902. **1**(3): p. 367-389.
72. van de Pavert, S.A. and R.E. Mebius, *Development of secondary lymphoid organs in relation to lymphatic vasculature.* Adv Anat Embryol Cell Biol, 2014. **214**: p. 81-91.
73. Vondenhoff, M.F., et al., *Lymph sacs are not required for the initiation of lymph node formation.* Development, 2009. **136**(1): p. 29-34.
74. Onder, L., et al., *Endothelial cell-specific lymphotoxin- receptor signaling is critical for lymph node and high endothelial venule formation.* Journal of Experimental Medicine, 2013. **210**(3): p. 465-473.
75. Cupedo, T. and R.E. Mebius, *Cellular interactions in lymph node development.* J Immunol, 2005. **174**(1): p. 21-5.
76. Moyron-Quiroz, J.E., et al., *Role of inducible bronchus associated lymphoid tissue (iBALT) in respiratory immunity.* Nat Med, 2004. **10**(9): p. 927-34.
77. Hess, E., et al., *RANKL induces organized lymph node growth by stromal cell proliferation.* J Immunol, 2012. **188**(3): p. 1245-54.
78. Sugiyama, M., et al., *Expression pattern changes and function of RANKL during mouse lymph node microarchitecture development.* Int Immunol, 2012. **24**(6): p. 369-78.
79. Cupedo, T., et al., *Presumptive lymph node organizers are differentially represented in developing mesenteric and peripheral nodes.* J Immunol, 2004. **173**(5): p. 2968-75.
80. Okuda, M., et al., *Distinct activities of stromal cells involved in the organogenesis of lymph nodes and Peyer's patches.* J Immunol, 2007. **179**(2): p. 804-11.
81. Luther, S.A., K.M. Ansel, and J.G. Cyster, *Overlapping Roles of CXCL13, Interleukin 7 Receptor , and CCR7 Ligands in Lymph Node Development.* Journal of Experimental Medicine, 2003. **197**(9): p. 1191-1198.
82. Ohl, L., et al., *Cooperating Mechanisms of CXCR5 and CCR7 in Development and Organization of Secondary Lymphoid Organs.* Journal of Experimental Medicine, 2003. **197**(9): p. 1199-1204.
83. van de Pavert, S.A., et al., *Chemokine CXCL13 is essential for lymph node initiation and is induced by retinoic acid and neuronal stimulation.* Nature Immunology, 2009. **10**(11): p. 1193-1199.
84. Berggren, K., et al., *Expression and regulation of the retinoic acid synthetic enzyme RALDH-2 in the embryonic chicken wing.* Dev Dyn, 2001. **222**(1): p. 1-16.
85. Niederreither, K. and P. Dolle, *Retinoic acid in development: towards an integrated view.* Nat Rev Genet, 2008. **9**(7): p. 541-53.
86. Bénézech, C., et al., *Lymphotoxin-β Receptor Signaling through NF-κB2-RelB Pathway Reprograms Adipocyte Precursors as Lymph Node Stromal Cells.* Immunity, 2012. **37**(4): p. 721-734.
87. Boehm, T., *Caught in the act: reprogramming of adipocytes into lymph-node stroma.* Immunity, 2012. **37**(4): p. 596-8.
88. Blum, K.S. and R. Pabst, *Keystones in lymph node development.* J Anat, 2006. **209**(5): p. 585-95.
89. Weih, F. and J. Caamano, *Regulation of secondary lymphoid organ development by the nuclear factor-kappaB signal transduction pathway.* Immunol Rev, 2003. **195**: p. 91-105.
90. Muller, G., U.E. Hopken, and M. Lipp, *The impact of CCR7 and CXCR5 on lymphoid organ development and systemic immunity.* Immunol Rev, 2003. **195**: p. 117-35.
91. Ruddle, N.H. and E.M. Akirav, *Secondary Lymphoid Organs: Responding to Genetic and Environmental Cues in Ontogeny and the Immune Response.* The Journal of Immunology, 2009. **183**(4): p. 2205-2212.

92. Roberts, N.A., et al., *Rank signaling links the development of invariant gammadelta T cell progenitors and Aire(+) medullary epithelium.* Immunity, 2012. **36**(3): p. 427-37.
93. Cupedo, T. and R.E. Mebius, *Role of chemokines in the development of secondary and tertiary lymphoid tissues.* Seminars in Immunology, 2003. **15**(5): p. 243-248.
94. Cupedo, T., et al., *Initiation of cellular organization in lymph nodes is regulated by non-B cell-derived signals and is not dependent on CXC chemokine ligand 13.* J Immunol, 2004. **173**(8): p. 4889-96.
95. Browning, J.L. and L.E. French, *Visualization of lymphotoxin-beta and lymphotoxin-beta receptor expression in mouse embryos.* J Immunol, 2002. **168**(10): p. 5079-87.
96. Browning, J.L., et al., *Lymphotoxin-beta receptor signaling is required for the homeostatic control of HEV differentiation and function.* Immunity, 2005. **23**(5): p. 539-50.
97. Benezech, C., et al., *Lymphotoxin-beta receptor signaling through NF-kappaB2-RelB pathway reprograms adipocyte precursors as lymph node stromal cells.* Immunity, 2012. **37**(4): p. 721-34.
98. Hashi, H., et al., *Compartmentalization of Peyer's patch anlagen before lymphocyte entry.* J Immunol, 2001. **166**(6): p. 3702-9.
99. Hoorweg, K. and T. Cupedo, *Development of human lymph nodes and Peyer's patches.* Semin Immunol, 2008. **20**(3): p. 164-70.
100. Mebius, R.E., et al., *A developmental switch in lymphocyte homing receptor and endothelial vascular addressin expression regulates lymphocyte homing and permits CD4+ CD3- cells to colonize lymph nodes.* Proc Natl Acad Sci U S A, 1996. **93**(20): p. 11019-24.
101. Mebius, R.E., I.L. Schadee-Eestermans, and I.L. Weissman, *MAdCAM-1 dependent colonization of developing lymph nodes involves a unique subset of CD4+CD3- hematolymphoid cells.* Cell Adhes Commun, 1998. **6**(2-3): p. 97-103.
102. Rennert, P.D., et al., *Surface lymphotoxin alpha/beta complex is required for the development of peripheral lymphoid organs.* J Exp Med, 1996. **184**(5): p. 1999-2006.
103. Rennert, P.D., J.L. Browning, and P.S. Hochman, *Selective disruption of lymphotoxin ligands reveals a novel set of mucosal lymph nodes and unique effects on lymph node cellular organization.* Int Immunol, 1997. **9**(11): p. 1627-39.
104. Ettinger, R., et al., *Effects of tumor necrosis factor and lymphotoxin on peripheral lymphoid tissue development.* Int Immunol, 1998. **10**(6): p. 727-41.
105. Hamada, H., et al., *Identification of multiple isolated lymphoid follicles on the antimesenteric wall of the mouse small intestine.* J Immunol, 2002. **168**(1): p. 57-64.
106. Lorenz, R.G., et al., *Isolated lymphoid follicle formation is inducible and dependent upon lymphotoxin-sufficient B lymphocytes, lymphotoxin beta receptor, and TNF receptor I function.* J Immunol, 2003. **170**(11): p. 5475-82.
107. Ngo, V.N., R.J. Cornall, and J.G. Cyster, *Splenic T zone development is B cell dependent.* J Exp Med, 2001. **194**(11): p. 1649-60.
108. Endres, R., et al., *Mature follicular dendritic cell networks depend on expression of lymphotoxin beta receptor by radioresistant stromal cells and of lymphotoxin beta and tumor necrosis factor by B cells.* J Exp Med, 1999. **189**(1): p. 159-68.
109. Matsumoto, M., et al., *Role of lymphotoxin and the type I TNF receptor in the formation of germinal centers.* Science, 1996. **271**(5253): p. 1289-91.
110. Le Hir, M., et al., *Differentiation of follicular dendritic cells and full antibody responses require tumor necrosis factor receptor-1 signaling.* J Exp Med, 1996. **183**(5): p. 2367-72.
111. Fu, Y.X., et al., *Lymphotoxin-alpha (LTalpha) supports development of splenic follicular structure that is required for IgG responses.* J Exp Med, 1997. **185**(12): p. 2111-20.
112. Matsumoto, M., et al., *Affinity maturation without germinal centres in lymphotoxin-alpha-deficient mice.* Nature, 1996. **382**(6590): p. 462-6.
113. Fu, Y.X., et al., *B lymphocytes induce the formation of follicular dendritic cell clusters in a lymphotoxin alpha-dependent fashion.* J Exp Med, 1998. **187**(7): p. 1009-18.

114. Withers, D.R., et al., *The role of lymphoid tissue inducer cells in splenic white pulp development.* Eur J Immunol, 2007. **37**(11): p. 3240-5.
115. Ngo, V.N., et al., *Lymphotoxin alpha/beta and tumor necrosis factor are required for stromal cell expression of homing chemokines in B and T cell areas of the spleen.* J Exp Med, 1999. **189**(2): p. 403-12.
116. Schneider, K., K.G. Potter, and C.F. Ware, *Lymphotoxin and LIGHT signaling pathways and target genes.* Immunol Rev, 2004. **202**: p. 49-66.
117. Tumanov, A.V., D.V. Kuprash, and S.A. Nedospasov, *The role of lymphotoxin in development and maintenance of secondary lymphoid tissues.* Cytokine & Growth Factor Reviews, 2003. **14**(3-4): p. 275-288.
118. Fu, Y.X., et al., *Independent signals regulate development of primary and secondary follicle structure in spleen and mesenteric lymph node.* Proc Natl Acad Sci U S A, 1997. **94**(11): p. 5739-43.
119. Tumanov, A.V., et al., *Lymphotoxin and TNF produced by B cells are dispensable for maintenance of the follicle-associated epithelium but are required for development of lymphoid follicles in the Peyer's patches.* J Immunol, 2004. **173**(1): p. 86-91.
120. Tumanov, A., et al., *Distinct role of surface lymphotoxin expressed by B cells in the organization of secondary lymphoid tissues.* Immunity, 2002. **17**(3): p. 239-50.
121. Wu, Q., et al., *The requirement of membrane lymphotoxin for the presence of dendritic cells in lymphoid tissues.* J Exp Med, 1999. **190**(5): p. 629-38.
122. Summers-DeLuca, L.E., et al., *Expression of lymphotoxin-alphabeta on antigen-specific T cells is required for DC function.* J Exp Med, 2007. **204**(5): p. 1071-81.
123. Eugster, H.P., et al., *Multiple immune abnormalities in tumor necrosis factor and lymphotoxin-alpha double-deficient mice.* Int Immunol, 1996. **8**(1): p. 23-36.
124. Rennert, P.D., et al., *Lymph node genesis is induced by signaling through the lymphotoxin beta receptor.* Immunity, 1998. **9**(1): p. 71-9.
125. Pasparakis, M., et al., *Immune and inflammatory responses in TNF alpha-deficient mice: a critical requirement for TNF alpha in the formation of primary B cell follicles, follicular dendritic cell networks and germinal centers, and in the maturation of the humoral immune response.* J Exp Med, 1996. **184**(4): p. 1397-411.
126. Mueller, S.N. and R.N. Germain, *Stromal cell contributions to the homeostasis and functionality of the immune system.* Nat Rev Immunol, 2009. **9**(9): p. 618-29.
127. Fu, Y.X. and D.D. Chaplin, *Development and maturation of secondary lymphoid tissues.* Annu Rev Immunol, 1999. **17**: p. 399-433.
128. Kiyono, H. and S. Fukuyama, *NALT- versus Peyer's-patch-mediated mucosal immunity.* Nat Rev Immunol, 2004. **4**(9): p. 699-710.
129. Garside, P., O. Millington, and K.M. Smith, *The anatomy of mucosal immune responses.* Ann N Y Acad Sci, 2004. **1029**: p. 9-15.
130. Mebius, R.E. and G. Kraal, *Structure and function of the spleen.* Nat Rev Immunol, 2005. **5**(8): p. 606-16.
131. Luther, S.A., T.K. Vogt, and S. Siegert, *Guiding blind T cells and dendritic cells: A closer look at fibroblastic reticular cells found within lymph node T zones.* Immunol Lett, 2011. **138**(1): p. 9-11.
132. Britschgi, M.R., et al., *Dynamic modulation of CCR7 expression and function on naive T lymphocytes in vivo.* J Immunol, 2008. **181**(11): p. 7681-8.
133. Luther, S.A., et al., *Coexpression of the chemokines ELC and SLC by T zone stromal cells and deletion of the ELC gene in the plt/plt mouse.* Proc Natl Acad Sci U S A, 2000. **97**(23): p. 12694-9.
134. Tomei, A.A., et al., *Fluid flow regulates stromal cell organization and CCL21 expression in a tissue-engineered lymph node microenvironment.* J Immunol, 2009. **183**(7): p. 4273-83.
135. Link, A., et al., *Fibroblastic reticular cells in lymph nodes regulate the homeostasis of naive T cells.* Nat Immunol, 2007. **8**(11): p. 1255-65.

136. Siegert, S. and S.A. Luther, *Positive and negative regulation of T cell responses by fibroblastic reticular cells within paracortical regions of lymph nodes.* Front Immunol, 2012. **3**: p. 285.
137. Siegert, S., et al., *Fibroblastic reticular cells from lymph nodes attenuate T cell expansion by producing nitric oxide.* PLoS ONE, 2011. **6**(11): p. e27618.
138. Lukacs-Kornek, V., et al., *Regulated release of nitric oxide by nonhematopoietic stroma controls expansion of the activated T cell pool in lymph nodes.* Nat Immunol, 2011. **12**(11): p. 1096-104.
139. Khan, O., et al., *Regulation of T cell priming by lymphoid stroma.* PLoS ONE, 2011. **6**(11): p. e26138.
140. Fletcher, A.L., et al., *Lymph node fibroblastic reticular cells directly present peripheral tissue antigen under steady-state and inflammatory conditions.* J Exp Med, 2010. **207**(4): p. 689-97.
141. Katakai, T., et al., *Lymph node fibroblastic reticular cells construct the stromal reticulum via contact with lymphocytes.* J Exp Med, 2004. **200**(6): p. 783-95.
142. Chai, Q., et al., *Maturation of Lymph Node Fibroblastic Reticular Cells from Myofibroblastic Precursors Is Critical for Antiviral Immunity.* Immunity, 2013. **38**(5): p. 1013-1024.
143. Cyster, J.G., et al., *Chemokines and B-cell homing to follicles.* Curr Top Microbiol Immunol, 1999. **246**: p. 87-92; discussion 93.
144. Cyster, J.G., et al., *Follicular stromal cells and lymphocyte homing to follicles.* Immunol Rev, 2000. **176**: p. 181-93.
145. Aguzzi, A., J. Kranich, and N.J. Krautler, *Follicular dendritic cells: origin, phenotype, and function in health and disease.* Trends Immunol, 2013.
146. Hase, H., et al., *BAFF/BLyS can potentiate B-cell selection with the B-cell coreceptor complex.* Blood, 2004. **103**(6): p. 2257-65.
147. Krautler, N.J., et al., *Follicular dendritic cells emerge from ubiquitous perivascular precursors.* Cell, 2012. **150**(1): p. 194-206.
148. Mackay, F. and J.L. Browning, *Turning off follicular dendritic cells.* Nature, 1998. **395**(6697): p. 26-7.
149. Katakai, T., *Marginal reticular cells: a stromal subset directly descended from the lymphoid tissue organizer.* Frontiers in Immunology, 2012. **3**.
150. Katakai, T., et al., *Organizer-like reticular stromal cell layer common to adult secondary lymphoid organs.* J Immunol, 2008. **181**(9): p. 6189-200.
151. Roozendaal, R., et al., *Conduits mediate transport of low-molecular-weight antigen to lymph node follicles.* Immunity, 2009. **30**(2): p. 264-76.
152. Junt, T., et al., *Subcapsular sinus macrophages in lymph nodes clear lymph-borne viruses and present them to antiviral B cells.* Nature, 2007. **450**(7166): p. 110-4.
153. Wolniak, K.L., S.M. Shinall, and T.J. Waldschmidt, *The germinal center response.* Crit Rev Immunol, 2004. **24**(1): p. 39-65.
154. Vinuesa, C.G., I. Sanz, and M.C. Cook, *Dysregulation of germinal centres in autoimmune disease.* Nat Rev Immunol, 2009. **9**(12): p. 845-57.
155. Victora, G.D. and M.C. Nussenzweig, *Germinal centers.* Annu Rev Immunol, 2012. **30**: p. 429-57.
156. Gatto, D. and R. Brink, *The germinal center reaction.* J Allergy Clin Immunol, 2010. **126**(5): p. 898-907; quiz 908-9.
157. Sacca, R., et al., *Lymphotoxin: from chronic inflammation to lymphoid organs.* J Inflamm, 1995. **47**(1-2): p. 81-4.
158. Picarella, D.E., et al., *Transgenic tumor necrosis factor (TNF)-alpha production in pancreatic islets leads to insulitis, not diabetes. Distinct patterns of inflammation in TNF-alpha and TNF-beta transgenic mice.* J Immunol, 1993. **150**(9): p. 4136-50.
159. Kratz, A., et al., *Chronic inflammation caused by lymphotoxin is lymphoid neogenesis.* J Exp Med, 1996. **183**(4): p. 1461-72.
160. Hjelmstrom, P., *Lymphoid neogenesis: de novo formation of lymphoid tissue in chronic inflammation through expression of homing chemokines.* J Leukoc Biol, 2001. **69**(3): p. 331-9.

161. Schrama, D., et al., *Targeting of lymphotoxin-alpha to the tumor elicits an efficient immune response associated with induction of peripheral lymphoid-like tissue.* Immunity, 2001. **14**(2): p. 111-21.
162. Wang, J., et al., *The complementation of lymphotoxin deficiency with LIGHT, a newly discovered TNF family member, for the restoration of secondary lymphoid structure and function.* Eur J Immunol, 2002. **32**(7): p. 1969-79.
163. Gommerman, J.L. and J.L. Browning, *Lymphotoxin/light, lymphoid microenvironments and autoimmune disease.* Nat Rev Immunol, 2003. **3**(8): p. 642-55.
164. Lee, Y., et al., *Recruitment and activation of naive T cells in the islets by lymphotoxin beta receptor-dependent tertiary lymphoid structure.* Immunity, 2006. **25**(3): p. 499-509.
165. Ruddle, N.H., *Lymphoid neo-organogenesis: lymphotoxin's role in inflammation and development.* Immunol Res, 1999. **19**(2-3): p. 119-25.
166. Guerder, S., et al., *Costimulator B7-1 confers antigen-presenting-cell function to parenchymal tissue and in conjunction with tumor necrosis factor alpha leads to autoimmunity in transgenic mice.* Proc Natl Acad Sci U S A, 1994. **91**(11): p. 5138-42.
167. Sarvetnick, N., et al., *Loss of pancreatic islet tolerance induced by beta-cell expression of interferon-gamma.* Nature, 1990. **346**(6287): p. 844-7.
168. Heath, W.R., et al., *Autoimmune diabetes as a consequence of locally produced interleukin-2.* Nature, 1992. **359**(6395): p. 547-9.
169. Luther, S.A., et al., *BLC expression in pancreatic islets causes B cell recruitment and lymphotoxin-dependent lymphoid neogenesis.* Immunity, 2000. **12**(5): p. 471-81.
170. Martin, A.P., et al., *A novel model for lymphocytic infiltration of the thyroid gland generated by transgenic expression of the CC chemokine CCL21.* J Immunol, 2004. **173**(8): p. 4791-8.
171. Lira, S.A., et al., *Mechanisms regulating lymphocytic infiltration of the thyroid in murine models of thyroiditis.* Crit Rev Immunol, 2005. **25**(4): p. 251-62.
172. Furtado, G.C., et al., *Lymphotoxin beta receptor signaling is required for inflammatory lymphangiogenesis in the thyroid.* Proc Natl Acad Sci U S A, 2007. **104**(12): p. 5026-31.
173. Fan, L., et al., *Cutting edge: ectopic expression of the chemokine TCA4/SLC is sufficient to trigger lymphoid neogenesis.* J Immunol, 2000. **164**(8): p. 3955-9.
174. Chen, S.C., et al., *Ectopic expression of the murine chemokines CCL21a and CCL21b induces the formation of lymph node-like structures in pancreas, but not skin, of transgenic mice.* J Immunol, 2002. **168**(3): p. 1001-8.
175. Luther, S.A., et al., *Differing activities of homeostatic chemokines CCL19, CCL21, and CXCL12 in lymphocyte and dendritic cell recruitment and lymphoid neogenesis.* J Immunol, 2002. **169**(1): p. 424-33.
176. Goya, S., et al., *Sustained interleukin-6 signalling leads to the development of lymphoid organ-like structures in the lung.* J Pathol, 2003. **200**(1): p. 82-7.
177. Salomonsson, S., et al., *Expression of the B cell-attracting chemokine CXCL13 in the target organ and autoantibody production in ectopic lymphoid tissue in the chronic inflammatory disease Sjogren's syndrome.* Scand J Immunol, 2002. **55**(4): p. 336-42.
178. Salomonsson, S., et al., *Cellular basis of ectopic germinal center formation and autoantibody production in the target organ of patients with Sj*  *gren's syndrome.* Arthritis & Rheumatism, 2003. **48**(11): p. 3187-3201.
179. Manzo, A., et al., *Systematic microanatomical analysis of CXCL13 and CCL21in situ production and progressive lymphoid organization in rheumatoid synovitis.* European Journal of Immunology, 2005. **35**(5): p. 1347-1359.
180. Barone, F., et al., *Association of CXCL13 and CCL21 expression with the progressive organization of lymphoid-like structures in Sjögren's syndrome.* Arthritis & Rheumatism, 2005. **52**(6): p. 1773-1784.
181. Astorri, E., et al., *Evolution of Ectopic Lymphoid Neogenesis and In Situ Autoantibody Production in Autoimmune Nonobese Diabetic Mice: Cellular and Molecular Characterization*

of Tertiary Lymphoid Structures in Pancreatic Islets. The Journal of Immunology, 2010. **185**(6): p. 3359-3368.
182. Manzo, A., et al., *Secondary and ectopic lymphoid tissue responses in rheumatoid arthritis: from inflammation to autoimmunity and tissue damage/remodeling.* Immunol Rev, 2010. **233**(1): p. 267-85.
183. Amft, N., et al., *Ectopic expression of the B cell-attracting chemokine BCA-1 (CXCL13) on endothelial cells and within lymphoid follicles contributes to the establishment of germinal center-like structures in Sjogren's syndrome.* Arthritis Rheum, 2001. **44**(11): p. 2633-41.
184. Takemura, S., et al., *Lymphoid neogenesis in rheumatoid synovitis.* J Immunol, 2001. **167**(2): p. 1072-80.
185. Rangel-Moreno, J., et al., *Inducible bronchus-associated lymphoid tissue (iBALT) in patients with pulmonary complications of rheumatoid arthritis.* J Clin Invest, 2006. **116**(12): p. 3183-94.
186. Hjelmstrom, P., et al., *Lymphoid tissue homing chemokines are expressed in chronic inflammation.* Am J Pathol, 2000. **156**(4): p. 1133-8.
187. Phillips, R.J., et al., *Circulating fibrocytes traffic to the lungs in response to CXCL12 and mediate fibrosis.* J Clin Invest, 2004. **114**(3): p. 438-46.
188. Weyand, C.M. and J.J. Goronzy, *Ectopic germinal center formation in rheumatoid synovitis.* Ann N Y Acad Sci, 2003. **987**: p. 140-9.
189. Magliozzi, R., et al., *Intracerebral expression of CXCL13 and BAFF is accompanied by formation of lymphoid follicle-like structures in the meninges of mice with relapsing experimental autoimmune encephalomyelitis.* J Neuroimmunol, 2004. **148**(1-2): p. 11-23.
190. Katakai, T., et al., *Th1-biased tertiary lymphoid tissue supported by CXC chemokine ligand 13-producing stromal network in chronic lesions of autoimmune gastritis.* J Immunol, 2003. **171**(8): p. 4359-68.
191. Winter, S., et al., *The chemokine receptor CXCR5 is pivotal for ectopic mucosa-associated lymphoid tissue neogenesis in chronic Helicobacter pylori-induced inflammation.* J Mol Med (Berl), 2010. **88**(11): p. 1169-80.
192. Wengner, A.M., et al., *CXCR5- and CCR7-dependent lymphoid neogenesis in a murine model of chronic antigen-induced arthritis.* Arthritis Rheum, 2007. **56**(10): p. 3271-83.
193. Grabner, R., et al., *Lymphotoxin beta receptor signaling promotes tertiary lymphoid organogenesis in the aorta adventitia of aged ApoE-/- mice.* J Exp Med, 2009. **206**(1): p. 233-48.
194. Bombardieri, M., et al., *Activation-induced cytidine deaminase expression in follicular dendritic cell networks and interfollicular large B cells supports functionality of ectopic lymphoid neogenesis in autoimmune sialoadenitis and MALT lymphoma in Sjogren's syndrome.* J Immunol, 2007. **179**(7): p. 4929-38.
195. Gause, A., et al., *The B lymphocyte in rheumatoid arthritis: analysis of rearranged V kappa genes from B cells infiltrating the synovial membrane.* Eur J Immunol, 1995. **25**(10): p. 2775-82.
196. Schroder, A.E., et al., *Differentiation of B cells in the nonlymphoid tissue of the synovial membrane of patients with rheumatoid arthritis.* Proc Natl Acad Sci U S A, 1996. **93**(1): p. 221-5.
197. Uccelli, A., F. Aloisi, and V. Pistoia, *Unveiling the enigma of the CNS as a B-cell fostering environment.* Trends Immunol, 2005. **26**(5): p. 254-9.
198. Qin, Y., et al., *Clonal expansion and somatic hypermutation of V(H) genes of B cells from cerebrospinal fluid in multiple sclerosis.* J Clin Invest, 1998. **102**(5): p. 1045-50.
199. Dorner, T., et al., *Immunglobulin repertoire analysis provides new insights into the immunopathogenesis of Sjogren's syndrome.* Autoimmun Rev, 2002. **1**(3): p. 119-24.
200. Sims, G.P., et al., *Somatic hypermutation and selection of B cells in thymic germinal centers responding to acetylcholine receptor in myasthenia gravis.* J Immunol, 2001. **167**(4): p. 1935-44.

201. Stott, D.I., et al., *Antigen-driven clonal proliferation of B cells within the target tissue of an autoimmune disease. The salivary glands of patients with Sjogren's syndrome.* J Clin Invest, 1998. **102**(5): p. 938-46.
202. Kim, H.J., et al., *Plasma cell development in synovial germinal centers in patients with rheumatoid and reactive arthritis.* J Immunol, 1999. **162**(5): p. 3053-62.
203. Gregorio, A., et al., *Lymphoid neogenesis in juvenile idiopathic arthritis correlates with ANA positivity and plasma cells infiltration.* Rheumatology (Oxford), 2007. **46**(2): p. 308-13.
204. Armengol, M.P., et al., *Thyroid autoimmune disease: demonstration of thyroid antigen-specific B cells and recombination-activating gene expression in chemokine-containing active intrathyroidal germinal centers.* Am J Pathol, 2001. **159**(3): p. 861-73.
205. Aust, G., et al., *The role of CXCR5 and its ligand CXCL13 in the compartmentalization of lymphocytes in thyroids affected by autoimmune thyroid diseases.* Eur J Endocrinol, 2004. **150**(2): p. 225-34.
206. Randen, I., et al., *The identification of germinal centres and follicular dendritic cell networks in rheumatoid synovial tissue.* Scand J Immunol, 1995. **41**(5): p. 481-6.
207. McMahon, E.J., et al., *Epitope spreading initiates in the CNS in two mouse models of multiple sclerosis.* Nat Med, 2005. **11**(3): p. 335-9.
208. Nasr, I.W., et al., *Tertiary lymphoid tissues generate effector and memory T cells that lead to allograft rejection.* Am J Transplant, 2007. **7**(5): p. 1071-9.
209. Yu, P., et al., *Priming of naive T cells inside tumors leads to eradication of established tumors.* Nat Immunol, 2004. **5**(2): p. 141-9.
210. Freni, M.A., et al., *Focal lymphocytic aggregates in chronic hepatitis C: occurrence, immunohistochemical characterization, and relation to markers of autoimmunity.* Hepatology, 1995. **22**(2): p. 389-94.
211. Wotherspoon, A.C., et al., *Regression of primary low-grade B-cell gastric lymphoma of mucosa-associated lymphoid tissue type after eradication of Helicobacter pylori.* Lancet, 1993. **342**(8871): p. 575-7.
212. Cupedo, T., et al., *Induction of Secondary and Tertiary Lymphoid Structures in the Skin.* Immunity, 2004. **21**(5): p. 655-667.
213. Link, A., et al., *Association of T-Zone Reticular Networks and Conduits with Ectopic Lymphoid Tissues in Mice and Humans.* The American Journal of Pathology, 2011. **178**(4): p. 1662-1675.
214. Rangel-Moreno, J., et al., *The development of inducible bronchus-associated lymphoid tissue depends on IL-17.* Nat Immunol, 2011. **12**(7): p. 639-46.
215. Moyron-Quiroz, J.E., et al., *Persistence and responsiveness of immunologic memory in the absence of secondary lymphoid organs.* Immunity, 2006. **25**(4): p. 643-54.
216. Lochner, M., et al., *Microbiota-induced tertiary lymphoid tissues aggravate inflammatory disease in the absence of ROR t and LTi cells.* Journal of Experimental Medicine, 2010. **208**(1): p. 125-134.
217. Marinkovic, T., *Interaction of mature CD3+CD4+ T cells with dendritic cells triggers the development of tertiary lymphoid structures in the thyroid.* Journal of Clinical Investigation, 2006. **116**(10): p. 2622-2632.
218. Muniz, L.R., et al., *A critical role for dendritic cells in the formation of lymphatic vessels within tertiary lymphoid structures.* J Immunol, 2011. **187**(2): p. 828-34.
219. Halle, S., et al., *Induced bronchus-associated lymphoid tissue serves as a general priming site for T cells and is maintained by dendritic cells.* J Exp Med, 2009. **206**(12): p. 2593-601.
220. GeurtsvanKessel, C.H., et al., *Dendritic cells are crucial for maintenance of tertiary lymphoid structures in the lung of influenza virus-infected mice.* J Exp Med, 2009. **206**(11): p. 2339-49.
221. Flavell, S.J., et al., *Fibroblasts as novel therapeutic targets in chronic inflammation.* Br J Pharmacol, 2008. **153 Suppl 1**: p. S241-6.
222. Barone, F., S. Nayar, and C.D. Buckley, *The role of non-hematopoietic stromal cells in the persistence of inflammation.* Front Immunol, 2012. **3**: p. 416.

223. Filer, A., et al., *The role of chemokines in leucocyte-stromal interactions in rheumatoid arthritis.* Front Biosci, 2008. **13**: p. 2674-85.
224. Suematsu, S. and T. Watanabe, *Generation of a synthetic lymphoid tissue-like organoid in mice.* Nat Biotechnol, 2004. **22**(12): p. 1539-45.
225. Lotzer, K., et al., *Mouse aorta smooth muscle cells differentiate into lymphoid tissue organizer-like cells on combined tumor necrosis factor receptor-1/lymphotoxin beta-receptor NF-kappaB signaling.* Arterioscler Thromb Vasc Biol, 2010. **30**(3): p. 395-402.
226. Peduto, L., et al., *Inflammation Recapitulates the Ontogeny of Lymphoid Stromal Cells.* The Journal of Immunology, 2009. **182**(9): p. 5789-5799.
227. Picarella, D.E., et al., *Insulitis in transgenic mice expressing tumor necrosis factor beta (lymphotoxin) in the pancreas.* Proc Natl Acad Sci U S A, 1992. **89**(21): p. 10036-40.
228. Manzo, A., et al., *CCL21 Expression Pattern of Human Secondary Lymphoid Organ Stroma Is Conserved in Inflammatory Lesions with Lymphoid Neogenesis.* The American Journal of Pathology, 2007. **171**(5): p. 1549-1562.
229. Stranford, S. and N.H. Ruddle, *Follicular dendritic cells, conduits, lymphatic vessels, and high endothelial venules in tertiary lymphoid organs: Parallels with lymph node stroma.* Front Immunol, 2012. **3**: p. 350.
230. Peters, A., et al., *Th17 Cells Induce Ectopic Lymphoid Follicles in Central Nervous System Tissue Inflammation.* Immunity, 2011. **35**(6): p. 986-996.
231. Amft, N. and S.J. Bowman, *Chemokines and cell trafficking in Sjogren's syndrome.* Scand J Immunol, 2001. **54**(1-2): p. 62-9.
232. Drayton, D.L., et al., *Ectopic LT Directs Lymphoid Organ Neogenesis with Concomitant Expression of Peripheral Node Addressin and a HEV-restricted Sulfotransferase.* Journal of Experimental Medicine, 2003. **197**(9): p. 1153-1163.
233. Humby, F., et al., *Ectopic lymphoid structures support ongoing production of class-switched autoantibodies in rheumatoid synovium.* PLoS Med, 2009. **6**(1): p. e1.
234. Rangel-Moreno, J., et al., *Role of CXC chemokine ligand 13, CC chemokine ligand (CCL) 19, and CCL21 in the organization and function of nasal-associated lymphoid tissue.* J Immunol, 2005. **175**(8): p. 4904-13.
235. Ware, C.F., *Targeting lymphocyte activation through the lymphotoxin and LIGHT pathways.* Immunol Rev, 2008. **223**: p. 186-201.
236. Barone, F., et al., *CXCL13, CCL21, and CXCL12 expression in salivary glands of patients with Sjogren's syndrome and MALT lymphoma: association with reactive and malignant areas of lymphoid organization.* J Immunol, 2008. **180**(7): p. 5130-40.
237. Bombardieri, M., et al., *Inducible tertiary lymphoid structures, autoimmunity, and exocrine dysfunction in a novel model of salivary gland inflammation in C57BL/6 mice.* J Immunol, 2012. **189**(7): p. 3767-76.
238. Noben-Trauth, N., et al., *An interleukin 4 (IL-4)-independent pathway for CD4+ T cell IL-4 production is revealed in IL-4 receptor-deficient mice.* Proc Natl Acad Sci U S A, 1997. **94**(20): p. 10838-43.
239. Noben-Trauth, N., et al., *Efficient targeting of the IL-4 gene in a BALB/c embryonic stem cell line.* Transgenic Res, 1996. **5**(6): p. 487-91.
240. McKenzie, G.J., et al., *A distinct role for interleukin-13 in Th2-cell-mediated immune responses.* Curr Biol, 1998. **8**(6): p. 339-42.
241. Mombaerts, P., et al., *RAG-1-deficient mice have no mature B and T lymphocytes.* Cell, 1992. **68**(5): p. 869-77.
242. Wang, B., et al., *A block in both early T lymphocyte and natural killer cell development in transgenic mice with high-copy numbers of the human CD3E gene.* Proc Natl Acad Sci U S A, 1994. **91**(20): p. 9402-6.
243. Cascalho, M., et al., *A quasi-monoclonal mouse.* Science, 1996. **272**(5268): p. 1649-52.

244. Cunningham, A.F., et al., *Salmonella induces a switched antibody response without germinal centers that impedes the extracellular spread of infection.* J Immunol, 2007. **178**(10): p. 6200-7.
245. Neill, D.R., et al., *Nuocytes represent a new innate effector leukocyte that mediates type-2 immunity.* Nature, 2010. **464**(7293): p. 1367-70.
246. Cyster, J.G., *Chemokines, sphingosine-1-phosphate, and cell migration in secondary lymphoid organs.* Annu Rev Immunol, 2005. **23**: p. 127-59.
247. Katakai, T., *A novel reticular stromal structure in lymph node cortex: an immuno-platform for interactions among dendritic cells, T cells and B cells.* International Immunology, 2004. **16**(8): p. 1133-1142.
248. Buckley, C.D., et al., *Fibroblasts regulate the switch from acute resolving to chronic persistent inflammation.* Trends Immunol, 2001. **22**(4): p. 199-204.
249. Burman, A., et al., *A chemokine-dependent stromal induction mechanism for aberrant lymphocyte accumulation and compromised lymphatic return in rheumatoid arthritis.* J Immunol, 2005. **174**(3): p. 1693-700.
250. Tumanov, A.V., et al., *Cellular source and molecular form of TNF specify its distinct functions in organization of secondary lymphoid organs.* Blood, 2010. **116**(18): p. 3456-3464.
251. Ruddle, N.H., et al., *Probing the mechanism of TNF-alpha(cachectin)- and TNF-beta(lymphotoxin)-induced pancreatic inflammation with transgenic mice.* Res Immunol, 1993. **144**(5): p. 336-42.
252. Nishikawa, S.I., et al., *Inflammation, a prototype for organogenesis of the lymphopoietic/hematopoietic system.* Curr Opin Immunol, 2000. **12**(3): p. 342-5.
253. Eberl, G., *From induced to programmed lymphoid tissues: the long road to preempt pathogens.* Trends Immunol, 2007. **28**(10): p. 423-8.
254. Huang, H.Y. and S.A. Luther, *Expression and function of interleukin-7 in secondary and tertiary lymphoid organs.* Semin Immunol, 2012. **24**(3): p. 175-89.
255. Hata, M., et al., *Immunoelectron microscopic study of podoplanin localization in mouse salivary gland myoepithelium.* Acta Histochem Cytochem, 2010. **43**(2): p. 77-82.
256. Benezech, C., et al., *Ontogeny of Stromal Organizer Cells during Lymph Node Development.* The Journal of Immunology, 2010. **184**(8): p. 4521-4530.
257. Gatumu, M.K., et al., *Blockade of lymphotoxin-beta receptor signaling reduces aspects of Sjogren's syndrome in salivary glands of non-obese diabetic mice.* Arthritis Res Ther, 2009. **11**(1): p. R24.
258. Humphreys-Beher, M.G. and A.B. Peck, *New concepts for the development of autoimmune exocrinopathy derived from studies with the NOD mouse model.* Arch Oral Biol, 1999. **44 Suppl 1**: p. S21-5.
259. Jonsson, M.V., N. Delaleu, and R. Jonsson, *Animal models of Sjogren's syndrome.* Clin Rev Allergy Immunol, 2007. **32**(3): p. 215-24.
260. Lee, B.H., et al., *Animal models in autoimmune diseases: lessons learned from mouse models for Sjogren's syndrome.* Clin Rev Allergy Immunol, 2012. **42**(1): p. 35-44.
261. Delaleu, N., et al., *Sjogren's syndrome: studying the disease in mice.* Arthritis Res Ther, 2011. **13**(3): p. 217.
262. Lavoie, T.N., B.H. Lee, and C.Q. Nguyen, *Current concepts: mouse models of Sjogren's syndrome.* J Biomed Biotechnol, 2011. **2011**: p. 549107.
263. Nguyen, C.Q., et al., *Pathogenic effect of interleukin-17A in induction of Sjogren's syndrome-like disease using adenovirus-mediated gene transfer.* Arthritis Res Ther, 2010. **12**(6): p. R220.
264. Fleck, M., et al., *Murine cytomegalovirus induces a Sjogren's syndrome-like disease in C57Bl/6-lpr/lpr mice.* Arthritis Rheum, 1998. **41**(12): p. 2175-84.
265. Fleck, M., et al., *Treatment of chronic sialadenitis in a murine model of Sjogren's syndrome by local fasL gene transfer.* Arthritis Rheum, 2001. **44**(4): p. 964-73.
266. Allen, C.D. and J.G. Cyster, *Follicular dendritic cell networks of primary follicles and germinal centers: phenotype and function.* Semin Immunol, 2008. **20**(1): p. 14-25.

267. Muramatsu, M., et al., *Specific expression of activation-induced cytidine deaminase (AID), a novel member of the RNA-editing deaminase family in germinal center B cells.* J Biol Chem, 1999. **274**(26): p. 18470-6.
268. Dorner, T. and A. Radbruch, *Selecting B cells and plasma cells to memory.* J Exp Med, 2005. **201**(4): p. 497-9.
269. Schneider, P., et al., *BAFF, a novel ligand of the tumor necrosis factor family, stimulates B cell growth.* J Exp Med, 1999. **189**(11): p. 1747-56.
270. Jonsson, M.V., et al., *Serological implications of germinal center-like structures in primary Sjogren's syndrome.* J Rheumatol, 2007. **34**(10): p. 2044-9.
271. Le Pottier, L., et al., *Ectopic germinal centers are rare in Sjogren's syndrome salivary glands and do not exclude autoreactive B cells.* J Immunol, 2009. **182**(6): p. 3540-7.
272. Farr, A., A. Nelson, and S. Hosier, *Characterization of an antigenic determinant preferentially expressed by type I epithelial cells in the murine thymus.* J Histochem Cytochem, 1992. **40**(5): p. 651-64.
273. Farr, A.G., et al., *Characterization and cloning of a novel glycoprotein expressed by stromal cells in T-dependent areas of peripheral lymphoid tissues.* J Exp Med, 1992. **176**(5): p. 1477-82.
274. Schacht, V., et al., *Up-regulation of the lymphatic marker podoplanin, a mucin-type transmembrane glycoprotein, in human squamous cell carcinomas and germ cell tumors.* Am J Pathol, 2005. **166**(3): p. 913-21.
275. Schacht, V., et al., *T1alpha/podoplanin deficiency disrupts normal lymphatic vasculature formation and causes lymphedema.* EMBO J, 2003. **22**(14): p. 3546-56.
276. Breiteneder-Geleff, S., et al., *[Podoplanin--a specific marker for lymphatic endothelium expressed in angiosarcoma].* Verh Dtsch Ges Pathol, 1999. **83**: p. 270-5.
277. Breiteneder-Geleff, S., et al., *Podoplanin, novel 43-kd membrane protein of glomerular epithelial cells, is down-regulated in puromycin nephrosis.* Am J Pathol, 1997. **151**(4): p. 1141-52.
278. Akashi, K., et al., *Lymphoid development from stem cells and the common lymphocyte progenitors.* Cold Spring Harb Symp Quant Biol, 1999. **64**: p. 1-12.
279. Mebius, R.E., *Organogenesis of lymphoid tissues.* Nat Rev Immunol, 2003. **3**(4): p. 292-303.
280. Yang, C.Y., et al., *Trapping of naive lymphocytes triggers rapid growth and remodeling of the fibroblast network in reactive murine lymph nodes.* Proc Natl Acad Sci U S A, 2014. **111**(1): p. E109-18.
281. Cupedo, T., *An unexpected role for IL-17 in lymphoid organogenesis.* Nat Immunol, 2011. **12**(7): p. 590-2.
282. Fleige, H., et al., *Induction of BALT in the absence of IL-17.* Nat Immunol, 2012. **13**(1): p. 1; author reply 2.
283. Peters, A., et al., *Th17 cells induce ectopic lymphoid follicles in central nervous system tissue inflammation.* Immunity, 2011. **35**(6): p. 986-96.
284. Heredia, J.E., et al., *Type 2 innate signals stimulate fibro/adipogenic progenitors to facilitate muscle regeneration.* Cell, 2013. **153**(2): p. 376-88.
285. Chomarat, P. and J. Banchereau, *Interleukin-4 and interleukin-13: their similarities and discrepancies.* Int Rev Immunol, 1998. **17**(1-4): p. 1-52.
286. Murata, T., et al., *Sharing of receptor subunits and signal transduction pathway between the IL-4 and IL-13 receptor system.* Int J Hematol, 1999. **69**(1): p. 13-20.
287. Doucet, C., et al., *IL-4 and IL-13 specifically increase adhesion molecule and inflammatory cytokine expression in human lung fibroblasts.* Int Immunol, 1998. **10**(10): p. 1421-33.
288. Doucet, C., C. Jasmin, and B. Azzarone, *Unusual interleukin-4 and -13 signaling in human normal and tumor lung fibroblasts.* Oncogene, 2000. **19**(51): p. 5898-905.
289. Poudrier, J., et al., *A novel monoclonal antibody, C41, reveals IL-13Ralpha1 expression by murine germinal center B cells and follicular dendritic cells.* Eur J Immunol, 2000. **30**(11): p. 3157-64.

290. Vega, F., et al., *Tissue-specific function of lymph node fibroblastic reticulum cells.* Pathobiology, 2006. **73**(2): p. 71-81.
291. Temann, U.A., et al., *IL9 leads to airway inflammation by inducing IL13 expression in airway epithelial cells.* Int Immunol, 2007. **19**(1): p. 1-10.
292. Nelms, K., et al., *The IL-4 receptor: signaling mechanisms and biologic functions.* Annu Rev Immunol, 1999. **17**: p. 701-38.
293. Wynn, T.A., *IL-13 effector functions.* Annu Rev Immunol, 2003. **21**: p. 425-56.
294. Munitz, A., et al., *Distinct roles for IL-13 and IL-4 via IL-13 receptor alpha1 and the type II IL-4 receptor in asthma pathogenesis.* Proc Natl Acad Sci U S A, 2008. **105**(20): p. 7240-5.
295. Mannon, P. and W. Reinisch, *Interleukin 13 and its role in gut defence and inflammation.* Gut, 2012. **61**(12): p. 1765-73.
296. Kain, M.J. and B.M. Owens, *Stromal cell regulation of homeostatic and inflammatory lymphoid organogenesis.* Immunology, 2013. **140**(1): p. 12-21.
297. Morimoto, M., et al., *Functional importance of regional differences in localized gene expression of receptors for IL-13 in murine gut.* J Immunol, 2006. **176**(1): p. 491-5.
298. Scharl, M., et al., *Interleukin-13 and transforming growth factor beta synergise in the pathogenesis of human intestinal fistulae.* Gut, 2013. **62**(1): p. 63-72.
299. Raza, K., et al., *Early rheumatoid arthritis is characterized by a distinct and transient synovial fluid cytokine profile of T cell and stromal cell origin.* Arthritis Res Ther, 2005. **7**(4): p. R784-95.
300. Chiaramonte, M.G., et al., *An IL-13 inhibitor blocks the development of hepatic fibrosis during a T-helper type 2-dominated inflammatory response.* J Clin Invest, 1999. **104**(6): p. 777-85.
301. Ohshima, K., et al., *Interleukin-13 and interleukin-13 receptor in Hodgkin's disease: possible autocrine mechanism and involvement in fibrosis.* Histopathology, 2001. **38**(4): p. 368-75.
302. Relic, B., et al., *Il-4 and IL-13, but not IL-10, protect human synoviocytes from apoptosis.* J Immunol, 2001. **166**(4): p. 2775-82.
303. Hallett, M.A., K.T. Venmar, and B. Fingleton, *Cytokine stimulation of epithelial cancer cells: the similar and divergent functions of IL-4 and IL-13.* Cancer Res, 2012. **72**(24): p. 6338-43.
304. Barron, L. and T.A. Wynn, *Fibrosis is regulated by Th2 and Th17 responses and by dynamic interactions between fibroblasts and macrophages.* Am J Physiol Gastrointest Liver Physiol, 2011. **300**(5): p. G723-8.
305. Zhu, J. and W.E. Paul, *CD4 T cells: fates, functions, and faults.* Blood, 2008. **112**(5): p. 1557-69.
306. Spits, H., et al., *Innate lymphoid cells--a proposal for uniform nomenclature.* Nat Rev Immunol, 2013. **13**(2): p. 145-9.
307. Chang, Y.J., et al., *Innate lymphoid cells mediate influenza-induced airway hyper-reactivity independently of adaptive immunity.* Nat Immunol, 2011. **12**(7): p. 631-8.
308. Halim, T.Y., et al., *Lung natural helper cells are a critical source of Th2 cell-type cytokines in protease allergen-induced airway inflammation.* Immunity, 2012. **36**(3): p. 451-63.
309. Gallichan, W.S., et al., *Pancreatic IL-4 expression results in islet-reactive Th2 cells that inhibit diabetogenic lymphocytes in the nonobese diabetic mouse.* J Immunol, 1999. **163**(3): p. 1696-703.
310. Wang, H.Y., W.E. Paul, and A.D. Keegan, *IL-4 function can be transferred to the IL-2 receptor by tyrosine containing sequences found in the IL-4 receptor alpha chain.* Immunity, 1996. **4**(2): p. 113-21.
311. Dumoutier, L., et al., *Human interleukin-10-related T cell-derived inducible factor: molecular cloning and functional characterization as an hepatocyte-stimulating factor.* Proc Natl Acad Sci U S A, 2000. **97**(18): p. 10144-9.
312. Xie, M.H., et al., *Interleukin (IL)-22, a novel human cytokine that signals through the interferon receptor-related proteins CRF2-4 and IL-22R.* J Biol Chem, 2000. **275**(40): p. 31335-9.

313. Zenewicz, L.A. and R.A. Flavell, *Recent advances in IL-22 biology.* Int Immunol, 2011. **23**(3): p. 159-63.
314. Wolk, K., et al., *IL-22 increases the innate immunity of tissues.* Immunity, 2004. **21**(2): p. 241-54.
315. Sonnenberg, G.F., et al., *CD4(+) lymphoid tissue-inducer cells promote innate immunity in the gut.* Immunity, 2011. **34**(1): p. 122-34.
316. Dudakov, J.A., et al., *Interleukin-22 drives endogenous thymic regeneration in mice.* Science, 2012. **336**(6077): p. 91-5.
317. Ota, N., et al., *IL-22 bridges the lymphotoxin pathway with the maintenance of colonic lymphoid structures during infection with Citrobacter rodentium.* Nat Immunol, 2011. **12**(10): p. 941-8.
318. Wohn, C., et al., *Langerinneg conventional dendritic cells produce IL-23 to drive psoriatic plaque formation in mice.* Proc Natl Acad Sci U S A, 2013. **110**(26): p. 10723-8.
319. Kirchberger, S., et al., *Innate lymphoid cells sustain colon cancer through production of interleukin-22 in a mouse model.* J Exp Med, 2013. **210**(5): p. 917-31.
320. Honma, M., et al., *Podoplanin expression in wound and hyperproliferative psoriatic epidermis: regulation by TGF-beta and STAT-3 activating cytokines, IFN-gamma, IL-6, and IL-22.* J Dermatol Sci, 2012. **65**(2): p. 134-40.
321. Puel, A., et al., *Autoantibodies against IL-17A, IL-17F, and IL-22 in patients with chronic mucocutaneous candidiasis and autoimmune polyendocrine syndrome type I.* J Exp Med, 2010. **207**(2): p. 291-7.
322. Yang, X. and S.G. Zheng, *Interleukin-22: A likely target for treatment of autoimmune diseases.* Autoimmun Rev, 2014.
323. Ikeuchi, H., et al., *Expression of interleukin-22 in rheumatoid arthritis: potential role as a proinflammatory cytokine.* Arthritis Rheum, 2005. **52**(4): p. 1037-46.
324. Khader, S.A., et al., *IL-23 is required for long-term control of Mycobacterium tuberculosis and B cell follicle formation in the infected lung.* J Immunol, 2011. **187**(10): p. 5402-7.
325. Lavoie, T.N., et al., *Expression of interleukin-22 in Sjogren's syndrome: significant correlation with disease parameters.* Scand J Immunol, 2011. **74**(4): p. 377-82.
326. Ma, H.L., et al., *IL-22 is required for Th17 cell-mediated pathology in a mouse model of psoriasis-like skin inflammation.* J Clin Invest, 2008. **118**(2): p. 597-607.
327. Zhao, L., et al., *IL-22+ CD4+ T cells in patients with rheumatoid arthritis.* Int J Rheum Dis, 2013. **16**(5): p. 518-26.
328. Zhao, L., et al., *IL-22+CD4+ T-cells in patients with active systemic lupus erythematosus.* Exp Biol Med (Maywood), 2013. **238**(2): p. 193-9.
329. Mitra, A., S.K. Raychaudhuri, and S.P. Raychaudhuri, *IL-22 induced cell proliferation is regulated by PI3K/Akt/mTOR signaling cascade.* Cytokine, 2012. **60**(1): p. 38-42.
330. Sonnenberg, G.F., L.A. Fouser, and D. Artis, *Functional biology of the IL-22-IL-22R pathway in regulating immunity and inflammation at barrier surfaces.* Adv Immunol, 2010. **107**: p. 1-29.
331. Sonnenberg, G.F., L.A. Fouser, and D. Artis, *Border patrol: regulation of immunity, inflammation and tissue homeostasis at barrier surfaces by IL-22.* Nat Immunol, 2011. **12**(5): p. 383-90.
332. Ciccia, F., et al., *Potential involvement of IL-22 and IL-22-producing cells in the inflamed salivary glands of patients with Sjogren's syndrome.* Ann Rheum Dis, 2012. **71**(2): p. 295-301.
333. Tohyama, M., et al., *IFN-alpha enhances IL-22 receptor expression in keratinocytes: a possible role in the development of psoriasis.* J Invest Dermatol, 2012. **132**(7): p. 1933-5.
334. Brand, S., et al., *IL-22 is increased in active Crohn's disease and promotes proinflammatory gene expression and intestinal epithelial cell migration.* Am J Physiol Gastrointest Liver Physiol, 2006. **290**(4): p. G827-38.
335. Beltman, J.B., et al., *B cells within germinal centers migrate preferentially from dark to light zone.* Proc Natl Acad Sci U S A, 2011. **108**(21): p. 8755-60.

336. Sisto, M., et al., *Autoantibodies from Sjogren's syndrome trigger apoptosis in salivary gland cell line.* Ann N Y Acad Sci, 2007. **1108**: p. 418-25.
337. Ciccia, F., et al., *Rituximab modulates the expression of IL-22 in the salivary glands of patients with primary Sjogren's syndrome.* Ann Rheum Dis, 2013. **72**(5): p. 782-3.
338. Eberl, G., et al., *An essential function for the nuclear receptor RORγt in the generation of fetal lymphoid tissue inducer cells.* Nature Immunology, 2003. **5**(1): p. 64-73.
339. Zhang, X. and B. Lu, *IL-17 initiates tertiary lymphoid organ formation.* Cell Mol Immunol, 2012. **9**(1): p. 9-10.
340. Columba-Cabezas, S., et al., *Suppression of established experimental autoimmune encephalomyelitis and formation of meningeal lymphoid follicles by lymphotoxin β receptor-Ig fusion protein.* Journal of Neuroimmunology, 2006. **179**(1-2): p. 76-86.
341. Gommerman, J.L. and J.L. Browning, *Lymphotoxin/LIGHT, lymphoid microenvironments and autoimmune disease.* Nature Reviews Immunology, 2003. **3**(8): p. 642-655.
342. Ware, C.F., et al., *Expression of surface lymphotoxin and tumor necrosis factor on activated T, B, and natural killer cells.* J Immunol, 1992. **149**(12): p. 3881-8.
343. Lane, P.J.L., *The Architects of B and T Cell Immune Responses.* Immunity, 2008. **29**(2): p. 171-172.
344. Androlewicz, M.J., J.L. Browning, and C.F. Ware, *Lymphotoxin is expressed as a heteromeric complex with a distinct 33-kDa glycoprotein on the surface of an activated human T cell hybridoma.* J Biol Chem, 1992. **267**(4): p. 2542-7.
345. Barone, F., et al., *Association of CXCL13 and CCL21 expression with the progressive organization of lymphoid-like structures in Sjogren's syndrome.* Arthritis Rheum, 2005. **52**(6): p. 1773-84.
346. Manzo, A., et al., *CCL21 expression pattern of human secondary lymphoid organ stroma is conserved in inflammatory lesions with lymphoid neogenesis.* Am J Pathol, 2007. **171**(5): p. 1549-62.
347. Rantapaa-Dahlqvist, S., et al., *Antibodies against cyclic citrullinated peptide and IgA rheumatoid factor predict the development of rheumatoid arthritis.* Arthritis Rheum, 2003. **48**(10): p. 2741-9.
348. Bos, W.H., et al., *Arthritis development in patients with arthralgia is strongly associated with anti-citrullinated protein antibody status: a prospective cohort study.* Ann Rheum Dis, 2010. **69**(3): p. 490-4.
349. Barra, L., et al., *Anti-citrullinated protein antibodies in unaffected first-degree relatives of rheumatoid arthritis patients.* Arthritis Rheum, 2013. **65**(6): p. 1439-47.
350. Lisi, S., et al., *Sjogren's syndrome autoantibodies provoke changes in gene expression profiles of inflammatory cytokines triggering a pathway involving TACE/NF-kappaB.* Lab Invest, 2012. **92**(4): p. 615-24.
351. Buckley, C.D., *Why does chronic inflammatory joint disease persist?* Clin Med, 2003. **3**(4): p. 361-6.
352. Filer, A., C. Pitzalis, and C.D. Buckley, *Targeting the stromal microenvironment in chronic inflammation.* Curr Opin Pharmacol, 2006. **6**(4): p. 393-400.
353. Cupedo, T., *An unexpected role for IL-17 in lymphoid organogenesis.* Nature Immunology, 2011. **12**(7): p. 590-592.
354. Douglas, M.R., et al., *Why does inflammation persist: a dominant role for the stromal microenvironment?* Expert Rev Mol Med, 2002. **4**(25): p. 1-18.
355. Haworth, O. and C.D. Buckley, *Resolving the problem of persistence in the switch from acute to chronic inflammation.* Proc Natl Acad Sci U S A, 2007. **104**(52): p. 20647-8.
356. Serhan, C.N., et al., *Resolution of inflammation: state of the art, definitions and terms.* FASEB J, 2007. **21**(2): p. 325-32.
357. Boulianne, B., et al., *Lymphotoxin-sensitive microenvironments in homeostasis and inflammation.* Front Immunol, 2012. **3**: p. 243.

358. McCarthy, D.D., et al., *The lymphotoxin pathway: beyond lymph node development.* Immunol Res, 2006. **35**(1-2): p. 41-54.
359. Iwano, M., et al., *Evidence that fibroblasts derive from epithelium during tissue fibrosis.* J Clin Invest, 2002. **110**(3): p. 341-50.
360. Parsonage, G., et al., *A stromal address code defined by fibroblasts.* Trends Immunol, 2005. **26**(3): p. 150-6.
361. Kalluri, R. and E.G. Neilson, *Epithelial-mesenchymal transition and its implications for fibrosis.* J Clin Invest, 2003. **112**(12): p. 1776-84.
362. Abe, R., et al., *Peripheral blood fibrocytes: differentiation pathway and migration to wound sites.* J Immunol, 2001. **166**(12): p. 7556-62.
363. LeBleu, V.S., et al., *Origin and function of myofibroblasts in kidney fibrosis.* Nat Med, 2013. **19**(8): p. 1047-53.
364. Malhotra, D., et al., *Transcriptional profiling of stroma from inflamed and resting lymph nodes defines immunological hallmarks.* Nat Immunol, 2012. **13**(5): p. 499-510.
365. Astarita, J.L., S.E. Acton, and S.J. Turley, *Podoplanin: emerging functions in development, the immune system, and cancer.* Frontiers in Immunology, 2012. **3**.
366. Shen, Y., et al., *SRC induces podoplanin expression to promote cell migration.* J Biol Chem, 2010. **285**(13): p. 9649-56.
367. Bekiaris, V., et al., *Role of CD30 in B/T segregation in the spleen.* J Immunol, 2007. **179**(11): p. 7535-43.
368. Balogh, P., V. Fisi, and A.K. Szakal, *Fibroblastic reticular cells of the peripheral lymphoid organs: Unique features of a ubiquitous cell type.* Molecular Immunology, 2008. **46**(1): p. 1-7.

Appendix 1

Publications

Benezech C, **Nayar S**, et al. Clec-2 is required for development and maintenance of lymph nodes. Blood, 2014.

Barone F, **Nayar S**, Buckley C.D. The role of non-hematopoiteic stromal cells in the persistence of inflammation. Front Immunol, 2013. 3: p.416.

Bombardieri M, Barone F, Luchessi D, **Nayar S,** et al. Inducible tertiary lymphoid structures, autoimmunity, and exocrine dysfunction in a novel model of salivary gland inflammation in C57BL/6 mice. J Immunol, 2012. **189**(7): p. 3767-76.